

NIST-GCR-97-713

**THE TRANSPORT OF HIGH CONCENTRATIONS
OF CARBON MONOXIDE TO LOCATIONS
REMOTE FROM THE BURNING
COMPARTMENT**

Brian Y. Lattimer and Uri Vandsburger
Virginia Polytechnic Institute and State University,
Blacksburg, VA 24061-0238

Richard J. Roby
Hughes Associates, Inc.
Baltimore, MD 21227

Building and Fire Research Laboratory
Gaithersburg, MD 20899-0001

NIST

United States Department of Commerce
Technology Administration
National Institute of Standards and Technology

**THE TRANSPORT OF HIGH CONCENTRATIONS
OF CARBON MONOXIDE TO LOCATIONS
REMOTE FROM THE BURNING
COMPARTMENT**

Brian Y. Lattimer and Uri Vandsburger
Virginia Polytechnic Institute and State University
Blacksburg, VA 24061-0238

Richard J. Roby
Hughes Associates, Inc.
Baltimore, MD 21227

April, 1997
Building and Fire Research Laboratory
National Institute of Standards and Technology
Gaithersburg, MD 20899-0001



U.S. Department of Commerce
William M. Daley, *Secretary*
Technology Administration
Mary L. Good, *Under Secretary for Technology*
National Institute of Standards and Technology
Robert E. Hebner, *Acting Director*

Notice

This report was prepared for the Building and Fire Research Laboratory of the National Institute of Standards and Technology under grant number 60NANB5D0136. The statement and conclusions contained in this report are those of the authors and do not necessarily reflect the views of the National Institute of Standards and Technology or the Building and Fire Research Laboratory.

**THE TRANSPORT OF HIGH CONCENTRATIONS OF
CARBON MONOXIDE TO LOCATIONS REMOTE FROM
THE BURNING COMPARTMENT**

ANNUAL REPORT

NIST/BFRL CONTRACT NO. 60NANB4D1651

Scientific Officer Dr. W. M. Pitts

by

**Brian Y. Lattimer
and
Uri Vandsburger
Mechanical Engineering Department
Virginia Tech
Blacksburg VA 24061-0238**

and

**Richard J. Roby
Hughes Associates Inc
3610 Commerce Dr, Suite 817
Baltimore MD 21227**

**Reporting Period
1 September 1995 - 31 August 1996**

THE TRANSPORT OF HIGH CONCENTRATIONS OF CARBON MONOXIDE TO LOCATIONS REMOTE FROM THE BURNING COMPARTMENT

by

Brian Y. Lattimer

Dr. Uri Vandsburger, Chairman

Mechanical Engineering

(ABSTRACT)

An experimental study was conducted to measure the effects of oxygen entrainment on the transport of CO in building fires, and to develop a procedure for estimating CO levels during a building fire. Experiments were performed with an insulated 1/4-scale room connected to the side of a 1/4-scale hallway forming a L-shape. Measurements of CO, unburned hydrocarbons (UHC), CO₂, and O₂ concentrations and temperature were performed within the compartment, the hallway and post-hallway in the exhaust duct.

The level of CO transported to remote locations from the burning room was hypothesized to be most significantly affected by the oxygen entrainment into the compartment fire gases entering the hallway. With a fixed size opening connecting the compartment to the hallway, the oxygen entrainment was varied by changing the depth of the oxygen deficient hallway upper-layer. In experiments where compartment fire gases entered the hallway completely surrounded by oxygen deficient combustion gases, post-hallway CO yields were measured to be as much as 23% greater than CO yields measured inside the compartment, despite the presence of external burning. With deep upper-layers in the hallway, geometric effects were not observed to significantly affect the transported level of CO. Instead, the CO level was a function of the compartment stoichiometry and the occurrence of external burning.

With the compartment on the side of the hallway, the movement of combustion products within the hallway was measured to be non-uniform. Gases containing high CO concentrations ($>1.9\%$) were measured first traveling across the hallway and then down the side of the hallway opposite the compartment. Only 1.0% CO was measured in the gases on the compartment side of the hallway. The CO concentrations were 2.0-2.3% when gas concentrations in the hallway reached a steady-state. This level of CO would result in death with less than 2 minutes of exposure.

A procedure for predicting CO levels in building fires was also developed. The procedure accounts for the effects of external burning, the non-uniform transport of toxic gases in the hallway, the hallway upper-layer depth and the stoichiometry of the system on the CO levels at remote locations.

TABLE OF CONTENTS

	PAGE
ABSTRACT	ii
DEDICATION	iv
ACKNOWLEDGEMENTS	v
LIST OF FIGURES	xiv
LIST OF TABLES	xxx
NOMENCLATURE	xxxii
1.0 INTRODUCTION	1
1.1 MOTIVATION.....	1
1.2 PREVIOUS WORK	3
1.2.1 Species Production in Compartment Fires.....	3
1.2.2 Species Transport to Locations Remote from Burning Compartment	4
1.3 FOCUS OF RESEARCH.....	10
2.0 EXPERIMENTAL METHODS	14
2.1 INTRODUCTION.....	14
2.2 EXPERIMENTAL FACILITY.....	14
2.2.1 Compartment	14
2.2.2 Hallway.....	19
2.2.3 Fume Hood and Exhaust System.....	25
2.2.4 Gas Sampling System.....	25
2.2.5 Gas Analysis	28
2.2.5.1 <i>Unburned Hydrocarbon Measurements</i>	29
2.2.5.2 <i>CO, CO₂ and O₂ Measurements</i>	31

2.2.6	Data Acquisition	33
2.3	DATA REDUCTION	34
2.3.1	Basic Data Reduction.....	34
2.3.1.1	<i>Temperature Data</i>	34
2.3.1.2	<i>Species Concentrations</i>	35
2.3.1.3	<i>Species Yields</i>	36
2.3.1.4	<i>Smoke Extinction Coefficient and Yield</i>	38
2.3.1.5	<i>Fire Size</i>	39
2.3.1.6	<i>Compartment Global Equivalence Ratio</i>	40
2.3.1.7	<i>Residence Times</i>	41
2.3.1.8	<i>Compartment Fire Growth and Steady-State</i>	41
2.3.2	Temporal Averaging of Data	42
2.3.2.1	<i>Averaging over a Single Window Time</i>	44
2.3.2.2	<i>Averaging over Several Windows of Time</i>	44
2.3.3	Ignition Index.....	45
2.3.4	Video Record of Experiments.....	46
2.4	TYPES OF EXPERIMENTS.....	47
2.4.1	Experimental Goals	47
2.4.2	General Experimental Procedure	48
2.4.3	Fuel Samples	49
2.4.4	Estimation of Compartment Fire Gas Jet Air Entrainment....	50
2.4.5	Study of Conditions Necessary for the Transport of High CO Levels.....	51
2.4.6	Study of Species Concentration Evolution within the Facility	52
3.0	RESULTS: TRANSPORT OF CHEMICAL SPECIES TO REMOTE LOCATIONS	56

3.1 INTRODUCTION.....	56
3.2 AIR ENTRAINMENT INTO COMPARTMENT FIRE EXHAUST GASES.....	56
3.2.1 Background on Air Entrainment into Ceiling Jets and Plumes	57
3.2.2 Air Entrainment Model for Compartment Fire Exhaust Gases.....	58
3.2.3 Air Entrainment into Ceiling Jets	60
3.2.4 Air Entrainment into Plumes.....	65
3.2.5 Additional Parameters Affecting Air Entrainment	68
3.3 EFFECT OF AIR ENTRAINMENT ON POST-HALLWAY SPECIES YIELDS	70
3.3.1 Effect of Opening Size	71
3.3.2 Effects of Air Inlet Orifice Diameter and Fire Size	71
3.3.3 Effect of Inlet Soffit Height.....	76
3.3.4 Effect of Exit Soffit Height	82
3.3.5 Effect of All Parameters with a Deep Hallway Upper-Layer .	87
3.3.6 Major Parameters Controlling Post-Hallway Species Yields.....	91
3.4 POST-HALLWAY SPECIES YIELDS FROM POLYURETHANE FOAM FIRES	93
4.0 RESULTS: EVOLUTION OF COMBUSTION GASES IN THE HALLWAY	96
4.1 INTRODUCTION.....	96
4.2 MOVEMENT OF COMBUSTION GASES IN THE HALLWAY	96
4.3 EVOLUTION IN HEXANE COMPARTMENT FIRES	99

4.3.1	Short Transient Time with No External Burning.....	100
4.3.2	Short Transient Time with External Burning	118
4.3.3	Long Transient Time with External Burning	143
4.4	EVOLUTION IN POLYURETHANE FOAM COMPARTMENT FIRES	175
4.4.1	Short Equilibration Time with No External Burning.....	179
4.5	SUMMARY OF SPECIES EVOLUTION IN THE HALLWAY.....	194
5.0	DISCUSSION: ANALYSIS OF RESULTS AND MODEL DEVELOPMENT	196
5.1	INTRODUCTION.....	196
5.2	PREDICTION OF EXTERNAL BURNING.....	196
5.3	PREDICTION OF SPECIES CONCENTRATION TRANSIENT TIME	201
5.4	CORRELATIONS FOR THE PREDICTION OF CO.....	204
5.4.1	Oxygen Entrainment into Gases Entering the Hallway	205
5.4.2	Global Equivalence Ratio of the Compartment-Hallway System.....	209
5.5	PROCEDURE FOR PREDICTING CO LEVELS IN BUILDING FIRES.....	213
5.6	APPLICATION OF RESULTS TO FULL-SCALE SITUATIONS....	215
6.0	ENGINEERING TOOLS FOR THE ESTIMATION OF CO LEVELS IN BUILDING FIRES.....	217
6.1	INTRODUCTION.....	217

6.2 PROGRAMS AND CHEMICAL KINETIC MECHANISMS.....	217
6.2.1 SENKIN, STANJAN and CHEMKIN	217
6.2.2 Chemical Kinetic Mechanisms for <i>n</i> -Hexane and Methane.....	218
6.3 ESTIMATION OF SPECIES PRODUCTION IN COMPARTMENT FIRES	219
6.3.1 Background	219
6.3.2 Description of the Compartment Fire Model.....	222
6.3.3 <i>n</i> -Hexane Compartment Fire Modeling Results	225
6.3.4 Methane Compartment Fire Modeling Results.....	227
7.0 CONCLUSIONS AND RECOMMENDATIONS	238
7.1 SUMMARY.....	238
7.2 CONCLUSIONS.....	244
7.3 RECOMMENDATIONS.....	246
REFERENCES	249
APPENDIX A. EFFECT OF ORIFICE DIAMETER ON AIR INLET DUCT VELOCITY PROFILES.....	255
APPENDIX B. DATA REDUCTION PROGRAMS	257
APPENDIX C. ENHANCED CO GENERATION IN THE COMPARTMENT	281
C.1 INTRODUCTION	281
C.2 DOORWAY EXPERIMENTS.....	281
C.2.1 Experimental Methodology	281
C.2.2 Flow Visualization	283
C.2.3 Results and Discussion.....	285
C.2.4 Summary and Conclusions.....	289

C.3	COMBUSTIBLE CEILING	
	INSIDE THE COMPARTMENT	290
	C.3.1 Background	290
	C.3.2 Experimental Methodology	290
	C.3.3 Results and Discussion.....	293
	C.3.4 Summary	298
APPENDIX D.	CHEMICAL KINETIC MODELING	
	OF THE HALLWAY GASES.....	299
D.1	INTRODUCTION	299
D.2	DERIVATION OF GOVERNING EQUATIONS.....	299
D.3	METHODOLOGY OF MODELING	304
	D.3.1 Transformation of Experimental	
	Results to a Temporal Coordinate System ...	304
	D.3.2 Transformation of Plug Flow Reactor	
	Results to Spatial Coordinate System	306
APPENDIX E.	EXPERIMENTAL ERROR ANALYSIS	308
E.1	INTRODUCTION	308
E.2	CALCULATION OF ERROR.....	308
E.3	ERROR IN PARAMETERS	309
	E.3.1 Measured Species Concentrations	309
	E.3.2 Wet Species Concentrations.....	310
	E.3.3 Gas Temperature.....	310
	E.3.4 Fuel Weight.....	311
	E.3.5 Air Mass Flow Rate into Compartment	312
	E.3.6 Global Equivalence Ratio	312
	E.3.7 Species Yields	313
	E.3.8 Fire Size.....	313

E.3.9	Nondimensional Hallway Upper-Layer	
	Depth	313
E.3.10	Entrainment Function.....	314
E.3.11	Richardson Number.....	314
E.3.12	Ignition Index	314
E.4	SUMMARY	315
VITA	316

LIST OF FIGURES

FIGURE	PAGE
Figure 1. 1 The location of the victims from the fire in the Hillhaven nursing home (Nelson and Tu, 1991)	2
Figure 1. 2 The CO yields produced in <i>n</i> -hexane compartment fires performed by Gottuk (1992a) when sampling inside the compartment (□). Beyler's (1983) (▲) <i>n</i> -hexane hood experiment data is also shown.....	5
Figure 1. 3 The toxicity of CO relative to (a) HCN and (b) acrolein in gases produced in a building fire (Morikawa et al., 1993).....	7
Figure 2. 1 The building fire research facility at Virginia Tech with the compartment on the side of the hallway.....	15
Figure 2. 2 A detailed view of the compartment and plenum	16
Figure 2. 3 A detailed view of the hallway showing the automated sampling cart..	20
Figure 2. 4 The automated sampling cart used to sample at various hallway locations during a single experiment.....	22
Figure 2. 5 A schematic of the electronics involved in computer controlling the motors on the automated sampling cart	23
Figure 2. 6 The exhaust duct system used to collect the combustion products exiting the hallway.....	26
Figure 2. 7 A schematic of the piping system used to sample combustion gases from different locations in the facility. Also shown are the CO, CO ₂ and O ₂ analyzers.....	27
Figure 2. 8 A schematic of the equipment and piping in the UHC analysis system.....	30
Figure 2. 9 The utilization of the fire growth parameter(○) and the compartment upper-layer temperature (—) to describe the different stages of growth occurring during a compartment fire.....	43
Figure 2. 10 Sample locations within the facility for <i>n</i> -hexane compartment fires .	53
Figure 2. 11 Sample locations within the facility for polyurethane foam compartment fires	55

Figure 3. 12 The simplified control volume analysis of the hallway upper-layer gases.....	58
Figure 3. 13 The entrainment into a ceiling jet produced from an overventilated compartment fire. The data is from experiments having opening sizes of \circ -0.12 m ² , \square -0.08 m ² , and Δ -0.04 m ² with the solid line being the curve fit to the data. The dashed line is the ceiling jet curve from Ellison and Turner (1959).....	64
Figure 3. 14 The mass flow rate of air entrainment into the overventilated compartment fire gases in experiments with a 0.20 m inlet soffit where the plume, the turning region and the ceiling jet were present in the initial 0.60 m of travel. Experiments utilized \circ -0.12 m ² , \square -0.08 m ² , and Δ -0.04 m ² opening sizes.	66
Figure 3. 15 The air entrainment function for the overventilated compartment fire gases in the first 0.60 m of the hallway in experiments with a 0.20 m inlet soffit where both a plume and a ceiling jet are present. The data is from experiments having opening sizes of \circ -0.12 m ² , \square -0.08 m ² , and Δ -0.04 m ² with the solid being the curve fit to this data. The dash-dot line is the ceiling jet curve from this study while the dotted line is the ceiling jet curve from Ellison and Turner (1959).....	69
Figure 3. 16 The effect of the opening size on the post-hallway \bullet -CO, \blacksquare -UHC and \blacktriangle -CO ₂ yields for the cases with $Q=448\pm 154$ kW, $\phi=2.57\pm 0.06$, a 0.20 m inlet soffit, and no exit soffit. Experimental data of Ewens (1994b).....	72
Figure 3. 17 The variation in the compartment upper-layer temperature profile with inlet orifice diameter of \circ -0.30m (no orifice), \square -0.25 m, Δ -0.20, and ∇ -0.15 m	74
Figure 3. 18 The variation in the fuel volatilization rate in <i>n</i> -hexane fires with inlet orifice diameter of ----0.30m (no orifice), $\bullet\bullet\bullet$ 0.25 m, $-\bullet-$ 0.20, and $-\bullet\bullet-$ 0.15 m.....	75
Figure 3. 19 The effect of the fire size on the momentum of the compartment fire gas jet entering the hallway for opening sizes of \circ -0.12 m ² , \square -0.08 m ² and Δ -0.04 m ² is demonstrated. Experimental data of Ewens (1994b).....	77
Figure 3. 20 The effect of the fire size on the post-hallway \bullet -CO, \blacksquare -UHC and \blacktriangle -CO ₂ yields with a 0.12 m ² opening, $\phi=2.35\pm 0.41$, no inlet soffit and 0.20 m exit soffit is shown. Experimental data of Ewens (1994b).	78

Figure 3. 21	The variation in the post-hallway CO yield with no inlet soffit (●) and a 0.20m inlet soffit (■) is shown. The experimental conditions were $Q=431\pm150$ kW, $\phi=2.64\pm0.17$, and no exit soffit. Experimental data of Ewens (1994b).	79
Figure 3. 22	The variation in the post-hallway UHC yield with no inlet soffit (●) and a 0.20m inlet soffit (■) is shown. The experimental conditions were $Q=431\pm150$ kW, $\phi=2.64\pm0.17$, and no exit soffit. Experimental data of Ewens (1994b).	80
Figure 3. 23	The variation in the post-hallway CO ₂ yield with no inlet soffit (●) and a 0.20m inlet soffit (■) is shown. The experimental conditions were $Q=431\pm150$ kW, $\phi=2.64\pm0.17$, and no exit soffit. Experimental data of Ewens (1994b).	81
Figure 3. 24	The effect the non-dimensional upper-layer height on the post-hallway ●- CO, ■-UHC, and ▲-CO ₂ yields for experiments with a 0.12 m ² opening, $Q=291\pm36$ kW, and $\phi=3.20\pm0.54$. Filled symbols represent experiments with external burning while open symbols were experiments with no external burning.	84
Figure 3. 25	The effect the non-dimensional upper-layer height on the post-hallway ●- CO, ■-UHC, and ▲-CO ₂ yields for experiments with a 0.08 m ² opening, $Q=322\pm64$ kW, and $\phi=2.56\pm0.41$. Filled symbols represent experiments with external burning while open symbols were experiments with no external burning.	86
Figure 3. 26	The effect the non-dimensional upper-layer height on the post-hallway ●- CO, ■-UHC, and ▲-CO ₂ yields for experiments with a 0.04 m ² opening, $Q=259\pm41$ kW, and $\phi=2.77\pm0.57$. Filled symbols represent experiments with external burning while open symbols were experiments with no external burning.	88
Figure 3. 27	The effect of varying all parameters on the post-hallway CO yield when a deep upper-layer, $\gamma>1.0$, was present in the hallway. Filled symbols represent experiments with external burning while open symbols were experiments with no external burning.	90
Figure 3. 28	The effect of varying all parameters on the post-hallway UHC yield when a deep upper-layer, $\gamma>1.0$, was present in the hallway. Filled symbols represent experiments with external burning while open symbols were experiments with no external burning.	92

Figure 3. 29	The effect of the nondimensional upper-layer depth on the post-hallway \circ -CO, \square -UHC and Δ -CO ₂ yield in experiments with polyurethane foam as the fuel inside the compartment. The experiments utilized a 0.04 m ² opening, a 0.20 m inlet soffit, Q=164±11 kW and ϕ =2.08±0.01. Filled symbols represent experiments with external burning while open symbols were experiments with no external burning.	94
Figure 4.1	An image of the external burning in the hallway when looking down the open end of the hallway underneath the fume hood.	98
Figure 4.2	The temperature 0.05 m below the ceiling inside the compartment in 10 different <i>n</i> -hexane fire experiments with a 0.04 m ² opening, a 0.60 m exit soffit, and no external burning in the hallway. The experiments were aligned with one another in time using the fire growth parameter.	101
Figure 4.3	The wet CO concentration distribution 0.05 m below the ceiling 12-16 seconds before flashover in <i>n</i> -hexane fire experiments with a 0.04 m ² opening, 0.20 m inlet soffit, 0.60 m exit soffit and no external burning.	102
Figure 4.4	The wet UHC concentration distribution 0.05 m below the ceiling 12-16 seconds before flashover in <i>n</i> -hexane fire experiments with a 0.04 m ² opening, 0.20 m inlet soffit, 0.60 m exit soffit and no external burning.	103
Figure 4.5	The wet CO ₂ concentration distribution 0.05 m below the ceiling 12-16 seconds before flashover in <i>n</i> -hexane fire experiments with a 0.04 m ² opening, 0.20 m inlet soffit, 0.60 m exit soffit and no external burning.	104
Figure 4.6	The wet O ₂ concentration distribution 0.05 m below the ceiling 12-16 seconds before flashover in <i>n</i> -hexane fire experiments with a 0.04 m ² opening, 0.20 m inlet soffit, 0.60 m exit soffit and no external burning.	105
Figure 4.7	The temperature distribution 0.05 m below the ceiling 12-16 seconds before flashover in <i>n</i> -hexane fire experiments with a 0.04 m ² opening, 0.20 m inlet soffit, 0.60 m exit soffit and no external burning.	106

Figure 4.8	The wet CO concentration distribution 0.05 m below the ceiling 16-20 seconds after flashover in <i>n</i> -hexane fire experiments with a 0.04 m ² opening, 0.20 m inlet soffit, 0.60 m exit soffit and no external burning.....	108
Figure 4.9	The wet UHC concentration distribution 0.05 m below the ceiling 16-20 seconds after flashover in <i>n</i> -hexane fire experiments with a 0.04 m ² opening, 0.20 m inlet soffit, 0.60 m exit soffit and no external burning.....	109
Figure 4.10	The wet CO ₂ concentration distribution 0.05 m below the ceiling 16-20 seconds after flashover in <i>n</i> -hexane fire experiments with a 0.04 m ² opening, 0.20 m inlet soffit, 0.60 m exit soffit and no external burning.....	110
Figure 4.11	The wet O ₂ concentration distribution 0.05 m below the ceiling 16-20 seconds after flashover in <i>n</i> -hexane fire experiments with a 0.04 m ² opening, 0.20 m inlet soffit, 0.60 m exit soffit and no external burning.....	111
Figure 4.12	The temperature distribution 0.05 m below the ceiling 16-20 seconds after flashover in <i>n</i> -hexane fire experiments with a 0.04 m ² opening, 0.20 m inlet soffit, 0.60 m exit soffit and no external burning.....	112
Figure 4.13	The wet CO concentration distribution 0.05 m below the ceiling 40-44 seconds after flashover in <i>n</i> -hexane fire experiments with a 0.04 m ² opening, 0.20 m inlet soffit, 0.60 m exit soffit and no external burning.....	113
Figure 4.14	The wet UHC concentration distribution 0.05 m below the ceiling 40-44 seconds after flashover in <i>n</i> -hexane fire experiments with a 0.04 m ² opening, 0.20 m inlet soffit, 0.60 m exit soffit and no external burning.....	114
Figure 4.15	The wet CO ₂ concentration distribution 0.05 m below the ceiling 40-44 seconds after flashover in <i>n</i> -hexane fire experiments with a 0.04 m ² opening, 0.20 m inlet soffit, 0.60 m exit soffit and no external burning.....	115
Figure 4.16	The wet O ₂ concentration distribution 0.05 m below the ceiling 40-44 seconds after flashover in <i>n</i> -hexane fire experiments with a 0.04 m ² opening, 0.20 m inlet soffit, 0.60 m exit soffit and no external burning.....	116

Figure 4.17	The temperature distribution 0.05 m below the ceiling 40-44 seconds after flashover in <i>n</i> -hexane fire experiments with a 0.04 m ² opening, 0.20 m inlet soffit, 0.60 m exit soffit and no external burning.	117
Figure 4.18	The temperature 0.05 m below the ceiling inside the compartment in 10 different <i>n</i> -hexane fire experiments with a 0.12 m ² opening, a 0.60 m exit soffit, and external burning in the hallway. The experiments were aligned with one another in time using the fire growth parameter.	120
Figure 4.19	The wet CO concentration distribution 0.05 m below the ceiling 12-16 seconds before flashover in <i>n</i> -hexane fire experiments with a 0.12 m ² opening, 0.20 m inlet soffit, 0.60 m exit soffit and external burning.	121
Figure 4.20	The wet UHC concentration distribution 0.05 m below the ceiling 12-16 seconds before flashover in <i>n</i> -hexane fire experiments with a 0.12 m ² opening, 0.20 m inlet soffit, 0.60 m exit soffit and external burning.	122
Figure 4.21	The wet CO ₂ concentration distribution 0.05 m below the ceiling 12-16 seconds before flashover in <i>n</i> -hexane fire experiments with a 0.12 m ² opening, 0.20 m inlet soffit, 0.60 m exit soffit and external burning.	123
Figure 4.22	The wet O ₂ concentration distribution 0.05 m below the ceiling 12-16 seconds before flashover in <i>n</i> -hexane fire experiments with a 0.12 m ² opening, 0.20 m inlet soffit, 0.60 m exit soffit and external burning.	124
Figure 4.23	The temperature distribution 0.05 m below the ceiling 12-16 seconds before flashover in <i>n</i> -hexane fire experiments with a 0.12 m ² opening, 0.20 m inlet soffit, 0.60 m exit soffit and external burning.	125
Figure 4.24	The wet CO concentration distribution 0.05 m below the ceiling 16-20 seconds after flashover in <i>n</i> -hexane fire experiments with a 0.12 m ² opening, 0.20 m inlet soffit, 0.60 m exit soffit and external burning.	126
Figure 4.25	The wet UHC concentration distribution 0.05 m below the ceiling 16-20 seconds after flashover in <i>n</i> -hexane fire experiments with a 0.12 m ² opening, 0.20 m inlet soffit, 0.60 m exit soffit and external burning.	128

Figure 4.26 The wet CO ₂ concentration distribution 0.05 m below the ceiling 16-20 seconds after flashover in <i>n</i> -hexane fire experiments with a 0.12 m ² opening, 0.20 m inlet soffit, 0.60 m exit soffit and external burning.....	129
Figure 4.27 The wet O ₂ concentration distribution 0.05 m below the ceiling 16-20 seconds after flashover in <i>n</i> -hexane fire experiments with a 0.12 m ² opening, 0.20 m inlet soffit, 0.60 m exit soffit and external burning.....	130
Figure 4.28 The temperature distribution 0.05 m below the ceiling 16-20 seconds after flashover in <i>n</i> -hexane fire experiments with a 0.12 m ² opening, 0.20 m inlet soffit, 0.60 m exit soffit and external burning.....	131
Figure 4.29 The wet CO concentration distribution 0.05 m below the ceiling 44-48 seconds after flashover in <i>n</i> -hexane fire experiments with a 0.12 m ² opening, 0.20 m inlet soffit, 0.60 m exit soffit and external burning.....	132
Figure 4.30 The wet UHC concentration distribution 0.05 m below the ceiling 44-48 seconds after flashover in <i>n</i> -hexane fire experiments with a 0.12 m ² opening, 0.20 m inlet soffit, 0.60 m exit soffit and external burning.....	133
Figure 4.31 The wet CO ₂ concentration distribution 0.05 m below the ceiling 44-48 seconds after flashover in <i>n</i> -hexane fire experiments with a 0.12 m ² opening, 0.20 m inlet soffit, 0.60 m exit soffit and external burning.....	134
Figure 4.32 The wet O ₂ concentration distribution 0.05 m below the ceiling 44-48 seconds after flashover in <i>n</i> -hexane fire experiments with a 0.12 m ² opening, 0.20 m inlet soffit, 0.60 m exit soffit and external burning.....	135
Figure 4.33 The temperature distribution 0.05 m below the ceiling 44-48 seconds after flashover in <i>n</i> -hexane fire experiments with a 0.12 m ² opening, 0.20 m inlet soffit, 0.60 m exit soffit and external burning.....	136
Figure 4.34 The wet CO concentration distribution 0.05 m below the ceiling 72-76 seconds after flashover in <i>n</i> -hexane fire experiments with a 0.12 m ² opening, 0.20 m inlet soffit, 0.60 m exit soffit and external burning.....	138

Figure 4.35	The wet UHC concentration distribution 0.05 m below the ceiling 72-76 seconds after flashover in <i>n</i> -hexane fire experiments with a 0.12 m ² opening, 0.20 m inlet soffit, 0.60 m exit soffit and external burning.....	139
Figure 4.36	The wet CO ₂ concentration distribution 0.05 m below the ceiling 72-76 seconds after flashover in <i>n</i> -hexane fire experiments with a 0.12 m ² opening, 0.20 m inlet soffit, 0.60 m exit soffit and external burning.....	140
Figure 4.37	The wet O ₂ concentration distribution 0.05 m below the ceiling 72-76 seconds after flashover in <i>n</i> -hexane fire experiments with a 0.12 m ² opening, 0.20 m inlet soffit, 0.60 m exit soffit and external burning.....	141
Figure 4.38	The temperature distribution 0.05 m below the ceiling 72-76 seconds after flashover in <i>n</i> -hexane fire experiments with a 0.12 m ² opening, 0.20 m inlet soffit, 0.60 m exit soffit and external burning.....	142
Figure 4.39	The wet CO concentration distribution 0.05 m below the ceiling 96-100 seconds after flashover in <i>n</i> -hexane fire experiments with a 0.12 m ² opening, 0.20 m inlet soffit, 0.60 m exit soffit and external burning.....	144
Figure 4.40	The wet UHC concentration distribution 0.05 m below the ceiling 96-100 seconds after flashover in <i>n</i> -hexane fire experiments with a 0.12 m ² opening, 0.20 m inlet soffit, 0.60 m exit soffit and external burning.....	145
Figure 4.41	The wet CO ₂ concentration distribution 0.05 m below the ceiling 96-100 seconds after flashover in <i>n</i> -hexane fire experiments with a 0.12 m ² opening, 0.20 m inlet soffit, 0.60 m exit soffit and external burning.....	146
Figure 4.42	The wet O ₂ concentration distribution 0.05 m below the ceiling 96-100 seconds after flashover in <i>n</i> -hexane fire experiments with a 0.12 m ² opening, 0.20 m inlet soffit, 0.60 m exit soffit and external burning.....	147
Figure 4.43	The temperature distribution 0.05 m below the ceiling 96-100 seconds after flashover in <i>n</i> -hexane fire experiments with a 0.12 m ² opening, 0.20 m inlet soffit, 0.60 m exit soffit and external burning..	148

Figure 4.44	The temperature 0.05 m below the ceiling inside the compartment in 10 different <i>n</i> -hexane fire experiments with external burning, a 0.04 m ² opening, and the exit of the hallway blocked leaving a 0.20 m high, 1.22 m wide opening. The experiments were aligned with one another in time using the fire growth parameter.....	150
Figure 4.45	The wet CO concentration distribution 0.05 m below the ceiling 12-16 seconds after flashover in <i>n</i> -hexane fire experiments with a 0.04 m ² opening, 0.20 m inlet soffit, 0.20 m high 1.22 m wide opening at top of hallway exit and external burning.	151
Figure 4.46	The wet UHC concentration distribution 0.05 m below the ceiling 12-16 seconds after flashover in <i>n</i> -hexane fire experiments with a 0.04 m ² opening, 0.20 m inlet soffit, 0.20 m high 1.22 m wide opening at top of hallway exit and external burning.	152
Figure 4.47	The wet CO ₂ concentration distribution 0.05 m below the ceiling 12-16 seconds after flashover in <i>n</i> -hexane fire experiments with a 0.04 m ² opening, 0.20 m inlet soffit, 0.20 m high 1.22 m wide opening at top of hallway exit and external burning.	153
Figure 4.48	The wet O ₂ concentration distribution 0.05 m below the ceiling 12-16 seconds after flashover in <i>n</i> -hexane fire experiments with a 0.04 m ² opening, 0.20 m inlet soffit, 0.20 m high 1.22 m wide opening at top of hallway exit and external burning.	154
Figure 4.49	The temperature distribution 0.05 m below the ceiling 12-16 seconds after flashover in <i>n</i> -hexane fire experiments with a 0.04 m ² opening, 0.20 m inlet soffit, 0.20 m high 1.22 m wide opening at top of hallway exit and external burning.	156
Figure 4.50	The wet CO concentration distribution 0.05 m below the ceiling 48-52 seconds after flashover in <i>n</i> -hexane fire experiments with a 0.04 m ² opening, 0.20 m inlet soffit, 0.20 m high 1.22 m wide opening at top of hallway exit and external burning.	157
Figure 4.51	The wet UHC concentration distribution 0.05 m below the ceiling 48-52 seconds after flashover in <i>n</i> -hexane fire experiments with a 0.04 m ² opening, 0.20 m inlet soffit, 0.20 m high 1.22 m wide opening at top of hallway exit and external burning.	158
Figure 4.52	The wet CO ₂ concentration distribution 0.05 m below the ceiling 48-52 seconds after flashover in <i>n</i> -hexane fire experiments with a 0.04 m ² opening, 0.20 m inlet soffit, 0.20 m high 1.22 m wide opening at top of hallway exit and external burning.	159

Figure 4.53	The wet O ₂ concentration distribution 0.05 m below the ceiling 48-52 seconds after flashover in <i>n</i> -hexane fire experiments with a 0.04 m ² opening, 0.20 m inlet soffit, 0.20 m high 1.22 m wide opening at top of hallway exit and external burning.	160
Figure 4.54	The temperature distribution 0.05 m below the ceiling 48-52 seconds after flashover in <i>n</i> -hexane fire experiments with a 0.04 m ² opening, 0.20 m inlet soffit, 0.20 m high 1.22 m wide opening at top of hallway exit and external burning.	161
Figure 4.55	The wet CO concentration distribution 0.05 m below the ceiling 64-68 seconds after flashover in <i>n</i> -hexane fire experiments with a 0.04 m ² opening, 0.20 m inlet soffit, 0.20 m high 1.22 m wide opening at top of hallway exit and external burning.	163
Figure 4.56	The wet UHC concentration distribution 0.05 m below the ceiling 64-68 seconds after flashover in <i>n</i> -hexane fire experiments with a 0.04 m ² opening, 0.20 m inlet soffit, 0.20 m high 1.22 m wide opening at top of hallway exit and external burning.	164
Figure 4.57	The wet CO ₂ concentration distribution 0.05 m below the ceiling 64-68 seconds after flashover in <i>n</i> -hexane fire experiments with a 0.04 m ² opening, 0.20 m inlet soffit, 0.20 m high 1.22 m wide opening at top of hallway exit and external burning.	165
Figure 4.58	The wet O ₂ concentration distribution 0.05 m below the ceiling 64-68 seconds after flashover in <i>n</i> -hexane fire experiments with a 0.04 m ² opening, 0.20 m inlet soffit, 0.20 m high 1.22 m wide opening at top of hallway exit and external burning.	166
Figure 4.59	The temperature distribution 0.05 m below the ceiling 64-68 seconds after flashover in <i>n</i> -hexane fire experiments with a 0.04 m ² opening, 0.20 m inlet soffit, 0.20 m high 1.22 m wide opening at top of hallway exit and external burning.	167
Figure 4.60	The wet CO concentration distribution 0.05 m below the ceiling 80-84 seconds after flashover in <i>n</i> -hexane fire experiments with a 0.04 m ² opening, 0.20 m inlet soffit, 0.20 m high 1.22 m wide opening at top of hallway exit and external burning.	168
Figure 4.61	The wet UHC concentration distribution 0.05 m below the ceiling 80-84 seconds after flashover in <i>n</i> -hexane fire experiments with a 0.04 m ² opening, 0.20 m inlet soffit, 0.20 m high 1.22 m wide opening at top of hallway exit and external burning.	170

Figure 4.62	The wet CO ₂ concentration distribution 0.05 m below the ceiling 80-84 seconds after flashover in <i>n</i> -hexane fire experiments with a 0.04 m ² opening, 0.20 m inlet soffit, 0.20 m high 1.22 m wide opening at top of hallway exit and external burning.	171
Figure 4.63	The wet O ₂ concentration distribution 0.05 m below the ceiling 80-84 seconds after flashover in <i>n</i> -hexane fire experiments with a 0.04 m ² opening, 0.20 m inlet soffit, 0.20 m high 1.22 m wide opening at top of hallway exit and external burning.	172
Figure 4.64	The temperature distribution 0.05 m below the ceiling 80-84 seconds after flashover in <i>n</i> -hexane fire experiments with a 0.04 m ² opening, 0.20 m inlet soffit, 0.20 m high 1.22 m wide opening at top of hallway exit and external burning.	173
Figure 4.65	The wet CO concentration distribution 0.05 m below the ceiling 108-112 seconds after flashover in <i>n</i> -hexane fire experiments with a 0.04 m ² opening, 0.20 m inlet soffit, 0.20 m high 1.22 m wide opening at top of hallway exit and external burning.	174
Figure 4.66	The wet UHC concentration distribution 0.05 m below the ceiling 108-112 seconds after flashover in <i>n</i> -hexane fire experiments with a 0.04 m ² opening, 0.20 m inlet soffit, 0.20 m high 1.22 m wide opening at top of hallway exit and external burning.	175
Figure 4.67	The wet CO ₂ concentration distribution 0.05 m below the ceiling 108-112 seconds after flashover in <i>n</i> -hexane fire experiments with a 0.04 m ² opening, 0.20 m inlet soffit, 0.20 m high 1.22 m wide opening at top of hallway exit and external burning.	176
Figure 4.68	The wet O ₂ concentration distribution 0.05 m below the ceiling 108-112 seconds after flashover in <i>n</i> -hexane fire experiments with a 0.04 m ² opening, 0.20 m inlet soffit, 0.20 m high 1.22 m wide opening at top of hallway exit and external burning.	177
Figure 4.69	The temperature distribution 0.05 m below the ceiling 108-112 seconds after flashover in <i>n</i> -hexane fire experiments with a 0.04 m ² opening, 0.20 m inlet soffit, 0.20 m high 1.22 m wide opening at top of hallway exit and external burning.	178
Figure 4.70	The temperature 0.05 m below the ceiling inside the compartment in 10 different polyurethane foam fire experiments with no external burning, a 0.04 m ² opening, and a 0.60 m exit soffit. The experiments were aligned with one another in time using the fire growth parameter.	180

Figure 4.71	The wet CO concentration distribution 0.05 m below the ceiling 32-36 seconds after flashover in polyurethane foam fire experiments with a 0.04 m ² opening, 0.20 m inlet soffit, 0.60 m exit soffit and no external burning.	181
Figure 4.72	The wet CO ₂ concentration distribution 0.05 m below the ceiling 32-36 seconds after flashover in polyurethane foam fire experiments with a 0.04 m ² opening, 0.20 m inlet soffit, 0.60 m exit soffit and no external burning.	183
Figure 4.73	The wet O ₂ concentration distribution 0.05 m below the ceiling 32-36 seconds after flashover in polyurethane foam fire experiments with a 0.04 m ² opening, 0.20 m inlet soffit, 0.60 m exit soffit and no external burning.	184
Figure 4.74	The temperature distribution 0.05 m below the ceiling 32-36 seconds after flashover in polyurethane foam fire experiments with a 0.04 m ² opening, 0.20 m inlet soffit, 0.60 m exit soffit and no external burning.	185
Figure 4.75	The wet CO concentration distribution 0.05 m below the ceiling 64-68 seconds after flashover in polyurethane foam fire experiments with a 0.04 m ² opening, 0.20 m inlet soffit, 0.60 m exit soffit and no external burning.	186
Figure 4.76	The wet CO ₂ concentration distribution 0.05 m below the ceiling 64-68 seconds after flashover in polyurethane foam fire experiments with a 0.04 m ² opening, 0.20 m inlet soffit, 0.60 m exit soffit and no external burning.	187
Figure 4.77	The wet O ₂ concentration distribution 0.05 m below the ceiling 64-68 seconds after flashover in polyurethane foam fire experiments with a 0.04 m ² opening, 0.20 m inlet soffit, 0.60 m exit soffit and no external burning.	188
Figure 4.78	The temperature distribution 0.05 m below the ceiling 64-68 seconds after flashover in polyurethane foam fire experiments with a 0.04 m ² opening, 0.20 m inlet soffit, 0.60 m exit soffit and no external burning.	189
Figure 4.79	The wet CO concentration distribution 0.05 m below the ceiling 92-96 seconds after flashover in polyurethane foam fire experiments with a 0.04 m ² opening, 0.20 m inlet soffit, 0.60 m exit soffit and no external burning.	190

Figure 4.80	The wet CO ₂ concentration distribution 0.05 m below the ceiling 92-96 seconds after flashover in polyurethane foam fire experiments with a 0.04 m ² opening, 0.20 m inlet soffit, 0.60 m exit soffit and no external burning.	191
Figure 4.81	The wet O ₂ concentration distribution 0.05 m below the ceiling 92-96 seconds after flashover in polyurethane foam fire experiments with a 0.04 m ² opening, 0.20 m inlet soffit, 0.60 m exit soffit and no external burning.	192
Figure 4.82	The temperature distribution 0.05 m below the ceiling 92-96 seconds after flashover in polyurethane foam fire experiments with a 0.04 m ² opening, 0.20 m inlet soffit, 0.60 m exit soffit and no external burning.	193
Figure 5.1	The ignition index for an experiment with external burning in the hallway.	199
Figure 5.2	The ignition index for an experiment with no external burning.	200
Figure 5.3	The well-stirred volume model for the estimation of species concentration transient time in the hallway.	202
Figure 5.4	The use of the oxygen entrainment parameter, Eqn. (5.5), to predict the hallway exit CO yield with external burning occurring in the hallway. Data from opening sizes of ●-0.12 m ² , ▲-0.08 m ² , and ■-0.04 m ² . The solid line is a curve fit to the data.	207
Figure 5.5	The use of the oxygen entrainment parameter, Eqn. (5.5), to predict the hallway exit UHC yield with external burning occurring in the hallway. Data from opening sizes of ●-0.12 m ² , ▲-0.08 m ² , and ■-0.04 m ² . The solid line is a curve fit to the data.	208
Figure 5.6	The post-hallway CO yields (●) plotted against the compartment equivalence ratio. The compartment yields (□) from the study of 209Gottuk (1992a) are also shown.	211
Figure 5.7	The post-hallway CO yields (●) plotted against the system global equivalence ratio. The compartment yields (□) from the study of Gottuk (1992a) are also shown. The solid line is a curve fit to the data of Gottuk.	212
Figure 5.8	The proposed procedure for estimating CO levels in building fires.	214

- Figure 6. 1 The CO experimental results of ○-Beyler and Δ-Gottuk compared with the modeling results of Gottuk. Using ○-Beyler's data as the initial concentrations in the model, the dotted line is the result using the upper-layer temperature of Beyler and the ▲-dashed line is the result using the upper-layer temperature of Gottuk. The ▼-solid line corresponds to CO levels where all of the UHC was assumed to be consumed in the plume. 221
- Figure 6. 2 A phenomenological representation of the conditions present inside an idealized compartment fire just prior to the onset of flashover. 223
- Figure 6. 3 Comparison of the ○-experimental and —modeling results of Gottuk(1992a) with the proposed model estimations of CO concentrations for *n*-hexane fires during the steady-state time with temperatures of ----900K, ••• 1000 K, and -•- 1100 K. 226
- Figure 6. 4 Comparison of the ○-experimental and — modeling results of Gottuk (1992a) with the proposed model estimations of CO₂ concentrations for *n*-hexane fires during the steady-state time with temperatures of --900K, ••• 1000 K, and -•- 1100 K..... 228
- Figure 6. 5 Comparison of the ○-experimental and — modeling results of Gottuk (1992a) with the proposed model estimations of O₂ concentrations for *n*-hexane fires during the steady-state time with temperatures of ---- 900K, ••• 1000 K, and -•- 1100 K..... 229
- Figure 6. 6 Model estimation of the major species concentrations present in the 1000 K compartment upper-layer during the steady-state time of a *n*-hexane fire. Symbols: ●-N₂, ○-H₂O, □-CO₂, Δ-O₂, ▽-CO, ◇-H₂ and ●-UHC. 230
- Figure 6. 7 Model estimation of the UHC concentrations present in the 1000 K compartment upper-layer during the steady-state time of a *n*-hexane fire. Open symbols, ○-C₂H₄, □-CH₄, Δ-C₃H₆, and ▽-C₂H₂, correspond to the left y-axis while closed symbols, ●-C₂H₆, ■-C₄H₆ and ▲-C₃H₈ correspond to the right y-axis..... 231
- Figure 6. 8 Comparison of the experimental results of Bryner, et al. (1994), in both the ○-front (1300 K) and the □-back (1000 K) of their compartment, with the proposed model estimations of CO concentrations for methane compartment fires during the steady-state time with temperatures of ----1000K and ••• 1300 K. 233

Figure 6. 9	Comparison of the experimental results of Bryner, et al. (1994), in both the O-front (1300 K) and the □-back (1000 K) of their compartment, with the proposed model estimations of CO ₂ concentrations for methane compartment fires during the steady-state time with temperatures of ----1000K and •••1300 K.	234
Figure 6. 10	Comparison of the experimental results of Bryner, et al. (1994), in both the O-front (1300 K) and the □-back (1000 K) of their compartment, with the proposed model estimations of O ₂ concentrations for methane compartment fires during the steady-state time with temperatures of ----1000K and •••1300 K.	235
Figure 6. 11	Model estimation of the major species concentrations present in the 1000 K compartment upper-layer during the steady-state time of a methane fire. Symbols: ●-N ₂ , ○-H ₂ O, □-CO ₂ , △-O ₂ , ▽-CO, ◇-H ₂ and ●-UHC.....	236
Figure 6. 12	Model estimation of the UHC concentrations present in the 1000 K compartment upper-layer during the steady-state time of a methane fire. The open symbol, ○-CH ₄ , corresponds to the left y-axis while closed symbols, ■-C ₂ H ₂ , ▲-C ₂ H ₄ , and ▼-C ₂ H ₆ correspond to the right y-axis.	237
Figure A. 1	The velocity profiles in the air inlet duct for with ●-no orifice (0.30 m), ■-0.25 m, ▲-0.20 m and ▼-0.15 m diameter orifices attached to the duct. The vertical lines represent average velocities of the profiles.	256
Figure C. 1	The compartment on the end of the hallway with the plenum blocked forcing a bi-directional flow of air into and combustion gases out of the compartment through the door.....	282
Figure C. 2	The external burning <i>n</i> -hexane fire experiments with (a) a door and (b) a 0.12m ² opening connecting the compartment to the hallway.	284
Figure C. 3	The normalized species concentrations (wet) and temperatures within the compartment and hallway for <i>n</i> -hexane fire experiments with a door. Symbols and normalization values: ●-CO (8.0%), ■-UHC (10%), ▲-CO ₂ (20%), ▼-O ₂ (10.5%), and ○-Temperature.....	286

Figure C. 4	The normalized species concentrations (wet) and temperatures within the compartment and hallway for <i>n</i> -hexane fire experiments with a 0.12 m ² opening. Symbols and normalization values: ●-CO (8.0%), ■-UHC (10%), ▲-CO ₂ (20%), ▼-O ₂ (10.5%), and ○-Temperature. ...	287
Figure C. 5	The effect of air being entrained into the compartment through (a) the plenum and (b) the doorway on the fire plume inside the compartment.	288
Figure C. 6	A side view of the facility showing wood suspended from the ceiling of the compartment.	291
Figure C. 7	A top view of the facility showing the orientation of the wood in the upper layer of the compartment and the gas sampling locations.	292
Figure C. 8	The mass loss rate of the wooden ceiling as a function of time. The sampling locations of the five different experiments: Experimental sampling in the compartment: –Rear, ----Front, and down the hallway: ••0.46 m, -•- 1.83 m, -••- 3.20 m. –Average.	294
Figure C. 9	The normalized species concentrations (dry) and temperatures within the compartment and hallway for <i>n</i> -hexane fire experiments with a 0.12 m ² opening. Symbols and normalization values: ●-CO (15.0%), ■-UHC (10%), ▲-CO ₂ (20%), ▼-O ₂ (10.5%), and ○-Temperature. ...	295
Figure C. 10	The normalized species concentrations (dry) and temperatures within the compartment and hallway for <i>n</i> -hexane fire experiments containing a wood ceiling with a 0.12 m ² opening . Symbols and normalization values: ●-CO (15.0%), ■-UHC (10%), ▲-CO ₂ (20%), ▼-O ₂ (10.5%), and ○-Temperature.	296
Figure D. 1	The plug flow reactor being used to model the hallway gases.....	299
Figure D. 2	The control volume showing the fluxes of momentum.....	300
Figure D. 3	The control volume showing the fluxes of energy and species.....	301
Figure D. 4	The bulk flow path of the compartment fire gases. The letters denote locations where temperature and air entrainment measurements were performed.....	304
Figure D. 5	The location of the data points within the plug flow reactor.	306

LIST OF TABLES

TABLE	PAGE
Table 2. 1 The composition and some properties of the fuels utilized in the study.	49
Table 3. 1 The experimental conditions in the overventilated fire experiments used to determine the air entrainment into the ceiling jet.....	62
Table 3. 2 The air entrainment into the ceiling jet using the overventilated compartment fire experimental results.	62
Table 3. 3 The experimental conditions in the overventilated fire experiments with a 0.20 m inlet soffit where the air entrainment into compartment fire gases in the initial 0.60 m of the hallway is determined.	67
Table 3. 4 Using overventilated compartment fire experimental results with a 0.20 m inlet soffit, the calculated air entrainment into the compartment fire gases in the initial 0.60 m where the plume, the area of impingement and the ceiling jet are all present.	67
Table 5. 1 The use of the ignition index and the nondimensional upper-layer depth to predict the occurrence of external burning in the hallway.....	198
Table 5. 2 The conditions in experiments with both short and long steady-state times in the hallway.	203
Table E. 1 The uncertainty induced in the measurement of the species concentrations.	310
Table E. 2 The uncertainty in the calculation of the wet concentrations of CO, CO ₂ and O ₂	311
Table E. 3 The uncertainty in the post-hallway yields for the different species measured in the study.	313
Table E. 4 The errors of all the parameters measured and calculated in the study.	315

NOMENCLATURE

SYMBOL	DESCRIPTION	UNITS
A	area	m^2
A_r	pre-exponential collision factor	
A_{wet}	wetted area	m^2
C	concentration	% volume
C_p	specific heat constant	$kJ/g\text{-mol K}$
CO	level of carbon monoxide exposure	ppm
$COHb$	carboxyhemoglobin level	%
D	volumetric flow rate	m^3/s
D_h	hydraulic diameter	m
D_{mass}	optical density	m^2/g
E	entrainment function	
E_a	activation energy	
F	flame extension in hallway	m
F_a	flow constant	
F_{comp}	flame extension inside compartment	m
Fr	Froude number	
G	fire growth parameter	
GER	global equivalence ratio	
H	height of ceiling in compartment	m
ΔH_c	heat of combustion	kJ/kg
I	light intensity	volts
I_o	reference light intensity	volts
$I.I.$	ignition index	
L	free flame height	m
MW	molecular weight	$kg/kmol$
P	pressure	Torr
P_{wet}	wetted perimeter	m
Q	fire size (power of fire)	kW
\dot{Q}	volumetric flow rate	m^3/s
R	ideal gas constant for air, 28.84	$kJ/(kg K)$
\bar{R}	ideal gas constant; 8.314	$kJ/(kmol K)$
Re	Reynolds number	
Ri	Richardson number	
RR	reaction rate	
T	temperature	K

T_{comp}	compartment temperature	K
\bar{T}_{hall}	average hallway temperature	K
T_O	initial temperature	K
T_{OV}	temperature from overventilated fire	K
T_{SL}	temperature at stoichiometric flammability limit	K
T_{UV}	temperature from underventilated fire	K
V	volume	m ³
\bar{V}_e	average entrainment velocity	m/s
\bar{V}_i	average velocity into control volume	m/s
V_s	velocity of at fire source	m/s
X	mole fraction	kmol / kmol
Y	yield	
c	flow constant	
d	fuel pan diameter	m
g	acceleration of gravity, 9.81	m/s ²
h	height of opening	m
h_e	enthalpy	kJ/(kg K)
k	reaction rate constant	
l	length along flow into hallway	m
l_p	optical path length	m
mf	mass fraction	
\dot{m}	mass flow rate	kg/s
n	moles	mol
\dot{n}	molar flow rate	mol/s
Δp	pressure drop across exhaust duct orifice plate	mm Hg
q''	heat flux	W/m ²
t	time	s
t_{tran}	transient time	s
t_{exp}	lethal exposure time	min
u	velocity in plug flow reactor	m/s
v	velocity in hallway from model	m/s
w	width of opening	m
x	axial direction in plug flow reactor	m
y	flow constant	
z	distance between bottom of opening and ceiling	m

Greek

α	non-Arrhenius temperature dependence power	
β	flow coefficient	
δ	halfway upper-layer depth	m
ε	oxygen entrainment parameter	
ϕ	equivalence ratio	
γ	nondimensional upper-layer depth	
η_{red}	concentration reduction parameter	
λ	wavelength of laser	μm
μ	kinematic viscosity	m^2/s
ρ	density	kg/m^3
σ	extinction coefficient	$1/\text{m}$
ξ	specific extinction coefficient	g/m^2
ζ	specific heat ratio	

Subscript

0	initial state
1	final state
<i>air</i>	air
<i>amb</i>	ambient
<i>c</i>	compartment
<i>CO</i>	carbon monoxide
<i>CO₂</i>	carbon dioxide
<i>d</i>	dry
<i>e</i>	entrained
<i>ex</i>	exhaust duct
<i>fs</i>	flame sheet
<i>fuel</i>	fuel
<i>g</i>	global
<i>hall</i>	hallway
<i>hallexit</i>	exit of hallway
<i>i</i>	into control volume or system
<i>j</i>	species
<i>o</i>	out of control volume or system
<i>open</i>	opening connecting compartment and hallway
<i>OV</i>	overventilated
<i>O₂</i>	oxygen
<i>p</i>	plume
<i>prod</i>	products of complete combustion

<i>res</i>	residence
<i>s</i>	fire source
<i>st</i>	stoichiometric
<i>smk</i>	smoke
<i>sys</i>	system
<i>UHC</i>	unburned hydrocarbons
<i>UL</i>	upper-layer
<i>UV</i>	underventilated
<i>w</i>	wet
<i>v</i>	fuel volatilization

CHAPTER 1.

INTRODUCTION

1.1 MOTIVATION

The total number of civilian deaths in home fires throughout the United States in 1994 dropped to an all time low of 3,425 people (Karter, 1995). Though this news is encouraging, the statistics for the cause of deaths in building fires reveals some less encouraging aspects regarding smoke inhalation deaths.

The cause of death in building fires continues to be dominated by smoke inhalation. Smoke inhalation was responsible for 76% of the deaths in building fires in 1990 (Hall and Hardwood, 1995). From 1980 to 1990, the percentage of smoke inhalation deaths in structure fires has risen 1% each year. If these numbers are extrapolated, smoke inhalation was responsible for 80% of the deaths in structure fires in 1994. Since the level of carboxyhemoglobin in a victim's blood stream (>50%) was the measure of whether or not death was caused by smoke inhalation, the smoke inhalation data conveys that an increasing percentage of deaths in building fires are the result of carbon monoxide poisoning.

Two-thirds of the smoke inhalation victims were found at locations distant from the room of fire origin (Gann et al., 1994). This situation is demonstrated vividly in two unfortunate fires during the last decade, both in nursing homes. On October 5, 1989 at the Hillhaven Nursing Home in Norfolk, Virginia, a fire in a patient's room resulted in the death of 13 people (Nelson and Tu, 1991). Each victim died of carbon monoxide poisoning with 12 of the victims found in a room or position down the hallway from the room containing the fire, see Fig. 1.1. Twenty-three (23) patients resided along the wing containing the burning room. Nine (9) of the victims were found in rooms on the

opposite side of the hallway from the burning room while only one (1) victim was found on the burning room side of the hallway. A similar type fire in a Southern Michigan hospice on December 15, 1985 claimed the lives of 8 people. Six (6) victims died of carbon monoxide poisoning and were found in rooms down the hallway from the burning room (Nelson, 1988). These incidents are examples of types of fires which claim the lives of hundreds of people annually.

The statistics on CO poisoning and the above cited incidents show a clear need in the fire science community for models which accurately predict the transport of CO to locations distant from the burning room. Further insight must first be gained on the phenomena controlling the transport of CO to remote locations before such a model can be produced. With this knowledge, measurements and analysis can be performed to produce models enabling fire protection engineers to predict the levels of CO at remote locations. Engineers could use such tools to design more fire-safe buildings, from a smoke inhalation hazard perspective, and to prevent tragic incidents such as those mentioned above from continuously reoccurring.

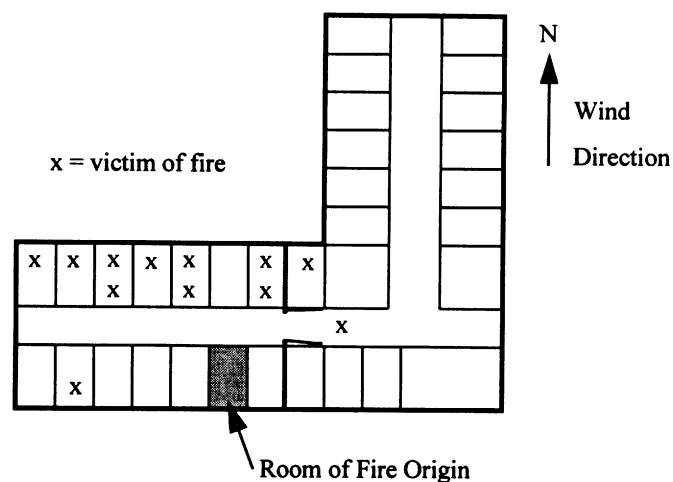


Figure 1.1 The location of the victims from the fire in the Hillhaven nursing home (Nelson and Tu, 1991)

1.2 PREVIOUS WORK

The fire science community has begun to address the problem of CO poisoning in building fires. Initial research in the area focused on understanding the formation of CO inside the burning room (compartment). More recently, research has begun to address the transport of CO away from the compartment.

1.2.1 Species Production in Compartment Fires

The “hood” experiments were the first investigations focusing on understanding the production of combustion gases in an idealized room fire containing a two-layer environment (cool air in the bottom portion of the room and hot combustion gases in the top portion of the room). In the experiments performed by Cetegen (1982), Beyler (1983), Zukoski (1985, 1991), Toner (1987) and Morehart (1990), combustion gases from a fire were caught inside a hood located some distance above the fire. The gases inside the hood simulated a compartment fire upper-layer. The air entrainment into the fire plume rising to upper-layer was varied by adjusting the distance between the fire source and the upper-layer. The global equivalence ratio (defined as the mass of the gas in the upper-layer from the fuel divided by the mass of the gas in the upper-layer from the air all normalized by the fuel stoichiometric ratio) could be varied by altering the mass loss rate of the fuel or the air entrainment rate into the fire plume. The global equivalence ratio (GER) was used to predict species yields in the upper-layer. The plume equivalence ratio,

$$\phi = \frac{\dot{m}_{fuel} / \dot{m}_{air}}{\left(\dot{m}_{fuel} / \dot{m}_{air} \right)_{st}}, \quad (1.1)$$

is defined as the ratio of the mass loss rate of fuel and the air entrainment rate into the fire plume normalized by the stoichiometric fuel-to-air ratio. This is equivalent to the global

equivalence ratio during the steady-state burning of the fire (assuming the fuel and air enter the upper-layer via the fire plume). The plume equivalence ratio is typically used to determine the global equivalence ratio since the global equivalence ratio is experimentally difficult to measure.

Gottuk (1992a,b,c), Tewarson (1984), Pitts (1994a) and Bryner et al. (1995) used the GER to predict species formation in compartment fires. From experiments by Gottuk (1992a), it was found that the hood experiments over-predicted the CO yields at global equivalence ratios from 0.4 up to 1.5, see Fig. 1.2. Pitts (1994 a,b) attributed the difference in the CO yields to the higher upper-layer temperatures in the compartment experiments.

When wood is placed on the ceiling of the compartment, CO concentrations of as high as 14%-dry have been measured inside the compartment. Such high concentrations are much greater than what would be predicted through the current GER concept (Pitts, 1994a). Some of the situations where the GER concept has difficulties predicting the CO levels in compartment fires, i.e. when wood is in the upper-layer of the compartment, are addressed and compensated for in an algorithm developed by Pitts (1994b).

1.2.2 Species Transport to Locations Remote from Burning Compartment

The transport of toxic gases away from the burning room has received minimal attention in the past. The majority of the smoke movement studies were performed to measure the temperature distribution, smoke layer depth and gas temperature distribution in the adjacent space (e.g. Heskestad and Hill (1987)). Studies on toxic gas movement away from the burning room have primarily been performed to verify that high levels of CO are transported to a location remote (a target room) from the burning room. More recently, experiments have been performed to investigate the evolution of compartment fire gases in the adjacent space.

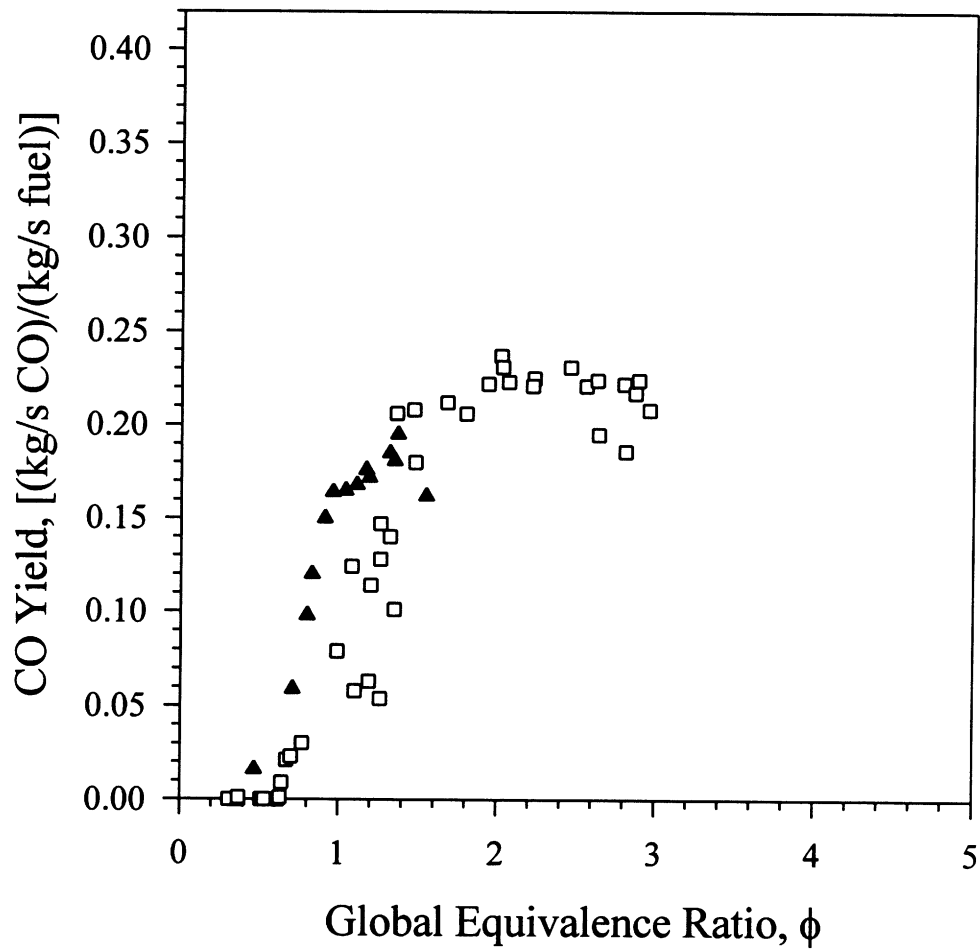
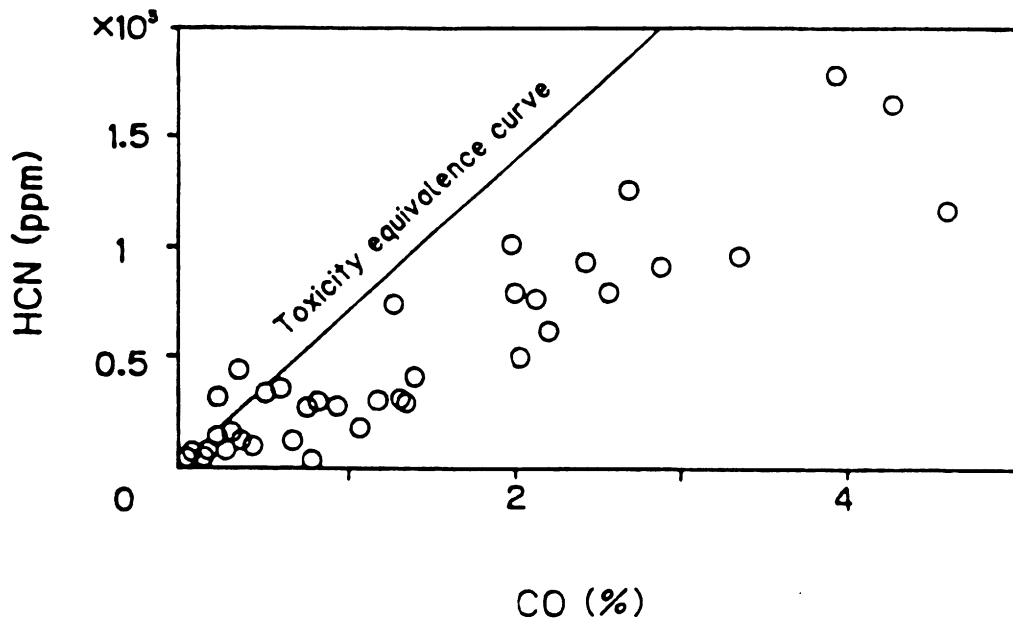


Figure 1.2 The CO yields produced in *n*-hexane compartment fires performed by Gottuk (1992a) when sampling inside the compartment (\square). Beyler's (1983) (\blacktriangle) *n*-hexane hood experiment data is also shown.

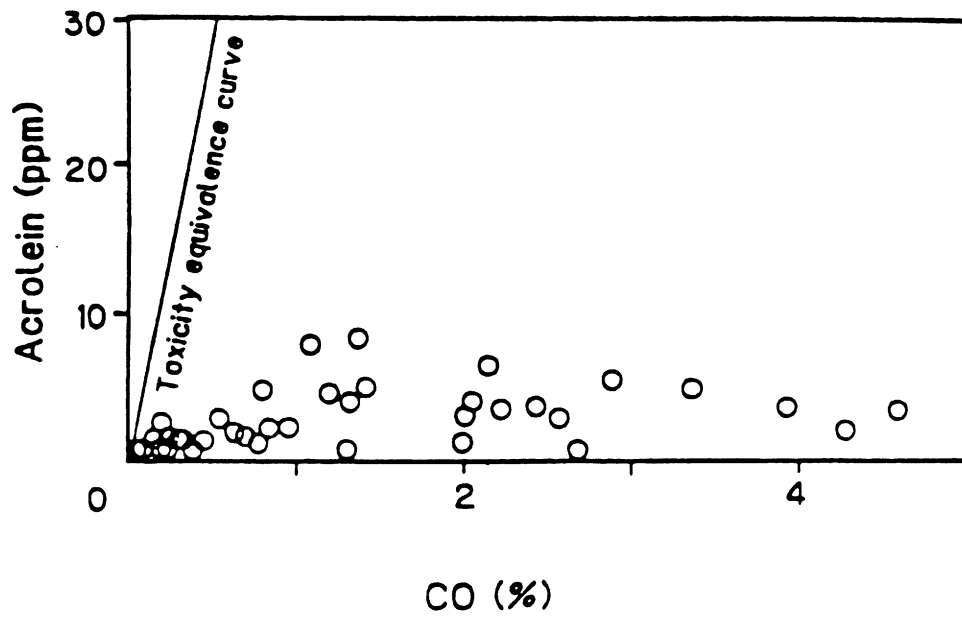
Full-scale room-hallway experiments were conducted by Fardell et al. (1986) to investigate the concentrations of different species produced in an underventilated fire environment. A gas chromatograph was used to analyze grab bag samples of gases taken from both the burning room and at the end of the hallway. In the course of measuring the levels of nearly forty different compounds, Fardell et al. (1986) assumed CO concentrations to be approximately 3.5-4.0%-dry in the gases entering the hallway.

Experiments were performed by Morikawa et al. (1990, 1993) inside a full-scale two level facility. A fire, fueled by furnishings typically found in a home, was present in a large room in the downstairs portion of the facility. Temperatures and gas concentrations were measured in the burn room and in an upstairs target room at different times during the fire. The majority of the fire experiments produced gases containing approximately 5.5-6.0%-dry CO, but levels as high as 8.0%-dry were measured. With the door open to the target room upstairs, CO levels reached as high as 4.5%-dry with levels typically in the 3-4%-dry range. The degree of toxicity of CO compared with HCN and acrolein was also studied, see Fig. 1.3. The toxicity equivalency curve shown in Fig. 1.3 is based on the lethal concentrations of CO, HCN and acrolein for 5-10 minutes of exposure (5000 ppm, 350 ppm and 30 ppm respectively). With the majority of the data points on the lower side of the toxicity curve, CO is seen in Fig. 1.3 to be equivalently or more toxic than both HCN and acrolein.

Levine and Nelson (1990) performed a full-scale simulation of a townhouse fire which occurred in Sharon, Pennsylvania. The fire resulted in the deaths of three people. One of the victim's bloodstream contained a carboxyhemoglobin level of 91%. This is much higher than the levels measured in most CO poisoning victims (65%). Large quantities of wood present in the kitchen (the room of fire origin) were found to be responsible for the production of extraordinarily high levels of CO. Carbon monoxide in excess of 8%-dry was measured in the burn room while 5%-dry CO was measured in the



(a)



(b)

Figure 1.3 The toxicity of CO relative to (a) HCN and (b) acrolein in gases produced in a building fire (Morikawa et al., 1993).

upstairs bedroom. The results of the study prompted researchers to perform the previously mentioned compartment fires with the wood ceiling.

The events of a fire which occurred in the Southern Michigan hospice fire mentioned earlier were simulated experimentally by Nelson (1988). Nelson hypothesized that the lack of oxygen in the hallway adjacent to the burning room was the mechanism which allowed the transport of high levels of CO. To test the hypothesis, a full-scale experiment was performed with the burning room connected to a hallway containing a target room. The burning room contained two openings, one connecting the room to the hallway and one connecting the room to the ambient surroundings (situated under a fume hood). The hallway contained a target room, with no openings, located approximately 12 m away from the burning room. The air flow into the hallway was restricted to the air which could enter from the burn room opening. The methane gas fire in the room replaced the air initially in the hallway and target room with combustion gases containing low O₂ levels. Carbon monoxide concentrations were measured to be as high as 4.5%-dry only 0.5 m above the floor in the target room approximately 200 seconds after ignition. The rapid cooling of the hot fire exhaust gases was also cited as being responsible for allowing high levels of CO to be transported to the target room.

The studies briefly described above verified that high concentrations of CO are generated and transported to locations remote from the fire origin, and that CO is the primary toxicant formed in these situations. None of these studies, however, investigated the evolution of the fire exhaust gas composition as the gases are transported to remote locations from the burning compartment. Only one study speculated on the phenomena which may be responsible for the transport of high levels of CO to remote locations from the fire origin (Nelson, 1988).

A study by Ewens (1994a) investigated the applicability of the compartment GER for the prediction of CO yields in the gases exiting the hallway, termed post-hallway CO

yields. The experiments performed by Ewens (1994a) contained a hallway (with unlimited available oxygen) connected to the compartment used in the study of Gottuk (1992a). In all experiments the compartment fires were underventilated and the burning inside the compartment extended out into the hallway, a phenomena termed external burning (i.e. the oxidation of fuel rich gases as they exhaust from a burning compartment and mix with ambient air). The presence of external burning was noted in a previous study by Gottuk (1992a,c) to significantly reduce CO levels downstream of the compartment. Ewens (1994a) found that the CO post-hallway yield was a function of both the fluid mechanics in the hallway and the stoichiometry of the gases entering the hallway. The conditions at the opening between the compartment and the hallway governed the hallway fluid mechanics. The fluid mechanics determined the degree of oxygen entrainment into the compartment fire gases entering the hallway. The air entrainment where the gases enter the hallway, which is mainly governed by the soffit size and the opening size at this location, was attributed to having the most significant effect on the CO levels post-hallway.

Studies by Ellison and Turner (1959), Alpert (1972), Hinkley et al. (1984) and Babrauskas (1980) demonstrated that the entrainment rate into a buoyant plume is much higher than the entrainment into a ceiling jet. In Ewens (1994) work, no soffit at the hallway entrance resulted in the gases traveling the length of the hallway as a ceiling jet (defined as hot flowing gases traveling along the ceiling). With a 0.20 m soffit at the hallway entrance, a buoyant jet of fire was seen leaving the compartment. The jet was observed to impinge upon the ceiling approximately 0.30 m downstream of the compartment, after which the gases flowed down the hallway as a ceiling jet. The additional oxygen entrainment induced by the buoyant jet resulted in better oxidation of CO and lower post-hallway yields in the 0.20 soffit case.

Ewens (1994 a) also performed sampling along the length of the hallway, and measured that unburned hydrocarbons (UHC) reduced in concentration more rapidly than CO. This result was consistent with the findings of Westbrook and Dryer (1984) which showed UHC (e.g. C_2H_4 , CH_4) having a higher oxidation rate of reaction compared with CO for temperatures less than 1100 K. The reduction in the levels of CO was also inhibited by the production of CO from the oxidation of the UHC. Ewens (1994a) also measured a significant reduction in CO oxidation when hallway temperatures fell below 850 K. This slow CO oxidation is consistent with modeling results (Pitts, 1992 and Yetter, et al., 1991).

In the experiments of Ewens (1994a), the fire gases exit the compartment into an overventilated hallway upper-layer. This situation resulted in the oxidation of CO to levels less than 0.50% by the exit of the hallway. These levels would be lethal to humans if exposed to them for approximately 20 minutes. Exposure to the levels of CO at remote locations in experiments performed by Morikawa et al. (1993) and Nelson (1988) (4.5%) would cause death in approximately 1 minute. The difference in the experiments appears to be the amount of oxygen allowed to entrain into the compartment fire gases entering the hallway.

1.3 FOCUS OF RESEARCH

The focus of the research discussed in this document is to investigate how and when high levels of CO are transported to locations remote from the fire origin. An experimental study was conducted to determine:

1. the levels of CO transported to remote locations,
2. the phenomena controlling the level of CO transported to remote locations,
3. the movement of CO away from a room on the side of a hallway, and
4. the effects of different fuels in the compartment.

The experimental findings will provide data which can be utilized to develop models, and to predict levels of CO transported to distant locations from the fire origin.

The level of CO transported to remote locations is mainly dependent upon

- the chemical composition of,
- the oxygen entrainment into, and
- the heat losses from

the high temperature compartment fire gases entering the hallway. For a fixed chemical composition of compartment fire gases, the entrainment into the fire gases is hypothesized to be the parameter which controls the level of CO transported to remote locations. The entrainment affects both the amount of oxygen entrained into the jet of compartment fire gases, and the heat losses from the jet. The entrainment of O₂ into the fire gases is necessary to oxidize CO. However, rapid entrainment of cooler O₂ containing gases increases the heat losses. This results in fire gas temperatures reduced to levels where CO oxidation cannot occur. The focus of the research was to measure the oxygen entrainment into fire exhaust gases from compartment fires of various GER.

The amount of oxygen entrained into the hot (>850 K) compartment fire gases entering and traveling within the hallway is the parameter believed to be controlling the level of CO transported away from the room. The oxygen entrainment into the gases was varied in the study by Ewens (1994a), but never quantified. The present research determined the physical parameters which most significantly affect the oxygen entrainment into the compartment fire gases entering the hallway. The effect of varying these parameters on the oxygen entrainment was then quantified.

In actual building fires, it is hypothesized that the accumulation of an oxygen deficient layer of combustion gases in the hallway during the beginning stages of the fire inhibits the amount of oxygen allowed to be entrained into the compartment fire gases

entering the hallway. The result is the transport of fatally high levels of CO to distant locations in the building. Experiments were performed to quantify the effect of varying the depth of the upper-layer in the hallway on the CO level transported to remote locations.

With the compartment on the side of the hallway, the fluid mechanics of the hallway gases are highly three-dimensional. The movement of toxic combustion gases within the hallway is believed to be non-uniform as evidenced by the location of the victims in the Hillhaven nursing home fire pictured in Fig. 1.1 (Nelson and Tu, 1991). To verify this theory, the movement of toxic gases away from the compartment was experimentally measured.

To investigate the effect of different fuels being burned inside the compartment, both liquid *n*-hexane fires and polyurethane foam fires were used in the study. The effect of the upper-layer depth in the hallway and the evolution of the hallway species concentrations were experimentally determined for the fires produced by each fuel.

A methodology was developed to estimate the level of CO transported to remote locations. The method considers

1. the uniformity of gas concentration in the adjacent space,
2. the occurrence and/or absence of external burning,
3. the hallway upper-layer depth,
4. the stoichiometry of the compartment and hallway, and
5. the entrainment into the compartment fires.

A tool was also developed to provide an estimation of combustion product concentrations produced inside the compartment. The tool considers only the chemical kinetics of the gases inside the compartment. The results of the model were compared

with existing experimental data. A model for estimating the oxidation of compartment fire gases in the hallway is also given, but not tested.

CHAPTER 2.

EXPERIMENTAL METHODS

2.1 INTRODUCTION

The following chapter is devoted to describing the experimental facility and the methodologies used to characterize the transport of high concentrations of CO away from a compartment on the side of a hallway. The chapter begins with a description of the experimental facility. A discussion of the experimental procedures used to acquire the data, and the treatment of the acquired data is then presented. The final portion of the chapter focuses on the types of experiments performed in the study.

2.2 EXPERIMENTAL FACILITY

The fire experiments were conducted in the fireproof structure which consists of a compartment placed on the side at the end of a hallway, see Fig. 2.1. The following sections describe the compartment, the hallway, the fume hood and exhaust system, and the gas analysis system. Details of the instrumentation in each of these areas of the experimental facility is also given. Lastly, the details of the data acquisition system are discussed.

2.2.1 Compartment

The compartment is seen in Fig. 2.2 to be divided into two levels to separate the flow of air into the compartment and the flow of combustion gases out of the compartment. The upper level of the compartment was 1.52 m wide, 1.22 m high, and 1.22 m deep, and was where the fire originated. This portion of the compartment was supported by a 6.35 mm thick, 50.8 mm steel angle iron frame with 6.35 mm thick, 50.8 mm bar stock supports. The floor, walls and ceiling were lined with 25.4 mm thick Fire Master, UL

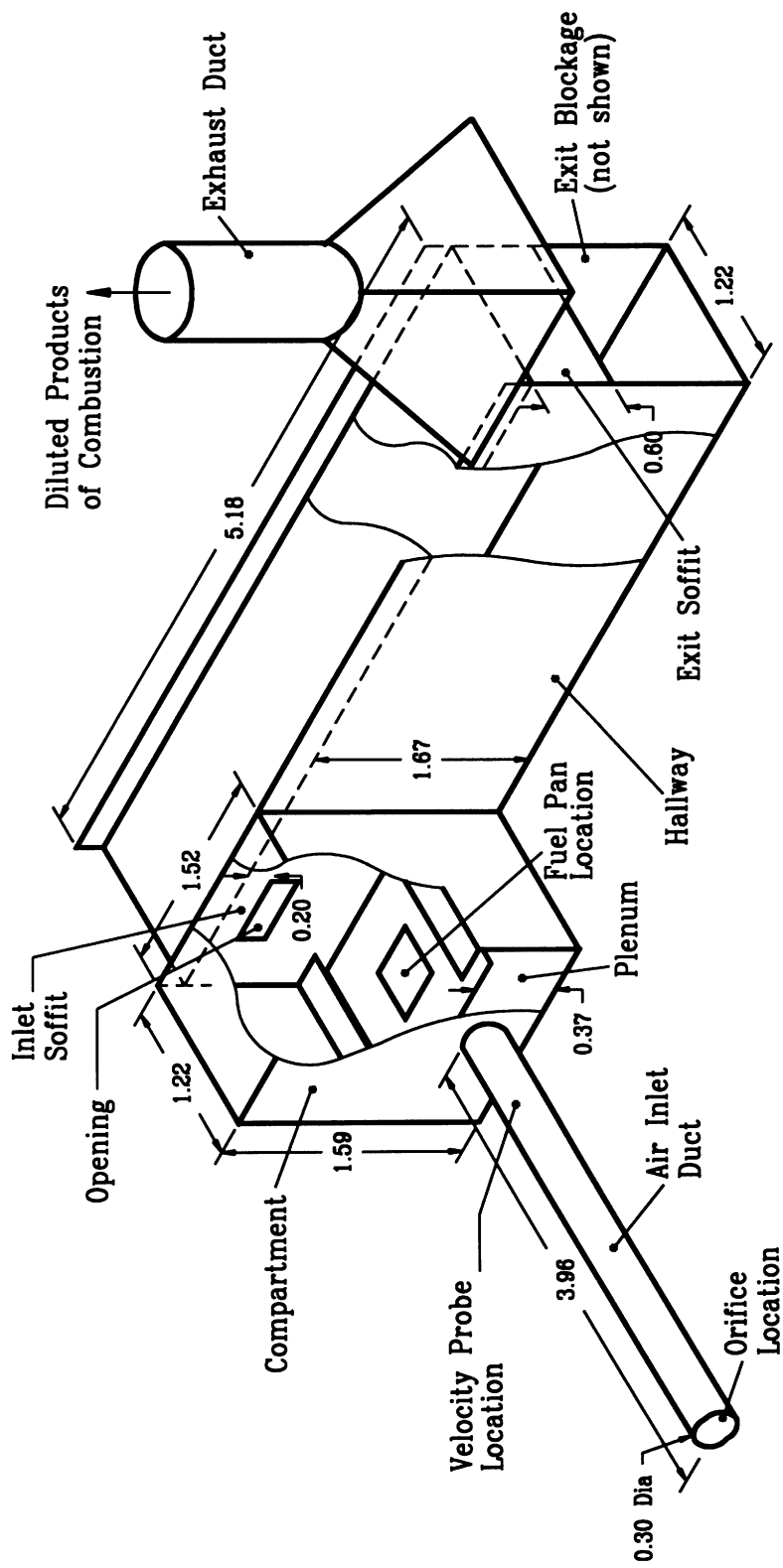


Figure 2.1 The building fire research facility at Virginia Tech with the compartment on the side of the hallway.

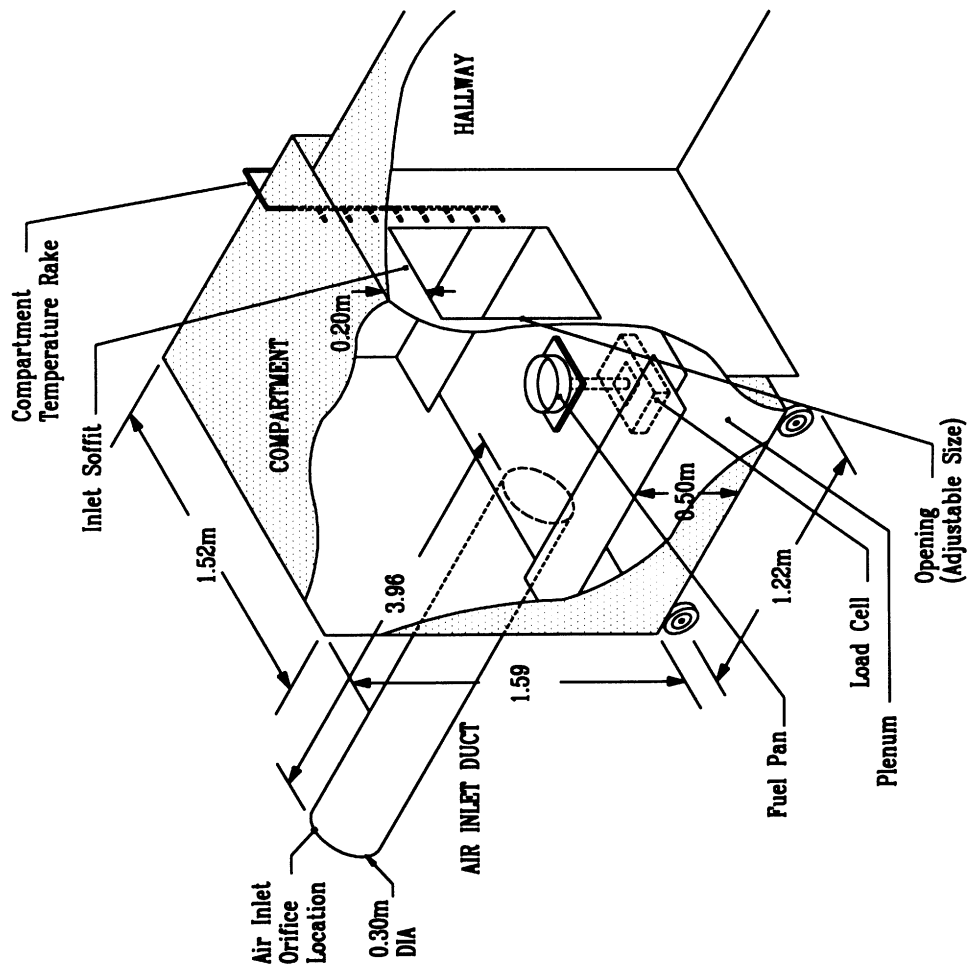


Figure 2.2 A detailed view of the compartment and plenum.

fire rated insulation board. The fire combustion products exit the compartment through a variable size opening with the maximum opening size, shown in Fig. 2.2, being 0.50 m wide, 0.75 m high (0.375 m^2). The three opening sizes utilized in the study were:

- 0.50 m wide, 0.25 m high (0.12 m^2 in area),
- 0.50 m wide, 0.16 m high (0.08 m^2 in area), and
- 0.25 m wide, 0.16 m high (0.04 m^2 in area).

The different opening sizes were achieved by blocking off the bottom portion of the opening. A 0.50 m wide, 0.63 m high hatch door was located on the wall opposite the wall containing the opening to allow easy and safe access to the inside of the compartment. To allow an upper-layer to form inside the compartment, there was a 0.20 m soffit (defined as the distance between the ceiling and the top of the opening where gases exit the compartment) inside the compartment.

The lower level of the structure was a 1.52 m wide, 0.37 m high, 1.22 m deep air distribution plenum constructed of 3.175 mm thick steel sheet metal. Air was naturally drawn into the plenum during a fire through a 0.30 m diameter, 3.96 m long circular duct attached to the plenum on the side of the compartment opposite the opening. The plenum was connected to the upper level of the compartment by two 1.22 m long, 0.13 m high thermally shielded openings located along the floor on either side of the compartment. The shields extended 0.28 m inward from the side walls.

The mass flow of air naturally drawn through the duct and into the compartment was controlled by attaching different diameter orifices on the inlet of the air duct (see Fig. 2.2). The orifice diameters utilized in the study were 0.30 m (no orifice), 0.25 m, 0.20 m, 0.15 m. The mass flow of air entrained into the compartment was determined by measuring the velocity of the air in the duct using a Kurz model 415, 0-2 m/s linear velocity hot film probe which had an accuracy of $\pm 2.5\%$. The probe was placed 3.0 m

(10 diameters) downstream of the air inlet where the orifices were attached to the duct. The velocity profiles were measured to be turbulent, with $Re=3,425$ to $9,675$, for each orifice diameter, and were found to be quite similar in shape, see Appendix A. The mean velocity was determined to be approximately 44.0 mm radially from the duct wall, and was at the same location for each orifice size considered. The probe could, therefore, remain in the same location for all experiments regardless of the attached orifice diameter. For further information on the procedure used to determine the velocity probe location see Appendix A. The mean temperature of the air flowing through the duct was also measured. The thermocouple was 3.35 m downstream of the duct air inlet. The air inlet of the duct was surrounded by a wooden cubical housing to minimize the external disturbances on measurement of air entrainment into the compartment.

Fires were burned in circular fuel pan positioned in the center of the compartment. Fuel pan diameters of 0.12, 0.15, 0.20, 0.23, and 0.28 m were utilized in the experiments. The fuel pan was located on a platform resting on a 15 kg range A&D load cell (1 gram resolution) situated in the plenum. The time derivative of the temporal fuel weight was used to determine the mass loss rate.

A spark ignition system was used to ignite the liquid pool fires. The system consisted of a voltage source and 14 gauge steel wire leads. The 120 V-AC powered source contained a transformer to generate the high voltages necessary for the spark. The two leads enter the compartment through the wall with the ends of the wires resting off to the side and just below the top of the fuel pan. After connecting the leads to the source, a spark was generated by flipping the power switch and turning the potentiometer. After the pool was ignited, the power source was turned off and disconnected from the leads. The development of the compartment fire was observed through three polished Vycor glass windows installed along the height of one wall.

An aspirated temperature rake was present in one corner of the compartment to measure the temperature profile of the upper-layer gases. The rake, constructed of 6.35 mm stainless steel tubing, consisted of eight type K (chromel-alumel) thermocouples vertically spaced 0.10 m apart with the top thermocouple which was 0.10 m below the ceiling. The rake was placed 0.10 m from either wall to avoid wall jet effects. Gases were drawn into the rake by a Dayton Speedaire diaphragm vacuum pump, model #4Z024. A water trap in an ice bath and a Gelman glass fiber filter were upstream of the pump to prevent water and particulates from flowing through pump. A bare thermocouple was located at the side of the opening to measure the temperature of the gases exiting the compartment.

2.2.2 Hallway

The combustion gases exited the compartment and entered into a 1.22 m wide, 5.18 m long hallway, see Fig. 2.3. The height of the hallway was dependent on the distance between the hallway ceiling and the top of the opening, termed the inlet soffit height. The hallway was 1.47 m high with an inlet soffit height of 0.0 m, and 1.67 m high with a 0.20 m inlet soffit. The hallway was constructed of 3 mm thick, 25.4 mm angle iron frame. The bottom 0.91 m of the hallway walls were constructed of 16.0 mm thick gypsum board lined with 1.5 mm thick Fiberfax ceramic fireproof paper. The upper portion of the hallway was fabricated of 25.4 mm thick Fire Master, UL rated, fire insulation board. Two Vycor glass access windows were placed in the upper portion of the wall at the dead end of the hallway where the compartment was located. The burning of the upper-layer gases within the hallway was observed through these windows.

Experiments were conducted with two types of blockage at the open end of the hallway. The open end, termed the hallway exit, was positioned underneath of the fume

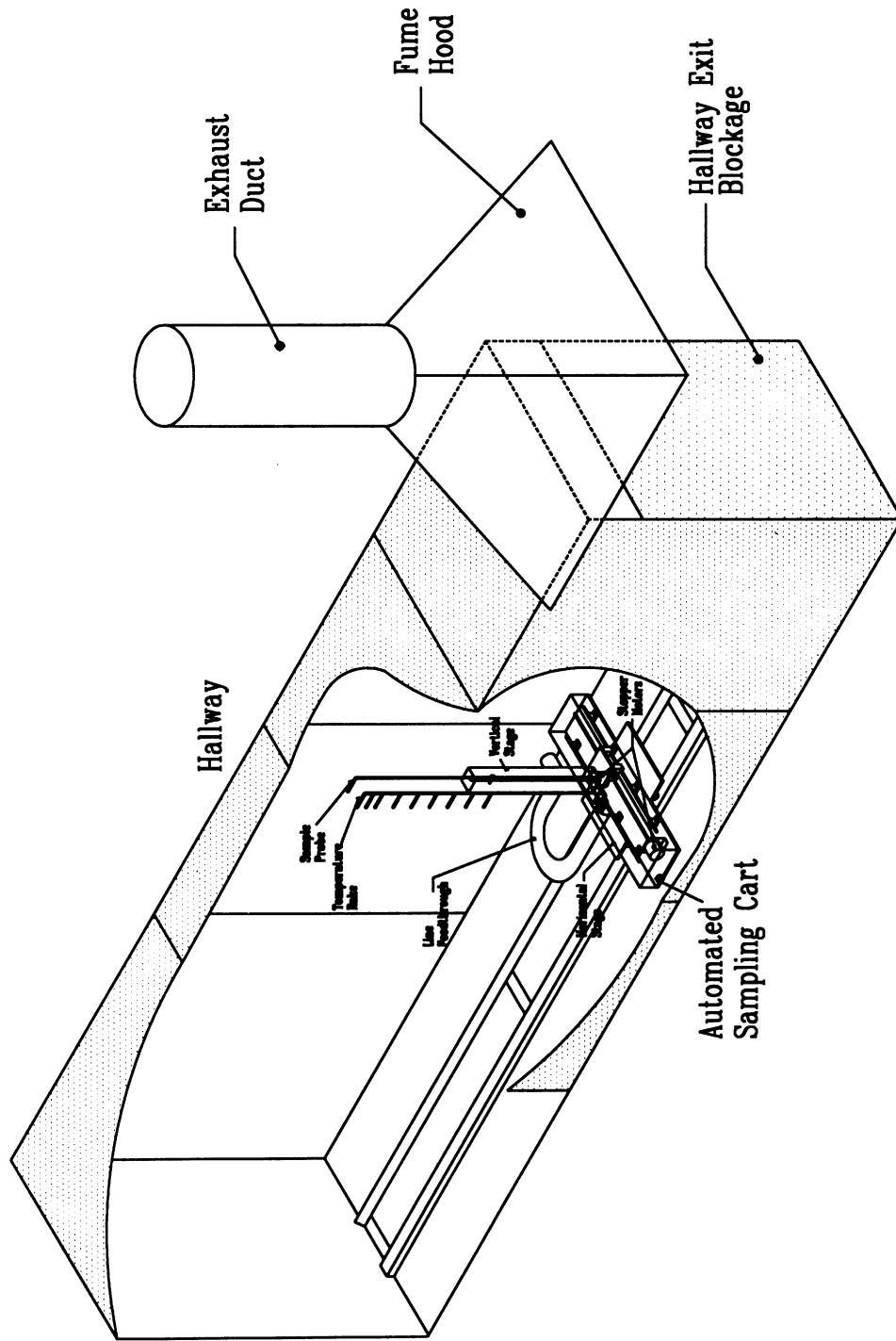


Figure 2.3 A detailed view of the hallway showing the automated sampling cart.

hood. The types of experiments were:

1. upper portion of the hallway blocked, termed an exit soffit, from 0.0 m to 0.80 m (see Fig. 2.1), and
2. bottom portion of the hallway blocked leaving a 1.22 m wide, 0.20 m high opening at the top of the hallway exit (see Fig. 2.3).

The upper portion of the hallway was blocked to control the upper-layer depth inside the hallway. The bottom portion of the hallway was blocked to highly restrict the amount of air entrainment into the hallway.

The automated sampling cart shown in Fig. 2.4 allowed the measurement of gas concentrations and temperature profiles at a variety of locations within the hallway during a single experiment. The cart contained a gas sampling probe, a vertical aspirated temperature rake with 9 type K thermocouples and two traversing assemblies. The cart was manually moved along the length of the hallway on a track. The two traversing assemblies, each consisting of a stepper motor, a lead screw and a driver nut, were used to move the gas sampling probe in either a vertical or horizontal direction via a computer. The vertical range of motion was 0.67 m while the horizontal range of motion is 0.76 m. The thermocouple rake was fixed in the vertical direction, and was only allowed to traverse in the horizontal direction. The wires from the motors, the Teflon tubing line necessary for the aspiration of the thermocouple rake, and the heated Teflon line used to transfer the gases from the hallway to the gas analyzers were all fed out of the hallway through a 0.10 m diameter flexible line feed-through duct.

The schematic of the control system for the 4.8 Amp stepper motors is seen in Fig. 2.5. A 486 DX66 personal computer containing an internal DT 2801-A Data Translation board controlled the movement of sample probe and thermocouple rake. An external DT 707 screw terminal board interfaced the DT 2801 with the two Servo Systems CMD-50

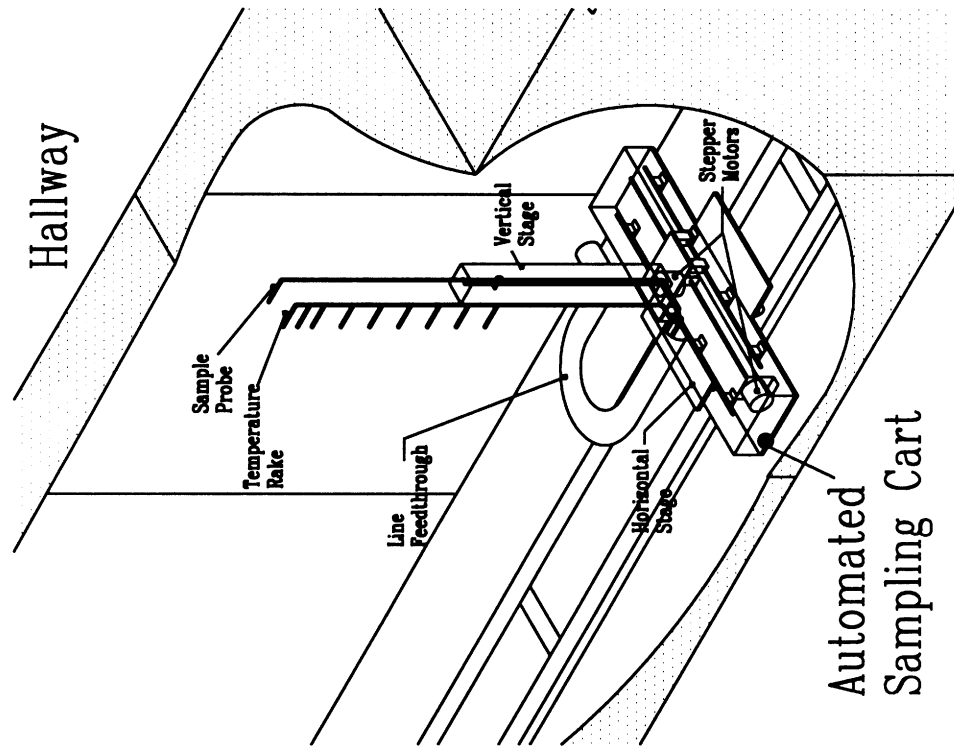


Figure 2.4 The automated sampling cart used to sample at various hallway locations during a single experiment.

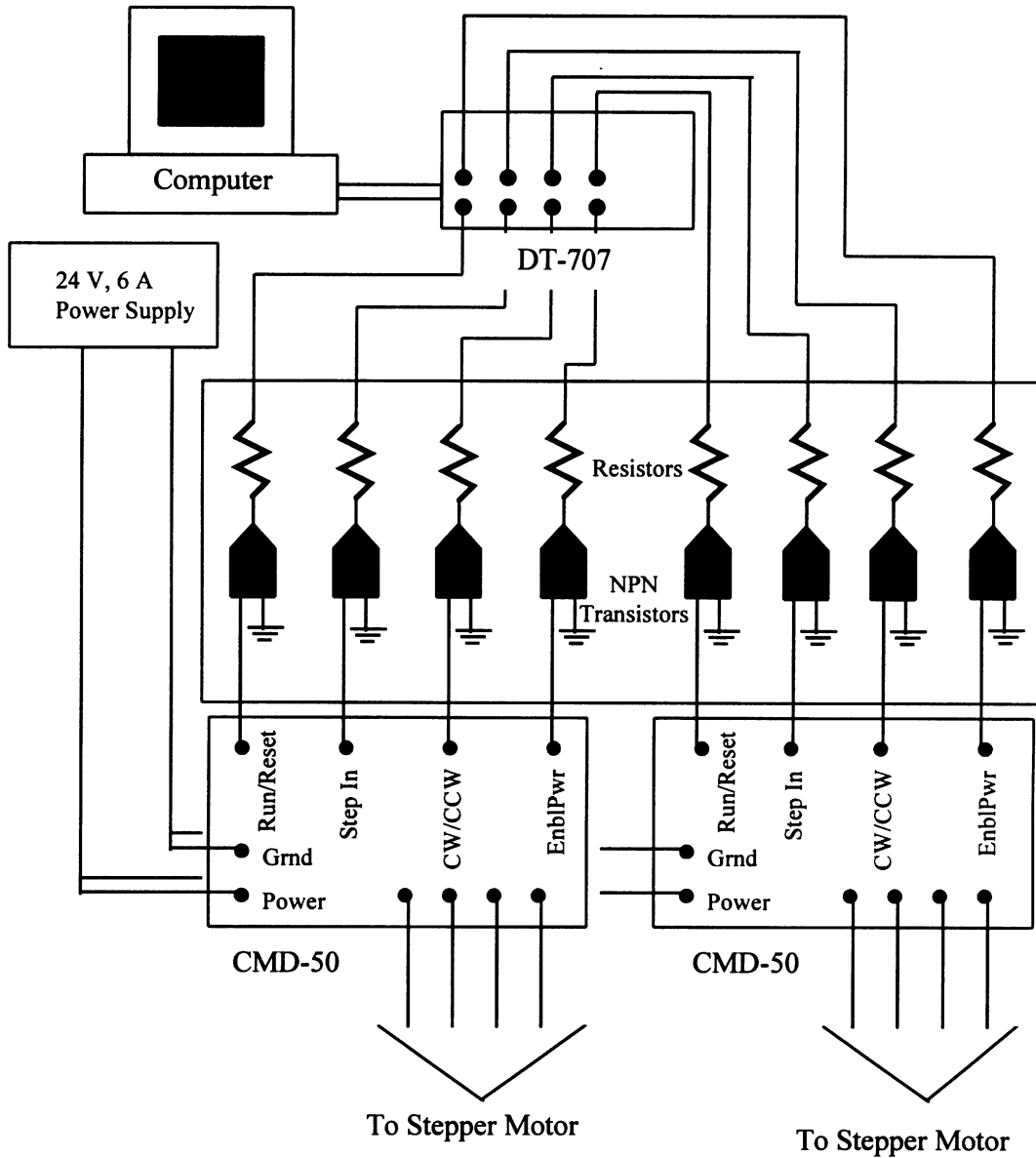


Figure 2.5 A schematic of the electronics involved in computer controlling the motors on the automated sampling cart

controllers, each of which was connected to a stepper motor. A FORTRAN program was written to control the movement of the two stepper motors. The program communicated with the data acquisition board using PCLAB subroutines. The user entered the distance the sample probe should move and the time it should remain at that location into a data file. This enabled the user to map out an entire sampling grid before the beginning experiment. The program can be activated at any time during the experiment.

The gas sampling probe was constructed of 6.35 mm diameter stainless steel tubing which had a 90 degree bend on one end forming an upside down L when mounted to the cart. Further information on the gas sampling system is given in section 2.2.4.

The aspirated temperature rake contained 9 type K thermocouples mounted inside 6.35 mm diameter stainless steel tubing. The top three thermocouples were 0.05 m apart with the top thermocouple 0.05 m below the ceiling to measure the large temperature variations near the ceiling. The remaining thermocouples were 0.10 m apart since more gradual temperature changes were expected this far below the ceiling. The thermocouple beads were recessed approximately 6.0 mm from the end of the aspirating tubes to shield the beads from radiation. To minimize the temperature effects of the aspirator tubes on the gases, the gas velocity in the tubes was greater than 5 m/s. With 5.5 m of 63.5 cm diameter Teflon tubing connecting the rake to the pump, a 1/3 hp rotary pump was used to achieve the desired velocities in the aspirator tubes. A water trap submerged in an ice bath and a Balston 915A, DX grade, glass fiber filter kept water and large particulates from flowing through the pump.

Located approximately 1.0 m outside of the end of the hallway was a video camera which was used to make visual record of each experiment. The camera recorded the experiment from the view point of a person standing at the end of the hallway under the fume hood looking down (upstream fluid mechanically) the hallway.

2.2.3 Fume Hood and Exhaust System

A 1.5 m by 1.5 m fume hood was situated directly over the exit of the hallway to collect the escaping combustion gas. As shown in Fig. 2.6, the hood was connected to a 0.46 m diameter duct, termed the exhaust duct. The duct contained an orifice plate, a probe for downstream gas sampling, and a laser extinction system for the measurement of soot. A 142 m³/min (5000 cfm) blower connected to the exhaust duct draws the combustion gases into the hood.

The 0.3048 m inside diameter, sharp edged orifice plate was designed in accordance with the A.S.T.M. standard for the measurement of the mass flow in a duct (Fluid Meters, 1971). The flow rate of air within the duct was determined by accessing the D and D/2 pressure taps.

Approximately 5 diameters upstream of the orifice plate, a 0.15 m long, 6.35 mm diameter sampling probe was positioned in the exhaust duct, see Fig. 2.6. To obtain a sample of the average concentration of gases flowing within the duct, numerous 3.2 mm holes were drilled along the length of the probe. The transport of the sample gases to the analyzers and the analysis of the sample gases is discussed in section 2.2.4.

A laser extinction system was present 3.7 diameters upstream of the orifice plate. The system consisted of a 5 mW, 670 nm visible red diode laser, an Oriel neutral density filter, an Oriel diffuser and a photodiode. Two 9.0 mm holes were made on opposite sides of the exhaust duct to allow the beam of light to pass through the gases flowing in the duct. After the light passed through the duct, the light was detected by the photodiode. The filter and diffuser were placed in front of the photodiode to generate a sensitive signal in the desired range.

2.2.4 Gas Sampling System

The piping system shown in Fig. 2.7 allowed gases to be drawn from the exhaust duct, the compartment, or the hallway. Gases were sampled from the facility through

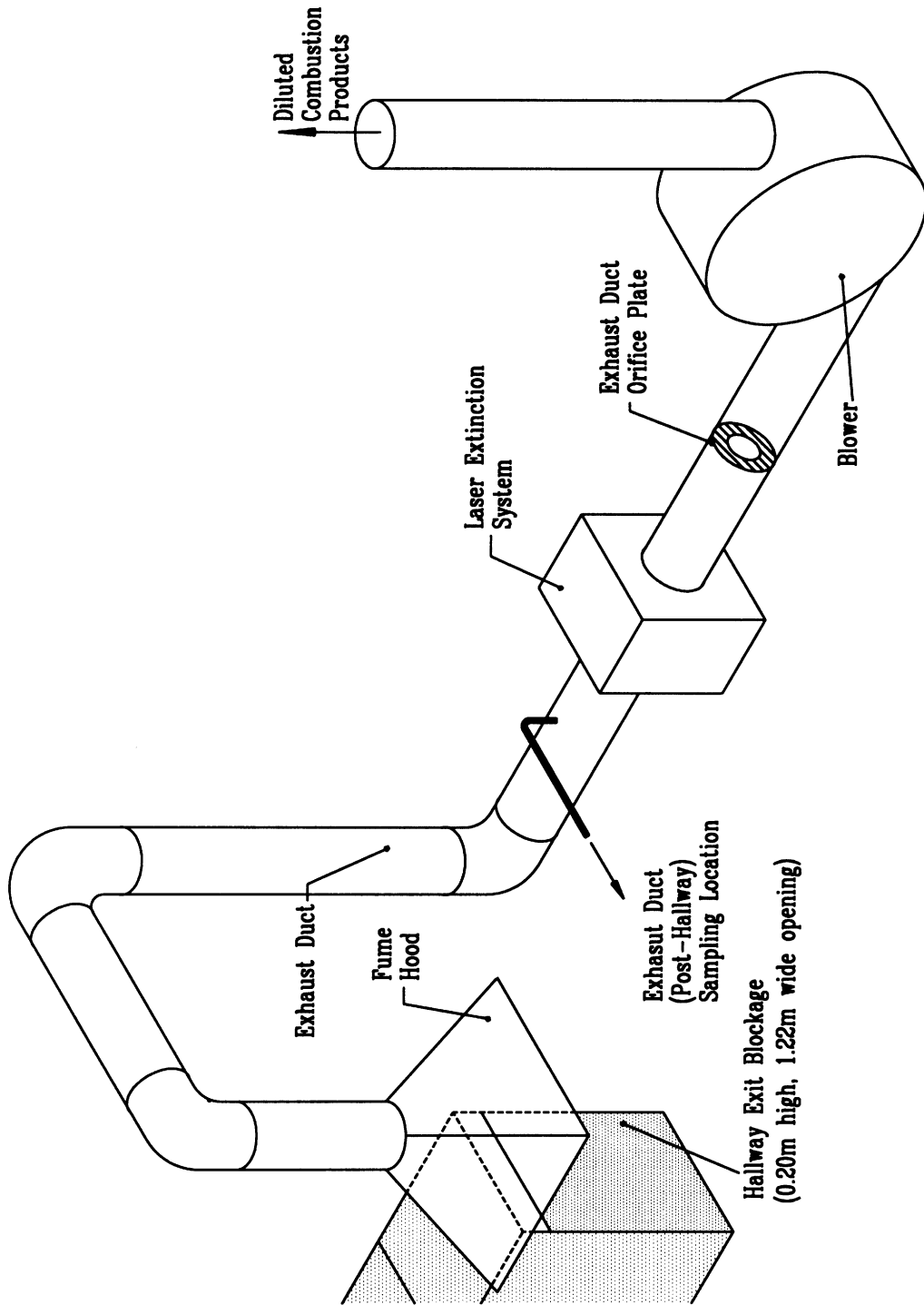


Figure 2.6 The exhaust duct system used to collect the combustion products exiting the hallway.

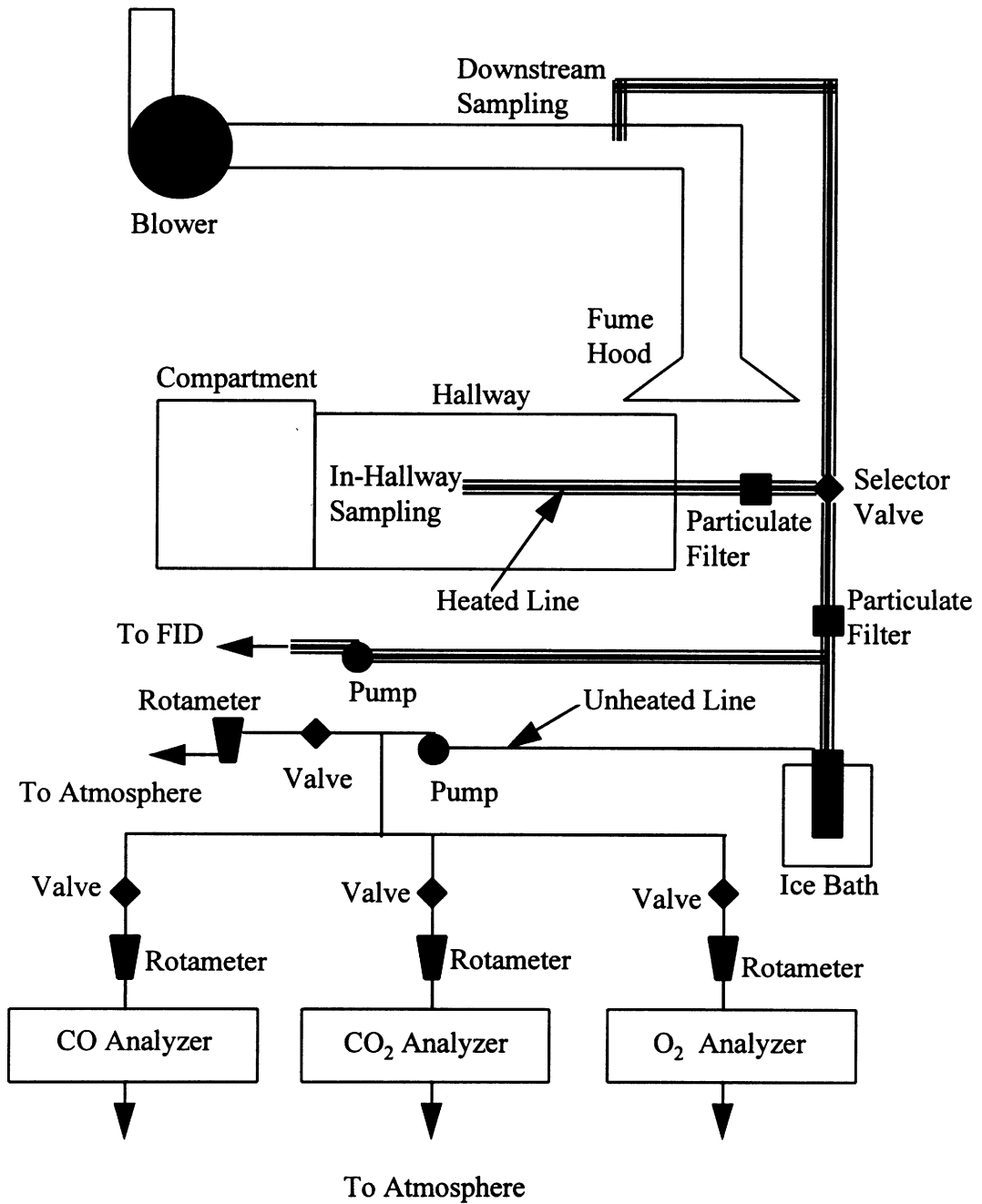


Figure 2.7 A schematic of the piping system used to sample combustion gases from different locations in the facility. Also shown are the CO, CO₂ and O₂ analyzers.

6.35 mm tubing by a suction produced from two Thomas 2107 CA18 diaphragm vacuum pumps. All heated lines and filters were insulated with approximately 10 mm thick fiber glass insulation, and were maintained at approximately 120°C using either Thermolyne electric resistant heating tapes or Hotwatt 360 W single glasrope resistance heaters. Lines were heated to prevent higher order hydrocarbons and water from condensing in the lines.

Gases sampled from the probe in the exhaust duct travel through a heated stainless steel line. A heated Gelman glass fiber filter was used to trap the soot particulates from entering the gas analysis equipment.

When gases were sampled from either the hallway or the upper-layer of the compartment, they were drawn out of the facility through a heated 5.5 m long Teflon line. The flexible Teflon line used allowed the sampling cart to move freely along the length of the hallway. The line was thermally shielded from radiant heat given off by the hallway external burning by placing the line inside of a flexible metal duct. The heavy soot content of the gases sampled from the hallway and compartment required the gases to be filtered twice to ensure the removal of soot particles from the sample. The Teflon line was connected to a heated Balston model #915A filter which contained a DX rated, borosilica glass fiber filter rated for the retention of 93% of particulates larger than 0.1 microns in diameter. The gases then proceeded through a heated stainless steel line which led to a heated Gelman glass fiber filter to retain any soot particulates remaining in the gases.

2.2.5 Gas Analysis

Once the gases had been filtered of soot, they branched off into two directions. A portion of the sampled gases remained wet and was drawn through a heated line by one of the vacuum pumps. The remaining gases were dried by being drawn through a water trap immersed in a Fisher model #910 refrigerated circulating bath held at -10°C. The unburned hydrocarbon (UHC) levels were measured using the wet gases with a flame

ionization detector (FID). The dry gases were passed through two non-dispersive infrared analyzers to measure CO and CO₂ concentrations, and through a paramagnetic analyzer to measure the O₂ concentration.

2.2.5.1 Unburned Hydrocarbon Measurements

The portion of the sampled gases which remained wet was drawn into an oven (maintained at 105°C) to measure the UHC wet concentration within the sample, see Fig. 2.8. Gases remain wet to prevent the loss of higher order hydrocarbons during the water trapping process. The measurement was performed using a model #12-800 Gow-Mac FID connected to a model #40-900 Gow-Mac electrometer for conditioning of the FID signal. The FID contained a hydrogen flame which was produced using a 40% hydrogen, 60% helium mixture as the fuel and purified air as the oxidant. Using Matheson rotameters, 270 cc/min of fuel and 470 cc/min of oxidant were continuously flowing to the FID.

As the sample gases entered the oven, they pass through a Fairchild 0-2 psig pressure regulator, model #10. For an accurate measurement of the sample, the pressure in the line was held at 1.5 psig using a flow meter and a pressure gauge downstream of the oven. The 0-10 SLPM Matheson rotameter controlled the bypass flow rate (typically ranging from 4.5-5.5 SLPM) to maintain a 1.5 psig reading on the Magnehelic 0-6 psig pressure gauge. The bypass flow rate also reduced the delay time of the sampling gas system to approximately 10 seconds. A portion of the gases flowing through the oven were directed through a capillary tube which led to the FID. The capillary tube was designed around the recommended flow rate of 20 to 40 cc/min. The products of the hydrogen flame were vented out of the oven through an opening in the top of the oven. Before the gases were vented to the ambient surroundings, the gases passed through a hydrogen detection system. If the flame was extinguished and high levels of hydrogen begin to be vented to the atmosphere, the hydrogen detector would automatically shut off the flow of

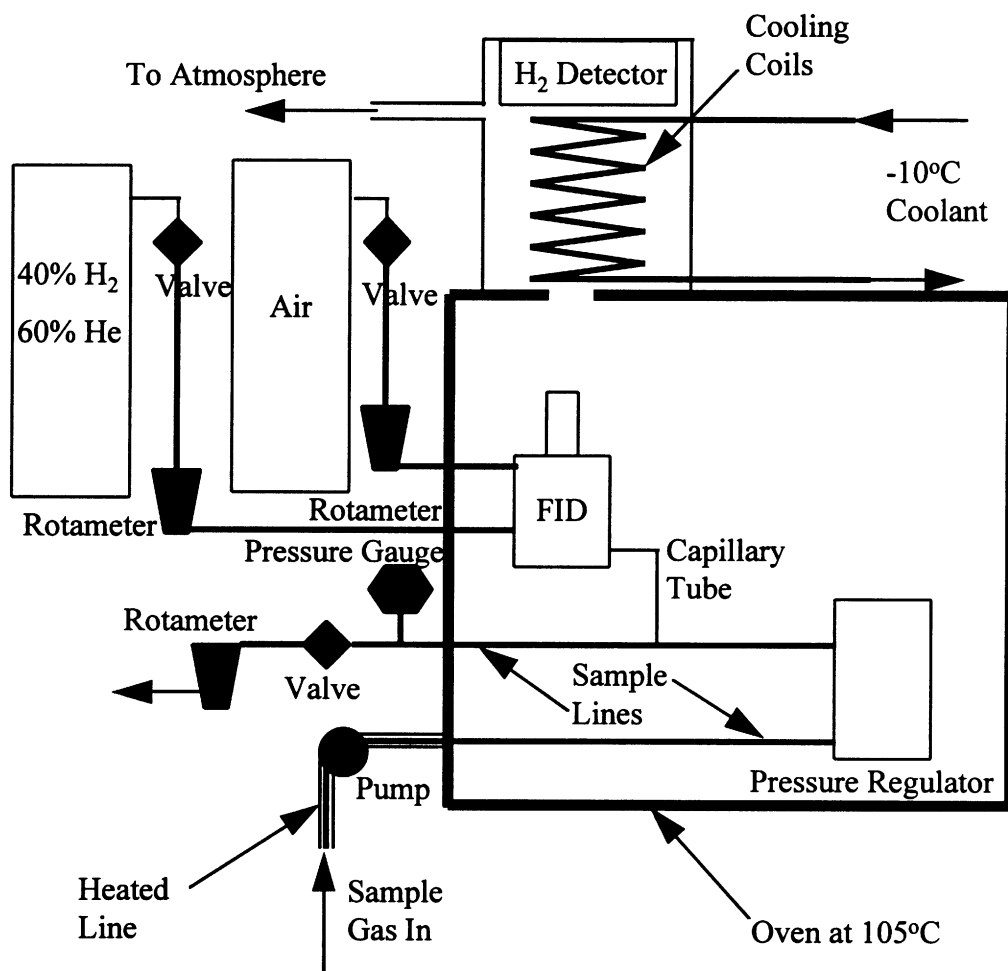


Figure 2.8 A schematic of the equipment and piping in the UHC analysis system.

hydrogen using a solenoid valve. Cooling coils at -10°C prevented the temperature around the hydrogen detector from exceeding the maximum operating condition of 49°C . The coils were cooled using -10°C coolant from a Fisher model #910 refrigerated circulating bath.

The FID signal was conditioned using the electrometer which contained four possible sensitivity ranges; three were commonly used in the experiments. Before the start of each experiment, the FID was calibrated by determining the zero point and the span point for the desired sensitivity range. At each of the ranges, the zero point was determined by passing nitrogen through the FID. The span point for a particular sensitivity range was generated by passing gases containing different concentrations of ethylene (C_2H_4) through the FID. Since the higher order hydrocarbons tend to pyrolyze to ethylene, using ethylene as a calibration gas for the measurement of UHC is a valid assumption (Westbrook and Dryer, 1984). Ethylene concentrations of 4.71%, 5456 ppm, 615 ppm were used to generate span points for each of the three sensitivity points. The lower ethylene concentration of 615 ppm was the range of UHC expected in the exhaust, and was used to calibrate the FID when sampling gases in the exhaust duct. The other two ranges were utilized when sampling gases in the compartment and hallway.

2.2.5.2 CO, CO₂ and O₂ Measurements

The portion of gases which was not drawn to the FID was dried to prevent the cells within the CO, CO₂ and O₂ analyzers from being damaged by condensation. After the gases were dried, they passed through the vacuum pump and were divided again. Part of the gases were directed to the analyzers while the remaining gases were vented to the surroundings (bypass flow). The bypass flow enabled the gases to be drawn into the analyzers at a faster rate allowing for sampling delay times of less than 10 seconds. The flow rate of gases into each of the three instruments was monitored at 1 l/min using 3 separate 0-3.5 SLPM range Matheson rotameters.

The dry CO and CO₂ concentrations were measured using Rosemont Analytical model 880 NDIR analyzers. The 0-5 volt output signal was linearized with respect to the gas concentration using a linearizer contained within the analyzer. The linearizer required a zero point and a span point for calibration of the instrument. The zero point was set by passing pure nitrogen through the analyzers. The span point was determined by passing a calibration gas containing a concentration equivalent to approximately 90% of the upper bound of the desired range. The CO analyzer ranges typically used in the experiments were 1000 ppm, 1% and 10%. The CO₂ analyzer ranges used in the experiments were 5000 ppm, 2%, 15% and 20%. The range was selected such that the concentration of the CO or CO₂ within the sample of the same order of magnitude and never exceeding the upper bound of the range. When sampling diluted exhaust duct gases, the lower concentration ranges (0 to 1000 ppm and 1% for CO and 0 to 5000 ppm and 2% CO₂) were used in the experiments. The higher ranges were used when sampling inside the hallway and compartment.

The dry concentration of O₂ was measured using a Siemens paramagnetic Oxymat 5E analyzer. The output from the instrument was 4-20 mA. This was converted to 1-5 volts using a 250 ohm resistor to enable the signal to be recorded in the computer. The analyzer operated in the 0 to 22% range, since concentrations of O₂ less than levels observed in the ambient surroundings (approximately 21%) were expected. The instrument was calibrated by first determining the zero point, and then setting the span point. Purified nitrogen was passed through the cell to determine the zero point. The span point was set using a gas mixture containing 4.75% O₂. Since the majority of sample gases where accurate O₂ measurements were necessary contained low concentrations of O₂, a low concentration calibration gas was used to calibrate the analyzer.

2.2.6 Data Acquisition

A 386 computer containing various Data Translation data acquisition boards was used to collect the data. The computer was equipped with three internal DT 2801-A digital-to-analog data acquisition boards containing 12-bit resolution. The internal boards were connected to three external boards, one DT 707 screw terminal board and two DT 756-Y amplified boards. The DT 707 was utilized to measure the differential outputs from the UHC, CO, CO₂, and O₂ analyzers, the load cell, the air duct velocity probe and the laser extinction system. One of the DT 756-Y boards was used to process the signals of the thermocouples in the compartment rake, the air inlet duct, the exhaust duct and the opening between the compartment and hallway. The other DT 756-Y board was used to process signals of the thermocouples in the hallway rake. The two DT 756-Y boards were amplified, multiplexing terminal boards containing cold junction compensation for thermocouple measurements. The boards were used to amplify the low voltage signals given by the thermocouples allowing the thermocouple signals to be read directly.

The data acquisition was controlled using a BASIC program. The program accessed PCLAB subroutines to acquire the data from the different measuring devices listed above. Before the acquisition began, the user was required to enter a file name where the computer will store the raw data. The data acquisition was started approximately 30 seconds before the ignition of the fire in the compartment. After the data acquisition program was activated, the program began to store data in the raw data file every 2 seconds. The raw data was determined by averaging the data samples sent to the computer 1 second before and 1 second after the recording time. There were typically 60 ± 2 samples of data which were averaged to generate a single raw data point for each of the 28 signals. The thermocouple signals were converted to degrees Celsius using a PCLAB subroutine and then stored in the raw data file. The data acquisition program was permitted to run 30 seconds after the compartment fire had extinguished to allow the

gases sampled at the end of the experiment to be analyzed. The reduction of the raw data file is described in section 2.3.

2.3 DATA REDUCTION

Once the numerical and visual data were collected, they needed to be reduced to a useful form. The basic data reduction converted the raw data to a useful form, in addition to performing other calculations. After the basic reduction, the temporal data was averaged over one or several time periods. The output from the basic reduction program was also used in other programs to calculate parameters such as the ignition index. Finally, visual data was analyzed in certain cases where external burning was particularly interesting. The remainder of the section describes in detail the basic data reduction, the data averaging, the calculation of the ignition index and the analysis of visual data.

2.3.1 Basic Data Reduction

A FORTRAN program titled *FIRERED3.FOR*, see Appendix B, was written to convert the raw data file into seven data files. Six of the output files contain columns of the temporal data for the calculated and measured values, while the seventh file contains descriptive information about the testing conditions. The treatment of the raw data and the methods used for calculating various parameters are described below.

2.3.1.1 Temperature Data

The temperature data was stored in the raw data file in units of degrees Celsius. The reduction program converted the raw temperature data to Kelvin. The temporal temperature data from the compartment, air inlet duct and exhaust duct were stored in one of the output files, while the hallway temperature data was stored in a separate output file.

2.3.1.2 Species Concentrations

The temporal CO, CO₂, O₂ and UHC concentrations were stored as voltages within the raw data file. The voltages associated with CO, CO₂ and O₂ were converted to dry concentrations by entering the sampling range used for each species during the experiment. The UHC voltages were converted to wet concentrations by entering the sensitivity range of the electrometer (either 1×10^{-9} , 10^{-10} , or 10^{-11} with 10^{-11} being the most sensitive range) used during the experiment and the voltage output of the FID with the span gas flowing through it.

The wet concentrations of CO, CO₂, and O₂ were calculated in the program using the dry concentrations and an assumption about the amount of H₂O within the sample gases. It was assumed that all of the H₂O in the sample gas was produced from the combustion, with a stoichiometric proportion of H₂O and CO₂ being produced. With hexane as the fuel, 6 moles of CO₂ and 7 moles of H₂O are produced when stoichiometric burning occurs. The dry concentration of a species j were converted to the wet concentration of species j , $C_{j,w}$, using the equation

$$C_{j,w} = \left[\frac{X_{j,d}}{1 + \frac{7}{6} X_{CO_2,d}} \right] 100, \quad [\%] \quad (2.1)$$

having knowledge of the dry mole fraction of species j ($X_{j,d}$) and the dry mole fraction of CO₂ ($X_{CO_2,d}$). Equation 2.1 becomes less accurate in very fuel rich environments, global equivalence ratio greater than 3.0.

A lag time exists between the data measured instantaneously (i.e. temperature) and the species concentration measurements. The lag time of the concentration measurements depended on the location of the sampling (hallway, compartment or exhaust duct) and the instrument measuring time. The lag time associated with sampling in the hallway and the compartment was measured to be 8-10 seconds by injecting CO₂ directly into the

sampling probe. Knowing the time in which the CO₂ injection occurred, the lag time was determined by subtracting the time which the CO₂ was sensed by the analyzer from the injection time. The hallway and compartment lag time was the same since the same sampling line was used to sample from these locations.

The lag time of the species concentrations sampled from the exhaust duct was defined slightly differently. When sampling in the exhaust duct, the measured species concentrations were aligned with the time of the fuel mass loss rate which produced the species. The concentrations and fuel vaporization were aligned so that the post-hallway yield calculations were performed accurately. The lag time was estimated by subtracting the ignition time of the fire from the time when CO₂ levels produced by the fire were first measured in the exhaust duct. The ignition time of the fire was estimated as the time in which a jump in the temperature of the top thermocouple in the compartment rake occurred. This lag time was sensitive to the residence time of the gases in the hallway which was governed by the blockage at the end of the hallway. The lag time ranged from 20-22 seconds with no blockage at the end of the hallway to 30-32 seconds with a 0.80 m high exit soffit.

2.3.1.3 Species Yields

In the past, Beyler (1986a,b) and Tewarson (1984) used mass based species yields to quantify the production and consumption of species in an upper-layer fire environment. In general, the mass based species yield,

$$Y_j = \frac{\dot{m}_j}{\dot{m}_{fuel}}, \quad (2.2)$$

is defined as the mass flow rate of species j (\dot{m}_j) divided by the fuel mass loss rate (\dot{m}_{fuel}). Except for O₂, all species yields calculated represented the production of species relative to the fuel mass loss rate. In the case of O₂, the yield represented the consumption of O₂ relative to the fuel mass loss rate. Species yields were calculated when sampling was

performed in the compartment and in the exhaust duct where the mass flow of the gases in and out of the system was well defined.

The species yields in the compartment upper-layer,

$$Y_{j,c} = \frac{X_{j,w} MW_j (\dot{m}_{fuel} + \dot{m}_{air})}{\dot{m}_{fuel} MW_{UL}}, \quad (2.3)$$

were calculated using the wet species concentration of interest, the air entrainment rate into the compartment and the fuel mass loss rate. The molecular weight of the upper-layer gases, MW_{UL} , was assumed to be equivalent to that of air. This assumption is accurate to within $\pm 5\%$.

The post-hallway species yields (the species yield of the gases exiting the hallway),

$$Y_{j,ex} = \frac{X_{j,w} MW_j \dot{n}_{ex}}{\dot{m}_{fuel}}, \quad (2.4)$$

were calculated using measurements of species concentrations in the exhaust duct and with the knowledge of the molar flow rate in the exhaust duct, \dot{n}_{ex} . The molar flow rate through the duct,

$$\dot{n}_{ex} = \dot{Q}_{ex} \left[\frac{(\bar{R}/MW_{air}) T_{ex}}{P_{ex} MW_{air}} \right], \quad [\text{mol/s}] \quad (2.5)$$

was determined by applying the ideal gas law, inserting the measured exhaust duct temperature, T_{ex} , and assuming the recorded ambient pressure, P_a , was equivalent to the exhaust duct pressure, P_{ex} . The general equation to calculate the volumetric flow rate through a duct, \dot{Q}_{ex} ,

$$\dot{Q}_{ex} = 0.52502 \left(\frac{cyd^2 F_a}{\sqrt{1-\beta^4}} \right) \sqrt{\Delta p / \rho'} \quad , \quad [\text{ft}^3/\text{s}] \quad (2.6)$$

was taken from Fluid Meters: Their Theory and Applications (1971). After determining the flow constants (c , γ and F_a) and the ratio between the orifice diameter and the duct diameter, the volumetric flow rate through the duct (in SI units) was calculated from the following equation:

$$\dot{Q}_{ex} = 1.2099 \sqrt{\frac{\Delta p T_{ex}}{P_a}}. \quad [\text{m}^3/\text{s}] \quad (2.7)$$

With the pressure drop across the orifice plate, Δp , measured to be 14.3 mm Hg, the volumetric flow rate through the duct was determined using the temperature of the gases flowing through the exhaust duct, T_{ex} , and the ambient pressure, P_a . Since the exhaust duct gases were highly diluted (approximately 30:1), the assumption of the properties (MW , ρ , and ζ) of the gases flowing through the exhaust duct being equivalent to that of air is well supported.

2.3.1.4 Smoke Extinction Coefficient and Yield

Downstream of the hallway in the exhaust duct, the smoke level was determined with the use of a laser extinction system previously described in section 2.2.3. The reference intensity, I_o , of light was measured by averaging the initial 10 seconds of the photodiode output when no combustion gases were present inside the exhaust duct. The signal produced by the photodiode, I , is proportional to the amount of attenuated laser light which impinged upon it.

The extinction coefficient,

$$\sigma = (1/l_p) \ln(I/I_o), \quad [1/\text{m}] \quad (2.8)$$

is defined as the natural log of the attenuated intensity, I , divided by the reference intensity, I_o , all divided by the optical path length, l_p . The optical path length is the distance between the laser and the photodiode and was taken to be 0.457 m. The mass optical density,

$$D_{mass} = \frac{1}{1000} \left(\frac{\sigma}{2.303} \right) \frac{\dot{Q}_{ex}}{\dot{m}_{fuel}}, \quad [\text{m}^2/\text{g}] \quad (2.9)$$

was calculated using the fuel mass loss rate, \dot{m}_{fuel} , the volumetric flow rate through the duct, \dot{Q}_{ex} , and the extinction coefficient, σ (Tewarson, 1988).

To account for the size of the smoke particles attenuating the laser light passing through the duct, the specific extinction coefficient,

$$\xi = \frac{3.213}{\lambda \rho_{smk}}, \quad [\text{g}/\text{m}^2] \quad (2.10)$$

was estimated using the correlation for overventilated fires. This was used because no correlation for underventilated fires was available (Newman and Steciak, 1987). The wave length of laser beam, λ , was 0.670 μm , while the smoke density, ρ_{smk} , was estimated from experimental data to be 1.1 g/cm^3 (Newman and Steciak, 1987).

Therefore, the smoke yield,

$$Y_{smk} = \frac{D_{mass}}{\xi}, \quad (2.11)$$

was calculated by dividing the optical mass density by the specific extinction coefficient (Tewarson, 1988).

2.3.1.5 Fire Size

The size of the fire was estimated as the ideal heat release of the mass loss rate of fuel. The ideal heat release,

$$Q = \dot{m}_{fuel} \Delta H_c, \quad [\text{kW}] \quad (2.12)$$

was determined by multiplying the mass loss rate of fuel by the lower heating value of the heat of combustion, ΔH_c , of the fuel.

The fuel mass loss rate was determined using the temporal fuel weight data. The fuel weight data was stored in the raw data file as 1-5 volt signal (which corresponded to a 0-10 kg weight), and was converted to units of mass, [kg], using the data reduction program. The temporal derivative of the fuel weight data was used to determine the fuel mass loss rate. The temporal derivative was determined numerically over points ± 10 seconds around the point of interest.

2.3.1.6 Compartment Global Equivalence Ratio

The degree to which the fire inside the compartment was ventilated was defined by the equivalence ratio. The global equivalence ratio, ϕ_g , is defined as the mass of gas in the upper-layer from the fuel divided by the mass of gas in the upper-layer from the air all normalized by the stoichiometric fuel-to-air ratio. The stoichiometric fuel-to-air ratio is defined as the ratio of fuel-to-air which results in only CO_2 and H_2O as products. The plume equivalence ratio,

$$\phi_p = \frac{\left(\frac{\dot{m}_{fuel}}{\dot{m}_{air}} \right)}{\left(\frac{\dot{m}_{fuel}}{\dot{m}_{air}} \right)_{st}}, \quad (2.13)$$

is the fuel mass loss rate divided by the air entrainment into the compartment, again, normalized by the stoichiometric fuel-to-air ratio.

Species production inside the compartment has previously been correlated to the global equivalence ratio, but this parameter is difficult to directly measure with any accuracy. The plume equivalence ratio of the compartment fire was easily calculated using the air entrainment rate into the compartment and the fuel mass loss rate. When the fire was fully developed (during the post-flashover period), a steady-state was reached inside the compartment. During the steady-state period, the fuel and the air entrained into the compartment was all assumed to enter the upper-layer through the plume. The values

of ϕ_p and ϕ_g , therefore, were equivalent to one another during this period. The value of ϕ_g is known during the steady-state time of the fire, and will be referred to herein as simply ϕ .

The air entrainment rate into the compartment was determined by measuring the mean velocity (see section 2.2.1) and temperature of the air flowing through the air inlet duct. The density of the air flowing through the duct was determined using the ideal gas law. The air entrainment into the compartment was, therefore, calculated using the mean velocity, the density of the gases and the cross sectional area of the duct. Refer to the previous section, 2.3.1.5, for details on how the fuel mass loss rate was determined.

2.3.1.7 Residence Times

The residence time is defined as the amount of time a unit volume of gases remains within the area of interest. The residence time inside the compartment,

$$t_{res,c} = \frac{V_{UL}}{\dot{Q}_{air}(T_{UL}/T_{air})}, \quad [s] \quad (2.14)$$

calculates the amount of time a unit volume of air (temperature corrected) remained in the upper-layer of the compartment (which was assumed to be 0.60 m deep) (Gottuk et al., 1992).

2.3.1.8 Compartment Fire Growth and Steady-State

The growth of a compartment fire has previously been defined using a number of measured variables (e.g. upper-layer temperature, fuel mass loss rate, equivalence ratio etc.). Since the growth of the fire is mainly governed by the fuel mass loss rate, the fire growth was defined by Gottuk et al. (1992c) as,

$$G = t_{res,c} \frac{\left(\frac{dm_{fuel}}{dt} \right)}{\dot{m}_{fuel}}, \quad (2.15)$$

the residence time of the gases in the compartment multiplied by temporal change in the fuel mass loss rate divided by the mass loss rate. The parameter G is termed the fire growth parameter. The term multiplying the residence time of the gases in the compartment defines the rate of growth of the fire. When the growth rate of the fire is small compared with the residence time of the compartment gases, G goes to zero and the compartment is considered to be in a steady-state.

A plot of the fire growth parameter with time, Fig. 2.9, shows the four stages of a typical compartment fire. The compartment temperature is often used to characterize fire growth inside a compartment. For comparison purposes, the temperature 0.05 m below the compartment ceiling is also shown in Fig. 2.9 with the fire growth parameter since. After the fire was ignited, a gradual growth of the fire (termed the pre-flashover period) was observed to occur within the compartment. As the fire became oxygen deficient ($\phi > 1$) and the fire growth parameter reached a maximum, flashover occurred inside the compartment. Flashover is defined as the point at which the entire upper-layer in the compartment ignites. After flashover, the fire growth parameter is near zero. The fire was considered to be in a steady-state (termed the post-flashover period). The fire enters the decay period of its life when it had depleted almost all of the fuel in the compartment. Extinguishment occurred when all of the fuel in the compartment had been depleted.

2.3.2 Temporal Averaging of Data

Two types of data averaging were performed, with the type of averaging depending on the sampling location. When gases were sampled in the exhaust duct, data was averaged over a single window of time which encompassed a large portion of the post-flashover period. Data was averaged over several windows of time when gases were sampled from the compartment and hallway. Details are given below for the procedures of both types of averaging.

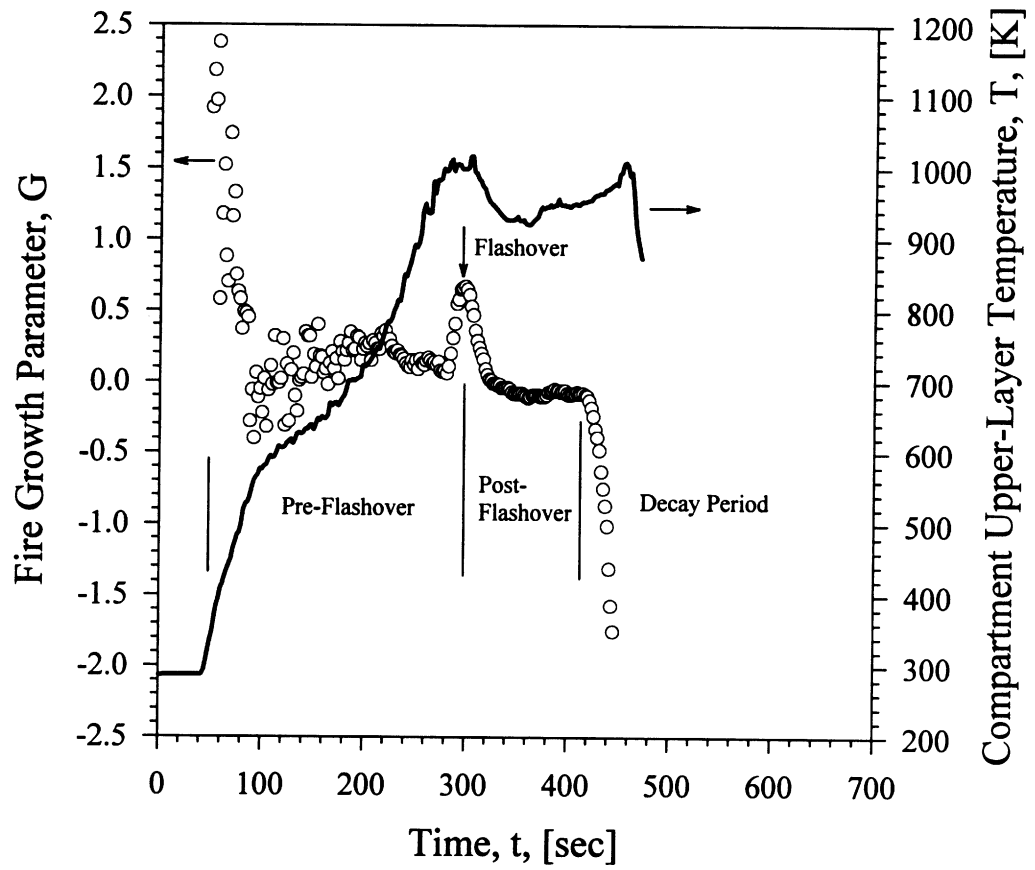


Figure 2.9 The utilization of the fire growth parameter(○) and the compartment upper-layer temperature (—) to describe the different stages of growth occurring during a compartment fire.

2.3.2.1 Averaging over a Single Window of Time

Post-hallway sampling was performed in the exhaust duct to determine the overall oxidation of the gases in the hallway. Since the highest levels of CO were formed in the post-flashover period of the fire (typically 140 seconds in length), the averaging was performed during this period of the fire. The species levels were quite uniform over the majority of the post-flashover period, thus averaging was performed near the middle of the period. If external burning occurred in the hallway during the post-flashover period, the data was averaged during this time window. The averaging window of time was typically 60 seconds in length. The data was averaged during a window of time where the fire growth parameter was approximately zero. The FORTRAN program *FIREAVG3.FOR*, see Appendix B, was used to average the data.

2.3.2.2 Averaging over Several Windows of Time

Sampling was performed in the compartment and the hallway to investigate the evolution of the gases within the facility. To study this transient phenomenon, the data was averaged over 4 second time periods before and after flashover.

Since sampling was performed at one location during an experiment, 25 separate experiments were performed to map the species concentrations in the hallway and compartment. To view the distribution of the gas concentrations within the hallway and compartment at a certain point in the fire, all of the experiments had to be temporally aligned with one another. Unfortunately, the time of ignition was not a good reference because the growth time of the fire to flashover was variable. The steady state time of each experiment, estimated as the time at which the fire growth parameter goes to zero, was instead used to align the experiments with one another.

A FORTRAN program was used to perform the multiple window averaging. Each of the output files produced from the program contained data from a single averaging window for all of the experiments of interest.

2.3.3 Ignition Index

From a fire safety point of view, it is important to be able to predict the ignition of gases in the hallway. A relationship based on classical empirical relations for lean flammability limits, termed the ignition index, was derived by Beyler (1984) to predict the occurrence of ignition of an upper-layer inside a compartment. The ignition index,

$$I. I. = \sum_j \frac{X_j \Delta H_{c,j}}{\int_{T_0}^{T_{SL,j}} n_{prod} C_p dT} \geq 1.0 \quad (2.16)$$

where,

j - fuel species of interest (CO, UHC and H₂ are considered)

X_j - wet mole fraction of the species j

$\Delta H_{c,j}$ - heat of combustion of the species j , [kJ/g-mol] (1411 kJ/g-mol for C₂H₄, 238 kJ/g-mol for CO, and 242 kJ/g-mol for H₂)

$T_{SL,j}$ - adiabatic flame temperature of the stoichiometric mixture for fuel species j at the lower flammability limit, [K] (1700 K for UHC, 1450 K for CO and 1080 K for H₂)

T_0 - temperature of the stoichiometric mixture of fuel species prior to reaction, [K]

n_{prod} - number of g-moles of products of complete combustion per g-mole of reactants (fuel species mixture)

$C_{p,j}$ - average heat capacity of products of complete combustion, [kJ/g-mol K],

was calculated using a FORTRAN program, and was used in this study to attempt to predict the occurrence of external burning in the hallway. The adiabatic flame temperature for a stoichiometric mixture at the lower flammability limit is approximately 100 K higher than the adiabatic flame temperature at the lower flammability limit. Note that the mixture at the lower limit is stoichiometric. The emphasis on having a stoichiometric mixture is that the ignition of a diffusion flame will locally occur where the mixture is at approximately stoichiometric conditions.

The ignition index is the ratio of the potential energy of the gases divided by the energy necessary for ignition of the gases. Once the potential energy is greater than the energy necessary for ignition, *II* rises above unity and ignition is expected to occur. This is of course assuming that some source of ignition, a pilot, is present.

The ignition index was calculated for gases sampled from the center of the opening connecting the compartment and the hallway. A few assumptions were applied in order to determine the *II*. The initial temperature of the reactants, T_O in Eqn. (2.16), was assumed to be equivalent to the average temperature of the top three thermocouples in the compartment upper-layer. The UHC were assumed to only consist of ethylene (C_2H_4). As previously mentioned, wet concentrations of the species were based on the fact that CO_2 and H_2O are present in stoichiometric proportions. Finally, the concentration of H_2 had to be estimated. In hood experiments performed by Beyler (1983) with liquid hexane, the concentration ratio of H_2 to CO varied from 0.26 to 0.67. Gottuk (1992) determined that a ratio of H_2 to CO of 0.5 yielded ignition index results which were $\pm 10\%$ of the expected value of *II*. The ratio of H_2 and CO equal to 0.5 was also utilized in this study.

The thermodynamic data was taken from several sources. The values of C_p for the products of complete combustion was found in Van Wylen and Sonntag (1986), while the values of ΔH_c were obtained from Beyler (1984) and Drysdale (1985). The adiabatic flame temperatures of a stoichiometric mixture at the lower flammability limit, T_{SLj} , were also obtained from Beyler (1984).

2.3.4 Video Record of Experiments

Each experiment was recorded using a VHS video camera which was located at the end of the hallway where the effluent enters the fume hood. Video taping provided a permanent record of each experiment, and allowed the opportunity to observe experiments again to document the occurrence of important events during the test.

The external burning in the hallway was one of the most important visual observations in the experiments. Video records of the experiments were viewed before data averaging was conducted to verify the occurrence(s) of external burning in the hallway. Accurately determining the times when the external burning begins and ends in the hallway was also important when attempting to predict the ignition of gases in the hallway, and verifying trends in the measured gas concentrations.

Video record of the experiments also played an integral role in visualizing the flow of gases in the hallway. Since laboratory techniques for measuring the flow field in the hallway were not practical for the reported experiments, the flame emissions in the hallway (external burning) were used to reveal how the gases were transported away from the compartment and down the hallway. The path of the combustion gases was most easily visualized when the most significant burning occurred in the hallway. This occurred when the gases exiting the compartment encountered concentrations of oxygen near those measured in the ambient surroundings (i.e. experiments with an exit soffit of 0.10 m or less).

2.4 TYPES OF EXPERIMENTS

The remainder of this chapter is dedicated to discussing the different types of experiments performed to measure the transport of CO away from a compartment on the side of a hallway. Initially, the goals of the experimental execution are explicitly defined. The experiments conducted to accomplish these goals are then described.

2.4.1 Experimental Goals

There were two main goals in the study. The first goal was to quantify the conditions where high concentrations of CO will be transported to locations downstream of the compartment where gas temperatures have decreased to levels where CO becomes

non-reactive, termed remote locations. The controlling factor in the transport of high levels of CO to remote locations was hypothesized to be the air entrainment into the plume of combustion gases exiting the compartment. Secondly, the study investigated the evolution of CO within a hallway when the burning compartment was located on the side. The evolution of CO in the hallway was hypothesized to be a function of the time necessary for the hallway gas concentrations to reach a steady-state, the occurrence of external burning in the hallway and possibly the type of fuel in the compartment.

2.4.2 General Experimental Procedure

Prior to the ignition of the compartment fire, several procedures were conducted to ensure the accuracy of the acquired data and to limit the number of experimental variables.

To be confident that the data acquired was accurate, the gas analyzers were calibrated for the desired range before each experiment. The load cell was calibrated at the beginning of the day of experimentation. After every 5 experiments, sampling lines and aspirated thermocouple lines were cleared of soot which had collected on the walls of the lines by blowing high pressure air through the lines.

The variations in the initial gas temperature in the compartment and hallway have previously been noted to have effects on CO formation and oxidation. For this reason, all experiments were conducted with a compartment temperature of 20-30°C, and a hallway temperature of 15-25°C. Wall temperatures also have an effect on the heat losses to the surroundings. To ensure approximately the same losses, the facility was allowed to cool (for 45 to 75 minutes depending on the ambient temperature) until the air temperatures within the facility were within the ranges state above. Lastly, the initial weight of the fuel inside the compartment was kept as constant as possible.

2.4.3 Fuel Samples

Three types of fuels were used in the investigation, liquid hexane, polyurethane foam, and Douglas fir plywood,. The majority of the experiments being conducted using liquid hexane. The composition of each fuel in addition to some of the fuel properties are shown in Table 2.1. The type of fuel was chosen based on the existence of experimental compartment data, and the levels of combustion gases produced by the compartment fire.

A number of experimental studies have utilized liquid hexane, C_6H_{14} , as a fuel since its composition is well characterized. Experiments performed by Beyler (1983) and Gottuk (1992a) were used as a basis for the species production in liquid *n*-hexane compartment fires. Liquid *n*-hexane was also used in the study by Ewens (1994a) where the oxidation of combustion gases down a hallway. To expand on this data base of information, liquid *n*-hexane was used in the majority of the experiments in this study. The liquid *n*-hexane was burned in 0.064 m deep steel fuel pans which were 0.15 m to 0.28 m in diameter. The pans were completely filled with liquid *n*-hexane just prior to the ignition of the fuel.

To validate that the experimental results were not fuel specific, polyurethane foam was also burned inside the compartment. The polyurethane foam had a density of 44.1 kg/m³ and an elemental composition of $CH_{1.74}O_{0.323}N_{0.70}$ (“Special Reference”, 1976). An elemental analysis performed by Galbraith Labs confirmed these results (Gottuk, 1992a). The foam contained a filler which accounted for 45% of the weight. After the

Table 2.1 The composition and some properties of the fuels utilized in the study.

Fuel	Volatiles Composition	(F/A) _{st} (by mass)	Heat of Combustion (LHV), ΔH_c , [kJ/kg]
Liquid <i>n</i> -Hexane	C_6H_{14}	0.0658	44,735
Polyurethane Foam	$CH_{1.74}O_{0.323}N_{0.698}$ *	0.113	26,570
Douglas fir Plywood	$CH_{2.506}O_{1.071}$ **	0.211	26,657

* Not including nonvolatile filler

** Assuming 15% char

foam compartment fire had extinguished, the filler remained as a powder and solid crust. A 0.457 m square, 0.30 m thick slab of polyurethane foam was burned in a stainless steel pan in the center of the compartment. Ignition of the foam block was instigated by placing two lit wooden matches on top of the block.

In a number of liquid hexane experiments, Douglas fir plywood was hung 0.05 m below the ceiling of the compartment to investigate the effects of an oxygen containing fuel in the upper-layer on species formation in the compartment upper-layer. Three 0.30 m wide, 0.91 m long 0.654 cm thick sections of Douglas Fir plywood were suspended below the ceiling so the mass loss rate of the plywood could be measured. The elemental composition of the plywood was determined to be $\text{CH}_{2.506}\text{O}_{1.071}$ (assuming 15% of the wood mass formed char) from an elemental analysis performed by Galbraith Labs. These experimental results are presented in Appendix C.

2.4.5 Estimation of Compartment Fire Gas Jet Air Entrainment

The oxygen entrainment into the compartment fire gas jet issuing into the hallway was hypothesized as the parameter which primarily governed the degree of CO oxidation. Overventilated compartment fires ($\phi < 1$) were performed to quantify the air entrainment into the compartment fire gases for different opening sizes (0.12, 0.08 and 0.04 m²) and for cases with no inlet soffit and with a 0.20 m inlet soffit. The automated cart was utilized in these experiments to generate species concentration profiles of the combustion gas layer present in the hallway during the steady-state time of the compartment fire. The entrainment was determined by the increase in O₂ concentration within the gases as they flowed away from the compartment.

2.4.5 Study of Conditions Necessary for the Transport of High CO Levels

Controlled experiments were conducted to determine the conditions under which high levels of CO were transported to remote locations. To quantify the overall effect of

each experimental variable on CO, CO₂ and UHC levels, gas sampling was performed in the exhaust duct.

The air entrainment into the combustion gases exiting the compartment was hypothesized as the primary variable in determining the yield of CO transported. The air entrainment was experimentally varied by changing:

1. the height of the inlet soffit,
2. the opening size, and
3. the depth of the upper-layer in the hallway.

The majority of the experiments were performed with a 0.20 m soffit, but some experiments were performed with no inlet soffit for comparison purposes. Opening sizes of 0.12 m², 0.08 m² and 0.04 m² were utilized in the study to vary the size of the jet entering the hallway. The depth of the low oxygen containing upper-layer in the hallway was experimentally controlled by the exit soffit height which was varied from 0.0 to 0.80 m in 0.10 m increments.

In addition to the air entrainment parameters, the investigation also included the effects of the compartment global equivalence ratio, the absence or presence of external burning and the type of fuel on the species levels transported downstream.

When a door connects the compartment and the hallway (instead of a window), air enters the compartment through the lower portion of the door and combustion gases exit the compartment through the upper portion. The fluid mechanics at the compartment and hallway interface are different than those in the case with a window containing unidirectional flow. The effects of having a 0.50 m wide, 0.75 m high door connecting the compartment and hallway on the species production inside of the compartment, the oxidation of gases in the hallway and the transport of gases to remote locations is discussed in Appendix C.

2.4.6 Study of Species Concentration Evolution within the Facility

The species evolution in the hallway was investigated under conditions where high post-hallway yields of CO (the yield of CO exiting the hallway) have been measured. The effects of the occurrence or absence external burning, the time necessary for hallway gas concentrations to reach a steady-state, and the fuel type in the compartment on the species levels in the hallway were investigated. The evolution of the species in these cases was measured by performing 25 different experiments at a variety of locations within the hallway and compartment, see Fig. 2.10. All samples were taken 0.05 m below the ceiling of the hallway and compartment except for the sample location at the opening (location b). At location b, the sampling was performed in the center of the opening, approximately 0.33 m below the ceiling. The sampling locations are shown on each plot of the species variation in the facility.

The upper-layer height in the hallway was observed to have an effect on the occurrence or absence of external burning in the hallway. Liquid *n*-hexane pool fire experiments were conducted with a 0.60 m exit soffit to study this effect.

The effect of the time necessary for the species concentrations in the hallway to reach a steady-state on the species evolution was investigated by varying the conditions at the hallway exit. In experiments with the bottom portion of the hallway exit blocked, nearly the entire post-flashover period (of the compartment fire) was necessary for the gas concentrations to reach a steady-state in the hallway. These experiments were termed as having a long transient time. Experiments containing exit soffit heights of 0.60 m resulted in the hallway gas concentrations reaching a steady-state approximately 50-60 seconds after flashover. These experiments were termed as having a short transient time experiments.

The effect of the compartment fire fuel on the evolution of species in the hallway was investigated by comparing liquid *n*-hexane fire experiments with polyurethane foam

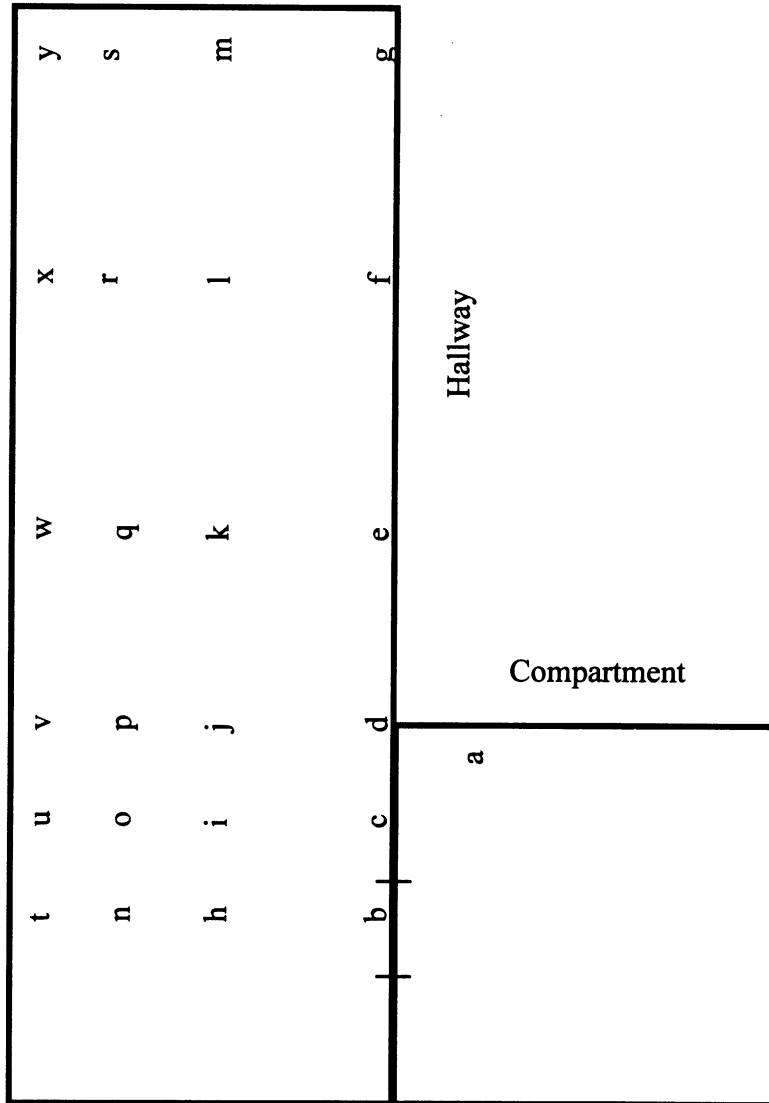


Figure 2.10 Sample locations within the facility for *n*-hexane compartment fires.

fire experimental results. A coarse mapping of the hallway was performed in the polyurethane foam experiments, see Fig. 2.11. The mapping was designed to capture the non-uniform concentration of CO across the hallway which was seen to exist in the *n*-hexane experiments.

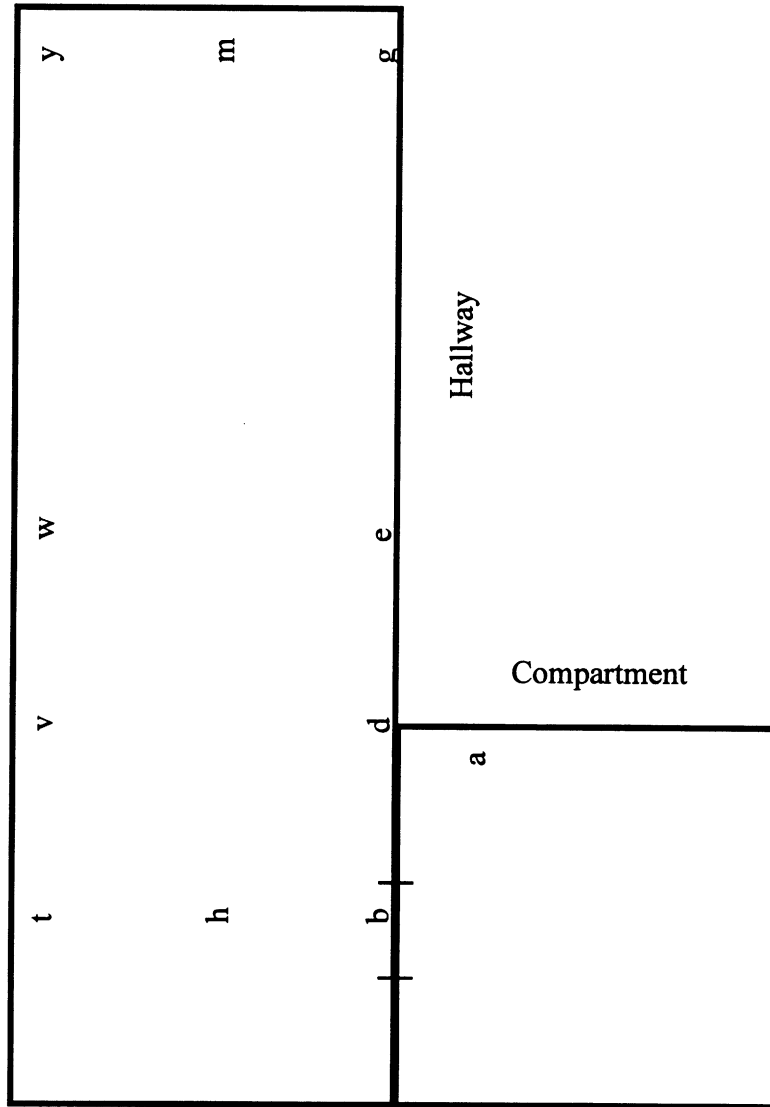


Figure 2.11 Sample locations within the facility for polyurethane foam compartment fires.

CHAPTER 3.

RESULTS: TRANSPORT OF CHEMICAL SPECIES TO REMOTE LOCATIONS

3.1 INTRODUCTION

The oxygen entrainment into compartment fire gases entering the hallway was hypothesized in section 1.3 as being the parameter which controls the level of species, particularly CO, transported to remote locations. Overventilated *n*-hexane compartment fire experiments were performed to measure air entrainment into the gases entering the hallway. The entrainment was measured for different opening sizes and different soffit heights above the opening. Underventilated fire tests were performed to measure the effect the experimental variables which alter the air entrainment on the post-hallway yield levels. The results of a parametric study quantifying the effects of the opening size, soffit height and upper-layer depth on the post-hallway CO, UHC, and CO₂ yields are presented. The effect of varying the compartment global equivalence ratio is also given.

3.2 AIR ENTRAINMENT INTO COMPARTMENT FIRE EXHAUST GASES

Oxygen entrainment is hypothesized as being the most significant parameter which determines the species levels transported to remote locations. Mullholland et al. (1991), Morehart et al. (1991), and Morehart et al. (1992) investigated limited air entrainment into compartment fire plumes, but the effects of oxygen entrainment into gases exiting the compartment has been addressed in only one study (Ewens, 1994a). In this section, a simplified model for determining the air entrainment into a non-reacting jet of combustion gases entering the hallway is derived from the conservation of mass. The

model is then applied to data produced from overventilated compartment fires to quantify the effects of different window and soffit sizes on the air entrainment into the jet.

3.2.1 Background on Air Entrainment into Ceiling Jets and Plumes

Air entrainment into a jet of gases is defined here, after Ellison and Turner (1959), in terms of the entrainment function,

$$E = \frac{\bar{V}_e}{\bar{V}_i}, \quad (3.1)$$

which is defined as the ratio of the average velocity of entrained gas \bar{V}_e with the average velocity of the jet, \bar{V}_i (Ellison and Turner, 1959). Air entrainment into ceiling jets and plumes is a function of the distance the gases have traveled from the source, the viscous effects between the jet gases and the surrounding gases (the Reynolds number), and the gravitational effects (the Richardson number).

In experiments with turbulent, unheated jets, Bakke (1957) and Poreh (1967) determined that the value of the entrainment function to be nearly independent of the distance traveled and the Reynolds number,

$$Re = \frac{\rho_i D_h \bar{V}_i}{\mu_i} \quad (3.2)$$

making the entrainment mainly a function of the Richardson number,

$$Ri = \frac{g D_h (\rho_e - \rho_i)}{\bar{V}_i^2 \rho_e} \quad (3.3a)$$

where

$$D_h = \frac{4 A_{open}}{P_{wet}}. \quad (3.3b)$$

These findings were supported by the salt water floor jet experiments performed by Ellison and Turner (1959). As a result of their work, Ellison and Turner (1959) determined that,

$$E = 0.075 \exp(-3.9 Ri), \quad (3.4)$$

the entrainment function decayed exponentially in magnitude with an increase in Richardson number.

3.2.2 Air Entrainment Model for Compartment Fire Exhaust Gases

To estimate the air entrainment into a non-reacting jet of compartment fire gases, a simplified model was derived using a control volume analysis. Shown in Fig. 3.1 is a control volume (CV) drawn around a portion of upper-layer gases in the hallway.

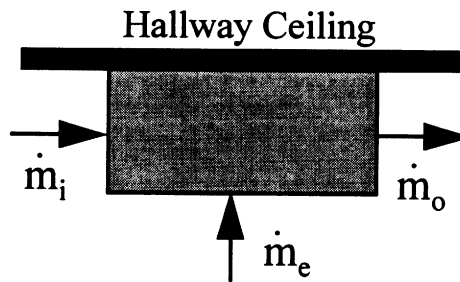


Figure 3.1 The simplified control volume analysis of the hallway upper-layer gases.

Assuming one-dimensional flow, the gases flowing into the CV, \dot{m}_i , are less diluted than those flowing out of the CV, \dot{m}_o , due to the entrainment of air, \dot{m}_e .

Applying the conservation of mass to this CV yields

$$\dot{m}_i + \dot{m}_e = \dot{m}_o. \quad (3.5)$$

Since the molecular weight of all the gases considered is nearly that of air, 28.84 kg/kmol, the above relation can be transformed to molar flow rate form;

$$\dot{n}_i + \dot{n}_e = \dot{n}_o. \quad (3.6)$$

Performing a similar analysis for the flow of O_2 within the system, the following relation is produced

$$\dot{n}_{i,O_2} + \dot{n}_{e,O_2} = \dot{n}_{o,O_2} \quad (3.7)$$

If equation (3.7) is divided by \dot{n}_o and equation (3.6) is applied, then

$$\frac{\dot{n}_{i,O_2}}{\dot{n}_i + \dot{n}_e} + \frac{\dot{n}_{e,O_2}}{\dot{n}_i + \dot{n}_e} = \frac{\dot{n}_{o,O_2}}{\dot{n}_o} \quad (3.8)$$

Dividing the top and the bottom of the first term on the left hand side by \dot{n}_i and dividing the top and the bottom of the second term on the left hand side by \dot{n}_e , equation (3.8) is transformed to

$$\frac{X_{i,O_2}}{1 + (\dot{n}_e/\dot{n}_i)} + \frac{X_{e,O_2}}{1 + (\dot{n}_i/\dot{n}_e)} = X_{o,O_2}, \quad (3.9)$$

where X denotes the oxygen volume fraction at the location denoted by the subscript. Through some algebra, a quadratic equation in terms of \dot{n}_e ,

$$\frac{(X_{e,O_2} - X_{o,O_2})}{\dot{n}_i^2} \dot{n}_e^2 + \frac{(X_{i,O_2} + X_{e,O_2} - 2X_{o,O_2})}{\dot{n}_i} \dot{n}_e + (X_{i,O_2} - X_{o,O_2}) = 0 \quad (3.10)$$

is formed. With the restriction of $\dot{n}_e > 0$, the quadratic formula yields

$$\dot{n}_e = \frac{-b + \sqrt{b^2 - 4ac}}{2a} \quad (3.11)$$

where;

$$a = \frac{(X_{e,O_2} - X_{o,O_2})}{\dot{n}_i^2}$$

$$b = \frac{(X_{i,O_2} + X_{e,O_2} - 2X_{o,O_2})}{\dot{n}_i}$$

$$c = (X_{i,O_2} - X_{o,O_2}).$$

The mass flow of the air entrainment into the CV,

$$\dot{m}_e = MW_{air}\dot{n}_e \quad (3.12)$$

is determined by multiplying by the molecular weight of air, MW_{air} .

In summary, to determine the air entrainment mass flow rate into a non-reacting jet of gases between two points, the following must be known:

- molar flow rate of gases into the CV,
- volume fraction of O₂ flowing into CV
- volume fraction of O₂ entrained into CV, and
- volume fraction of O₂ flowing out of CV.

Since the mass flow rate out of the compartment was known, the molar flow rate into the control volume was estimated by dividing the mass flow rate by the molecular weight of the gases (assumed to be that of air). By measuring the concentration of the gases exiting the compartment and at some location downstream of the compartment, the air entrainment which has occurred between these two points can be determined assuming that the O₂ concentration in the gases being entrained is known.

3.2.3 Air Entrainment into Ceiling Jets

A ceiling jet is defined as hot gases flowing along the ceiling of the hallway. The compartment fire gases entered the hallway as a ceiling jet when no inlet soffit was present. These tests are termed ceiling jet experiments. The air entrainment into overventilated compartment fire gases entering the hallway as a ceiling jet was estimated for three different window sizes, 0.12, 0.08 and 0.04 m². A 0.10 m diameter fuel pan filled with liquid *n*-hexane was utilized in the experiments to produce global equivalence ratios ranging from $\phi=0.1-0.4$. Experiments were performed with no exit soffit or blockage at the exit of the hallway.

Since the species concentrations in the upper-layer were not constant with height, species concentration profiles at a particular location in the hallway were experimentally determined by moving the sampling probe during the steady-state time of the fire. The sampling probe was moved from 0.05 m below the ceiling to 0.30 m below the ceiling in 0.05 m increments. With the steady-state lasting approximately 300 seconds in these experiments, the probe remained at each location for 20 seconds before being moved down another 0.05 m. In the underventilated fire experiments, the majority of species oxidation was measured to occur as the combustion gases exit the compartment and move across the hallway. The measurement of species profiles at the opening and 0.60 m across the hallway was, therefore, deemed sufficient for quantifying the difference in the entrainment between the three opening sizes.

To apply Eqn. (3.11), the volume fraction of O_2 at each location must be known. An integrated average of the measured O_2 profile was used as the volume fraction of O_2 in the upper-layer at each sampling location. Air was assumed to be entrained into the upper-layer gases, so X_{e,O_2} was assumed to be 0.21. Note that the entraining gases may not always contain 21% O_2 (i.e. when deep upper-layers are accumulated in the hallway). This is an important point to be considered when determining the oxygen entrainment into the compartment fire exhaust gas jet. This is addressed in Chapter 5 when correlations to predict CO and UHC post-hallway yields are developed based on the oxygen entrainment.

Since the mass flow rate of the gases exiting the compartment was known, an oxygen profile was measured at the opening where the compartment fire gases entered the hallway. The other O_2 profile was measured at a location 0.60 m downstream of the compartment opening. The mass flow rate of gases entering the hallway was converted to molar flow rate by dividing by the molecular weight of the gases (assumed to be equivalent to air).

Table 3.1 The experimental conditions in the overventilated fire experiments used to determine the air entrainment into the ceiling jet.

Opening Area, m ²	Opening Height, m	Opening Width, m	Mass Flow through Opening, kg/s	Velocity of Gases at Opening, m/s	Upper-Layer Gas Density (as air), kg/m ³	Entrained Gas Density (as air), kg/m ³
0.12	0.24	0.50	0.0630	0.74	0.7105	0.8905
0.08	0.16	0.50	0.0533	0.94	0.7105	0.8905
0.04	0.16	0.25	0.0366	1.29	0.7105	0.8905

Table 3.2 The air entrainment into the ceiling jet using the overventilated compartment fire experimental results.

Opening Area, m ²	Oxygen In, mole fraction	Oxygen Out, mole fraction	Mass Flow Air Entrained, kg/s	Velocity of Entrained Air, m/s	Richardson Number, Ri	Entrainment Function, E
0.12	0.185	0.187	0.0063	0.012	1.78	0.016
0.08	0.173	0.181	0.0135	0.031	0.88	0.033
0.04	0.143	0.168	0.0213	0.070	0.34	0.054

The conditions and the results of the analysis are tabulated in Table 3.1 and Table 3.2, respectively. To compare the air entrainment results with those of Ellison and Turner (1959), the entrainment function, see Eqn. (3.1), must be determined for each case. The average velocity entering the hallway, \bar{V}_i , was determined by dividing the mass flow of gases through the opening by the density (taken to be the density of air at the gas temperature) and the opening area. An average entrainment velocity,

$$\bar{V}_e = \frac{\dot{m}_e}{\rho_e A_{wet}}, \quad (3.13)$$

was determined by dividing the mass flow of entrainment by the density of the entrained air (density of air at the gas temperature below the upper-layer) and the wetted area of the jet. The wetted area of the jet,

$$A_{wet} = l(2h + w), \quad (3.14)$$

was defined as the product of the length, l , between the two sampling points (0.60 m) and twice the height, h , plus the width, w , of the opening. For the ceiling jet experiments, the Richardson number,

$$Ri = \frac{4\rho_i^2 g A_{open}^3 (\rho_e - \rho_i)}{\dot{m}_i^2 (2h + w) \rho_e}, \quad (3.15a)$$

where;

$$D_h = \frac{4 A_{open}}{(2h + w)} \quad (3.15b)$$

was determined using the conditions at the opening.

The air entrainment function is observed in Fig. 3.2 to exponentially decrease with respect to the Richardson Number, and is represented by the curve:

$$E = 0.07 \exp(-1.1 Ri) + 0.006. \quad (3.16)$$

The variation of the entrainment function with the Richardson number is similar to that found by Ellison and Turner (1959), see Eqn. (3.4), in their salt-water experiments, but is slightly shifted upward. The upward shift in the value of E is attributed to both not considering the expansion of the ceiling-jet as it entrains air and the wall effects. Not accounting for the jet expansion results in a smaller surface area, A_{wet} , over which the gases are entrained into the jet. This results in a calculation of a higher average entrainment velocity, see Eqn. (3.13). The wall effects were noted by Ellison and Turner (1959) to induce further entrainment into the jet by forcing mixing near the wall. The model does, however, provide a reasonable estimation of the air entrainment into the compartment fire gases.

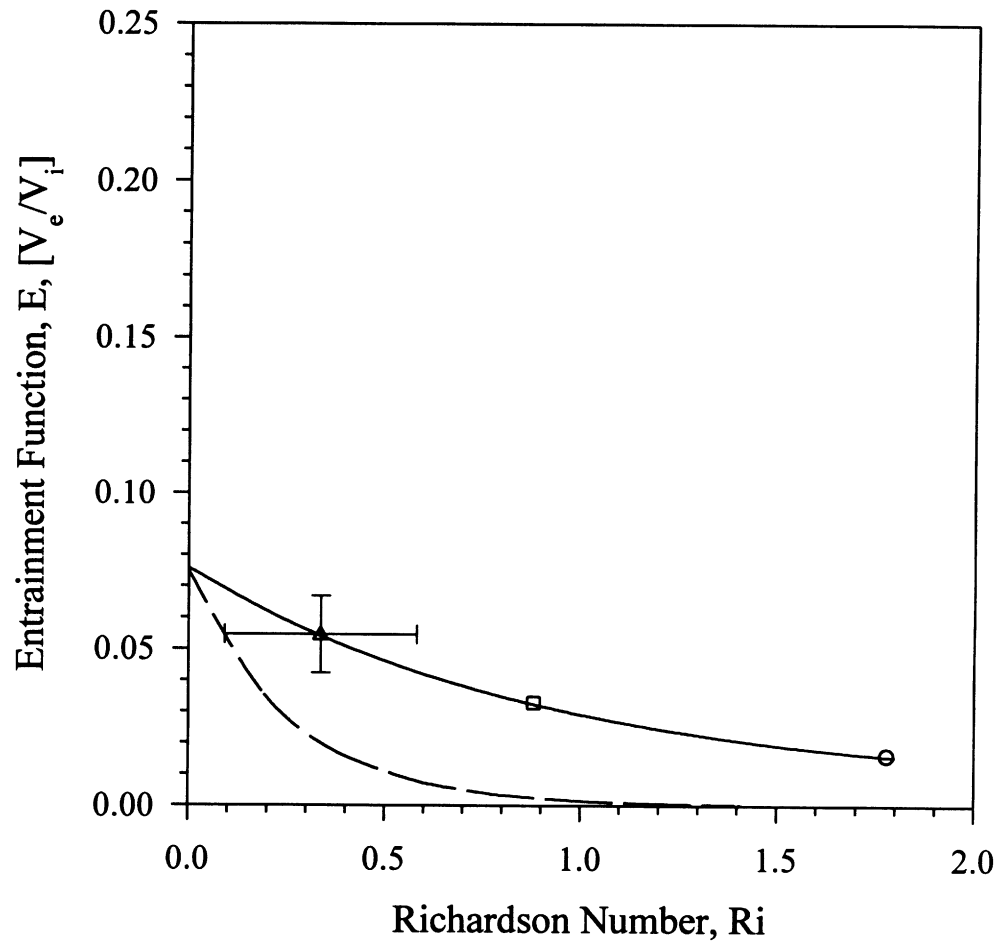


Figure 3.2 The entrainment into a ceiling jet produced from an overventilated compartment fire. The data is from experiments having opening sizes of ○-0.12 m², □-0.08 m², and Δ-0.04 m² with the solid line being the curve fit to the data. The dashed line is the ceiling jet curve from Ellison and Turner (1959).

The effect of the opening size on the mass flow of air entrainment is also seen in Fig. 3.2. As the opening size was decreased, the air entrainment was measured to increase.

3.2.4 Air Entrainment into Plumes

A plume is defined as a jet of hot gases which are permitted to rise vertically due to buoyancy. In experiments with a 0.20 m soffit, the gases exiting the compartment were allowed to rise 0.20 m until they impinged upon the ceiling approximately 0.30 m downstream of the opening. After ceiling impingement, the gases traveled across the hallway as a ceiling jet. Air entrainment into plumes has been noted by Ellison and Turner (1959), Alpert (1972, 1980) and Hinkely et al. (1984) to be considerably larger than that observed in ceiling jets. The turning region, where the jet impinges on the ceiling, was noted as having the next highest entrainment rate, while the ceiling jet had the least efficient air entrainment. The air entrainment into the fire gases as they flowed across the hallway first as a plume and then a ceiling jet is quantified in this section.

Overventilated compartment fire experiments were performed with a 0.15 m diameter fuel pan and no orifice on the air inlet duct. The three different opening sizes (0.12, 0.08 and 0.04) used in the ceiling jet study were also used in these experiments. To capture the three regions of the flow (the plume, the turning region and the ceiling jet) present as the gases moved across the hallway, species concentration profiles were measured at the opening (0.0 m), 0.15 m, 0.30 m, 0.45 m, 0.60 m and 0.90 m across the hallway. The profiles were produced by varying the sampling location from 0.05 m to at least 0.35 m below the ceiling in 0.05 m increments (remaining at each location for 20 seconds) during the steady-state time of the experiment. The molar flow rate into the initial control volume, \dot{n}_i , was determined from the mass flow of gases out of the compartment with each subsequent control volume using the value of \dot{n}_o for its value of \dot{n}_i .

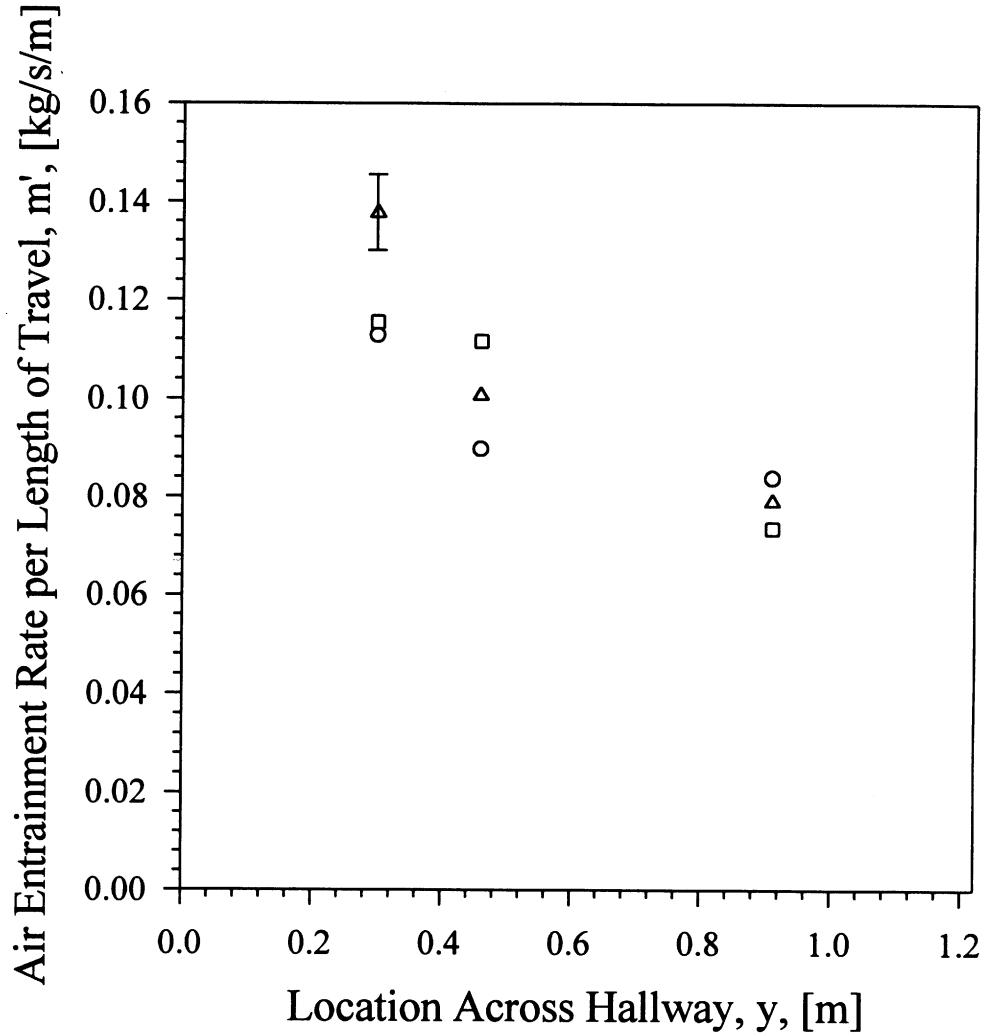


Figure 3.3 The mass flow rate of air entrainment into the overventilated compartment fire gases in experiments with a 0.20 m inlet soffit where the plume, the turning region and the ceiling jet were present in the initial 0.60 m of travel. Experiments utilized \circ -0.12 m², \square -0.08 m², and Δ -0.04 m² opening sizes.

Table 3.3 The experimental conditions in the overventilated fire experiments with a 0.20 m inlet soffit where the air entrainment into compartment fire gases in the initial 0.60 m of the hallway is determined.

Opening Area, m ²	Opening Height, m	Opening Width, m	Mass Flow through Opening, kg/s	Velocity of Gases at Opening, m/s	Upper-Layer Gas Density (as air), kg/m ³	Entrained Gas Density (as air), kg/m ³
0.12	0.24	0.50	0.0731	0.86	0.7105	0.8905
0.08	0.16	0.50	0.0613	1.08	0.7105	0.8905
0.04	0.16	0.25	0.0379	1.33	0.7105	0.8905

Table 3.4. Using overventilated compartment fire experimental results with a 0.20 m inlet soffit, the calculated air entrainment into the compartment fire gases in the initial 0.60 m where the plume, the area of impingement and the ceiling jet are all present.

Opening Area, m ²	Oxygen In, mole fraction	Oxygen Out, mole fraction	Mass Flow Air Entrained, kg/s	Velocity of Entrained Air, m/s	Richardson Number, Ri	Entrainment Function, E
0.12	0.179	0.192	0.052	0.08	0.87	0.093
0.08	0.175	0.193	0.060	0.10	0.41	0.097
0.04	0.149	0.190	0.074	0.20	0.22	0.15

For all three opening sizes, the air entrainment is seen in Fig. 3.3 to be the most significant in the first 0.30 m of the hallway where the plume was present. As noted in previous experiments performed by Hinkely, et al. (1984), less significant was measured to occur in the impingement area ($0.30 < y < 0.45$ m) and in the area of the ceiling jet ($0.45 < y < 0.90$ m), see Fig. 3.3. Also, the entrainment into the compartment fire gases was measured to increase as the area of the opening was decreased.

The entrainment function for the first 0.60 m of the hallway was calculated, see Table 3.3 and 3.4, so quantities could be compared with the ceiling jet data. Assuming the plume impinges on the ceiling 0.3 m across the hallway, the wetted area of the jet is

$$A_{wet} = 0.3(4h + 3w). \quad (3.17)$$

The Richardson number of the gases entering the hallway was defined as

$$Ri = \frac{4\rho_i^2 g A_{open}^3 (\rho_e - \rho_i)}{\dot{m}_i^2 (2h + 2w) \rho_e} \quad (3.18a)$$

where;

$$D_h = \frac{4 A_{open}}{(2h + 2w)}. \quad (3.18b)$$

Utilizing the new definitions for the wetted area and the Richardson number, the entrainment function was calculated to be significantly higher than that measured in the ceiling jet experiments, see Fig. 3.4 and Table 3.4. The entrainment function

$$E = 0.14 \exp(-4.0 Ri) + 0.084 \quad (3.19)$$

still, however, decreases exponentially with an increase in the Richardson number. As before, the entrainment functions for the 0.12 m² and the 0.08 m² openings are shown in Fig. 3.4 to be nearly equivalent, but the magnitude of E has risen to 0.10. The presence of a 0.04 m² opening resulted in a 50% increase in the entrainment function to a value of 0.15.

3.2.5 Additional Parameters Affecting Air Entrainment

Average velocities were used in the air entrainment model since the measurement of the flow field was not possible. It should be mentioned that combustion instabilities and higher gas temperatures play a role in the actual air entrainment into compartment fire gases in experiments where the compartment fire is underventilated. The air entrainment model only considers a one-dimensional flow field, thus decreasing the accuracy of the model in areas where two and three-dimensional flow field effects

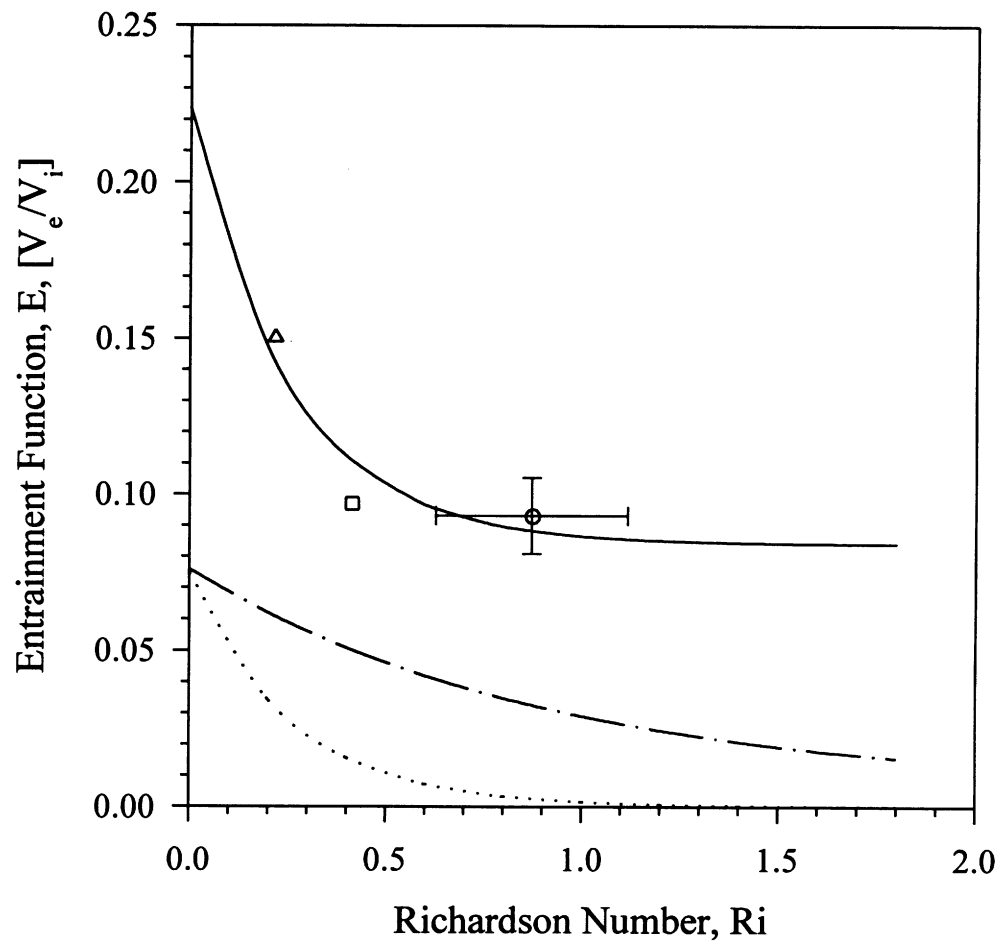


Figure 3.4 The air entrainment function for the overventilated compartment fire gases in the first 0.60 m of the hallway in experiments with a 0.20 m inlet soffit where both a plume and a ceiling jet are present. The data is from experiments having opening sizes of \circ -0.12 m², \square -0.08 m², and \triangle -0.04 m² with the solid being the curve fit to this data. The dash-dot line is the ceiling jet curve from this study while the dotted line is the ceiling jet curve from Ellison and Turner (1959).

are significant. For this reason, the measurement of the entrainment was confined to regions close to the compartment where wall effects on the flow field were not as significant. These experiments, however, do provide a basis for comparing the effects of different opening sizes and the presence of a 0.20 m inlet soffit on the air entrainment.

3.3 EFFECT OF ENTRAINMENT ON POST-HALLWAY SPECIES YIELDS

The oxygen entrainment into the compartment fire gases entering the hallway was experimentally altered in a number of ways:

- changing the opening size,
- changing the size of the fire,
- changing the air inlet orifice diameter,
- changing the inlet soffit height, and
- changing the exit soffit height (or exit blockage).

The first three experimental variables changed the entrainment into the compartment fire gases by altering the velocity of the gases entering the hallway, \bar{V}_i . The inlet soffit height at the opening determined whether the gases entered the hallway as a ceiling jet or as a plume. The inlet soffit, therefore, governed the entrainment into the compartment fire gases at the entrance of the hallway where the highest temperatures were present and chemical kinetics rates were fastest. The height of the exit soffit determined the O₂ concentration of the gases being entrained into the compartment fire products by defining the depth of the oxygen deficient combustion gas layer in the hallway. The effects of each of these variables on the post-hallway species yields (the yields of the species in the gases exiting the hallway) is discussed in the following sections.

3.3.1 Effect of Opening Size

Opening sizes of 0.12, 0.08 and 0.04 m² were utilized in the study to alter the air entrainment into the compartment fire gases entering the hallway. As seen in Fig. 3.2 and Fig. 3.4, a decrease in the opening size results in an increase in the entrainment. The oxidation of incomplete compartment fire products entering the hallway is dependent on the amount of oxygen available. A decrease in the opening size is, therefore, expected to result in lower post-hallway yields of CO and UHC (with the four remaining effects mentioned in the beginning of the section held relatively constant). It should be noted that the reduction in the yield is related to the oxygen entrainment which occurred in the region of the hallway where temperatures were high enough (>850 K for CO and 800 K for UHC) for oxidation to occur. After this point, gases were merely diluted by the process of entrainment since the chemical kinetics were frozen.

As stated in section 1.2.2., Ewens (1994a) investigated the oxidation of compartment fire gases down a hallway with near ambient levels of oxygen being entrained into the compartment fire gas jet entering the hallway. Reevaluating the data taken by Ewens (1994b), the effects of the opening size on the post-hallway species yields are shown in Fig. 3.5. As anticipated from the air entrainment results seen in Fig. 3.4, the CO and UHC yields are seen in Fig. 3.5 to decrease in magnitude with a decrease in the opening size. The increase in the oxidation of CO and UHC is also observed in Fig. 3.5 by an increase in the CO₂ yield. It should be noted that these trends become invalid when the compartment fire gas jet entering the hallway is entraining gases containing oxygen levels significantly lower than those observed in the ambient surroundings. This topic is addressed specifically in section 3.3.3.

3.3.2 Effects of Air Inlet Orifice Diameter and Fire Size

The size of the fire and the diameter of the orifice attached to the air inlet duct also control the mass flow rate of the compartment fire gases entering the hallway. As

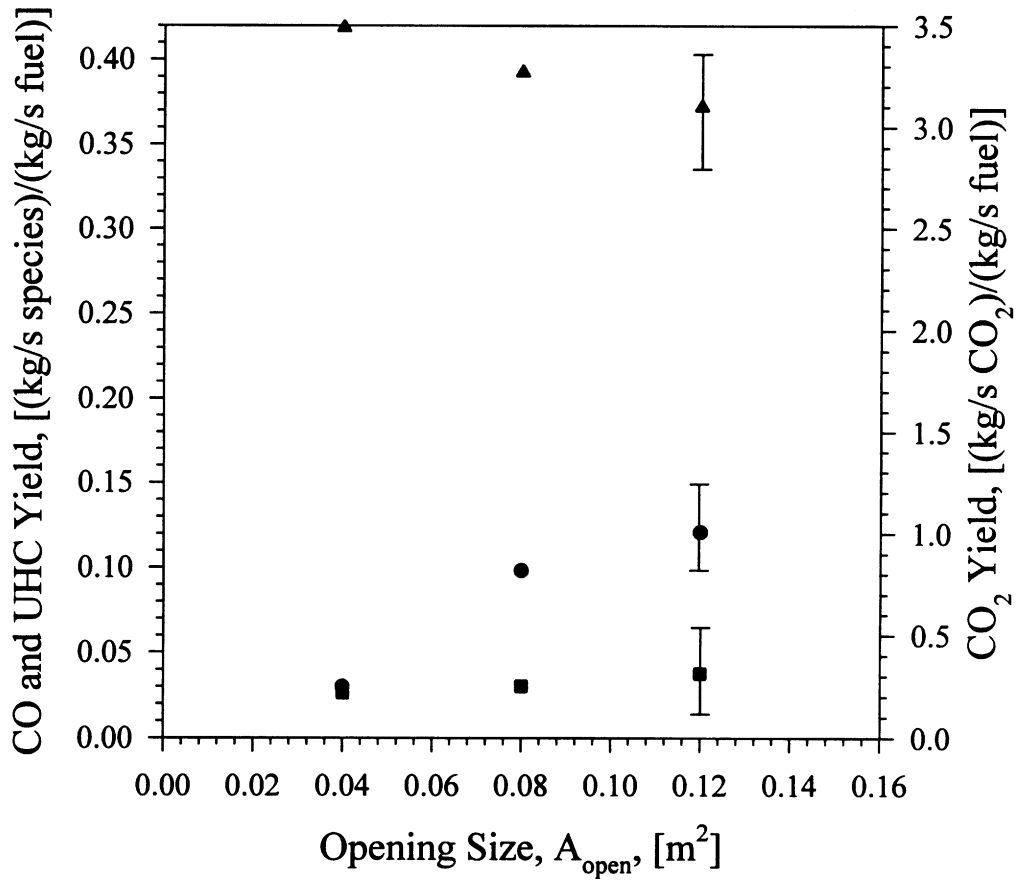


Figure 3.5 The effect of the opening size on the post-hallway ●-CO, ■-UHC and ▲-CO₂ yields for the cases with $Q=448\pm 154$ kW, $\phi=2.57\pm 0.06$, a 0.20 m inlet soffit, and no exit soffit. Experimental data of Ewens (1994b).

mentioned in section 2.2.1, the size of the fire is controlled by the diameter of the fuel pan. The larger fuel pan diameters resulted in a larger fire size. The air mass flow rate into the compartment was controlled by the diameter of the orifice placed on the end of the air inlet duct. A decrease in the orifice diameter resulted in a decrease in the air mass flow rate. These two experimental variables, pan diameter and orifice diameter, were used in the study to control the compartment GER and the mass flow rate of the gases entering the hallway through a particular opening size.

With the diameter of the fuel pan controlling the fuel mass loss rate and the orifice diameter controlling the air mass flow rate, the compartment GER was affected by altering these two parameters. A decrease in the orifice diameter reduced the air mass flow rate into the compartment causing an increase in the compartment GER for a given fire size. The decrease in the orifice diameter resulted in a deeper upper-layer within the compartment. The compartment upper-layer temperature fell by 125 K when the orifice diameter was decreased from 0.30 m (no orifice) to 0.10 m, see Fig. 3.6. The temperature drop was attributed to less complete combustion of the volatilized fuel. With the fuel volatilization rate dependent on the radiation incident upon the exposed fuel surface, the drop in upper-layer temperature could drastically affect the mass loss rate of fuel. The fuel mass loss rate, however, is shown in Fig. 3.7 to remain relatively unchanged with a decrease in orifice diameter. The decrease in the incident radiation from the fall in the upper-layer temperature was obviously compensated by a decrease in the distance between the upper-layer and the fuel surface (an increase in the upper-layer depth). For a particular fire size, the compartment GER could, therefore, be increased by decreasing the diameter of the orifice connected to the air inlet duct.

The effects of fire size on the post-hallway species yields with no orifice attached to the air inlet duct (0.30 m diameter) were determined through further analysis of the data of Ewens (1994b). An increase in the fire size resulted in an increase in the mass flow of air drawn into the compartment. This resulted in an increase in the mass flow rate of

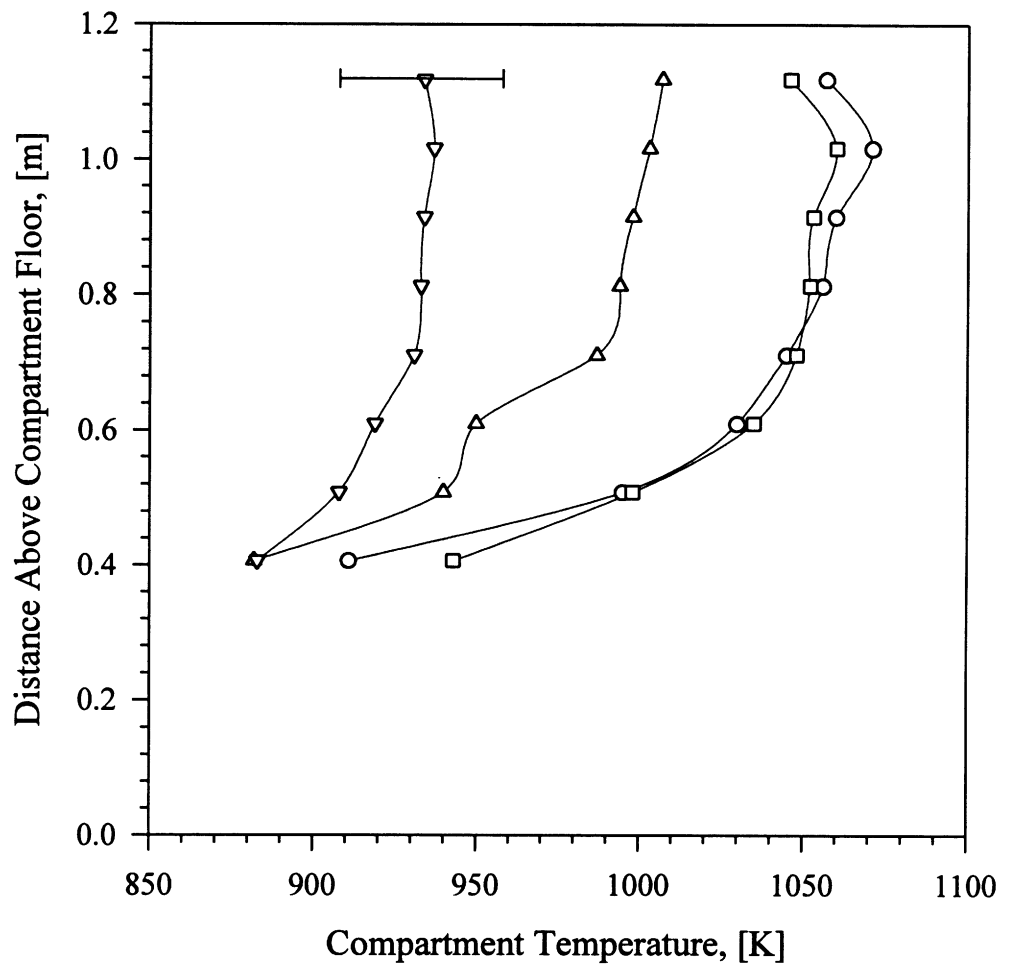


Figure 3.6 The variation in the compartment upper-layer temperature profile with inlet orifice diameter of \circ -0.30m (no orifice), \square -0.25 m, Δ -0.20, and ∇ -0.15 m

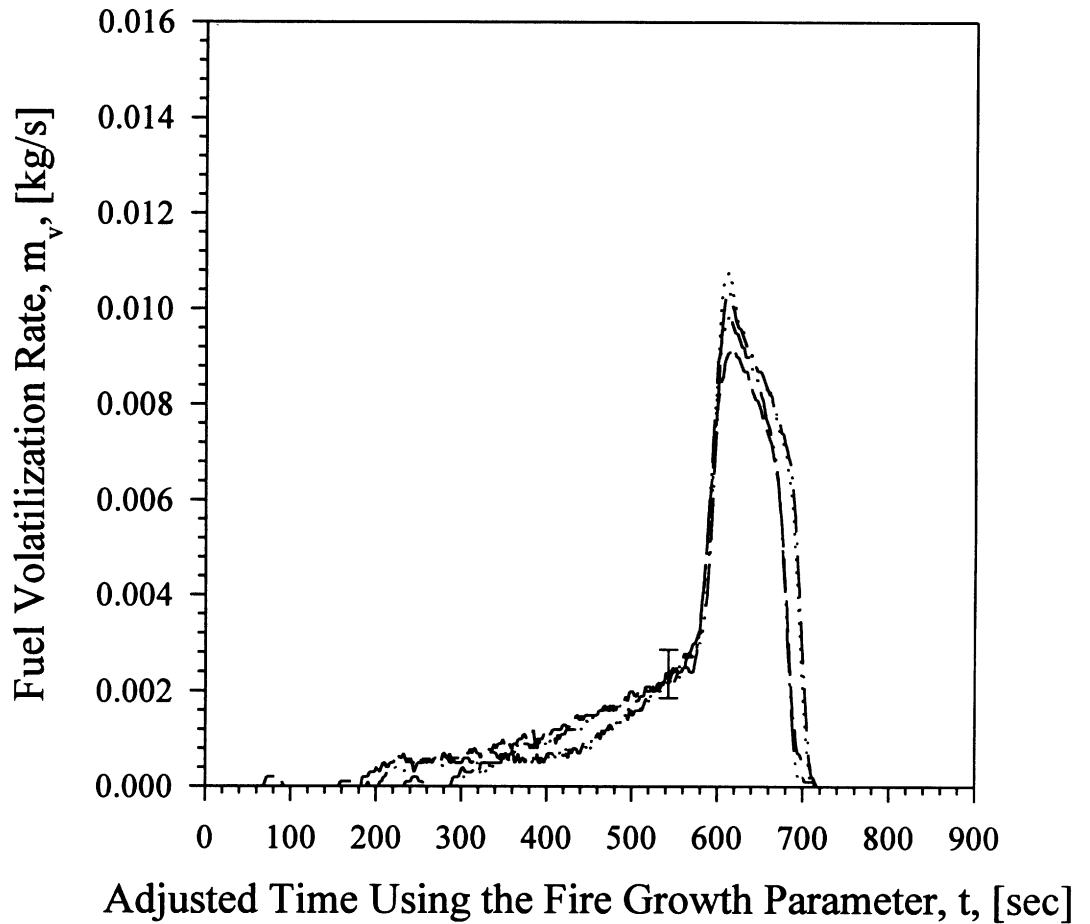


Figure 3.7 The variation in the fuel volatilization rate in *n*-hexane fires with inlet orifice diameter of ----0.30m (no orifice), •••0.25 m, -•-0.20, and -••-0.15 m.

gases exiting the compartment into the hallway. For a fixed opening size, a large increase in fire size is, however, seen in Fig. 3.8 to only slightly increase the momentum of the jet entering the hallway. An increase in the jet momentum (lower Richardson number) of compartment fire gases entering the hallway was seen in Fig. 3.2 and Fig. 3.4 to result in a significant increase in the entrainment of surrounding gases into the jet. The effect of the opening size on the momentum of the jet entering the hallway is seen in Fig. 3.8 to be much more significant than the effect of the fire size.

The effect of fire size on the post-hallway species yields was determined from further evaluation of Ewens (1994b) data. A broad increase in fire size (for a fixed opening size and compartment GER) is shown in Fig. 3.9 to result in only a slight increase in the CO and UHC yields with a corresponding decrease in CO₂ yield.

3.3.3 Effect of Inlet Soffit Height

The height of the soffit above the opening connecting the compartment and hallway determines whether the gases enter the hallway as a ceiling jet (0.0 m soffit) or as a plume (0.20 m soffit). The entrainment into a plume was seen in Fig. 3.4 to be significantly higher compared to the entrainment into a ceiling jet (see Fig. 3.2). The effects of the ceiling jet and the plume on the post-hallway yields is described in this section.

The effect of a 0.0 m inlet soffit versus a 0.20 m soffit was determined by reevaluating the data of Ewens (1994b). The experiments of Ewens (1994a) were with a well-ventilated hallway allowing the effect of the inlet conditions on species yields to be studied. The post-hallway CO yields in experiments with a 0.20 m are shown in Fig. 3.10 to be significantly lower compared with experiments having a 0.0 m soffit. Lower post-hallway UHC yields were also measured for experiments with a 0.20 m inlet soffit compared to levels measured in 0.0 m inlet soffit experiments, see Fig. 3.11. Conversely, an increase in the CO₂ post-hallway yields is observed in Fig. 3.12 for experiments with a 0.20 m inlet soffit compared with experiments having 0.0 m inlet soffit.

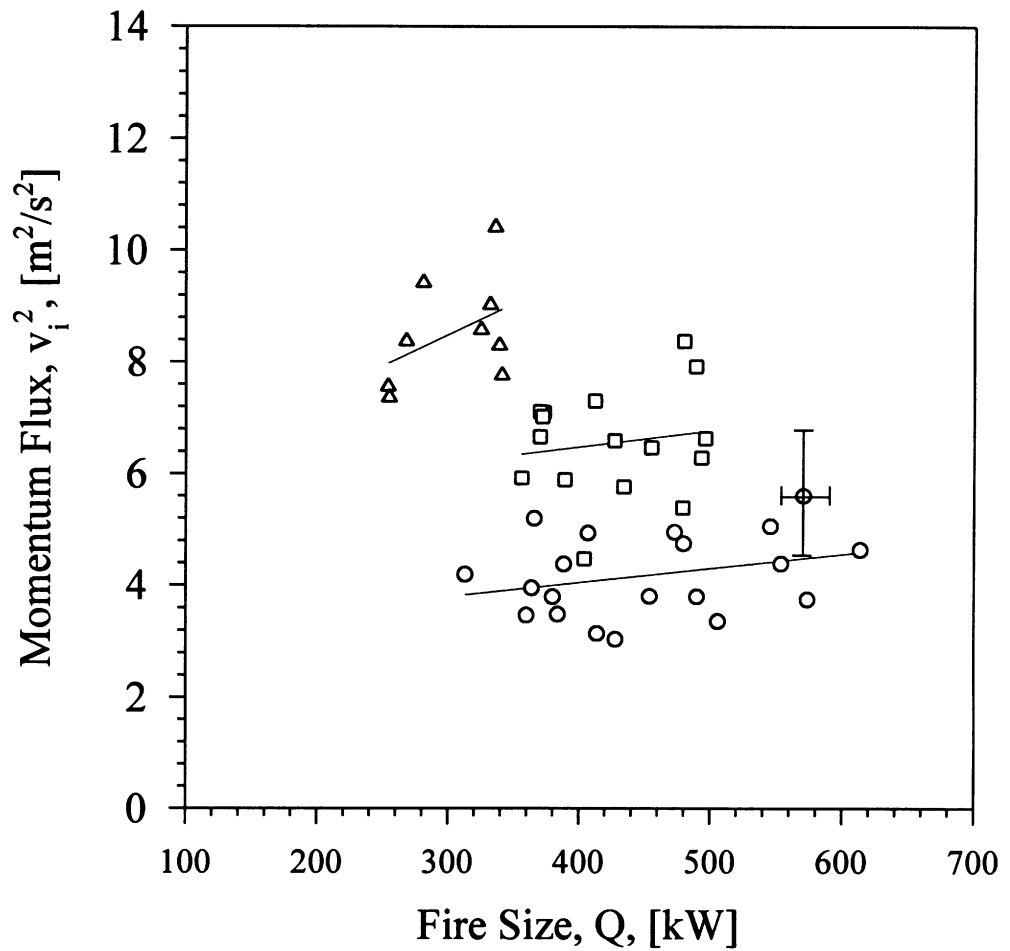


Figure 3.8 The effect of the fire size on the momentum of the compartment fire gas jet entering the hallway for opening sizes of \circ - $0.12 m^2$, \square - $0.08 m^2$ and Δ - $0.04 m^2$ is demonstrated. Experimental data of Ewens (1994b).

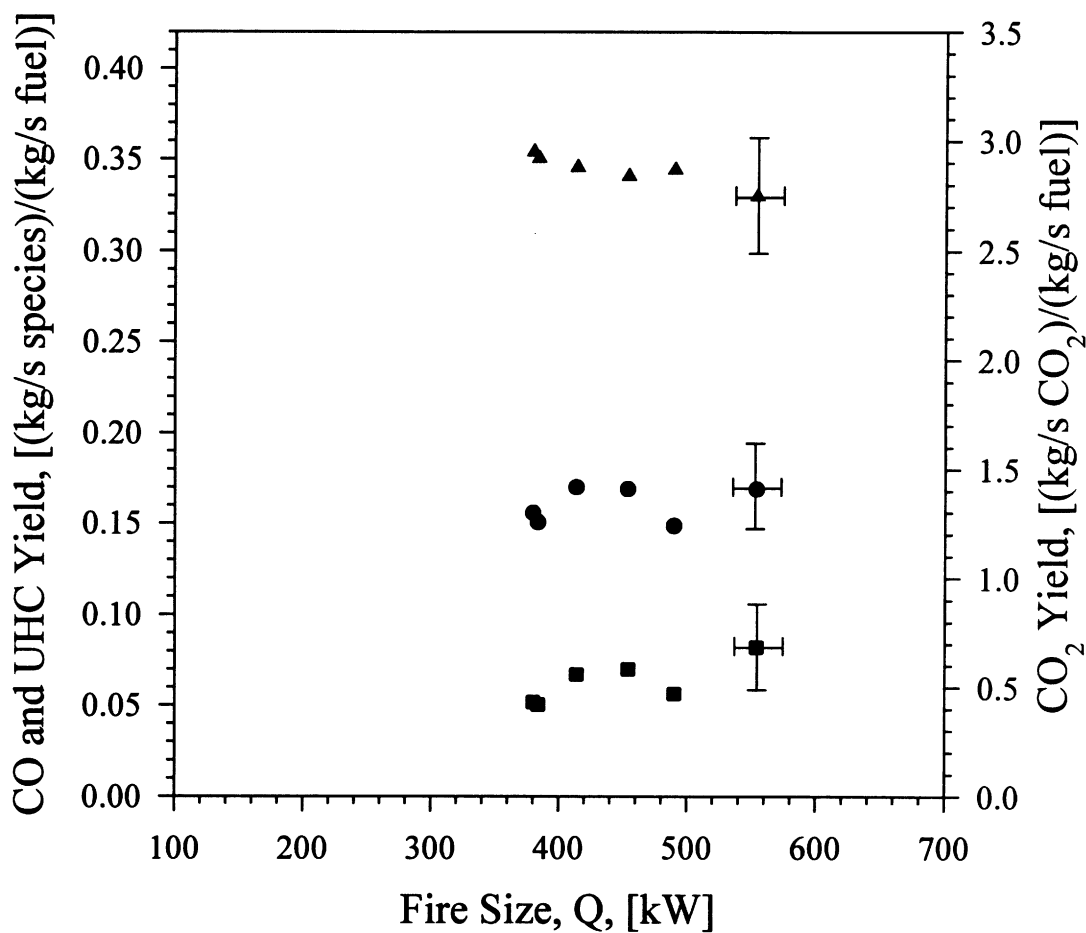


Figure 3.9 The effect of the fire size on the post-hallway ●-CO, ■-UHC and ▲-CO₂ yields with a 0.12 m² opening, $\phi=2.35\pm0.41$, no inlet soffit and 0.20 m exit soffit is shown. Experimental data of Ewens (1994b).

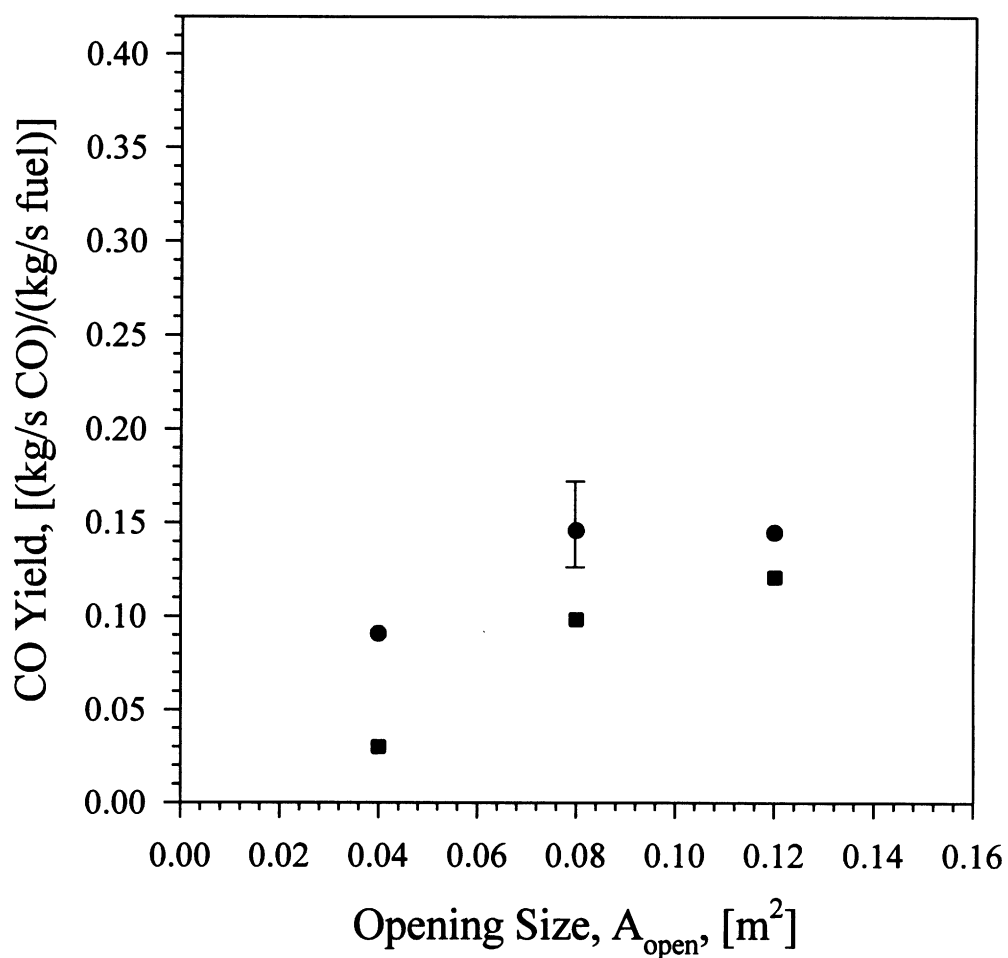


Figure 3.10 The variation in the post-hallway CO yield with no inlet soffit (●) and a 0.20m inlet soffit (■) is shown. The experimental conditions were $Q=431\pm 150$ kW, $\phi=2.64\pm 0.17$, and no exit soffit. Experimental data of Ewens (1994b).

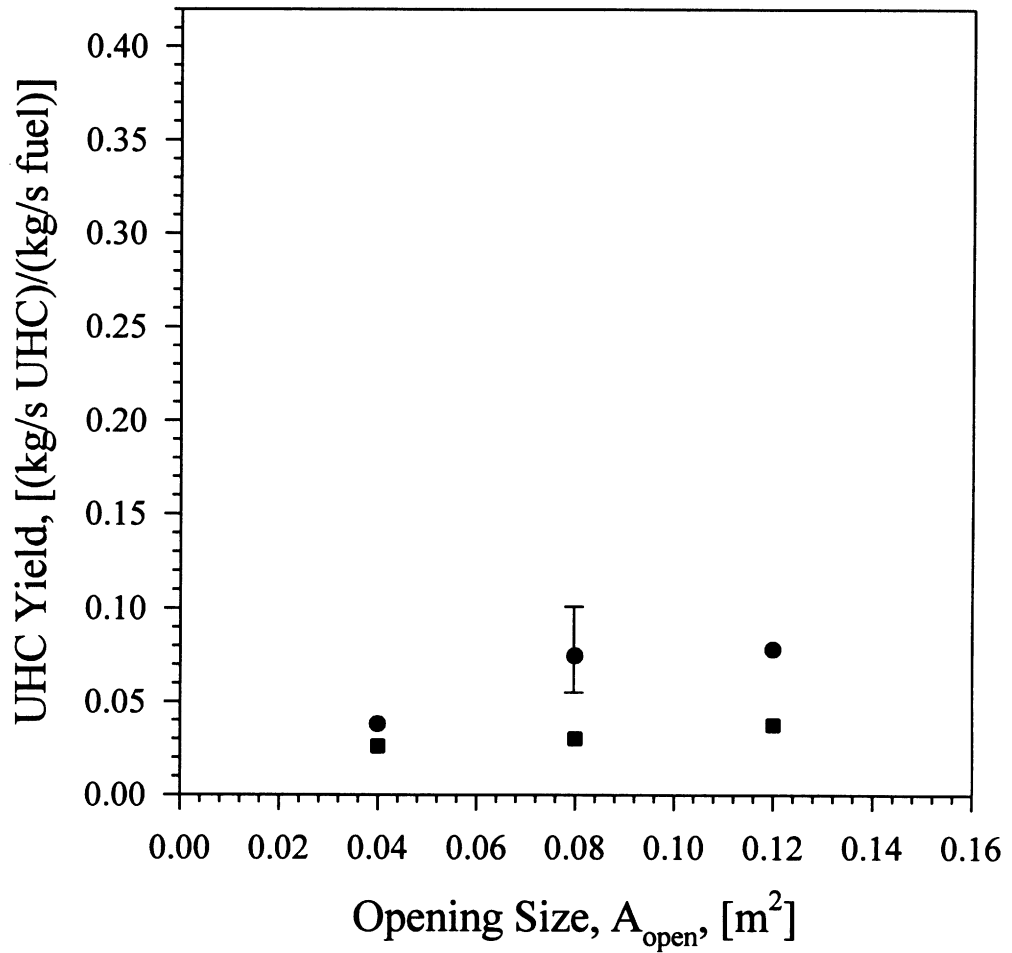


Figure 3.11 The variation in the post-hallway UHC yield with no inlet soffit (●) and a 0.20m inlet soffit (■) is shown. The experimental conditions were $Q=431\pm 150$ kW, $\phi=2.64\pm 0.17$, and no exit soffit. Experimental data of Ewens (1994b).

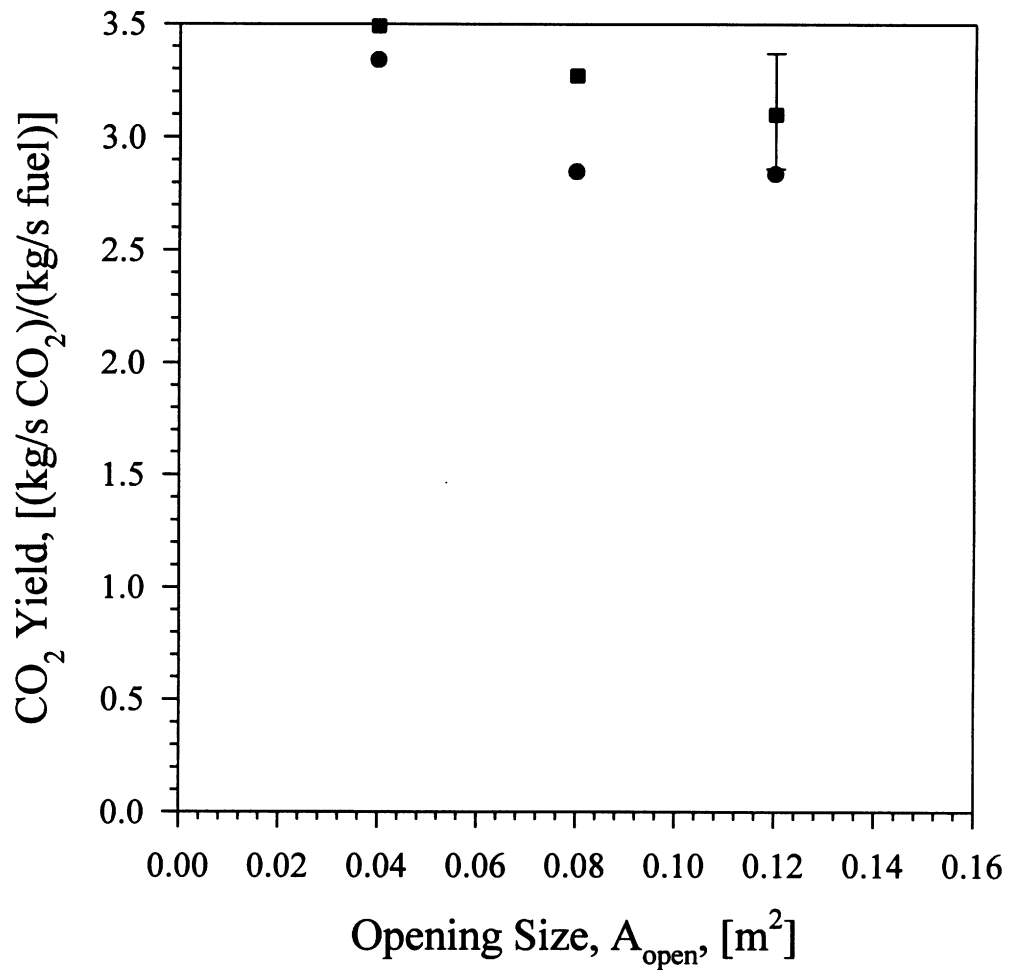


Figure 3.12 The variation in the post-hallway CO₂ yield with no inlet soffit (●) and a 0.20m inlet soffit (■) is shown. The experimental conditions were $Q=431\pm 150$ kW, $\phi=2.64\pm 0.17$, and no exit soffit. Experimental data of Ewens (1994b).

The significant difference in the post-hallway yields was attributed to the difference in entrainment between experiments with a 0.20 m soffit and with a 0.0 m soffit. The higher entrainment rate in the 0.20 m soffit experiments (compared with the 0.0 m soffit experiments) resulted in lower CO and UHC yields and higher CO₂ yields.

3.3.4 Effect of Exit Soffit Height

The exit soffit height was utilized in the experiments to control the depth of combustion gas layer which accumulated in the hallway during the pre-flashover period of the compartment fire. In actual building fires, it is hypothesized that the accumulation of such a layer in the space adjacent to the burning room results in lower oxygen concentration in the gases being entrained into the compartment fire gases entering that space. The effects of deepening the hallway upper-layer on the downstream species levels is explored in this section. All experiments were performed with a 0.20 m inlet soffit unless otherwise noted.

The exit soffit height was varied in the experiments from 0.0 m to 0.80 m in 0.10 m increments. The upper-layer depth was visually observed to be approximately equivalent to the exit soffit height except for experiments with an exit soffit equal to or less than 0.20 m. In the cases with exit soffits of 0.0, 0.10 and 0.20 m, the upper-layer depth was determined from the hallway vertical temperature profiles, and was found to be equivalent to approximately 0.20 m in all three instances.

The post-hallway yields of CO, UHC and CO₂ are plotted versus a nondimensional upper-layer depth,

$$\gamma = \delta/z, \quad (3.20)$$

which is defined as the upper-layer depth, δ , divided by the distance between the ceiling and the bottom of the opening, z , connecting the compartment and the hallway. Physically, γ represents the degree to which the plume of compartment fire gases entering

the hallway was surrounded by oxygen deficient combustion gases. Opening sizes of 0.12, 0.08 and 0.04 m² corresponded to values of z of 0.44, 0.36 and 0.36 m, respectively. For each opening size, the effect of varying the upper-layer depth on the post-hallway CO, UHC and CO₂ yields was measured. The data points were generated by averaging 60 seconds of temporal data during the compartment post-flashover period.

With an opening of 0.12 m² and an upper-layer depth no greater than the inlet soffit height, $\gamma=0.45$, the post-hallway species yields are shown in Fig. 3.13 to be relatively constant. The average yield of 0.098 for CO and 0.046 for UHC were the lowest measured yields, while the CO₂ was at its highest level of 2.58.

With a hallway upper-layer depth below the top of the 0.12 m² opening, the sides of the jet started to become surrounded by oxygen deficient combustion gases. This resulted in the entrainment of oxygen deficient combustion gases into the jet. The limited oxygen entrainment is evident in Fig. 3.13 with the gradual increase in the CO and UHC yields and decrease in CO₂ yield. From the work of Westbrook and Dryer (1984), the reduction in available O₂ reduces the pool of radicals (H, HO₂, OH, O, HCO, etc.) available for the oxidation of CO and UHC. The rapid generation of radicals is critical to the oxidation of CO. Carbon monoxide will not begin to oxidize until the UHC have been reduced to levels where the CO oxidation reactions are competitive with the UHC oxidation reactions (Westbrook and Dryer, 1984). If the generation of radicals is inhibited, less CO will be oxidized before the gas temperature falls below 850 K where the CO oxidation rate decreases drastically (Gottuk, 1992a, Pitts, 1992, Yetter et al., 1991). The gradual increase in CO and UHC yields is seen in Fig. 3.13 to continue until $\gamma>1.4$.

When the hallway upper-layer depth was increased such that $\gamma>1.4$, the post-hallway species yields were measured to be less dependent on the upper-layer depth and more dependent on the presence or absence of external burning in the hallway. With external burning occurring in the hallway and $\gamma>1.4$, the post-hallway CO yields were

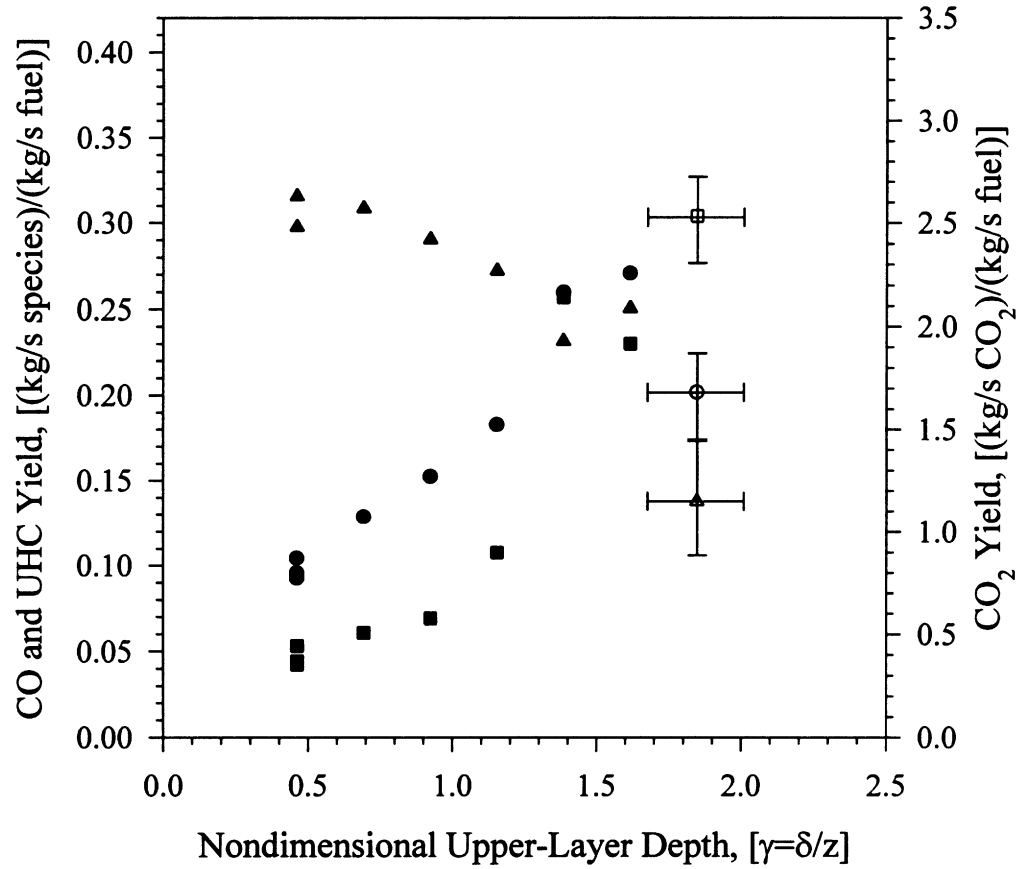


Figure 3.13 The effect the non-dimensional upper-layer height on the post-hallway ●-CO, ■-UHC, and ▲-CO₂ yields for experiments with a 0.12 m² opening, Q=291±36 kW, and $\phi=3.20\pm0.54$. Filled symbols represent experiments with external burning while open symbols were experiments with no external burning.

measured to be 0.27 (on average), see Fig. 3.13. These post-hallway yields are approximately 23% higher than yields measured inside the compartment by Gottuk (1992a) (on average 0.22 for $\phi > 1.8$). The post-hallway UHC yields were measured to be 0.24 which is approximately 27% lower than the yields measured inside the compartment (on average 0.33 for $\phi > 1.8$) (Gottuk, 1992b). Again, the lack of oxidation of CO and UHC is attributed to the limited radical pool generated in the oxygen deficient environment surrounding the jet of hot compartment fire gases entering the hallway (Westbrook and Dryer, 1984). From the data, it appears the limited oxidation of CO is less than the production of CO from the UHC oxidation. The increase in the post-hallway CO yields was, therefore, attributed to the oxidation of UHC which was visually evident by the external burning.

If the upper-layer depth was increased to levels where $\gamma > 1.7$, the jet of compartment fire gases issued into a hallway upper-layer environment with low oxygen levels which inhibited the ignition of the combustion gases. The post-hallway yields of CO, UHC, and CO₂ were all measured to be equivalent in magnitude to levels measured inside the compartment, see Fig. 3.13.

With a 0.08 m² opening connecting the compartment to the hallway, the distance between the ceiling and the bottom of the opening was decreased to 0.36 m. The jet issuing from the 0.08 m² opening was also measured to have a slightly higher entrainment compared with the jet from a 0.12 m² opening, see Fig. 3.4. The post-hallway yields are seen in Fig. 3.14 to show a trend similar to that observed with a 0.12 m² opening (see Fig. 3.13), but magnitudes are shifted downward when $\gamma < 1.7$. The downward shift is attributed to the slightly better O₂ entrainment in the 0.08 m² opening case. With γ slightly less than 1.7 and external burning occurring, post-hallway CO yields are observed in Fig. 3.14 to be 5% greater than compartment levels. The post-hallway UHC yields are, however, seen in Fig. 3.14 to decrease to levels 65% less than in-compartment yields. Again, the slight increase in CO and UHC oxidation compared with the 0.12 m²

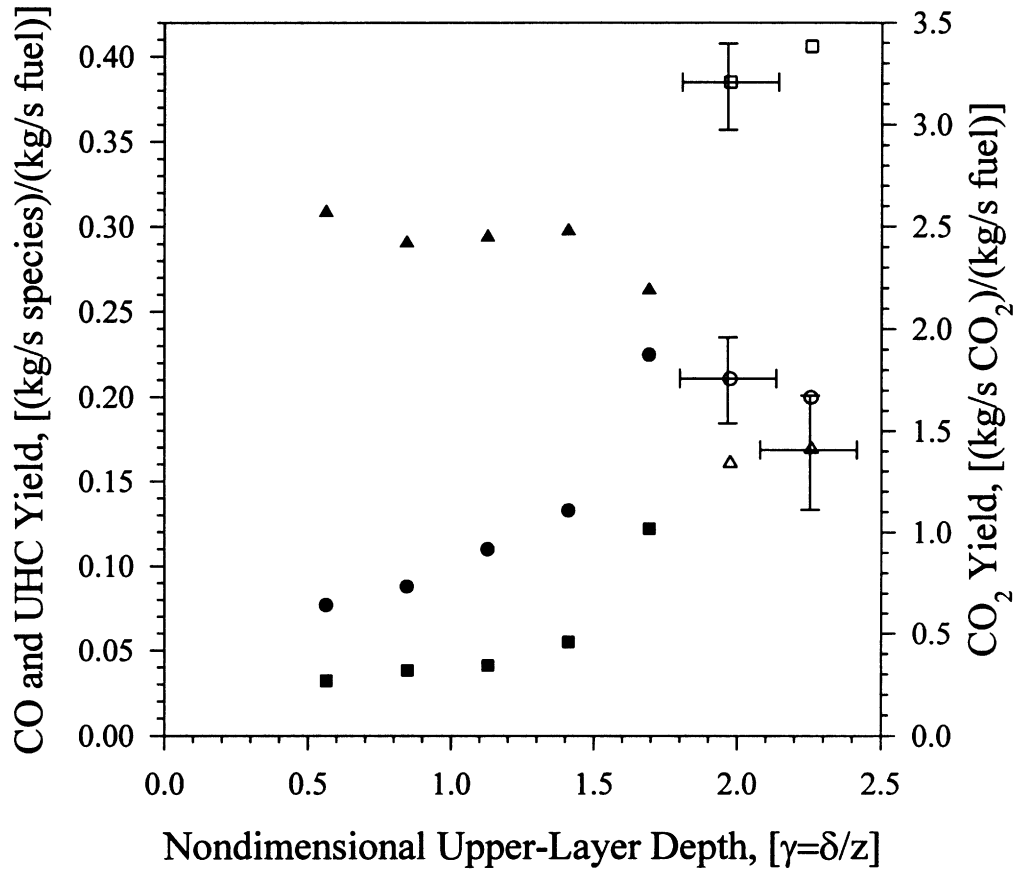


Figure 3.14 The effect the non-dimensional upper-layer height on the post-hallway ●-CO, ■-UHC, and ▲-CO₂ yields for experiments with a 0.08 m² opening, Q=322±64 kW, and $\phi=2.56\pm0.41$. Filled symbols represent experiments with external burning while open symbols were experiments with no external burning.

opening case was attributed to the increase in oxygen entrainment. The post-hallway CO yields were measured to be greater than compartment levels only at a $\gamma=1.68$.

A 0.04 m^2 opening was utilized to investigate the effect of significantly increasing the O_2 entrainment on the post-hallway yields. The distance between the ceiling and the bottom of the opening was 0.36 m (the same as the 0.08 m^2 opening case). The CO and UHC post-hallway yields are seen in Fig. 3.15 to remain nearly equivalent at a magnitude of approximately 0.025 for $\gamma \leq 1.2$. For a $1.2 < \gamma < 1.7$, the CO and UHC yields increase to levels observed inside the compartment. Unlike the other two cases, the post-hallway CO yields were never measured to be greater than those measured inside the compartment. As before, the absence of external burning occurred at a value of γ equal to 1.7 .

3.3.5 Effect of All Parameters with a Deep Hallway Upper-Layer

From the results presented in section 3.3.4, it appears that the accumulation of a deep, $\gamma \geq 1.0$, oxygen deficient upper-layer in the hallway during pre-flashover limits the oxygen entrained into the compartment fire gases entering the hallway by reducing the oxygen concentration of the gases surrounding the jet. The post-hallway species yields, therefore, become less sensitive to the entrainment induced by the size of the opening, the fire size, and the inlet soffit height. To demonstrate this point, a series of experiments were conducted with an upper-layer depth of $\delta \approx 0.50$. The effects of varying the opening size, the fire size, the inlet soffit height and the compartment global equivalence ratio on the post-hallway species yields were measured. The value of γ for these experiments varied depending upon the opening size and the inlet soffit height (2.1 for 0.12 m^2 and 3.1 for 0.08 m^2 and 0.04 m^2 with no inlet soffit, and 1.1 for 0.12 m^2 and 1.4 for 0.08 m^2 and 0.04 m^2 with a 0.20 m inlet soffit).

The post-hallway CO yield data shown in Fig. 3.16 was generated from experiments where the opening size, the fire size, the inlet soffit height and the compartment global equivalence ratio were all varied. The shape of the curve is similar to that of the

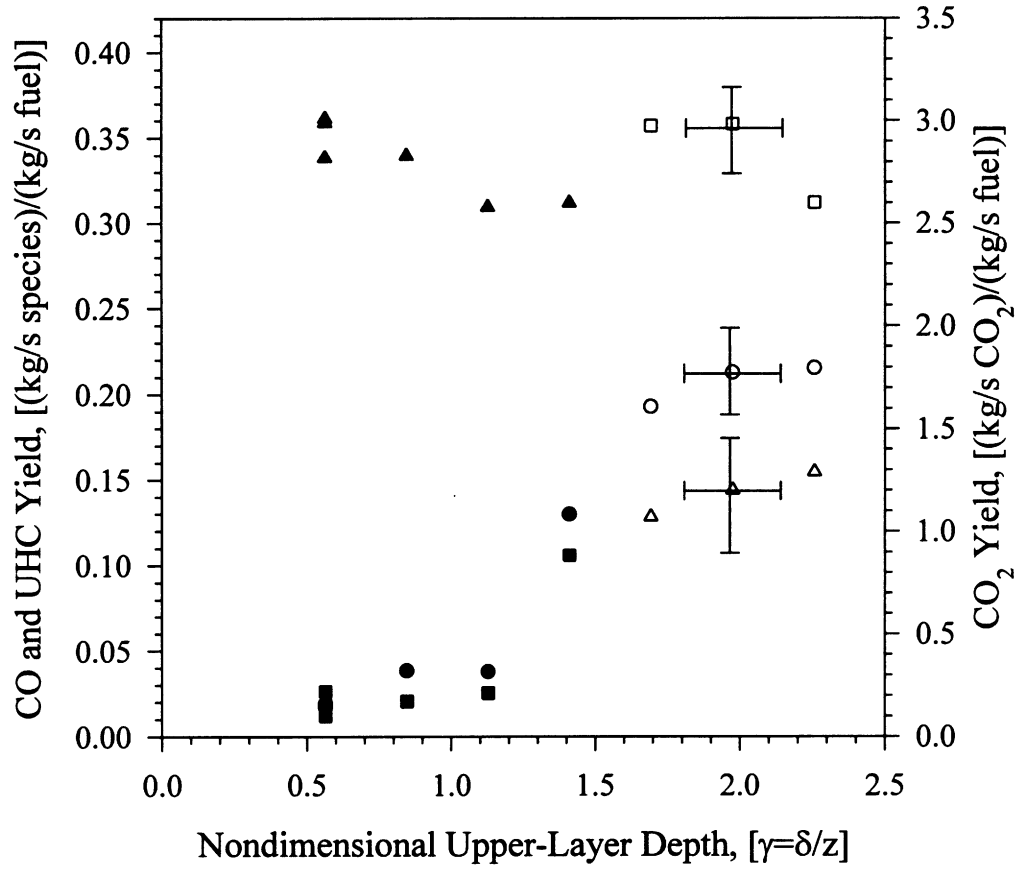


Figure 3.15 The effect the non-dimensional upper-layer height on the post-hallway ●-CO, ■-UHC, and ▲-CO₂ yields for experiments with a 0.04 m² opening, Q=259±41 kW, and φ=2.77±0.57. Filled symbols represent experiments with external burning while open symbols were experiments with no external burning.

compartment CO yield versus global equivalence ratio curve determined by Gottuk (1992a). In experiments with no external burning, downstream CO yields were similar in shape and magnitude compared with yields measured inside the compartment. With external burning in the hallway, the downstream CO yields were equivalent to the no external burning yields up to a ϕ of 2.0. With $\phi > 2.0$, the yield in experiments with external burning was approximately 0.16 compared with 0.22 in experiments without external burning. The post-hallway CO yield appeared to be relatively insensitive to the other variables (i.e. inlet soffit height, fire size, and opening size) with a deep upper-layer present in the hallway.

The plot of CO yield versus global equivalence ratio can be divided into three regions: low, transitional and high toxicity. In the low toxicity region, $0 < \phi < 0.6$, an undetectable amount of CO is transported downstream of the compartment. This is expected since there is virtually no CO being produced inside the compartment in this ϕ range. Characteristic of the transitional toxicity region, $0.6 < \phi < 2.0$, is a steep rise in the CO yield with an increasing ϕ . The slope of the rise depends on whether or not external burning occurs within the hallway. The slope is 0.16 with no external burning and 0.11 with external burning. The region is broader and the rise in the CO yield is less steep compared to the in-compartment data taken by Gottuk (1992a) where the transitional toxicity region was $0.6 < \phi < 1.5$ and the slope was 0.24 (see Fig. 1.2). The high toxicity region in Fig. 3.16 encompasses all $\phi > 2.0$. The CO yields plateau in this region and remain fairly constant. The level at which the CO plateaus depends on whether or not external burning occurred inside the hallway. The CO yield averages 0.22 with no external burning and 0.16 with external burning. The plateau level with no external burning is consistent with the in-compartment results reported by Gottuk (1992a). Overall, the CO yield in experiments with external burning decreases by 0.05-0.06 from the no external burning case for all ϕ greater than 1.2, see Fig. 3.16.

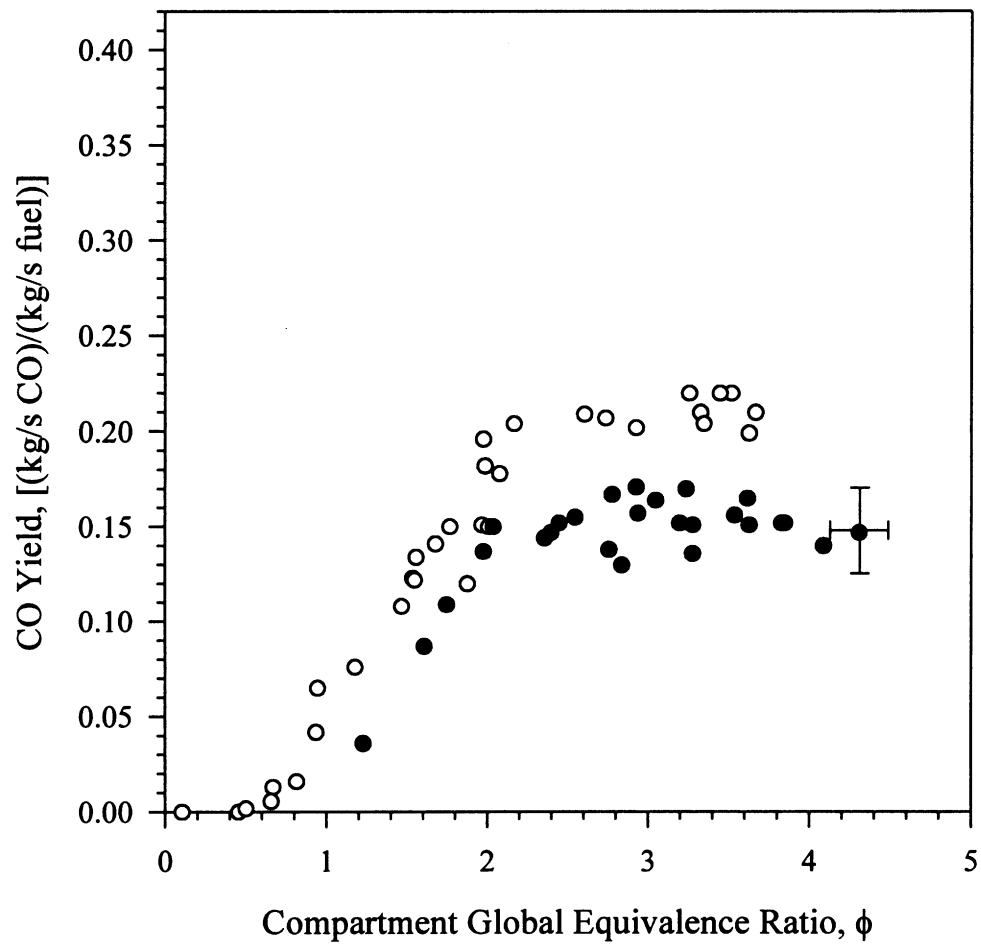


Figure 3.16 The effect of varying all parameters on the post-hallway CO yield when a deep upper-layer, $\gamma > 1.0$, was present in the hallway. Filled symbols represent experiments with external burning while open symbols were experiments with no external burning.

The post-hallway UHC yields are seen in Fig. 3.17 to also have a strong dependence on the occurrence of external burning in the hallway. The UHC yields are slightly scattered for the experiments with no external burning. The post-hallway UHC yields in experiments with external burning are seen in Fig. 3.17 to rise vary with an increase in ϕ . It is interesting to notice that the post-hallway UHC yields were not at a measurable level until ϕ was greater than 1.5. External burning in the hallway prevented measurable levels of UHC downstream until a $\phi > 1.5$.

3.3.6 Major Parameters Controlling Post-Hallway Species Yields

The parameters having the most significant effect on the post-hallway species yields were the:

- opening size,
- inlet soffit height,
- depth of upper-layer in hallway (hallway exit height),
- occurrence of external burning, and
- global equivalence ratio of the compartment fire.

The first two of the parameters are the variables which affected the entrainment into the compartment fire gas jet entering the hallway, while the third parameter controlled the oxygen concentration entrained into the jet. The last two parameters govern the chemistry which occurred in the hallway and compartment.

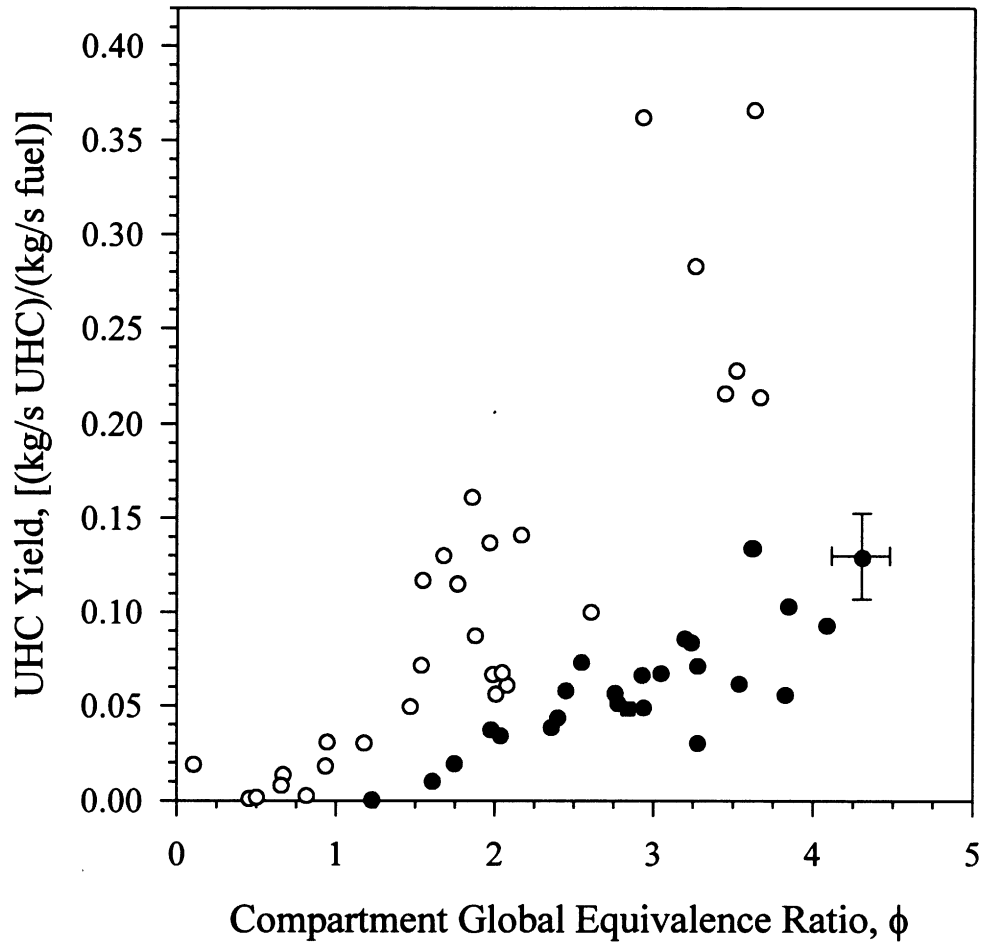


Figure 3.17 The effect of varying all parameters on the post-hallway UHC yield when a deep upper-layer, $\gamma > 1.0$, was present in the hallway. Filled symbols represent experiments with external burning while open symbols were experiments with no external burning.

3.4 POST-HALLWAY SPECIES YIELDS FROM POLYURETHANE FOAM FIRES

A series of experiments were conducted using polyurethane foam as the fuel inside of the compartment. The experiments exhibited an upper-layer temperature of 960 K, on average, at $\phi=2.1$ which is approximately 25 K lower than that observed in *n*-hexane experiments (985 K on average). The post-hallway yields from polyurethane fires are presented in this section, and compared to the post-hallway yields of the *n*-hexane fire experiments.

The experiments were conducted using a 0.20 m inlet soffit, a 0.04 m² opening and a compartment global equivalence ratio of 2.1. No sustained external burning occurred in the hallway regardless of the exit soffit height. The result of the absence of external burning in the hallway on the post-hallway CO yields was a yield greater than 0.15 at all hallway upper-layer depths tested, see Fig. 3.18. The post-hallway CO yields were measured to be approximately 0.15 at a $\gamma=0.55$, and increased to a level of 0.19 with $\gamma>1.0$. The post-hallway CO yields for $\gamma>1.0$ were equal to the yields measured inside the compartment by Gottuk (1992a). The low post-hallway CO₂ yields shown in Fig. 3.18 further demonstrates the lack of oxidation of CO in the hallway. The UHC yields plotted in Fig. 3.18 are approximately 4 times lower than yields measured in *n*-hexane fires. The low UHC yields were attributed to polyurethane fires producing high levels of oxygenated hydrocarbons (C₂H₄O), unsaturated hydrocarbons (C₂H₂) and higher order hydrocarbons. Oxygenated hydrocarbons (i.e. aldehydes and ketones) and unsaturated hydrocarbons were reported by Colket et al. (1974) to produce FID responses significantly lower than expected from the calibration. For example, C₂H₄O and C₂H₂ produces a signal 60% and 65%, respectively, lower than that of C₂H₆ (Colket, et al., 1974). The other source of possible error in the UHC measurements was the higher order hydrocarbons condensing in the sampling lines.

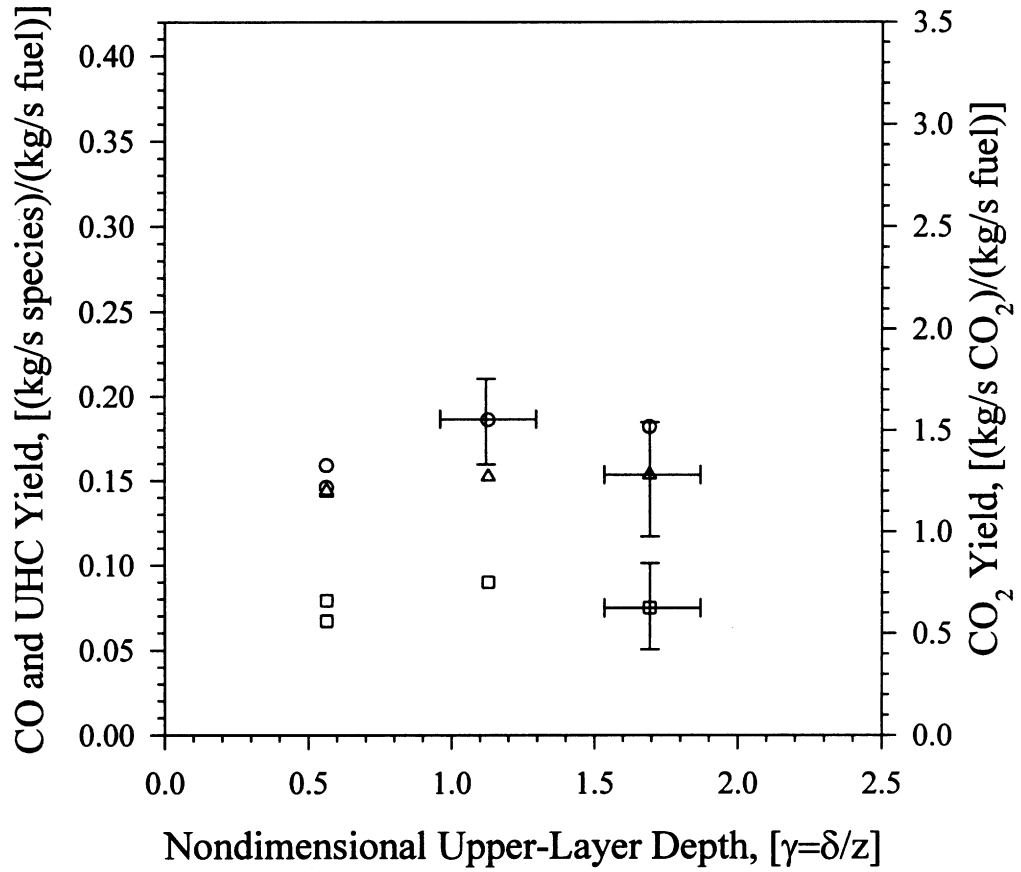


Figure 3.18 The effect of the nondimensional upper-layer depth on the post-hallway \circ -CO, \square -UHC and Δ -CO₂ yield in experiments with polyurethane foam as the fuel inside the compartment. The experiments utilized a 0.04 m² opening, a 0.20 m inlet soffit, $Q=164\pm 11$ kW and $\phi=2.08\pm 0.01$. Filled symbols represent experiments with external burning while open symbols were experiments with no external burning.

Compared with the *n*-hexane experiments, the polyurethane foam experiments contained higher post-hallway CO yields at lower values of γ due to the absence of external burning. The post-hallway CO yields in the foam experiments were measured to be approximately 14% less than the yields in the *n*-hexane experiments with no external burning. The low post-hallway CO₂ yields of 1.3 were consistent with the post-hallway yields measured in the *n*-hexane experiments with no external burning.

CHAPTER 4.

RESULTS: EVOLUTION OF SPECIES CONCENTRATIONS IN THE HALLWAY

4.1 INTRODUCTION

The effect of experimental conditions on temporal and spatial distributions of species concentration and temperature in the hallway cannot be measured post-hallway. In-hallway sampling was performed to measure the distribution of CO, UHC, CO₂, O₂ and temperature in the hallway. The data is used to develop a more detailed understanding of the parameters controlling the oxidation of CO. The experimental conditions for the in-hallway sampling experiments were consistent with those where high CO yields were measured post-hallway. The time necessary for hallway species concentrations to reach a steady-state (termed transient time), the absence or presence of external burning, and the type of fuel burning inside the compartment were experimentally varied. The effects of these parameters on the species concentrations and temperatures in the hallway were measured and are presented in this chapter.

4.2 MOVEMENT OF COMBUSTION GASES IN THE HALLWAY

With the compartment-hallway orientation shown in Fig. 2.1, the flow field in the hallway is highly three-dimensional. Since laboratory techniques for measuring the flow field in the hallway were not practical for the reported experiments, flame luminosity in the hallway (external burning) was used as a flow visualization tool to reveal the flow field present in the hallway. The path of the combustion gases was most easily visualized with the most intense burning in the hallway. This occurred when the gases exiting the

compartment encountered concentrations of oxygen near those observed in the ambient surroundings (i.e. experiments with an exit soffit of 0.10 m or less). The visualization was performed using a video camera placed at the hallway exit, and is described from this point of view (as if one were standing at the exit looking down the hallway toward the compartment).

An image of the typical external during the steady-state period (termed the post-flashover period) of the compartment fire is shown in Fig. 4.1. As the combustion gases exited the compartment, a buoyant plume was formed at the hallway entrance due to the presence of a 0.20 m soffit. The plume impinged upon the ceiling resulting in three major paths for the combustion gases transport down the hallway. Since there was an inlet soffit, the first means of transport was a counterclockwise rotating vortex formed at the top left corner of the hallway. From the size of the vortex, it was inferred to be a minor path of transport for this geometry. This mechanism of transport disappeared in the absence of an inlet soffit. The impingement of the buoyant plume was observed to force some of the gases to take on a trajectory which resulted in their transport down the center of the hallway. This constitutes the second path of transport. The majority of the external burning was observed to be present both across the hallway and along the upper right corner of the hallway, see Fig. 4.1. Based on this observation, the bulk of the combustion gases were driven across the hallway by the momentum of the jet exiting the compartment. The bulk flow of combustion gases then impinged upon the opposite wall causing a large clockwise rotating vortex to develop in the upper right corner of the hallway, see Fig. 4.1. The size of the vortex was estimated to be approximately 0.20-0.30 m in diameter. The size of the vortex is determined by the velocity of the gases impinging on the wall opposite the compartment. The velocity of the gases impinging on the wall is expected to primarily depend on the distance the gases need to travel before reaching the wall. The vortex is, therefore, believed to be scaled to the hallway width.

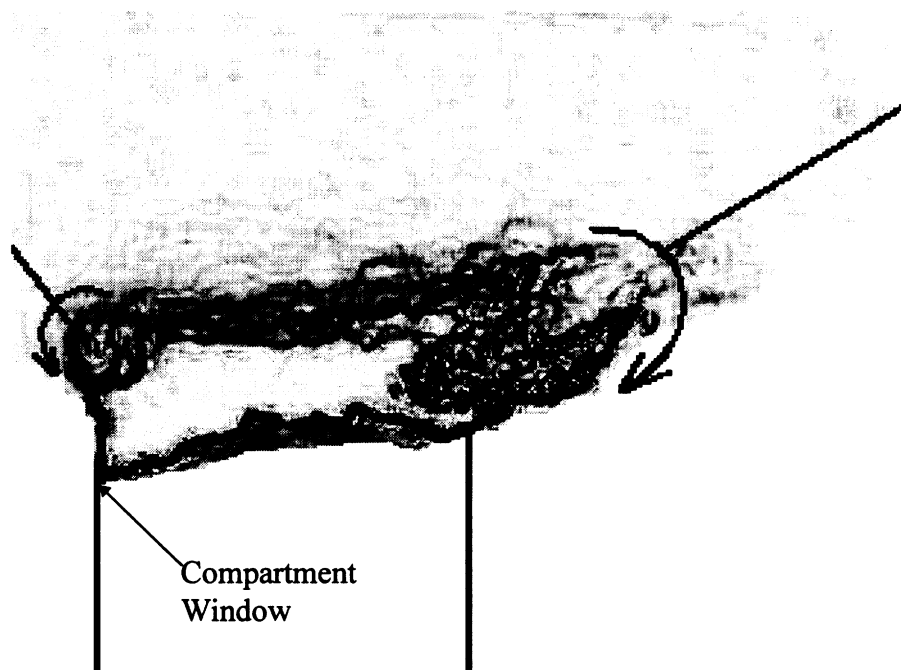


Figure 4.1 An image of the external burning in the hallway when looking down the open end of the hallway underneath the fume hood.

4.3 EVOLUTION IN HEXANE COMPARTMENT FIRES

Experiments using liquid *n*-hexane fires examined the effects of transient time of the species concentrations in the hallway and external burning. The evolution of CO, UHC, CO₂, O₂ (all reported on a wet-basis) and temperature within the hallway are presented for the different situations studied. All experiments were performed with a 0.20 m diameter fuel pan, a 0.20 m inlet soffit and a global equivalence ratio of 3.0 ± 0.50 . Note that these conditions are similar to those used in experiments to produce the data showing the effect of the exit soffit (upper-layer in the hallway) on the post-hallway yields seen in Fig. 3.13, Fig. 3.14 and Fig. 3.15. The 25 sampling locations within the facility were shown in Fig. 2.10 and are denoted by the lower case letters on the contour plots to follow. Note the y-axis in all contour plots corresponds to the center of the compartment-hallway opening.

Since gas sampling could only be performed at one location during an experiment, 25 different experiments were performed to generate the data to map the facility. The growth rate in each of the 25 fires was slightly different. The experiments had to be aligned with one another for the averaged data from each experiment to represent the same period in the fire growth. Carbon monoxide concentrations were measured to be highest just after the onset of flashover inside (termed post-flashover) of the compartment fire. The fire growth parameter, *G*, defined in Eqn. (2.15) was utilized to determine the beginning of the post-flashover period inside the compartment fire. Post-flashover was assumed inside the compartment when *G* was approximately zero.

The amount of time after flashover for the hallway species concentrations to reach a steady-state is termed the transient time. Species concentrations were considered to reach a steady-state when a less than 5% change occurred over a 30 second period. The transient time was determined by the conditions at the exit of the hallway. Experiments

which contained an exit soffit resulted in a short transient time, while longer transient times were achieved by blocking the bottom portion of the hallway exit.

4.3.1 Short Transient Time with No External Burning

Experiments were performed with a 0.04 m^2 opening and an upper-layer depth of 0.60 m (exit soffit of 0.60 m) to investigate the evolution of species concentrations and temperatures when no external burning occurred in the hallway. The nondimensional upper-layer depth for these conditions was $\gamma=1.7$. The experimental results previously seen in Fig. 3.15 indicate no external burning for this value of γ . With the 0.60m exit soffit present, species concentrations and temperatures were anticipated to have a short transient time.

The 25 experiments necessary to map the hallway concentrations were aligned with one another using the fire growth parameter, G . Compartment temperature data from 10 experiments was used to verify the validity of the alignment method. The temperatures during the post-flashover period of the compartment fires are shown in Fig. 4.2 to be aligned with one another. Noting the different times of ignition in Fig 4.2, the alignment compensates for differences in the initial growth of the compartment fire. With the data aligned, a description of the temporal and spatial evolution of the species concentration and temperature in the hallway upper-layer is given.

Approximately 12-16 seconds before flashover inside the compartment, 1.5% CO and 1.5% UHC, see Fig. 4.3 and Fig. 4.4, respectively, were measured in the compartment upper-layer. The CO and UHC levels were measured to rapidly be diluted as the gases were transported across the hallway. A CO_2 concentration of 7.0% was measured to be uniform throughout the hallway upper-layer, see Fig. 4.5. An O_2 concentration was also measured to be uniform within the hallway at a level of 8.5% , see Fig. 4.6. A plot of the temperature in the hallway is seen in Fig. 4.7. The gases were

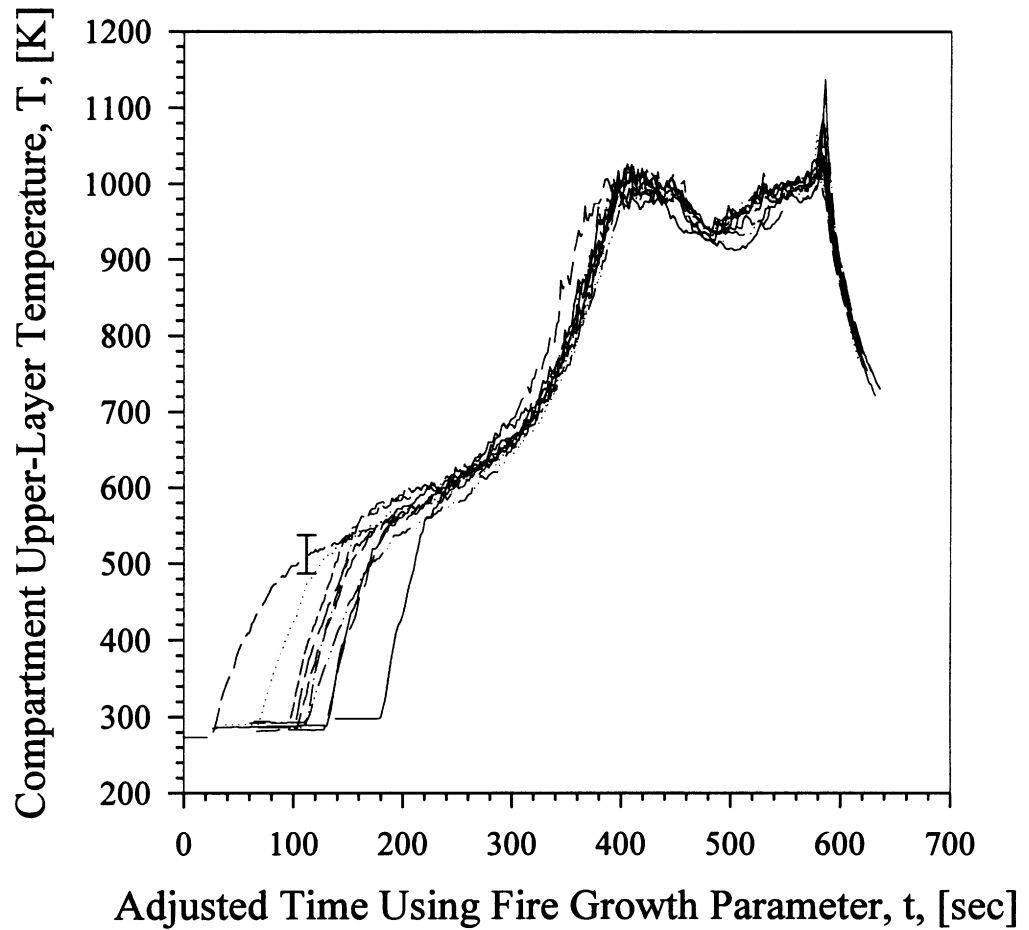


Figure 4.2 The temperature 0.05 m below the ceiling inside the compartment in 10 different *n*-hexane fire experiments with a 0.04 m² opening, a 0.60 m exit soffit, and no external burning in the hallway. The experiments were aligned with one another in time using the fire growth parameter.

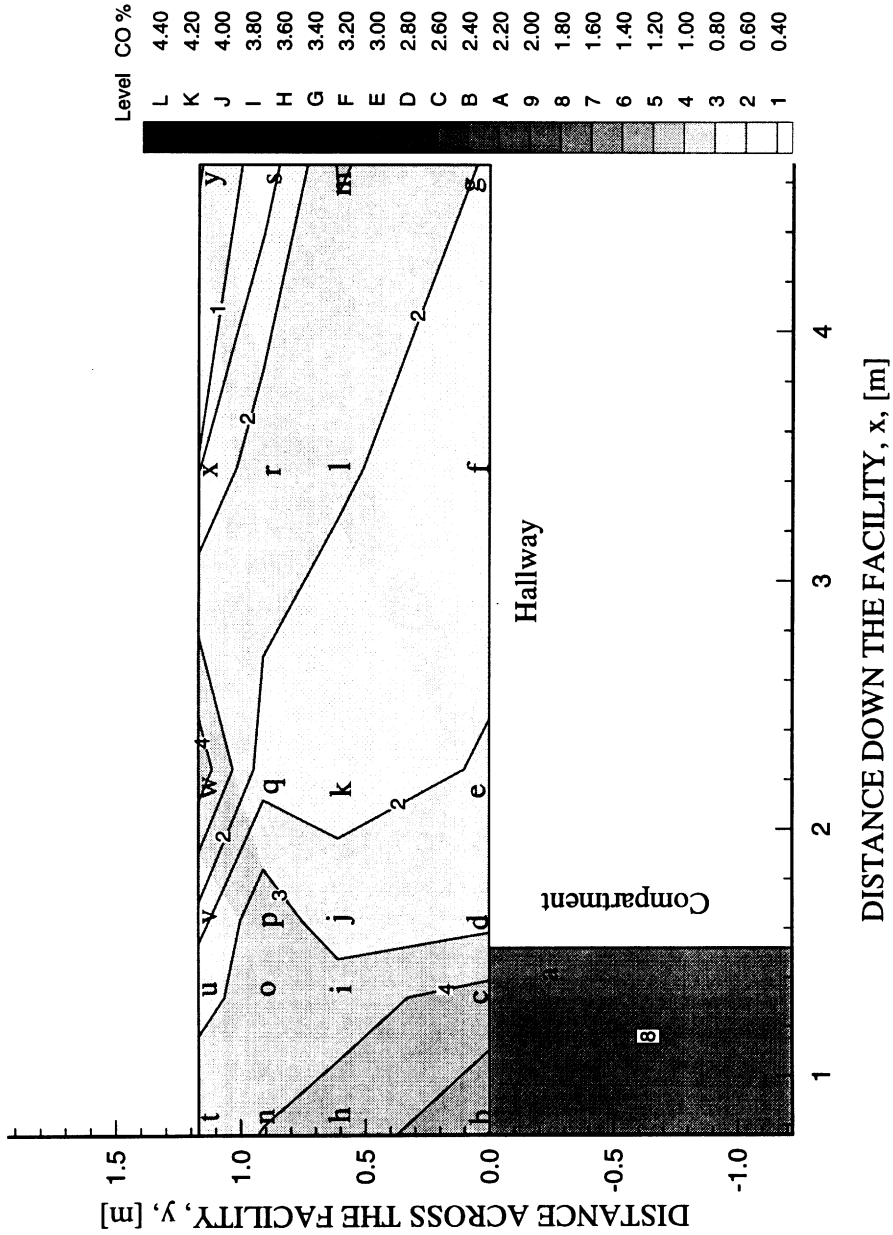


Figure 4.3 The wet CO concentration distribution 0.05 m below the ceiling 12-16 seconds before flashover in *n*-hexane fire experiments with a 0.04 m² opening, 0.20 m inlet soffit, 0.60 m exit soffit and no external burning.

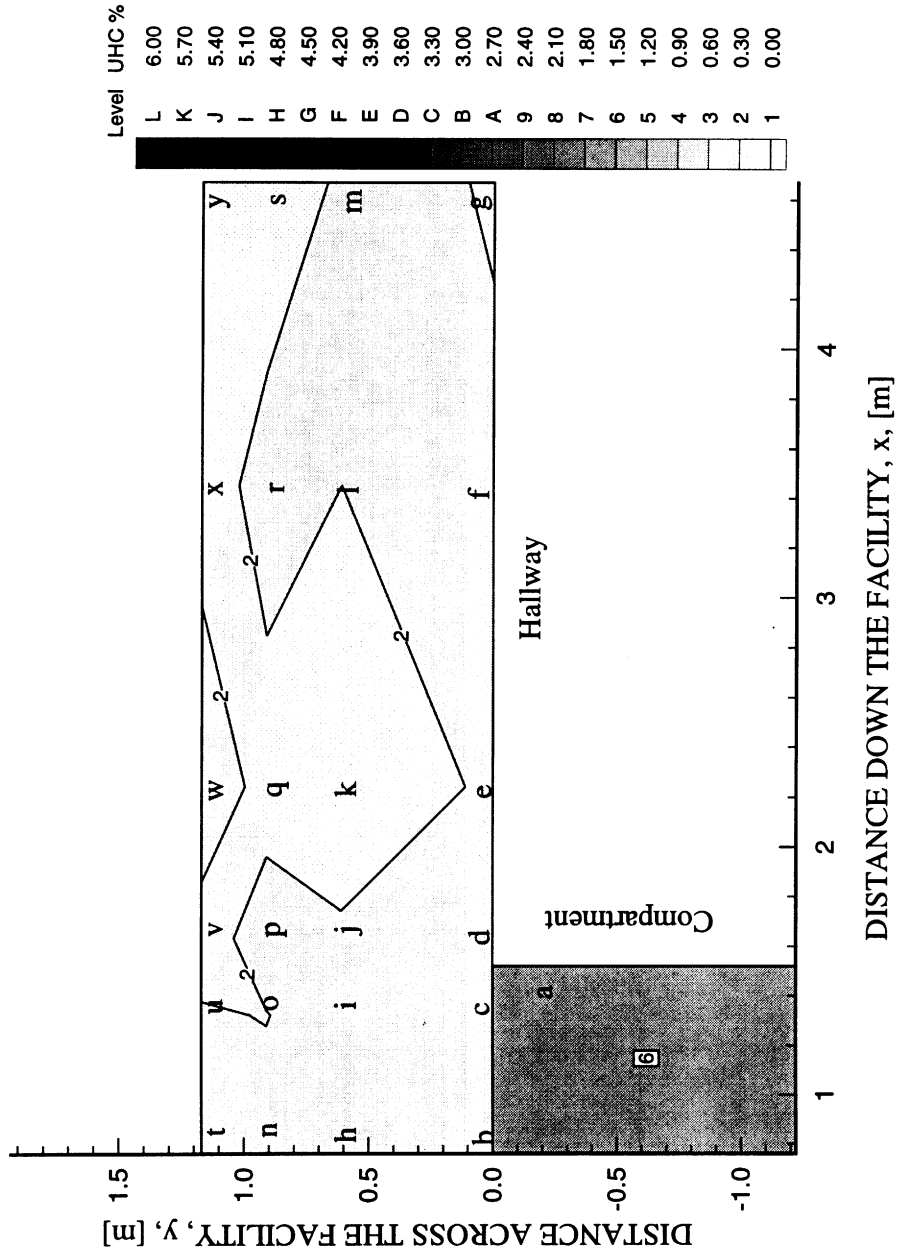


Figure 4.4 The wet UHC concentration distribution 0.05 m below the ceiling 12-16 seconds before flashover in *n*-hexane fire experiments with a 0.04 m² opening, 0.20 m inlet soffit, 0.60 m exit soffit and no external burning.

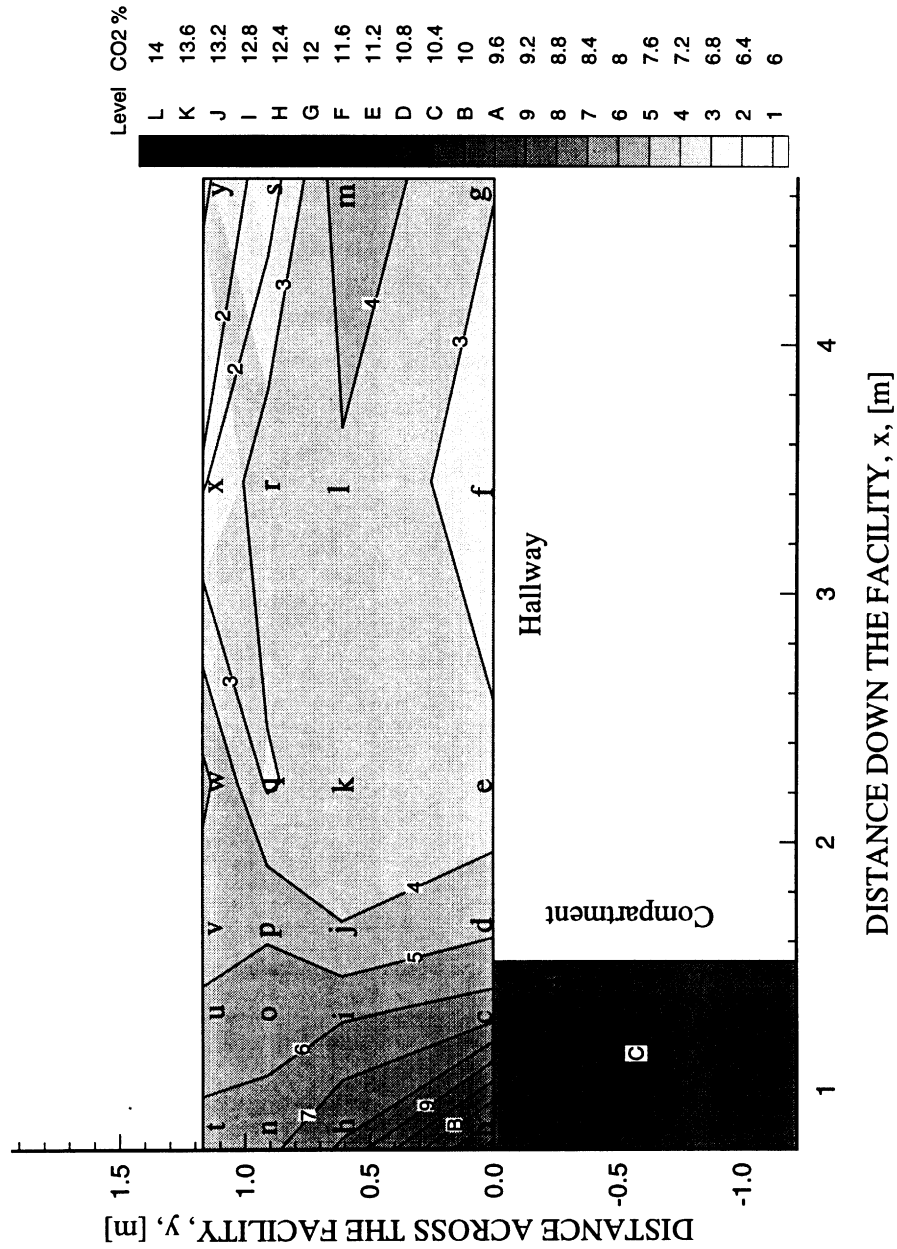


Figure 4.5 The wet CO₂ concentration distribution 0.05 m below the ceiling 12-16 seconds before flashover in *n*-hexane fire experiments with a 0.04 m² opening, 0.20 m inlet soffit, 0.60 m exit soffit and no external burning.

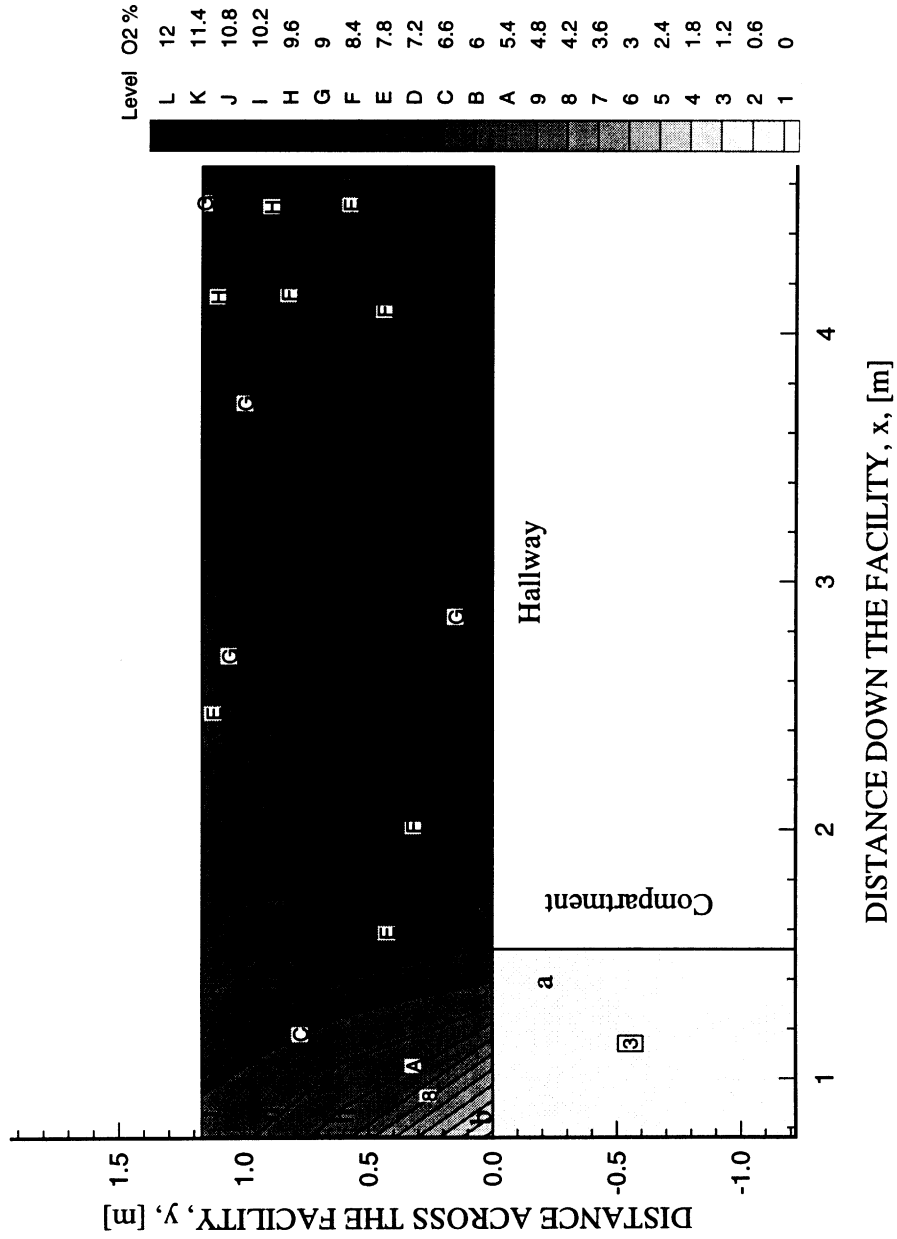


Figure 4.6 The wet O₂ concentration distribution 0.05 m below the ceiling 12-16 seconds before flashover in *n*-hexane fire experiments with a 0.04 m² opening, 0.20 m inlet soffit, 0.60 m exit soffit and no external burning.

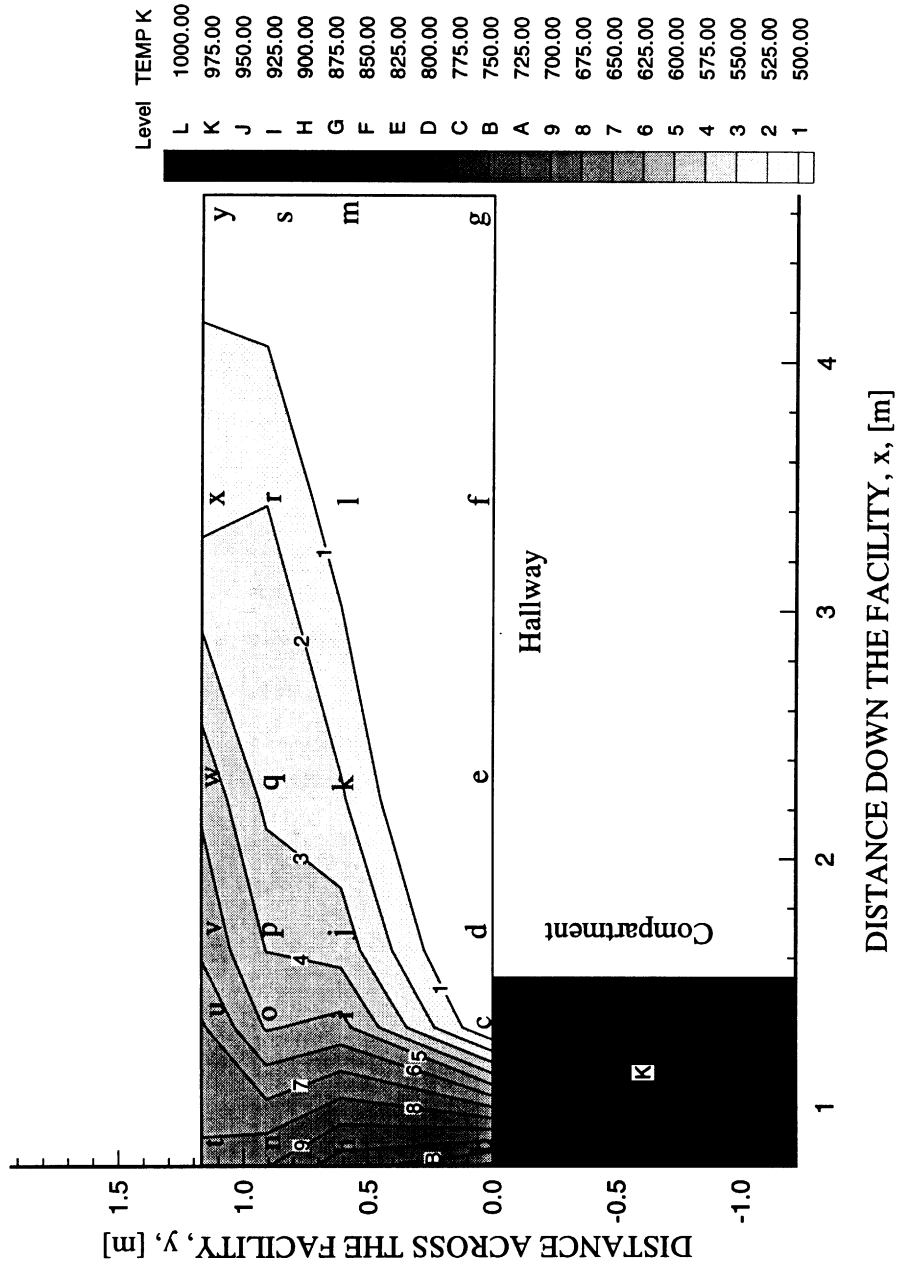


Figure 4.7 The temperature distribution 0.05 m below the ceiling 12-16 seconds before flashover in *n*-hexane fire experiments with a 0.04 m² opening, 0.20 m inlet soffit, 0.60 m exit soffit and no external burning.

measured to enter the hallway at temperatures of 780 K (see Fig. 4.7), but cooled rapidly to approximately 450 K by the end of the hallway.

Post-flashover was reached in the compartment 16-20 seconds after the onset of flashover. High concentrations of CO and UHC, see Fig. 4.8 and Fig. 4.9, respectively, were measured in the gases flowing across the hallway and along the wall opposite the compartment (the path of the bulk flow). The compartment fire gases entered the hallway with 2.4% CO, see Fig. 4.8. Carbon monoxide concentrations of 1.6% or greater were measured in gases flowing across the hallway and traveling down the side of the hallway opposite the compartment. Only 0.9% CO was measured in the gases on the compartment side of the hallway which is nearly half the levels measured on the opposite side of the hallway. The measured UHC concentrations are shown in Fig. 4.9 to be non-uniform in the hallway. Over 2.0 % UHC was measured on the side of the hallway opposite the compartment and 1.3% on the compartment side of the hallway. Plots of the measured concentrations of 7.0% CO₂ and 7.5% O₂ are seen in Fig. 4.10 and Fig. 4.11, respectively, to be uniform within the hallway upper-layer. A plot of the measured hallway gas temperatures is seen Fig. 4.12. The temperatures are slightly higher than the levels 12-16 before flashover, but spatially vary in approximately the same manner.

At approximately 40-44 seconds after the onset of flashover in the compartment, all measured species concentrations were uniform within the hallway upper-layer. The hallway species concentrations reached a steady state 56 seconds after CO levels of greater than 1% were measured in the gases entering the hallway. The upper-layer gases 0.05 m below the ceiling were measured to contain concentrations of 1.9% CO and 2.9% UHC along the length of the hallway, see Figs. 4.13 and 4.14. The gases were also measured to contain concentrations of 6.5% CO₂ and 7.2% O₂ along the hallway length, see Fig. 4.15 and 4.16, respectively. From the plot of the gas temperature (see Fig. 4.17), temperatures are seen to cool from 850 K at the window to less than 500 K by the end of

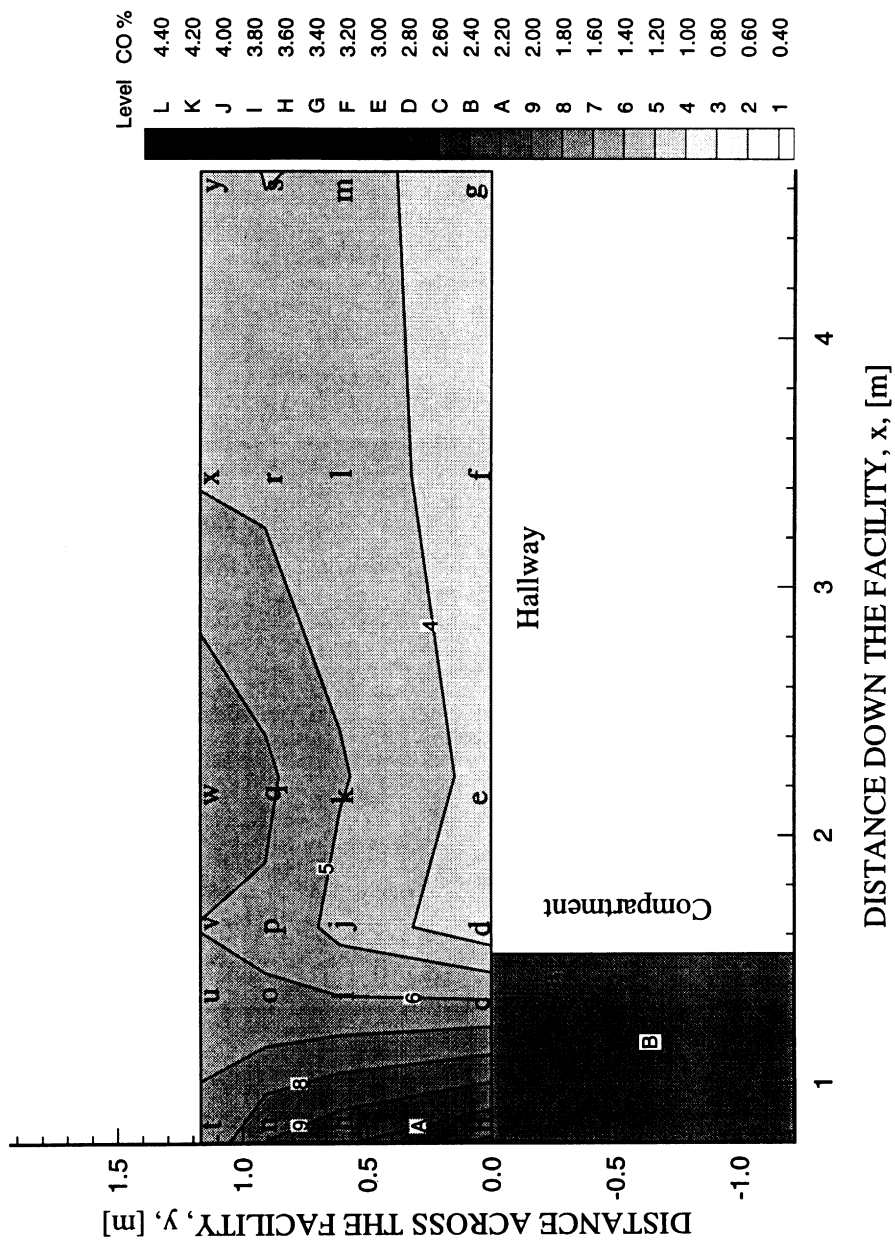


Figure 4.8 The wet CO concentration distribution 0.05 m below the ceiling 16-20 seconds after flashover in *n*-hexane fire experiments with a 0.04 m² opening, 0.20 m inlet soffit, 0.60 m exit soffit and no external burning.

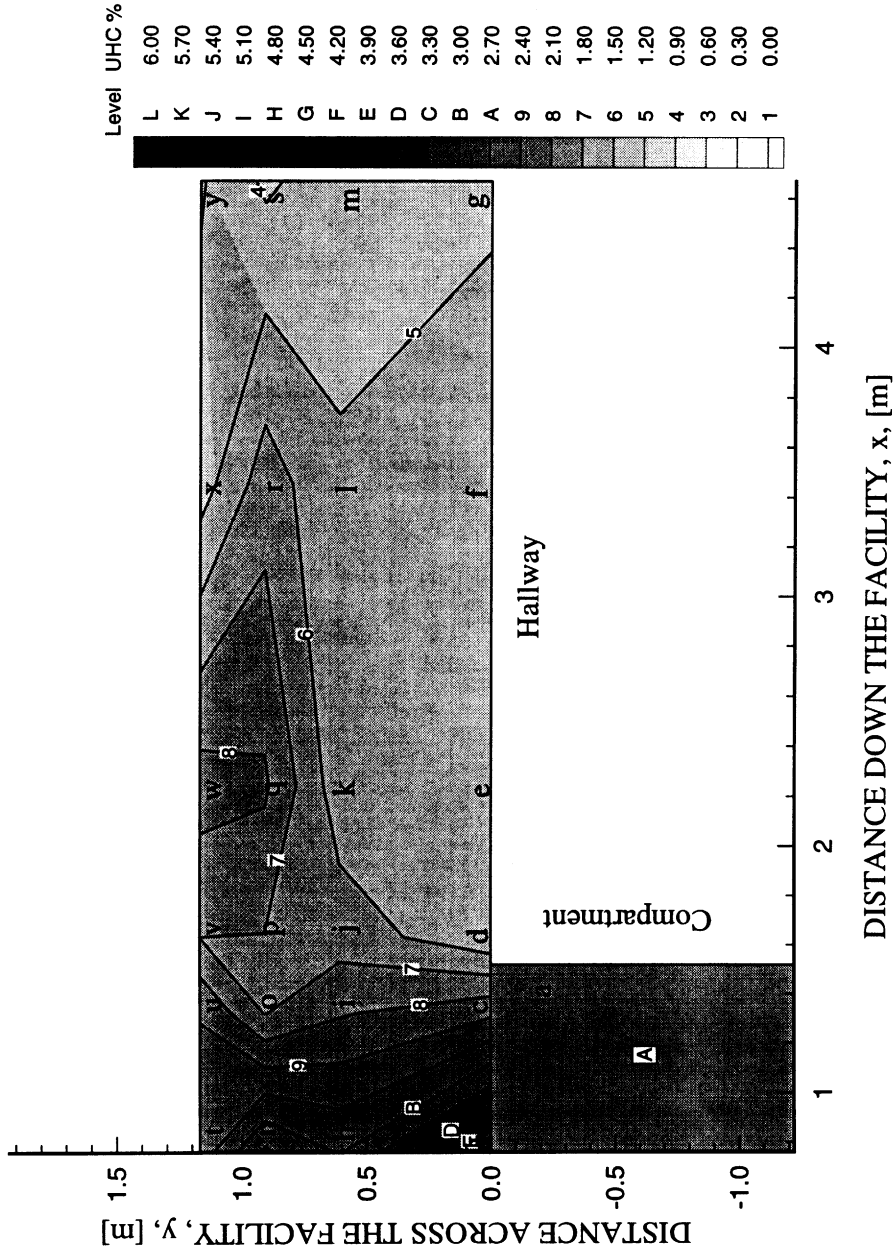


Figure 4.9 The wet UHC concentration distribution 0.05 m below the ceiling 16-20 seconds after flashover in *n*-hexane fire experiments with a 0.04 m² opening, 0.20 m inlet soffit, 0.60 m exit soffit and no external burning.

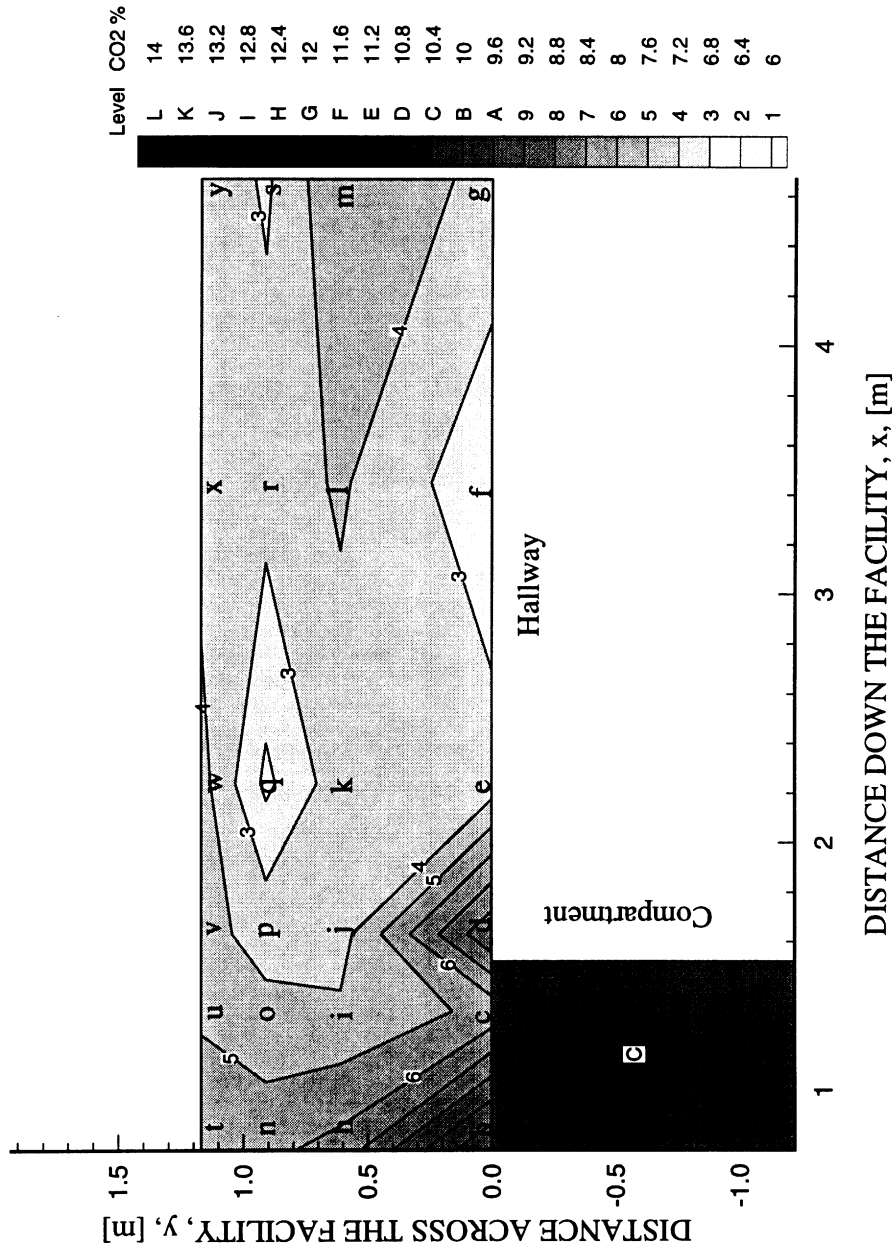


Figure 4.10 The wet CO₂ concentration distribution 0.05 m below the ceiling 16-20 seconds after flashover in *n*-hexane fire experiments with a 0.04 m² opening, 0.20 m inlet soffit, 0.60 m exit soffit and no external burning.

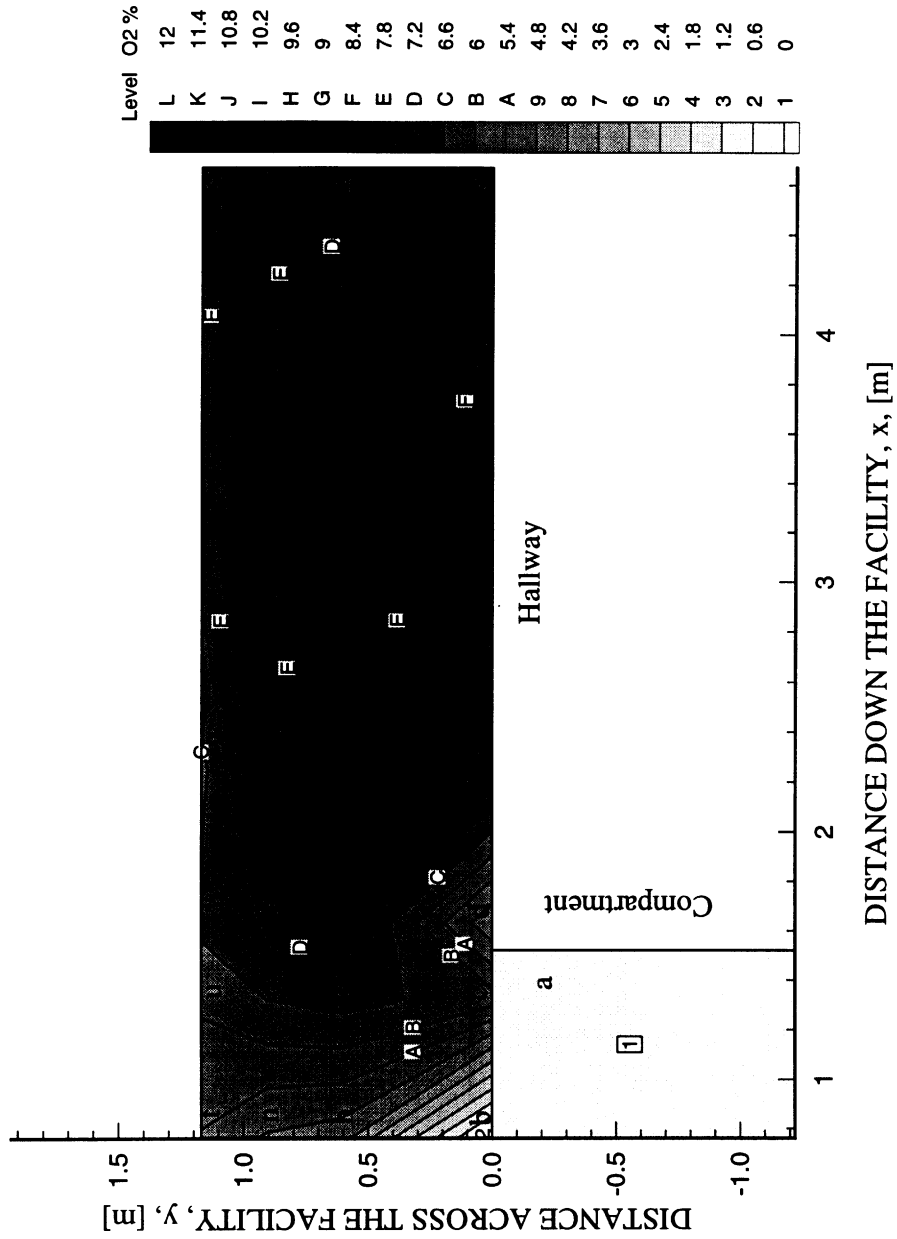


Figure 4.11 The wet O₂ concentration distribution 0.05 m below the ceiling 16-20 seconds after flashover in *n*-hexane fire experiments with a 0.04 m² opening, 0.20 m inlet soffit, 0.60 m exit soffit and no external burning.

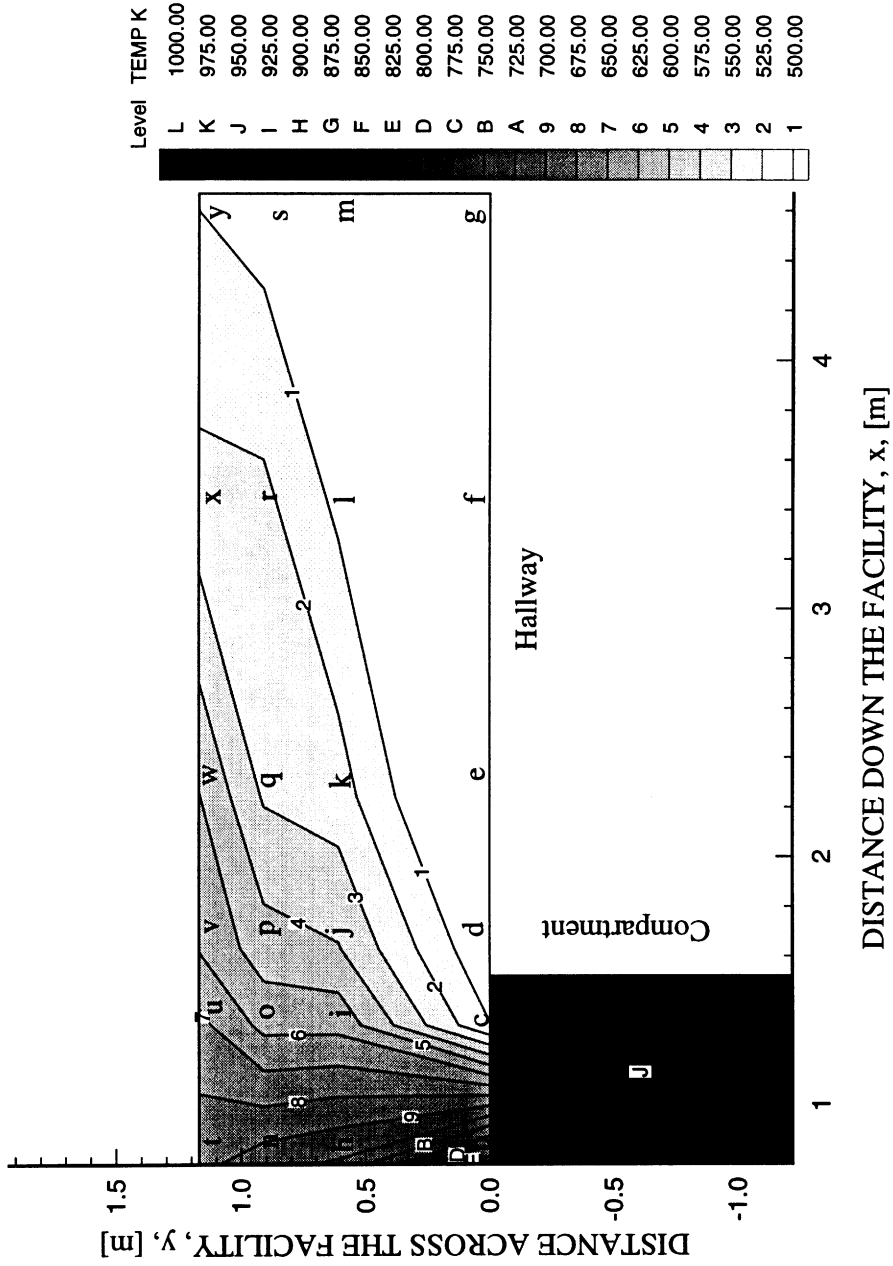


Figure 4.12 The temperature distribution 0.05 m below the ceiling 16-20 seconds after flashover in *n*-hexane fire experiments with a 0.04 m² opening, 0.20 m inlet soffit, 0.60 m exit soffit and no external burning.

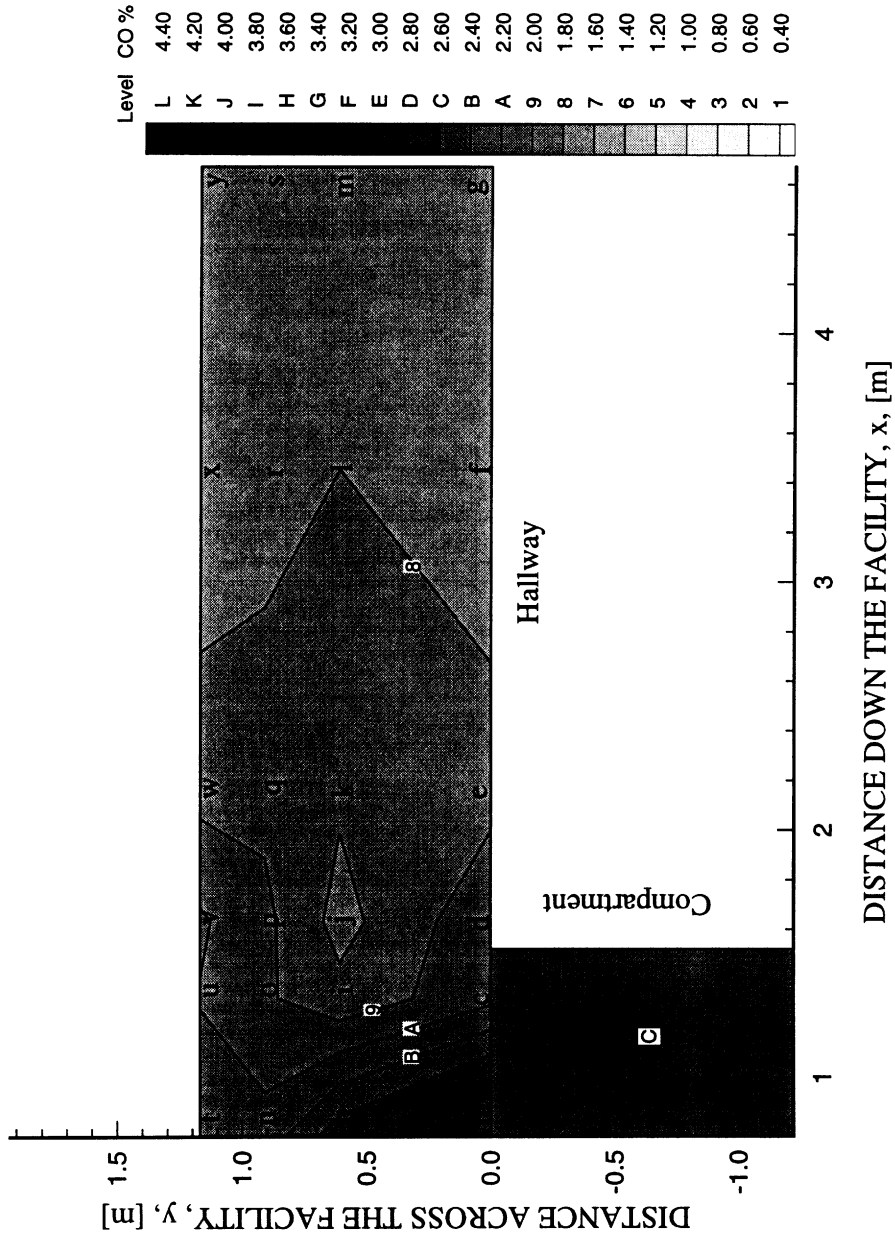


Figure 4.13 The wet CO concentration distribution 0.05 m below the ceiling 40–44 seconds after flashover in *n*-hexane fire experiments with a 0.04 m² opening, 0.20 m inlet soffit, 0.60 m exit soffit and no external burning.

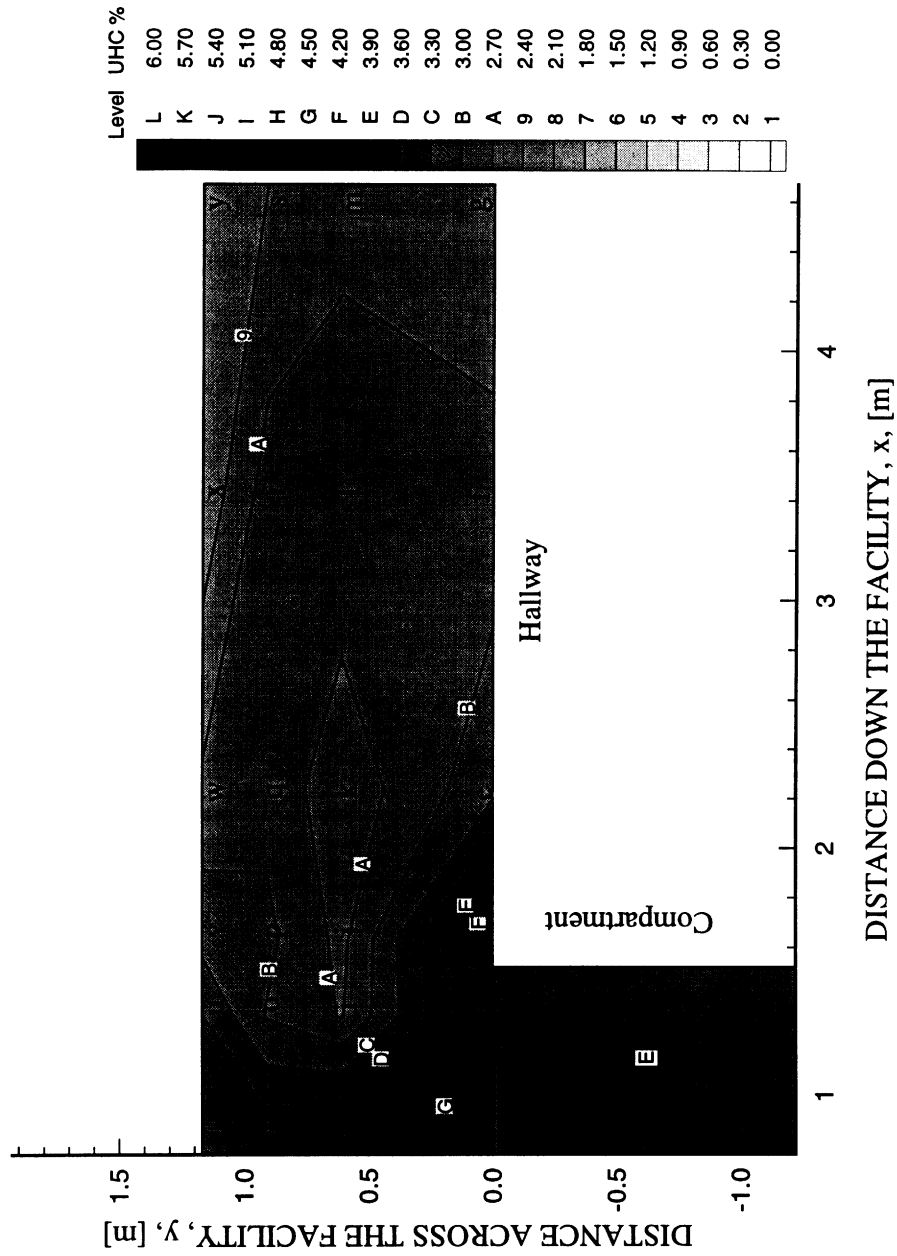


Figure 4.14 The wet UHC concentration distribution 0.05 m below the ceiling 40-44 seconds after flashover in *n*-hexane fire experiments with a 0.04 m² opening, 0.20 m inlet soffit, 0.60 m exit soffit and no external burning.

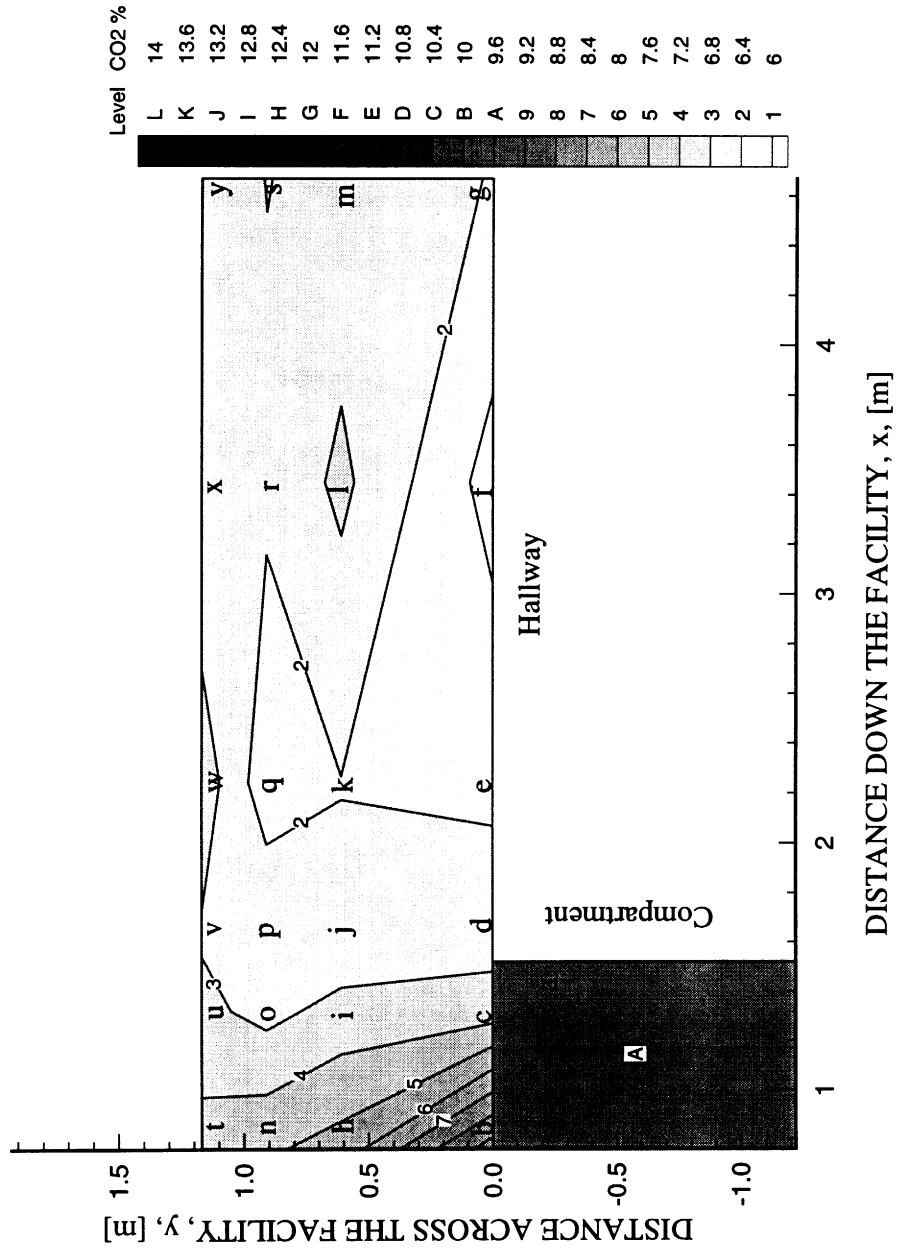


Figure 4.15 The wet CO₂ concentration distribution 0.05 m below the ceiling 40-44 seconds after flashover in *n*-hexane fire experiments with a 0.04 m² opening, 0.20 m inlet soffit, 0.60 m exit soffit and no external burning.

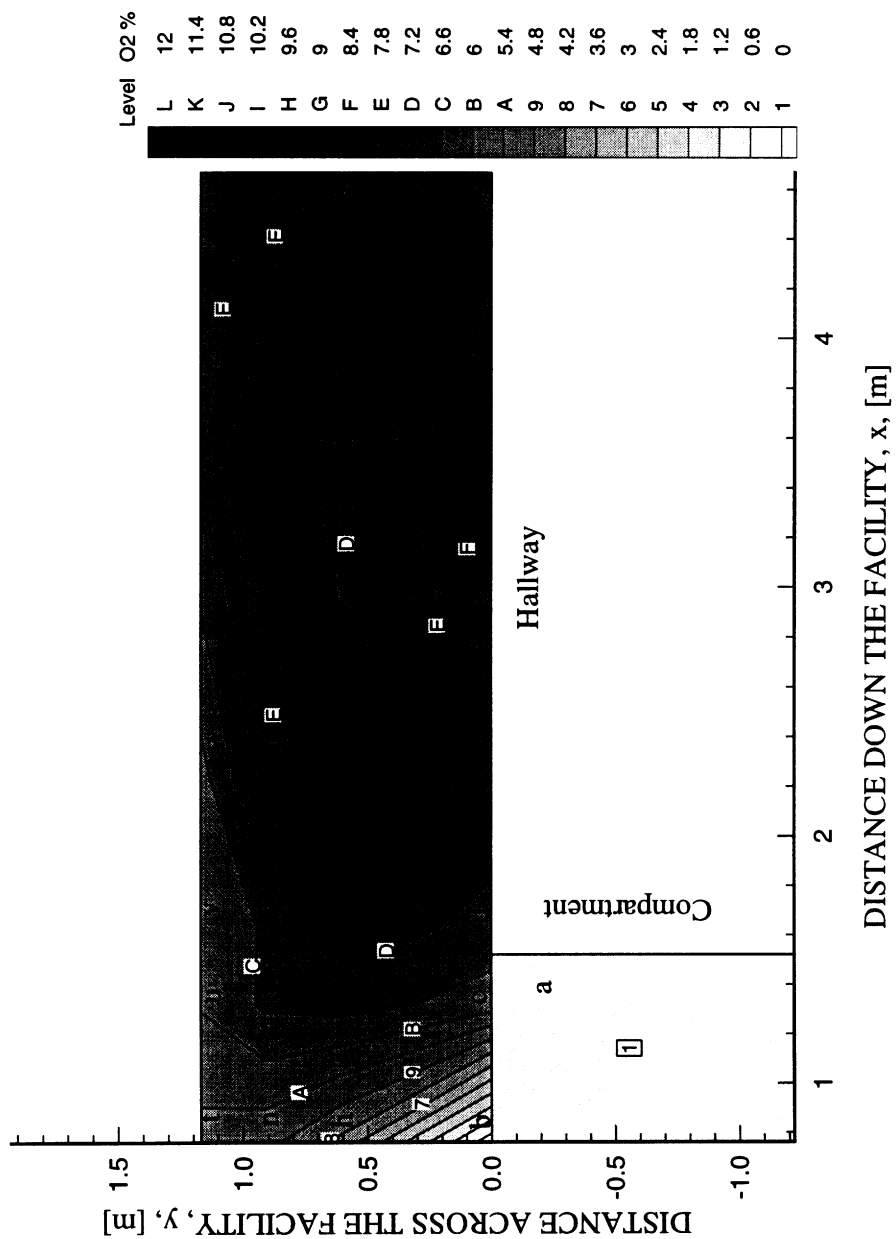


Figure 4.16 The wet O₂ concentration distribution 0.05 m below the ceiling 40-44 seconds after flashover in *n*-hexane fire experiments with a 0.04 m² opening, 0.20 m inlet soffit, 0.60 m exit soffit and no external burning.

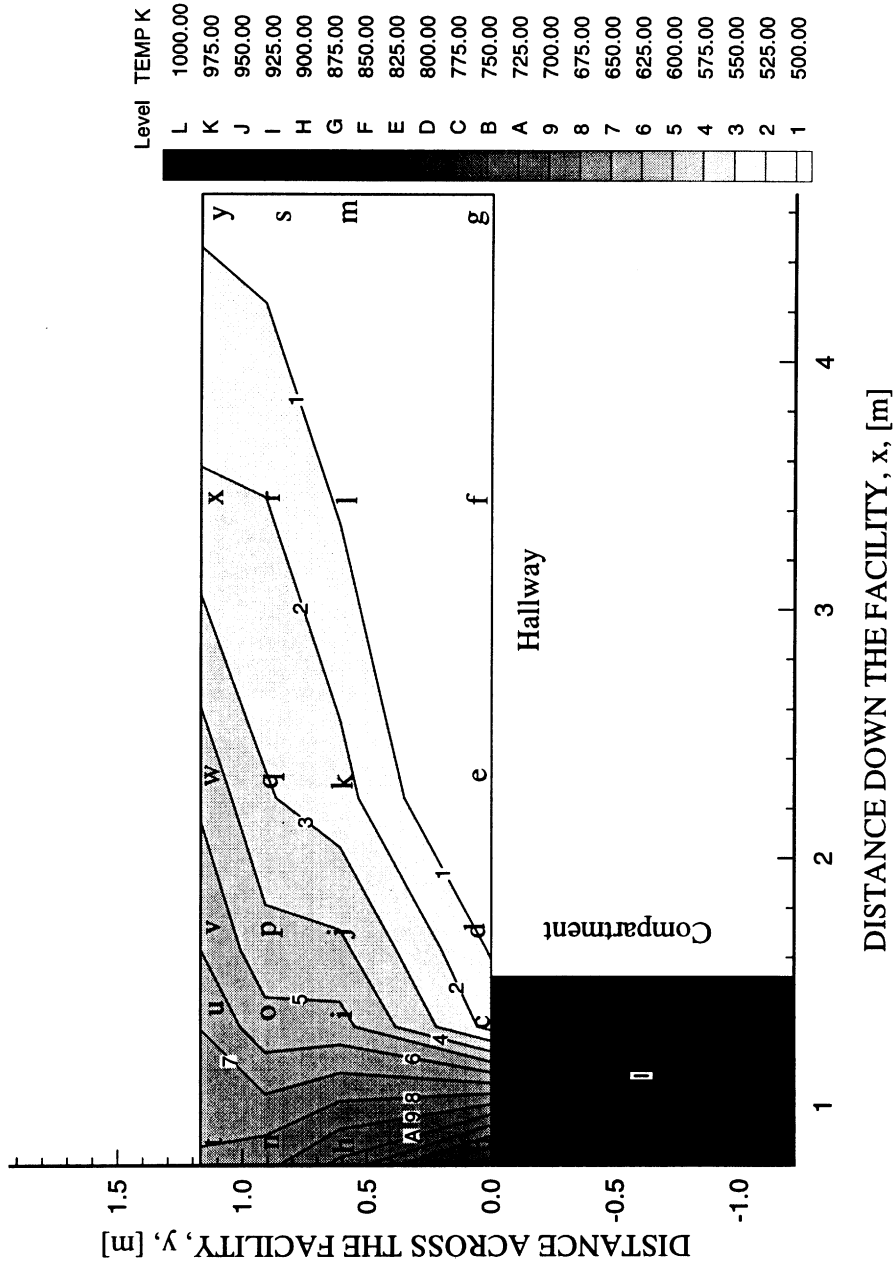


Figure 4.17 The temperature distribution 0.05 m below the ceiling 40-44 seconds after flashover in *n*-hexane fire experiments with a 0.04 m² opening, 0.20 m inlet soffit, 0.60 m exit soffit and no external burning.

the hallway. The species concentrations and temperatures within the hallway upper-layer at 40-44 seconds after flashover were measured to be relatively constant ($\pm 5\%$) until the end of the post-flashover period at 112-116 seconds.

The hallway upper-layer is considered to be in steady-state between 40 and 112 seconds after flashover since minimal changes in the species concentrations and temperatures were measured during this time period.

The exposure time,

$$t_{exp} = \left(\frac{197(COHb)}{CO^{0.858}} \right)^{1.587} \quad [\text{min}] \quad (4.1)$$

where;

t_{exp} - exposure time, [minutes]

$COHb$ - carboxyhemoglobin level in the blood, [%]

CO - level of carbon monoxide exposure, [ppm],

necessary for a particular concentration of CO (in ppm) to result in a fatally high concentration of carboxyhemoglobin (COHb) in the bloodstream can be estimated by assuming a 50% COHb level causes death (Peterson and Stewart, 1970). The CO concentration (1.9% or 19,000 ppm) measured in the hallway upper-layer gases during steady-state was estimated to result in death after 3.25 minutes of exposure.

4.3.2 Short Transient Time with External Burning

The post-hallway CO yields were measured to be as much as 25% greater than measured in-compartment yields (see Figs. 3.13 and 3.14) for experiments with a deep hallway upper-layer ($1.3 < \gamma < 1.7$) and external burning. In-hallway sampling was performed for experiments with a 0.12 m^2 opening and a 0.60 m exit soffit (0.60 m upper-layer depth and $\gamma = 1.36$) because these experimental conditions resulted in the highest post-hallway CO yields. The measurement species concentrations and temperatures in the hallway was conducted to investigate the effects of external burning on the temporal and spatial distribution of CO. Again, the presence of the 0.60 m exit soffit is anticipated

to result in a short transient time for the species concentrations and temperatures in the hallway.

The alignment of the 25 experiments was again performed using the fire growth parameter. Using 10 experiments as a representative set of the 25 experiments performed for this case, the compartment temperatures during the steady-state of the compartment fire are observed in Fig. 4.18 to be aligned with one another after shifting them in time using the fire growth parameter. The contour plots of measured species concentrations and temperatures in the hallway are presented in the remaining paragraphs of the section.

Gases containing 1.3 % CO and 1.0% UHC were measured in the compartment upper-layer, see Fig. 4.19 and Fig. 4.20, respectively, 12-16 seconds before the onset of flashover inside the compartment. The CO and UHC concentrations were measured to rapidly be diluted upon entering the hallway. The hallway upper-layer was measured to contain a uniform concentration of 8.0% CO₂, see Fig. 4.21. Approximately 7.0% O₂ (see Fig. 4.22) was measured in the upper-layer gases within the hallway. From the plot of measured gas temperatures in the hallway shown in Fig. 4.23, the gas temperature is seen to be less than 750 K at the opening. Temperatures were measured to cool to less than 500 K by the end of the hallway. The measured results shown in Figs. 4.19 - 4.23 are comparable to those measured in experiments with no external burning at this stage of the fire (see Figs. 4.3-4.7).

The beginning of the post-flashover period in the compartment occurred approximately 16-20 seconds after the onset of flashover. The species concentrations and temperatures of the gases in the hallway begin to change rapidly in a manner similar to that seen in experiments with no external burning, see Figs. 4.8-4.12. Non-uniform concentrations of CO and UHC were measured to be present in the hallway. The gases traveling on the side of the hallway opposite the compartment were measured to contain CO levels of 1.6%, see Fig. 4.24, while gases on the compartment side of the hallway contained 0.9% CO. The gases on the side of the hallway opposite the compartment also

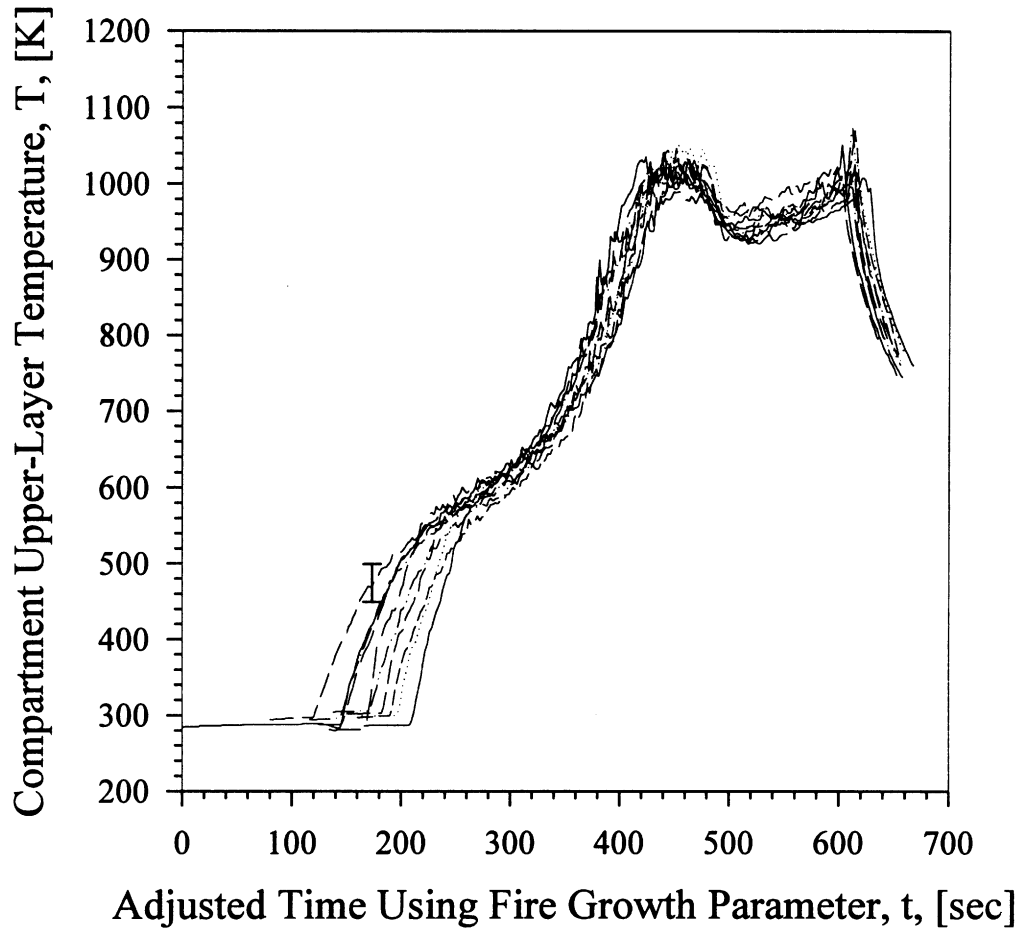


Figure 4.18 The temperature 0.05 m below the ceiling inside the compartment in 10 different *n*-hexane fire experiments with a 0.12 m² opening, a 0.60 m exit soffit, and external burning in the hallway. The experiments were aligned with one another in time using the fire growth parameter.

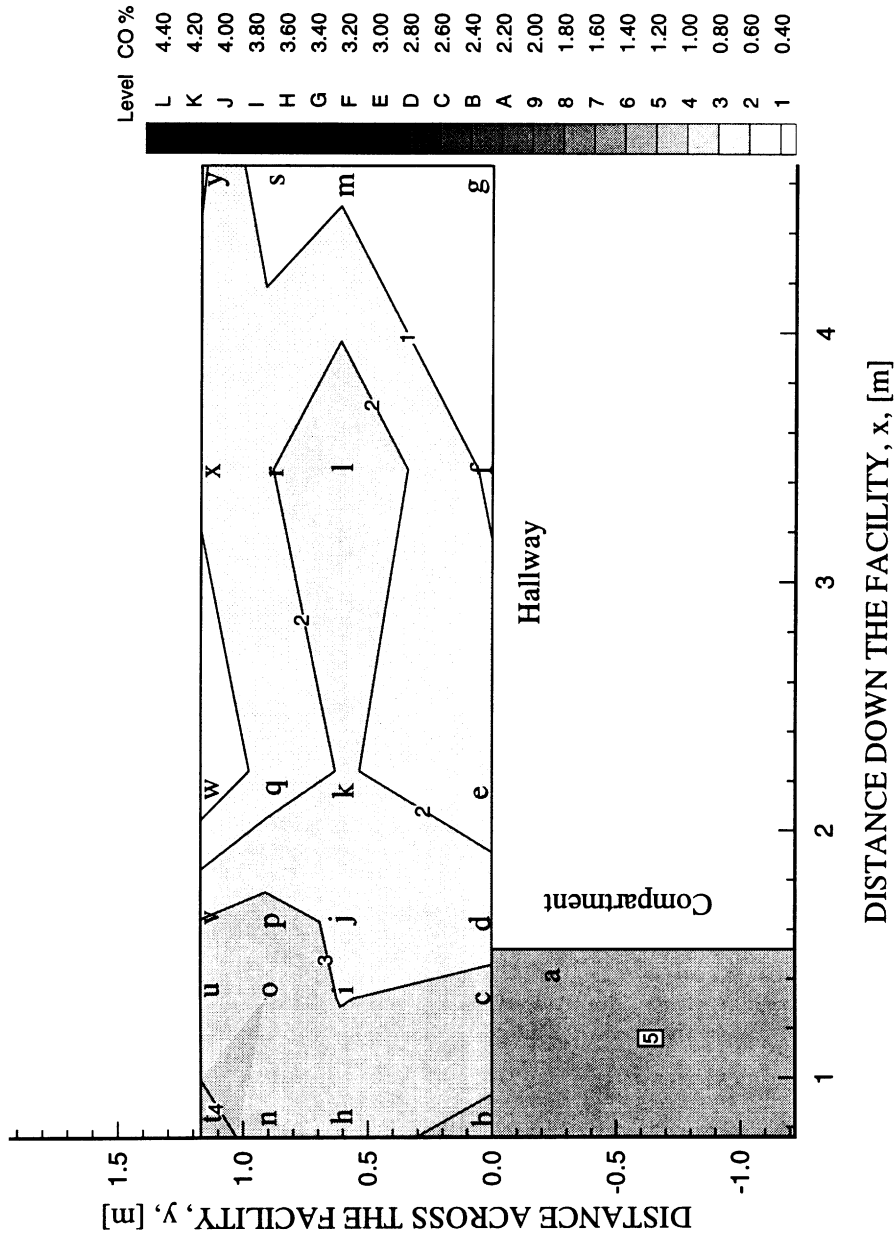


Figure 4.19 The wet CO concentration distribution 0.05 m below the ceiling 12-16 seconds before flashover in *n*-hexane fire experiments with a 0.12 m² opening, 0.20 m inlet soffit, 0.60 m exit soffit and external burning.

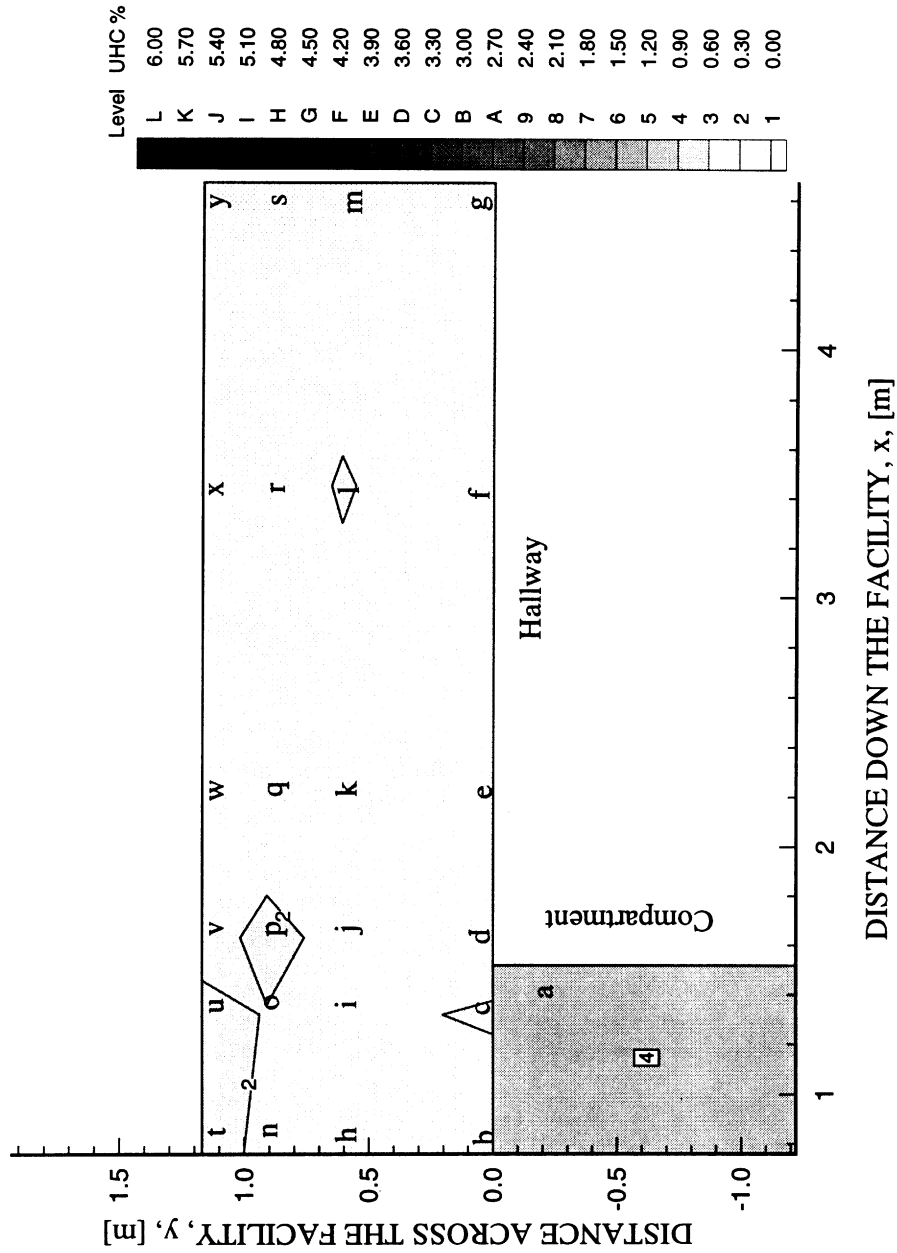


Figure 4.20 The wet UHC concentration distribution 0.05 m below the ceiling 12-16 seconds before flashover in *n*-hexane fire experiments with a 0.12 m² opening, 0.20 m inlet soffit, 0.60 m exit soffit and external burning.

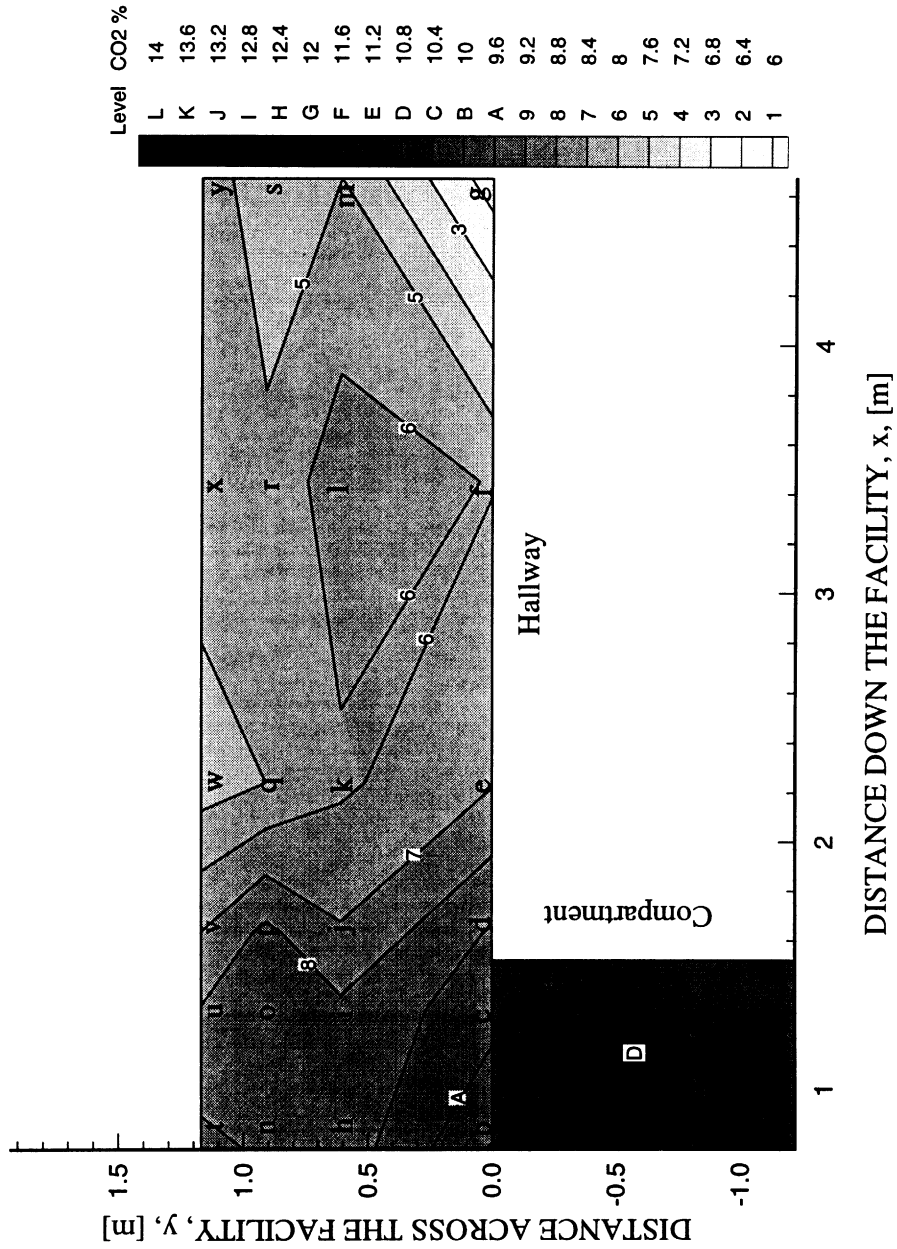


Figure 4.21 The wet CO₂ concentration distribution 0.05 m below the ceiling 12-16 seconds before flashover in *n*-hexane fire experiments with a 0.12 m² opening, 0.20 m inlet soffit, 0.60 m exit soffit and external burning.

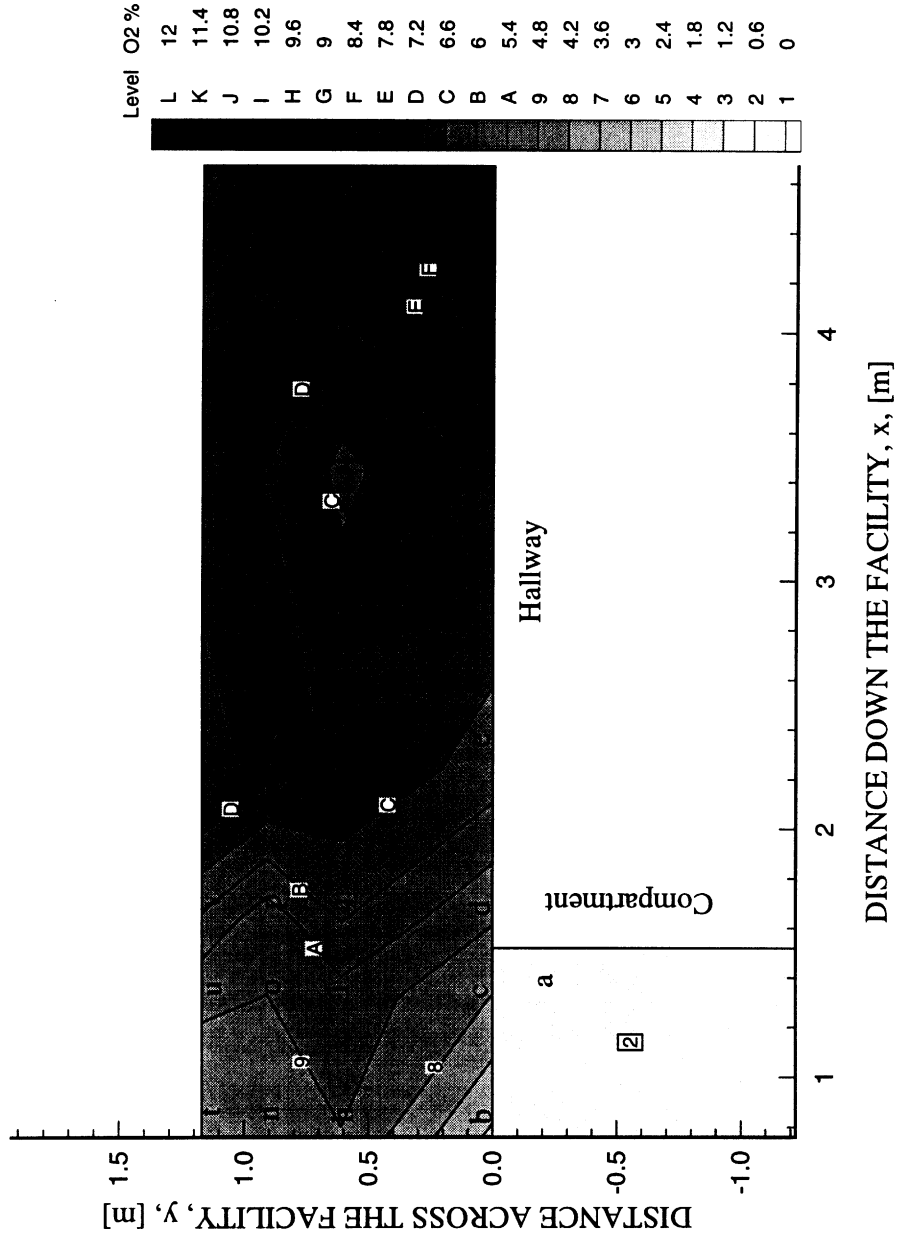


Figure 4.22 The wet O₂ concentration distribution 0.05 m below the ceiling 12-16 seconds before flashover in *n*-hexane fire experiments with a 0.12 m² opening, 0.20 m inlet soffit, 0.60 m exit soffit and external burning.

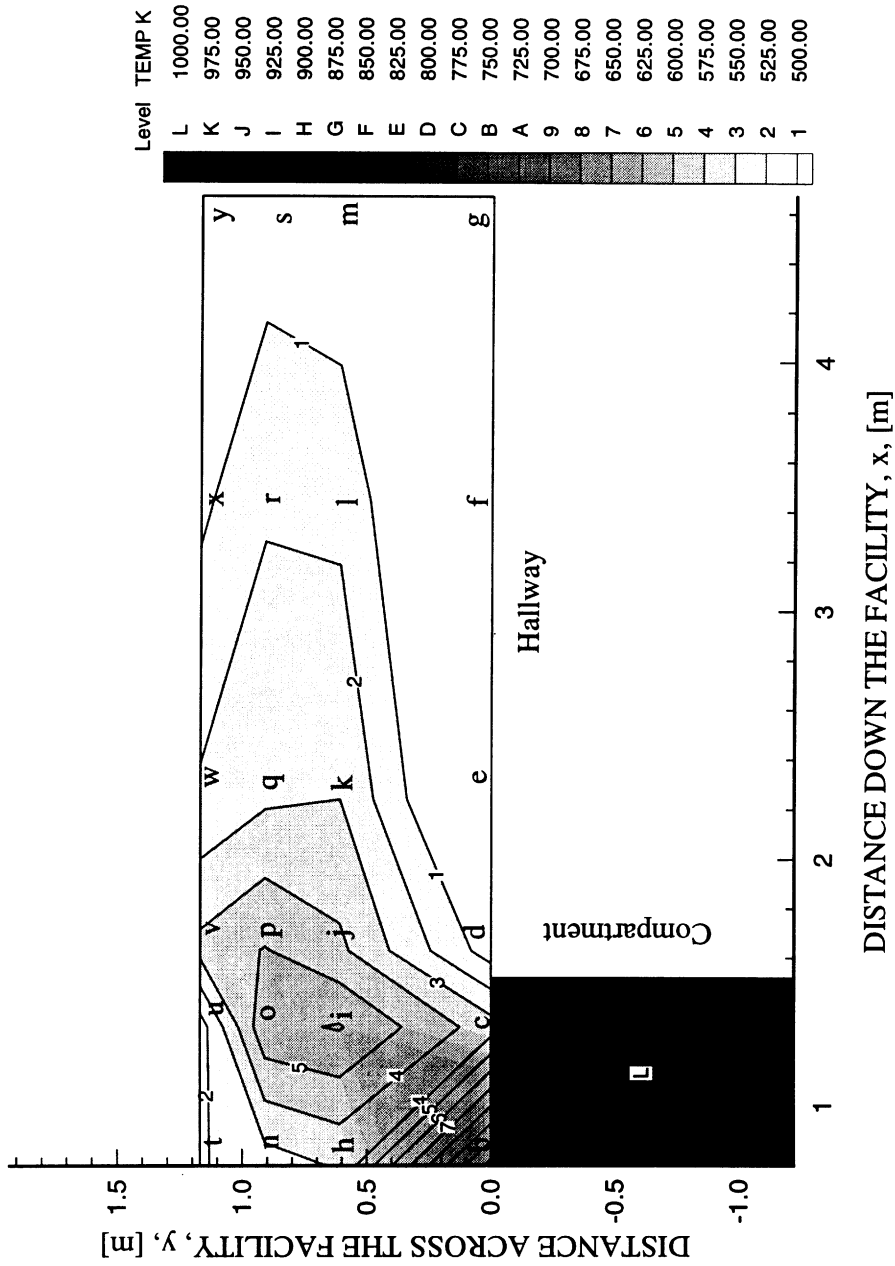


Figure 4.23 The temperature distribution 0.05 m below the ceiling 12-16 seconds before flashover in *n*-hexane fire experiments with a 0.12 m² opening, 0.20 m inlet soffit, 0.60 m exit soffit and external burning.

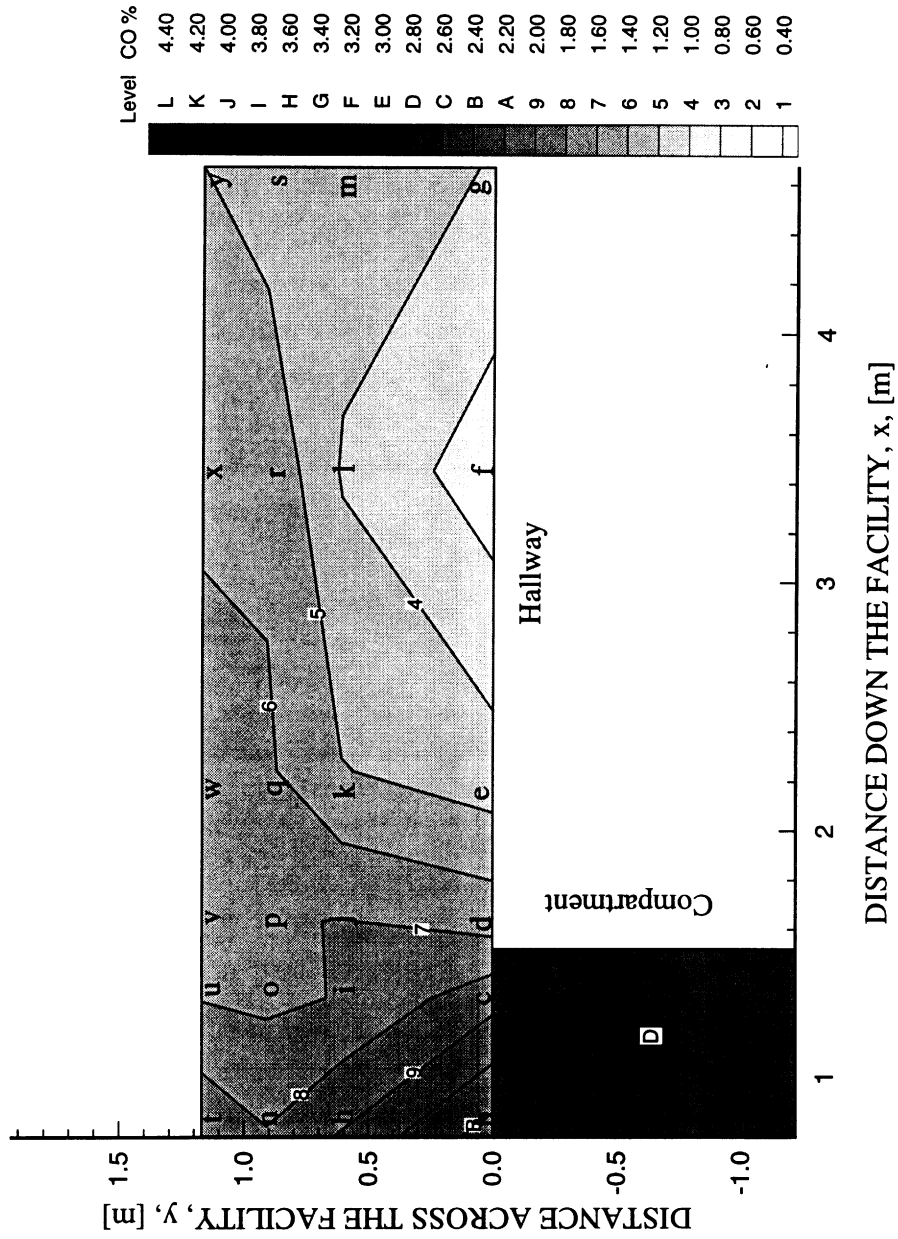


Figure 4.24 The wet CO concentration distribution 0.05 m below the ceiling 16-20 seconds after flashover in *n*-hexane fire experiments with a 0.12 m² opening, 0.20 m inlet soffit, 0.60 m exit soffit and external burning.

contained higher UHC concentrations (1.3%) compared with the UHC levels (0.7%) in the gases on the compartment side of the hallway, see Fig. 4.25. Plots of the measured CO₂ and O₂ concentrations are seen in Figs. 4.26 and 4.27. Approximately 8.7% CO₂ and 4.8% O₂ were measured to be relatively uniform within the hallway upper-layer. The gas temperatures were measured to be slightly higher in magnitude (see Fig. 4.28) compared with levels at the 16-20 before flashover (see Fig. 4.23).

Just prior to the onset of external burning, all species concentrations were measured to be uniform within the hallway 44-48 seconds after flashover, see Figs. 4.29-4.32. The steady-state is observed 60 seconds after gases containing greater than 1% CO were measured entering the hallway. The plot of the measured CO and UHC concentrations is seen in Figs. 4.29 and 4.30, respectively. Upper-layer gases downstream of the compartment were measured to contain 2.3% CO and 2.5% UHC (see Fig. 4.29 and 4.30, respectively). Concentrations of approximately 8.5% CO₂ and 3.6% O₂ were also measured to be uniform within the upper-layer, see Fig. 4.31 and Fig. 4.32, respectively. Gas temperatures were measured to be 825 K at the opening (see Fig. 4.33), but were only 500 K at the exit of the hallway.

To this point, the species concentrations and temperatures of the gases within the hallway are similar to that observed in experiments without external burning. This is expected since the global equivalence ratio and the mass flow of the gases into the hallway was similar in the two experiments.

External burning occurred in the hallway 50-60 seconds after flashover. The burning was difficult to observe, since it was almost entirely surrounded by the dark upper-layer of combustion gases already present in the hallway. Burning gases were observed crossing the hallway and traveling along the wall opposite the compartment for approximately 2.0 m. External burning was observed to be attached to the vent.

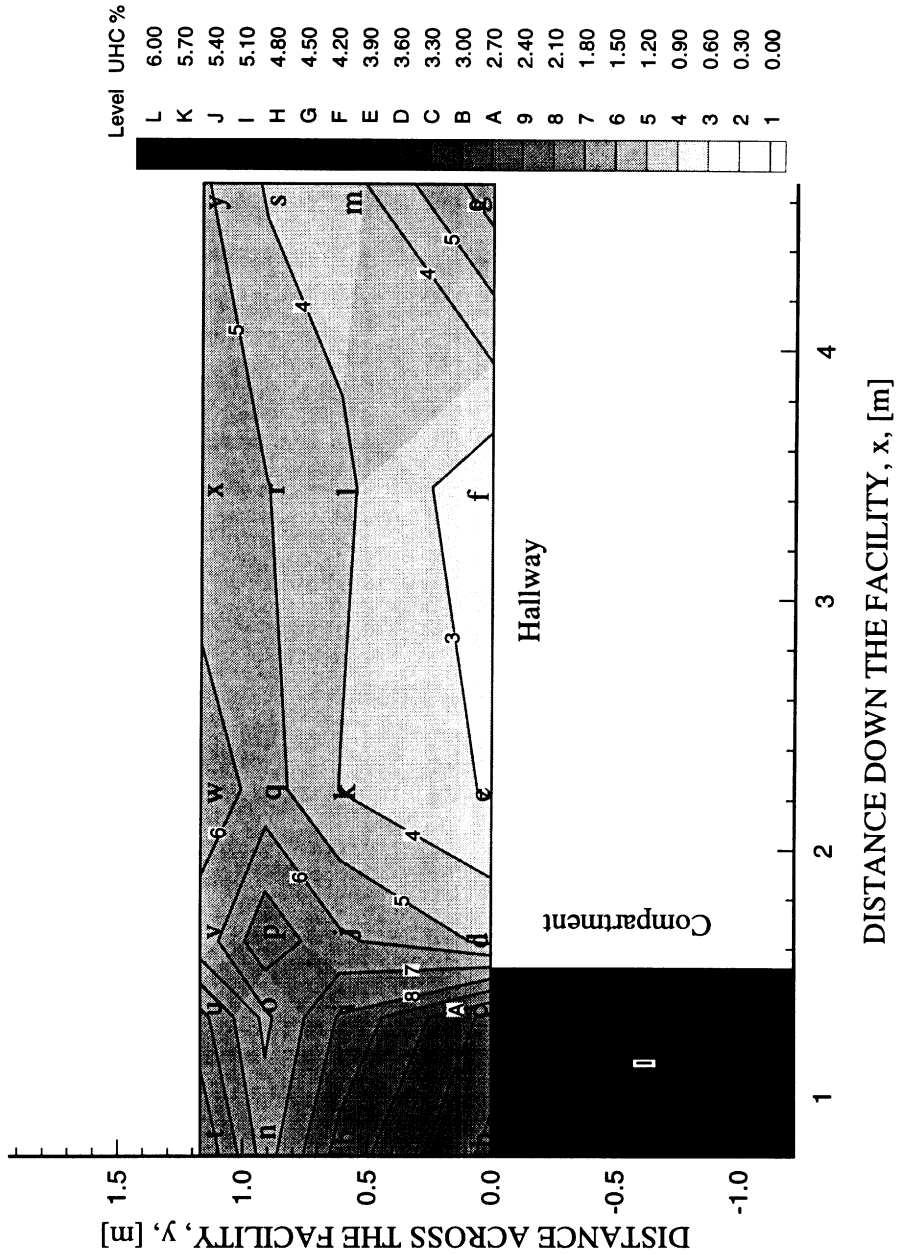


Figure 4.25 The wet UHC concentration distribution 0.05 m below the ceiling 16-20 seconds after flashover in *n*-hexane fire experiments with a 0.12 m² opening, 0.20 m inlet soffit, 0.60 m exit soffit and external burning..

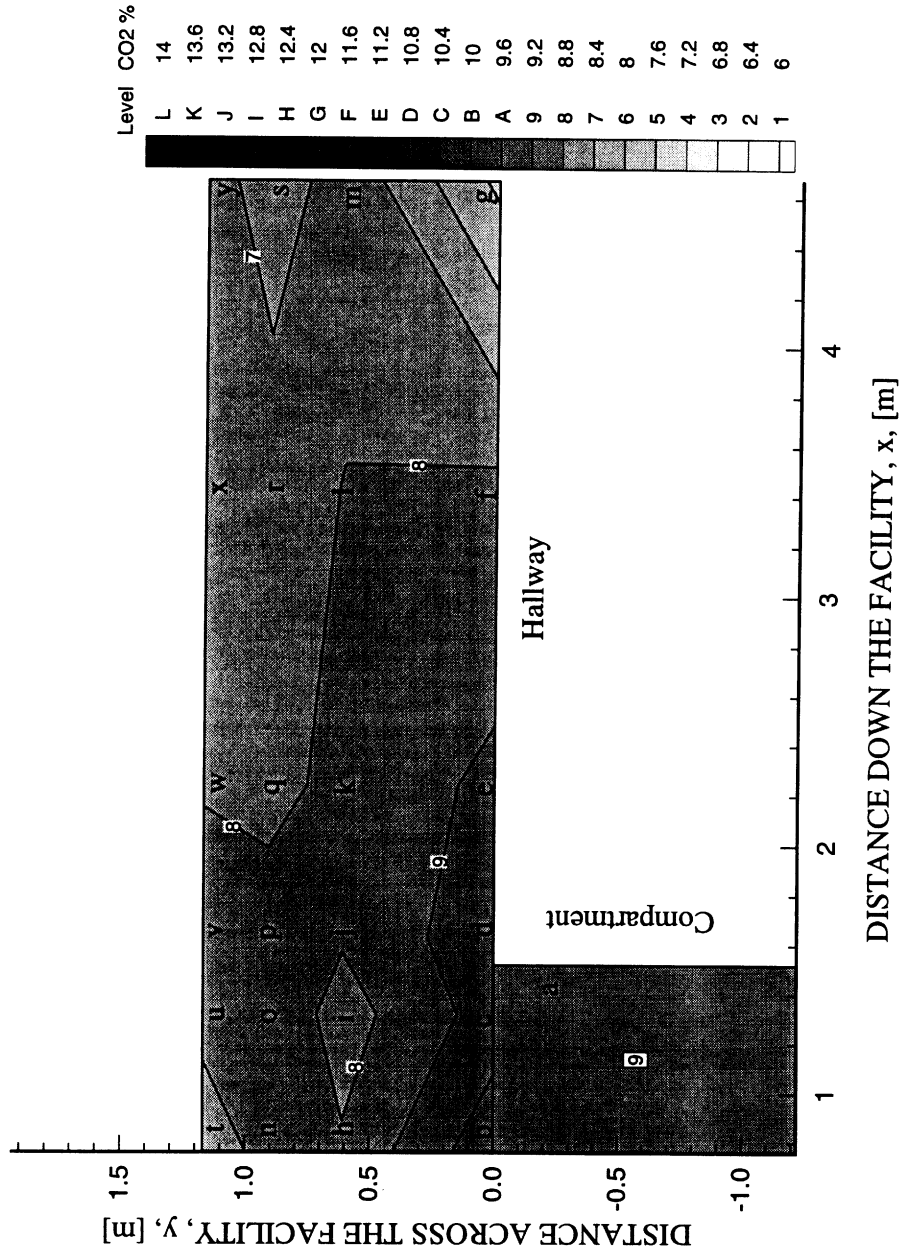


Figure 4.26 The wet CO₂ concentration distribution 0.05 m below the ceiling 16-20 seconds after flashover in *n*-hexane fire experiments with a 0.12 m² opening, 0.20 m inlet soffit, 0.60 m exit soffit and external burning.

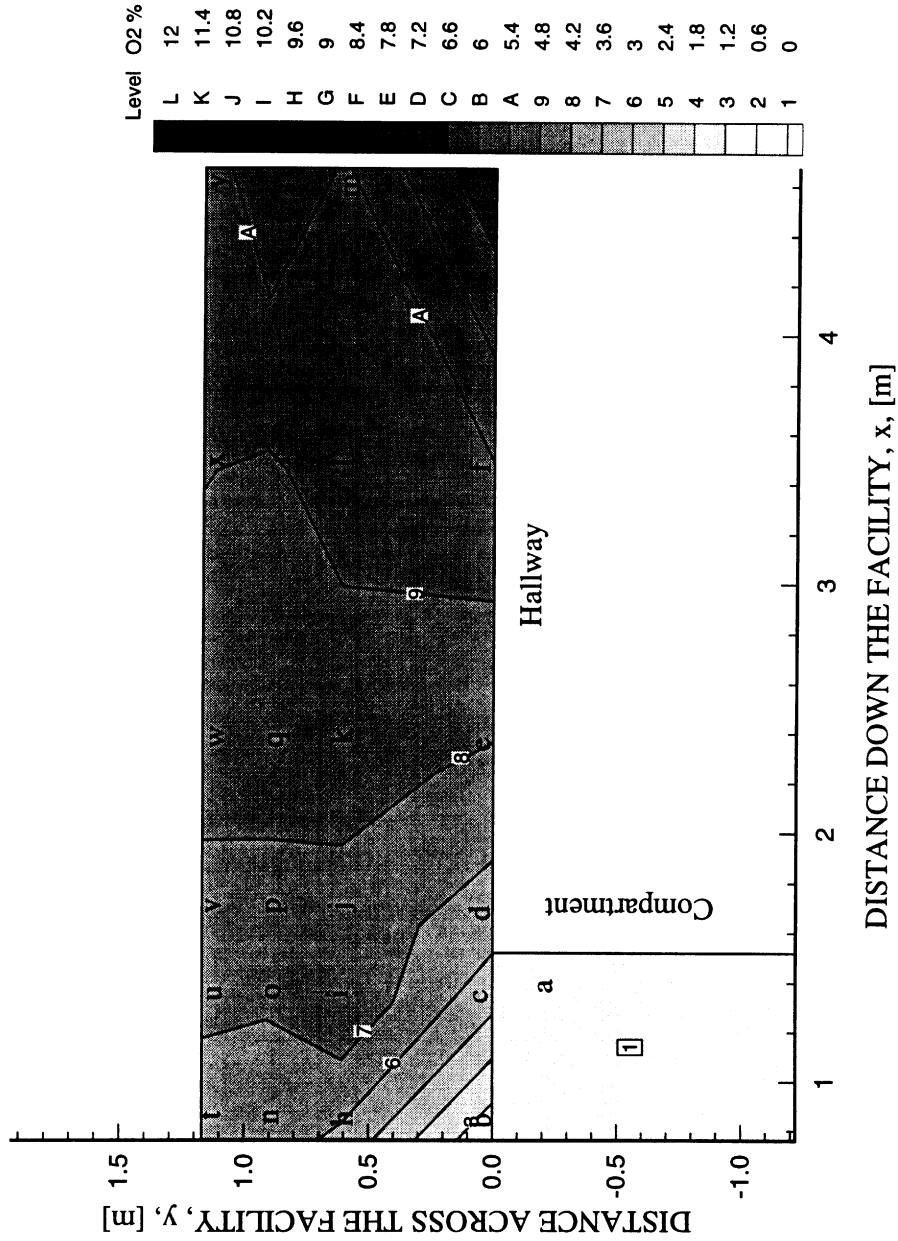


Figure 4.27 The wet O₂ concentration distribution 0.05 m below the ceiling 16-20 seconds after flashover in *n*-hexane fire experiments with a 0.12 m² opening, 0.20 m inlet soffit, 0.60 m exit soffit and external burning.

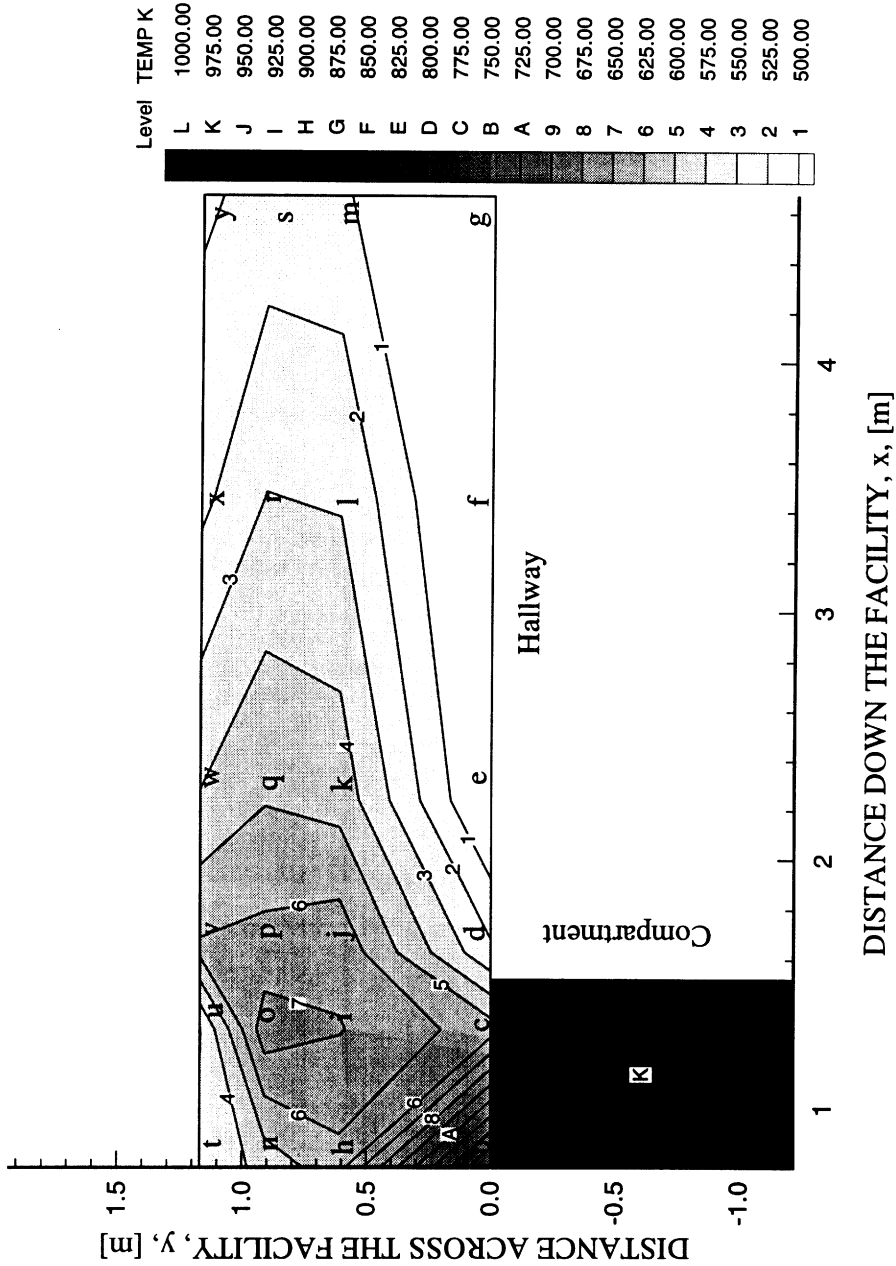


Figure 4.28 The temperature distribution 0.05 m below the ceiling 16-20 seconds after flashover in *n*-hexane fire experiments with a 0.12 m² opening, 0.20 m inlet soffit, 0.60 m exit soffit and external burning.

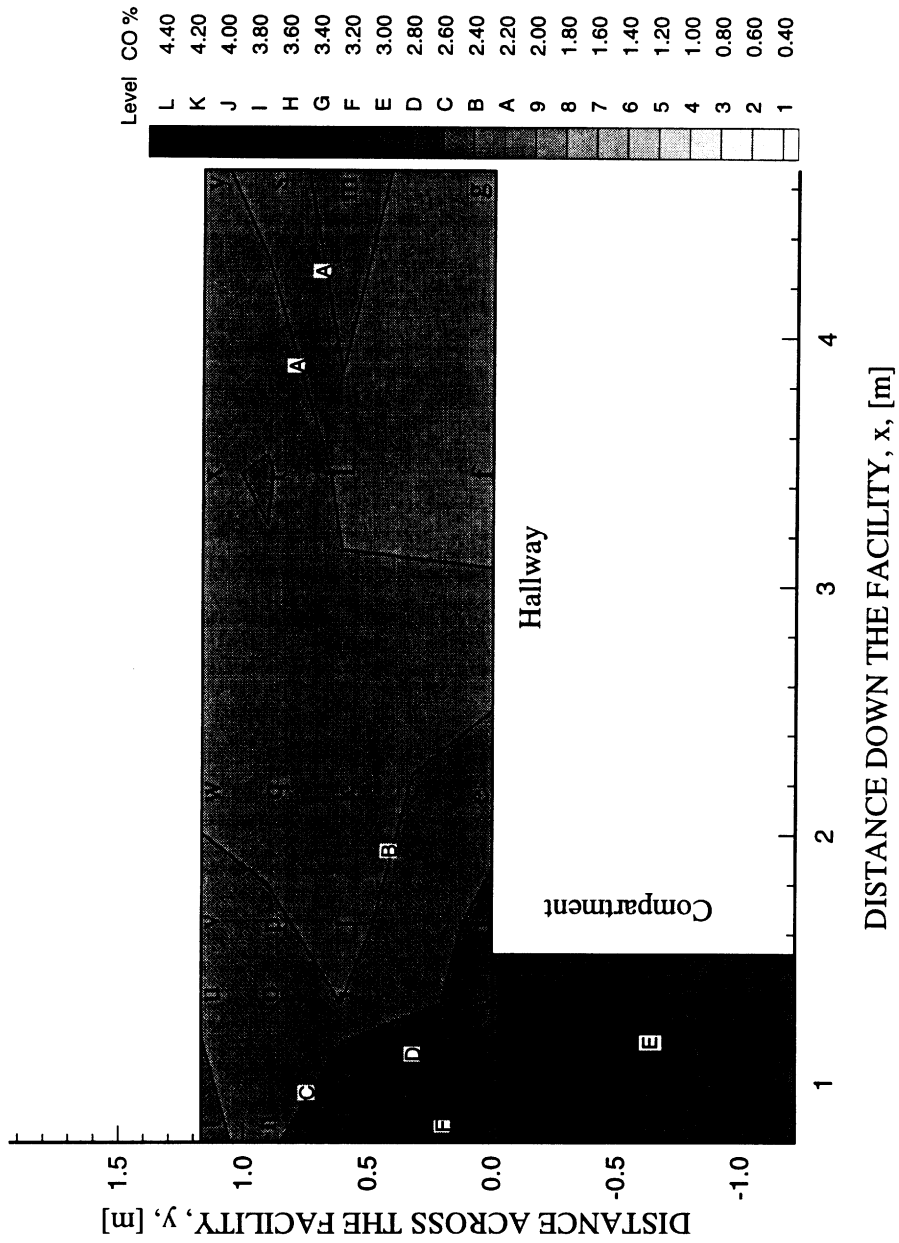


Figure 4.29 The wet CO concentration distribution 0.05 m below the ceiling 44-48 seconds after flashover in *n*-hexane fire experiments with a 0.12 m² opening, 0.20 m inlet soffit, 0.60 m exit soffit and external burning.

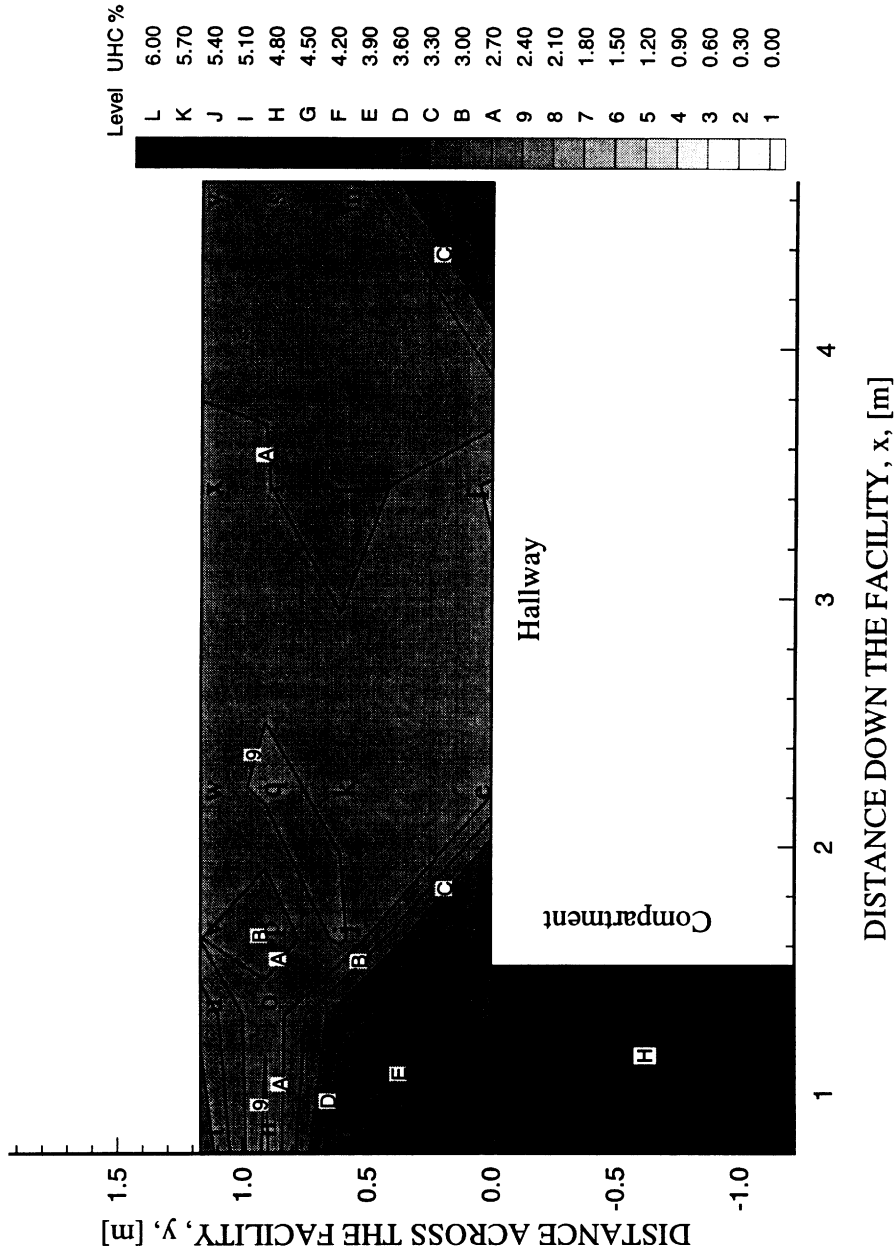


Figure 4.30 The wet UHC concentration distribution 0.05 m below the ceiling 44-48 seconds after flashover in *n*-hexane fire experiments with a 0.12 m² opening, 0.20 m inlet soffit, 0.60 m exit soffit and external burning.

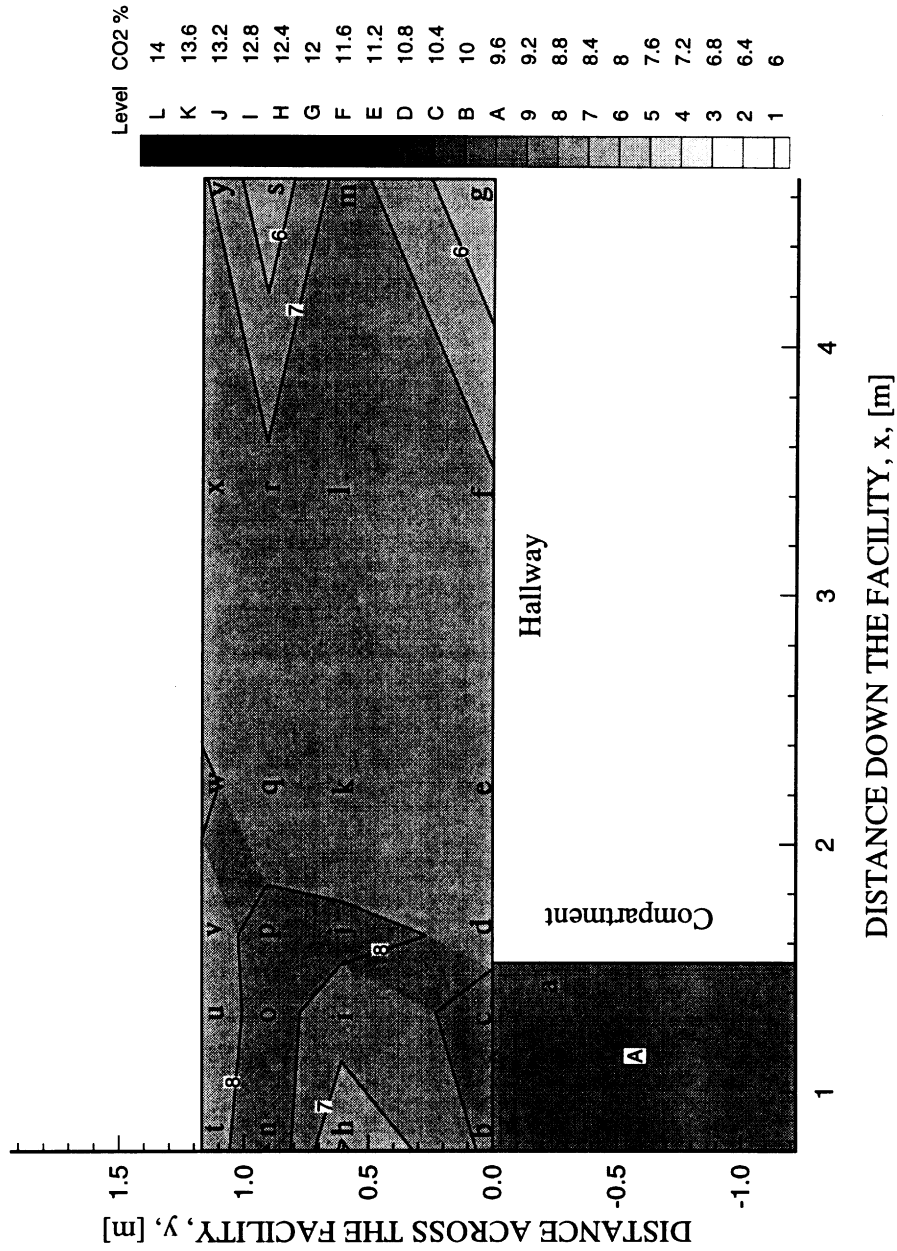


Figure 4.31 The wet CO₂ concentration distribution 0.05 m below the ceiling 44–48 seconds after flashover in *n*-hexane fire experiments with a 0.12 m² opening, 0.20 m inlet soffit, 0.60 m exit soffit and external burning.

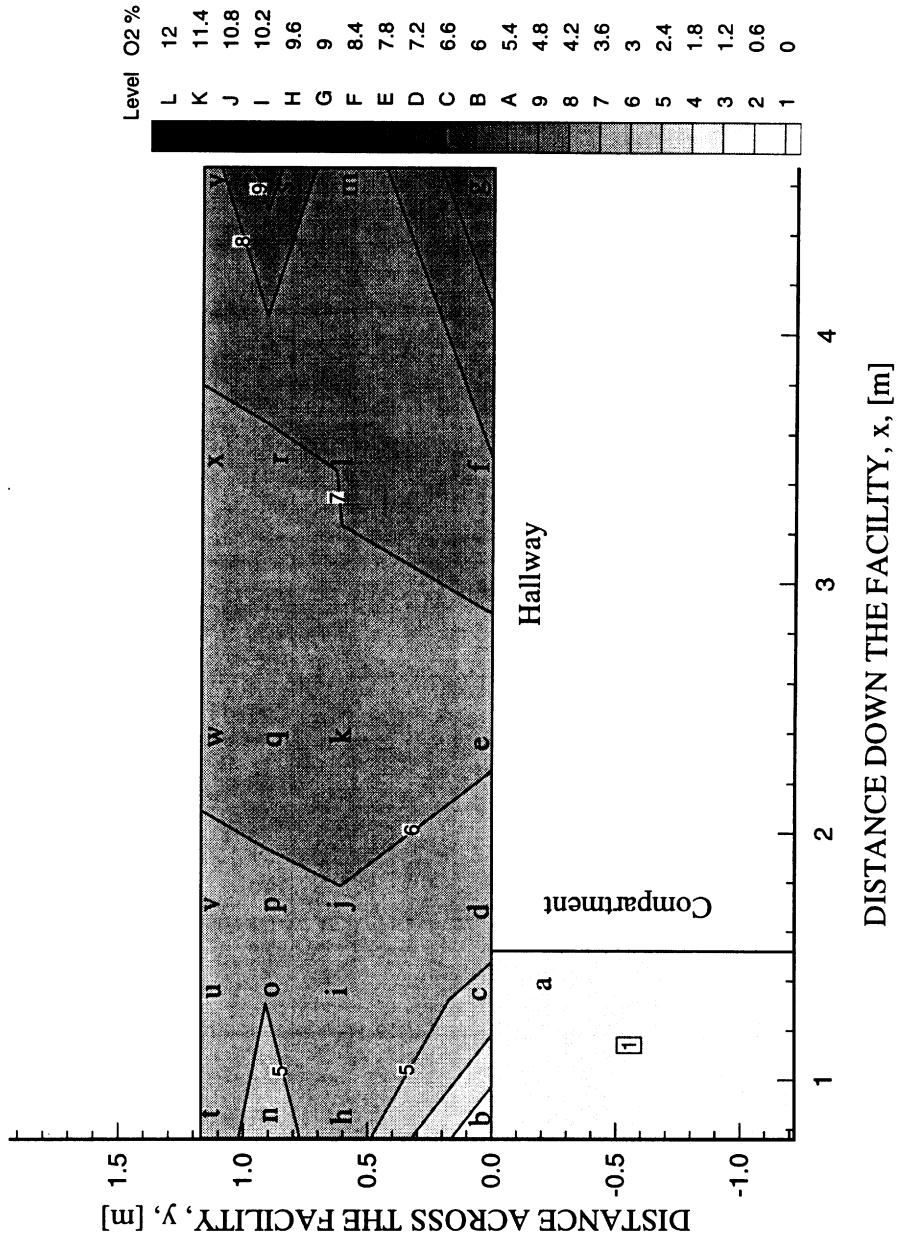


Figure 4.32 The wet O₂ concentration distribution 0.05 m below the ceiling 44-48 seconds after flashover in *n*-hexane fire experiments with a 0.12 m² opening, 0.20 m inlet soffit, 0.60 m exit soffit and external burning.

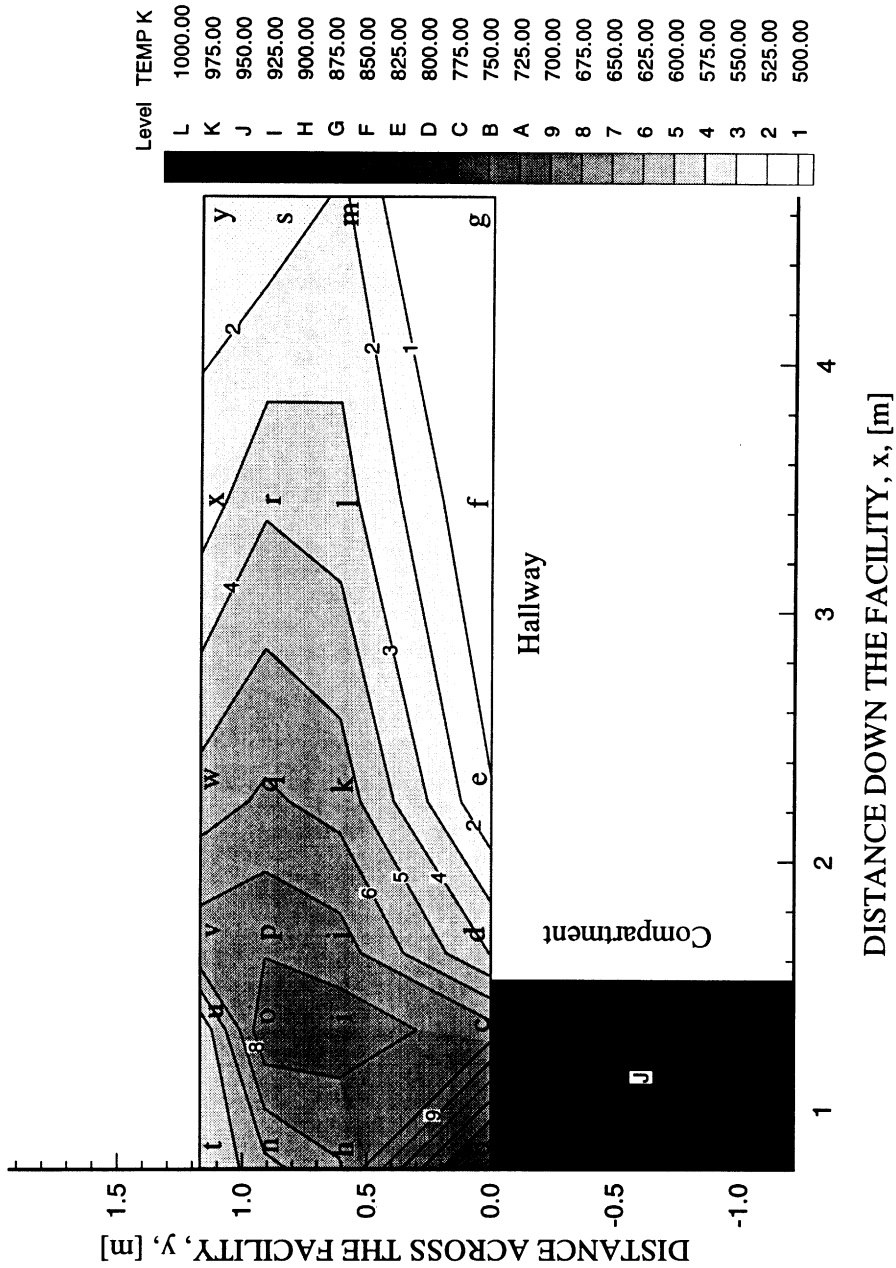


Figure 4.33 The temperature distribution 0.05 m below the ceiling 44-48 seconds after flashover in *n*-hexane fire experiments with a 0.12 m² opening, 0.20 m inlet soffit, 0.60 m exit soffit and external burning.

The effect of external burning on species concentrations and temperatures is evident 72-76 seconds after flashover. The CO concentration was measured to decrease slightly to 2.1% (see Fig. 4.34) on the side of the hallway opposite the compartment where the burning was visually apparent. The concentration of CO on the compartment side of the hallway was, however, measured to be slightly higher at 2.5%. The effect of external burning on the UHC concentration in the hallway is seen in Fig. 4.35. The gases along the side of the hallway opposite the compartment were measured to contain low UHC concentrations (1.5%). The CO₂ concentration of 9.7% was measured in the gases where burning was observed, see Fig. 4.36. The CO₂ concentration was measured to be nearly 1.0% higher than those levels on the compartment side of the hallway. The O₂ concentration in upper-layer gases was measured to gradually increase from 1.2% near the compartment to 3.6% by the end of the hallway, see Fig. 4.37. Note that the concentrations of UHC, CO₂ and O₂ measured on the compartment side of the hallway are approximately equal to the species levels just prior to external burning 44-48 seconds after flashover, see Fig. 4.30-4.32. The oxidation of mainly UHC in the hallway is observed in Fig. 4.38 to result in only a 50 K rise in the upper-layer temperature with levels near the compartment approximately 750 K. These temperatures were typically measured above the flame front and are, therefore, cooler than the flame temperature. Slow response times of the aspirated thermocouples, approximately 1 second, prevented the measurement of the turbulent flame temperature with flames at the thermocouple.

The high CO concentrations was attributed to the oxidation of the UHC. According to Westbrook and Dryer (1984), UHC have a higher rate of reaction with radicals (i.e. H, OH, H₂O, O) compared with CO. Also, the oxidation of UHC forms additional CO. Through the law of mass action, the ratio of the UHC concentration to the CO concentration must be low (i.e. low UHC concentration or high CO concentration) for the oxidation reactions of CO to become competitive. In these experiments, the oxidation of UHC and CO is believed to occur at or very close to the flame front where temperatures

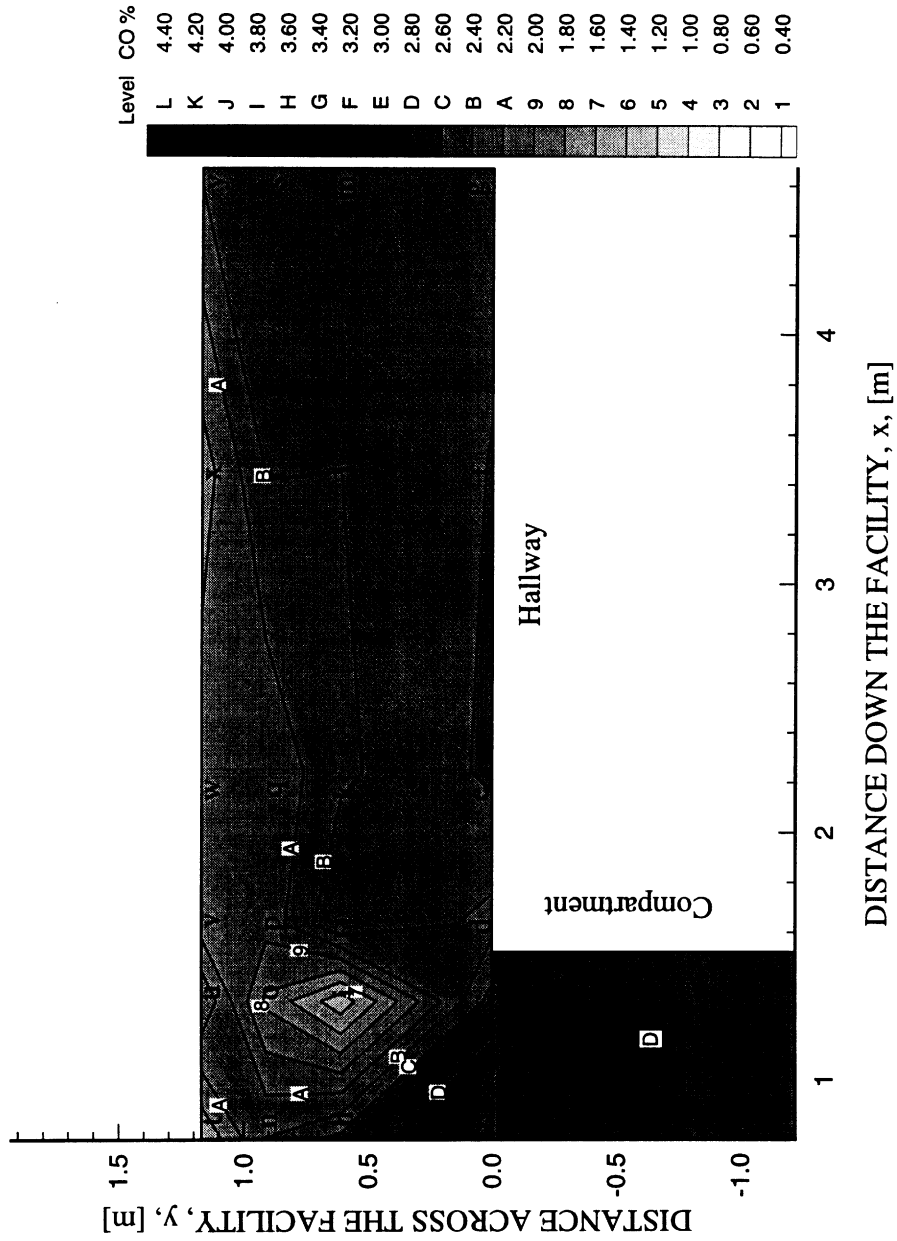


Figure 4.34 The wet CO concentration distribution 0.05 m below the ceiling 72-76 seconds after flashover in *n*-hexane fire experiments with a 0.12 m² opening, 0.20 m inlet soffit, 0.60 m exit soffit and external burning.

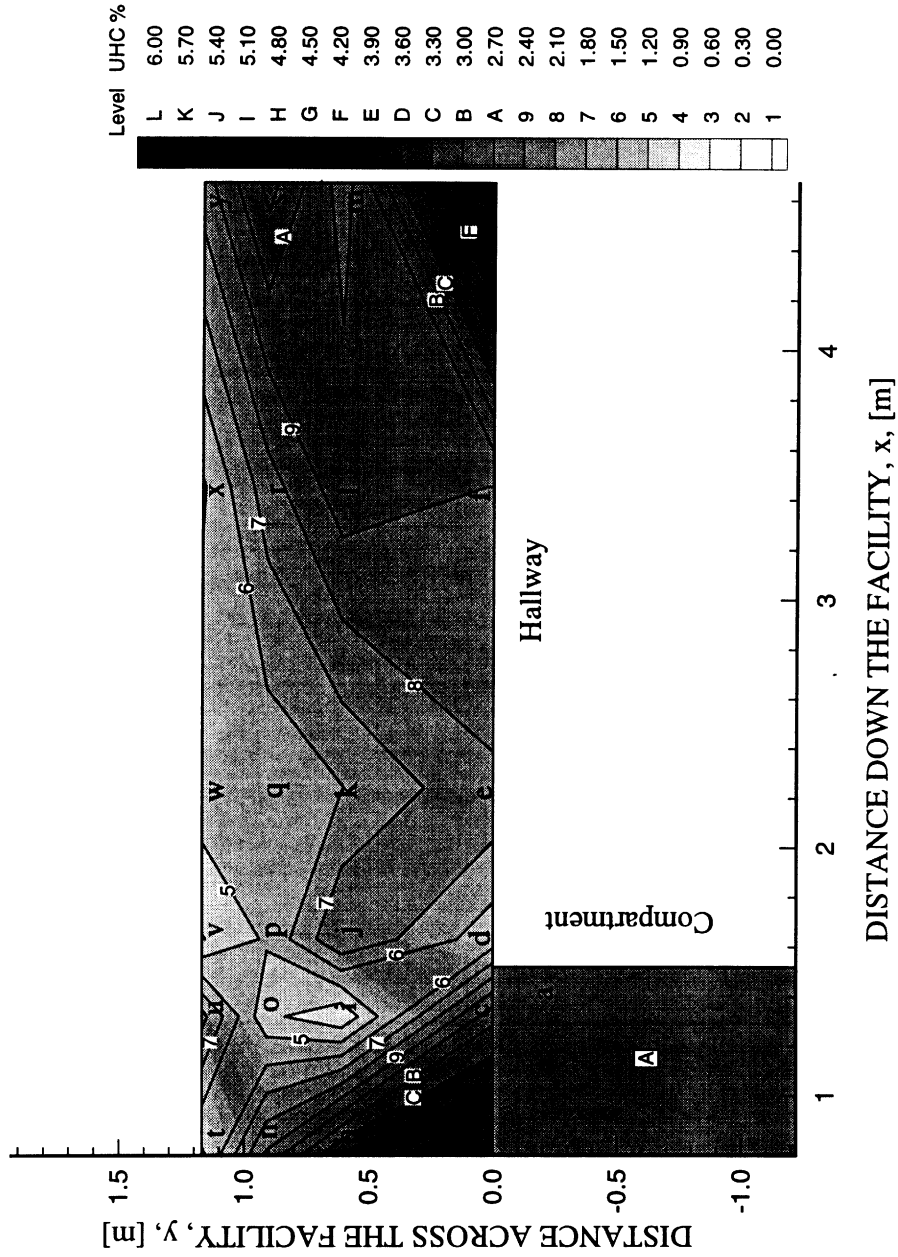


Figure 4.35 The wet UHC concentration distribution 0.05 m below the ceiling 72-76 seconds after flashover in *n*-hexane fire experiments with a 0.12 m² opening, 0.20 m inlet soffit, 0.60 m exit soffit and external burning.

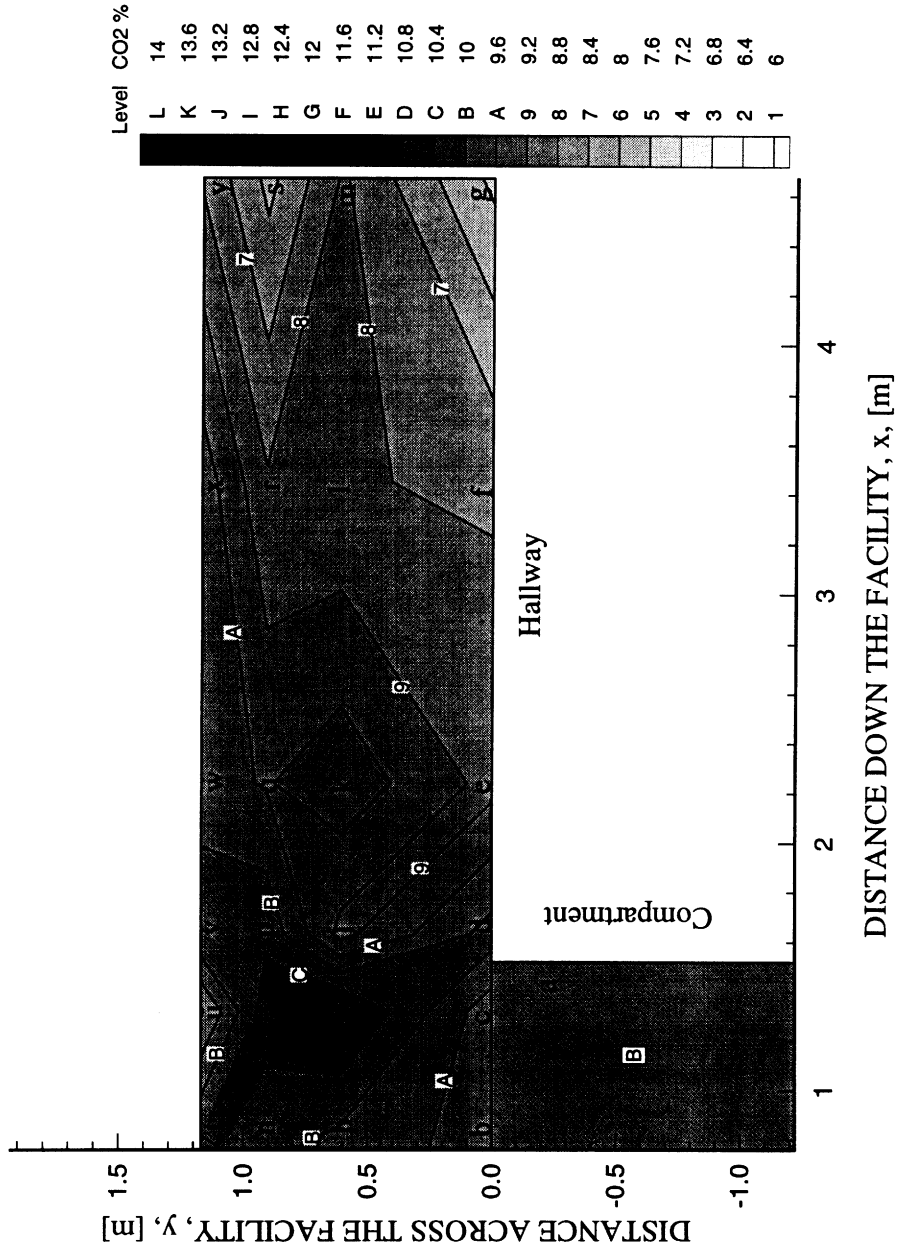


Figure 4.36 The wet CO₂ concentration distribution 0.05 m below the ceiling 72-76 seconds after flashover in *n*-hexane fire experiments with a 0.12 m² opening, 0.20 m inlet soffit, 0.60 m exit soffit and external burning.

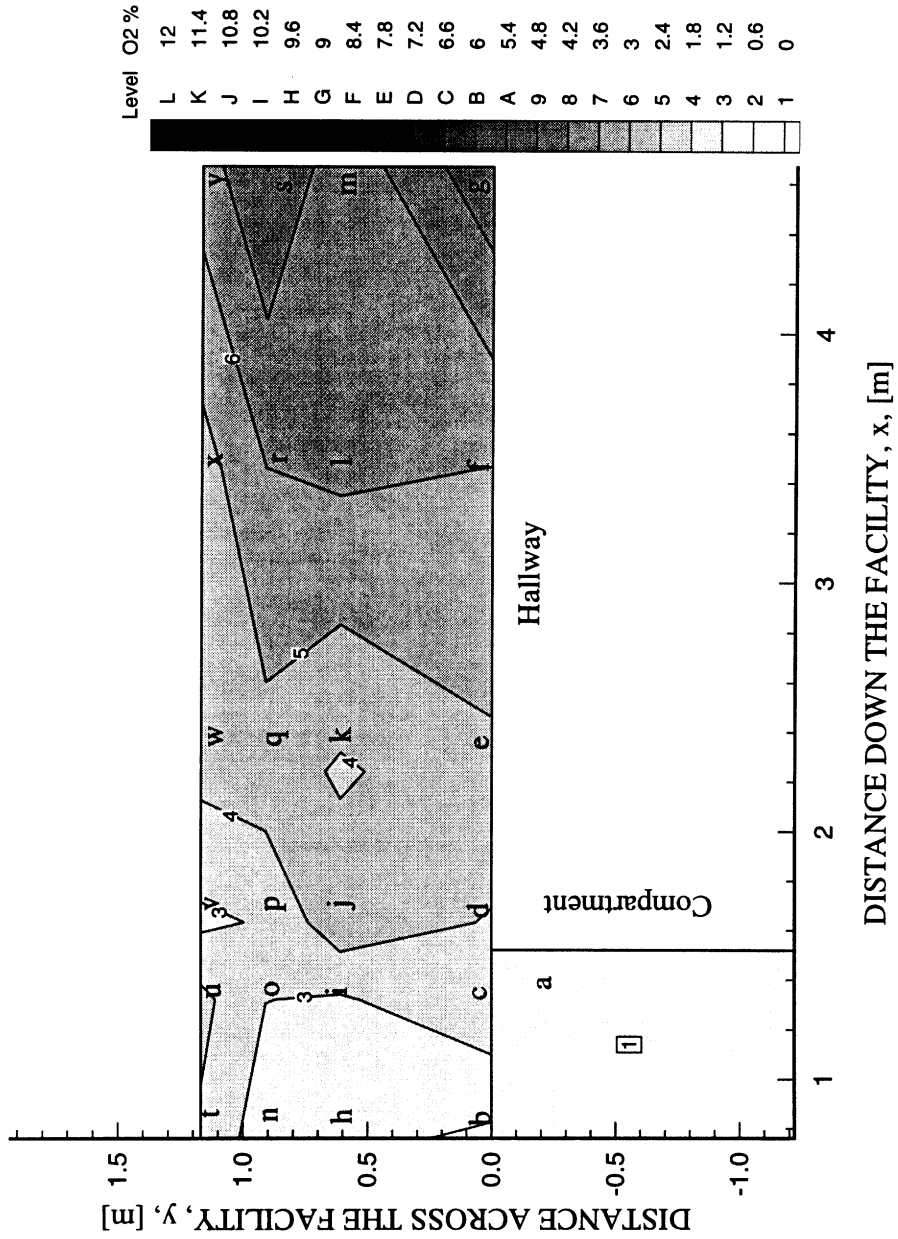


Figure 4.37 The wet O₂ concentration distribution 0.05 m below the ceiling 72-76 seconds after flashover in *n*-hexane fire experiments with a 0.12 m² opening, 0.20 m inlet soffit, 0.60 m exit soffit and external burning.

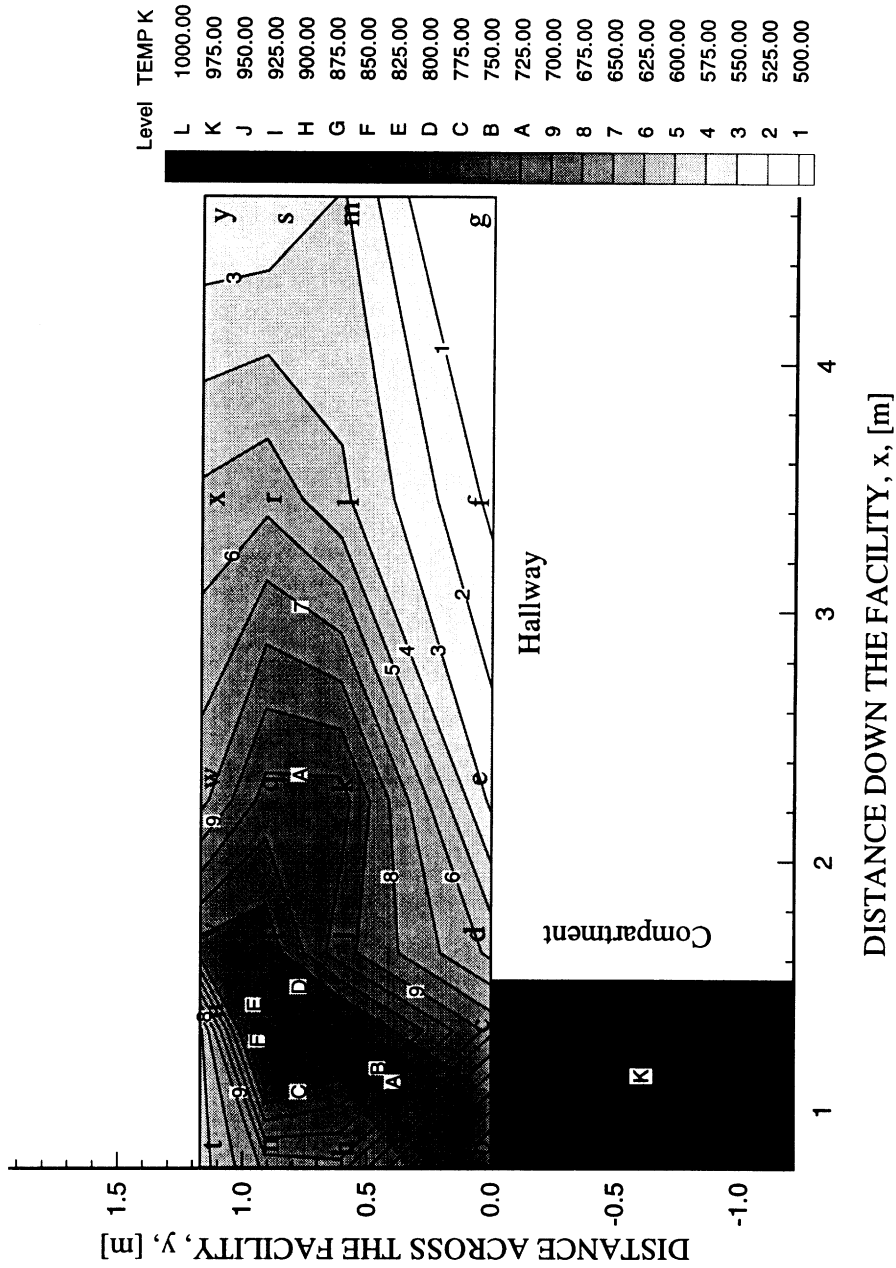


Figure 4.38 The temperature distribution 0.05 m below the ceiling 72-76 seconds after flashover in *n*-hexane fire experiments with a 0.12 m² opening, 0.20 m inlet soffit, 0.60 m exit soffit and external burning.

are greater than 1100 K. Temperatures were typically measured above the flame front, and were estimated to be less than 800 K within 3 seconds after entering the hallway. No oxidation is believed to be occurring above the flame front where the temperatures were measured since a residence of at least 6 seconds is necessary for UHC or CO oxidation to occur at 800 K (Pitts, 1992). The deep upper-layer in the hallway reduced the concentration of O₂ in contact with the gases entering the hallway. From Westbrook and Dryer (1984), limited O₂ results in less radicals available for the oxidation of CO and UHC. From the data, it appears that the majority of the radicals were utilized to reduce the UHC concentration. With the measured increase in CO₂ concentrations, CO oxidation was occurring in the hallway. The CO concentration was, however, only reduced to 2.0-2.4% before the heat losses prevented further reaction from occurring.

The species concentrations and temperatures in the upper-layer gases were measured to be uniform within the hallway 96-100 seconds after flashover. The CO concentrations were measured to be approximately 2.0%, see Fig. 4.39. This CO level was estimated to cause death with less than 3 minutes of exposure. The UHC concentration in the upper-layer gases was measured to be reduced from 4.0% to 1.2% after the gases had traveled across the hallway, see Fig. 4.40. Downstream of the compartment, the UHC concentration was measured to be 1.0%. Upper-layer gases were measured to contain 9.9% CO₂ and 1.8% O₂ along the length of the hallway, see Fig. 4.41 and 4.42. The external burning resulted in gas temperatures of approximately 900 K at the opening, see Fig. 4.43. These temperatures were measured to cool to 700 K by the hallway exit.

4.3.3 Long Transient Time with External Burning

Hallway species concentrations and temperatures were mapped (see Fig. 2.10) 0.05 m below the ceiling in experiments with a 0.04 m² opening and the bottom portion of the hallway exit blocked. The blockage resulted in a 0.20 m high, 1.22 m wide opening at the top of the hallway exit. The upper-layer gases containing high combustion product concentrations exited the hallway through the opening at the exit and were collected in

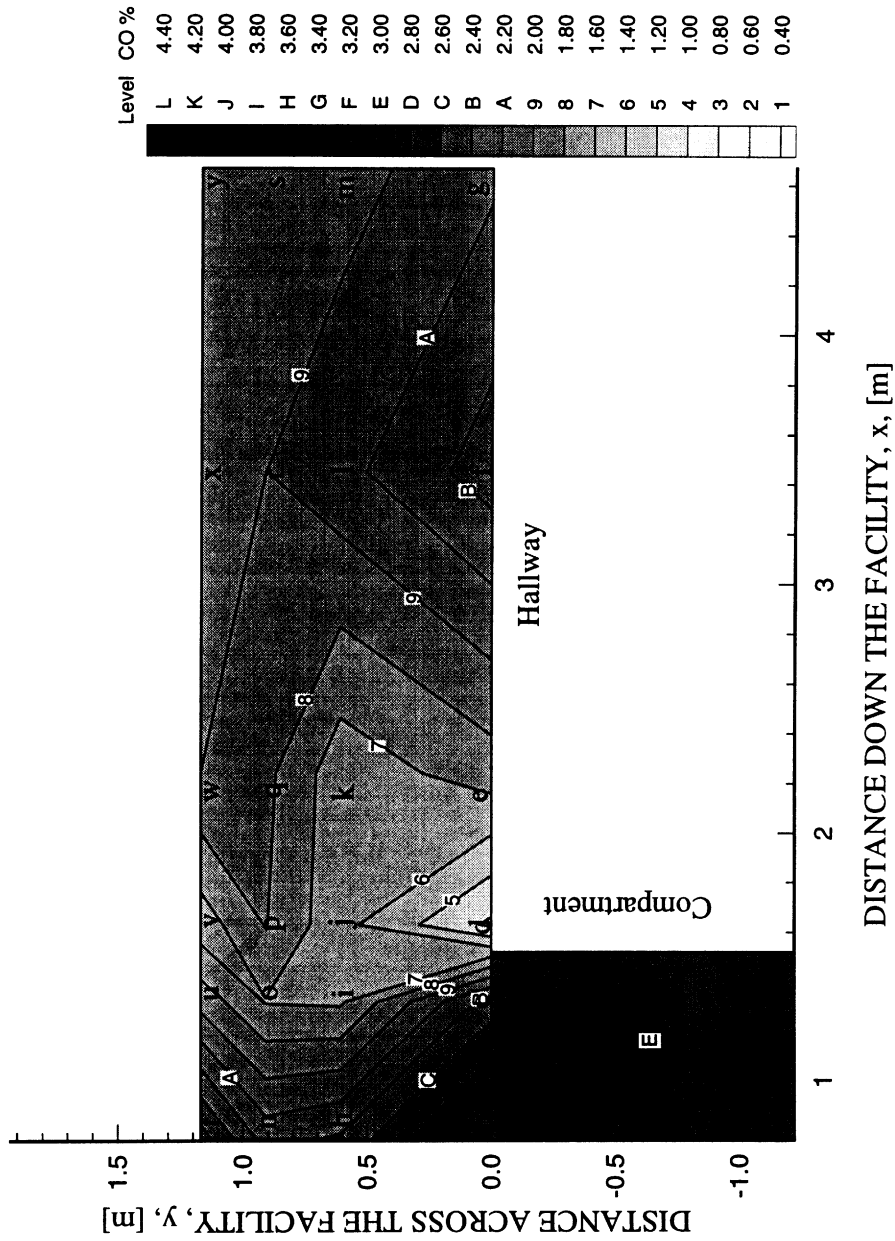


Figure 4.39 The wet CO concentration distribution 0.05 m below the ceiling 96-100 seconds after flashover in *n*-hexane fire experiments with a 0.12 m² opening, 0.20 m inlet soffit, 0.60 m exit soffit and external burning.

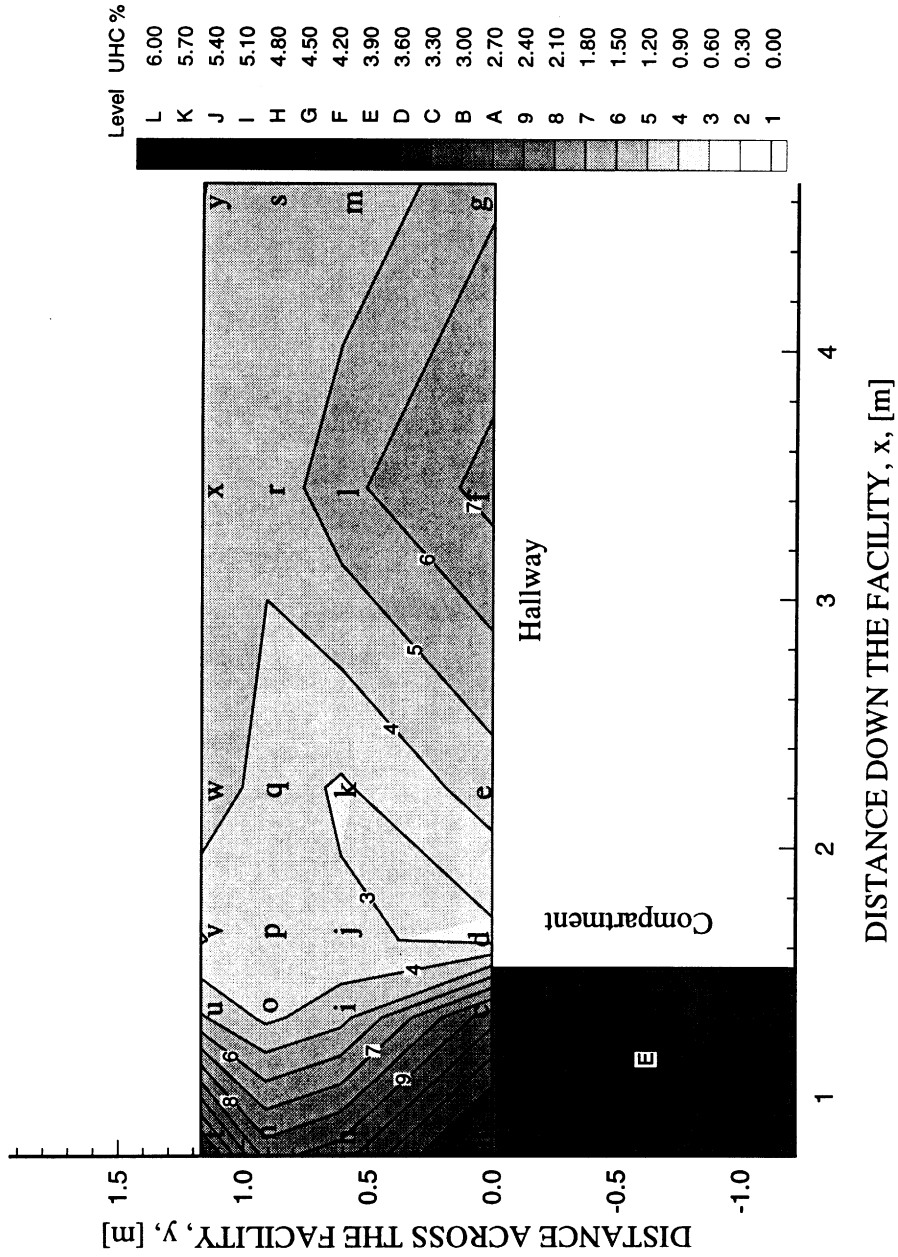


Figure 4.40 The wet UHC concentration distribution 0.05 m below the ceiling 96-100 seconds after flashover in *n*-hexane fire experiments with a 0.12 m² opening, 0.20 m inlet soffit, 0.60 m exit soffit and external burning.

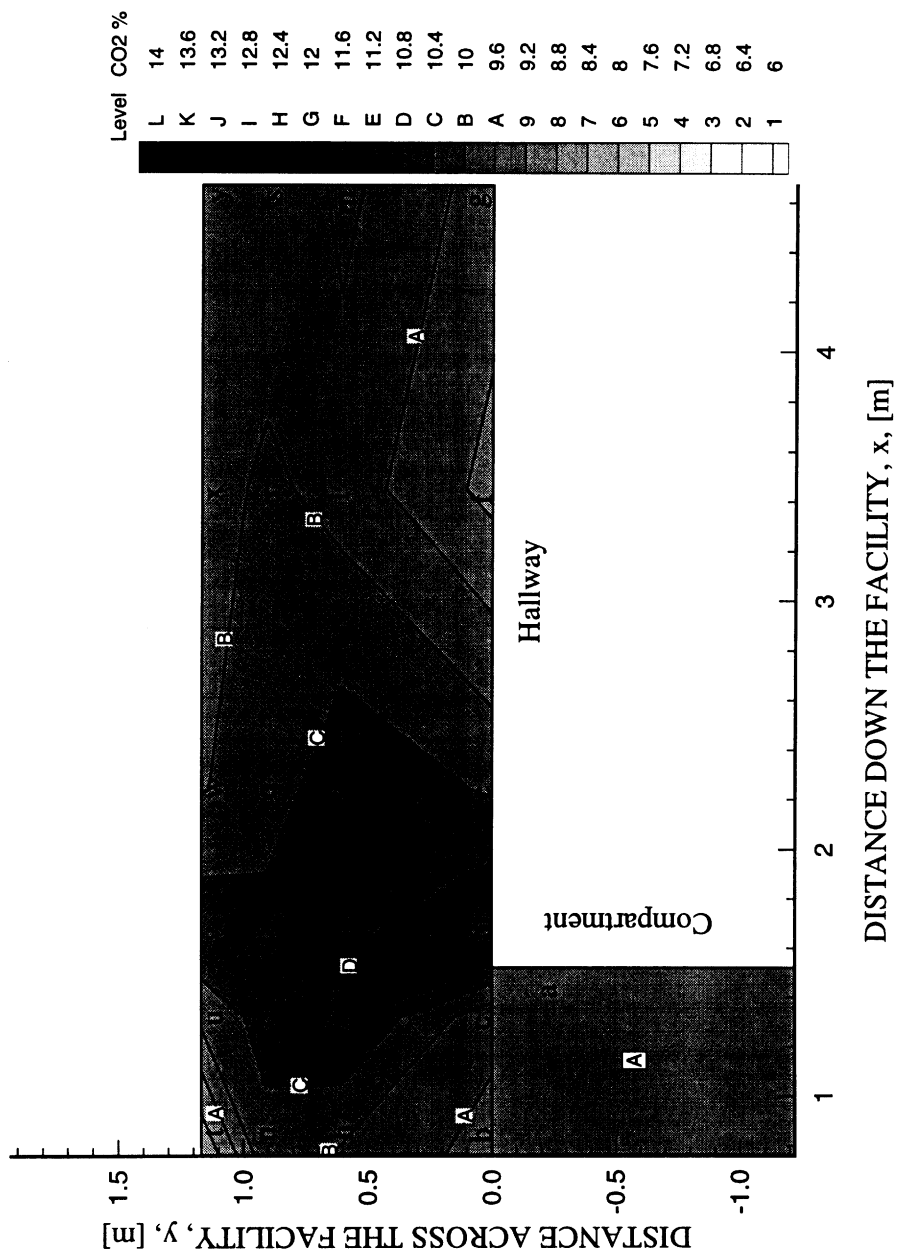


Figure 4.41 The wet CO₂ concentration distribution 0.05 m below the ceiling 96-100 seconds after flashover in *n*-hexane fire experiments with a 0.12 m² opening, 0.20 m inlet soffit, 0.60 m exit soffit and external burning.

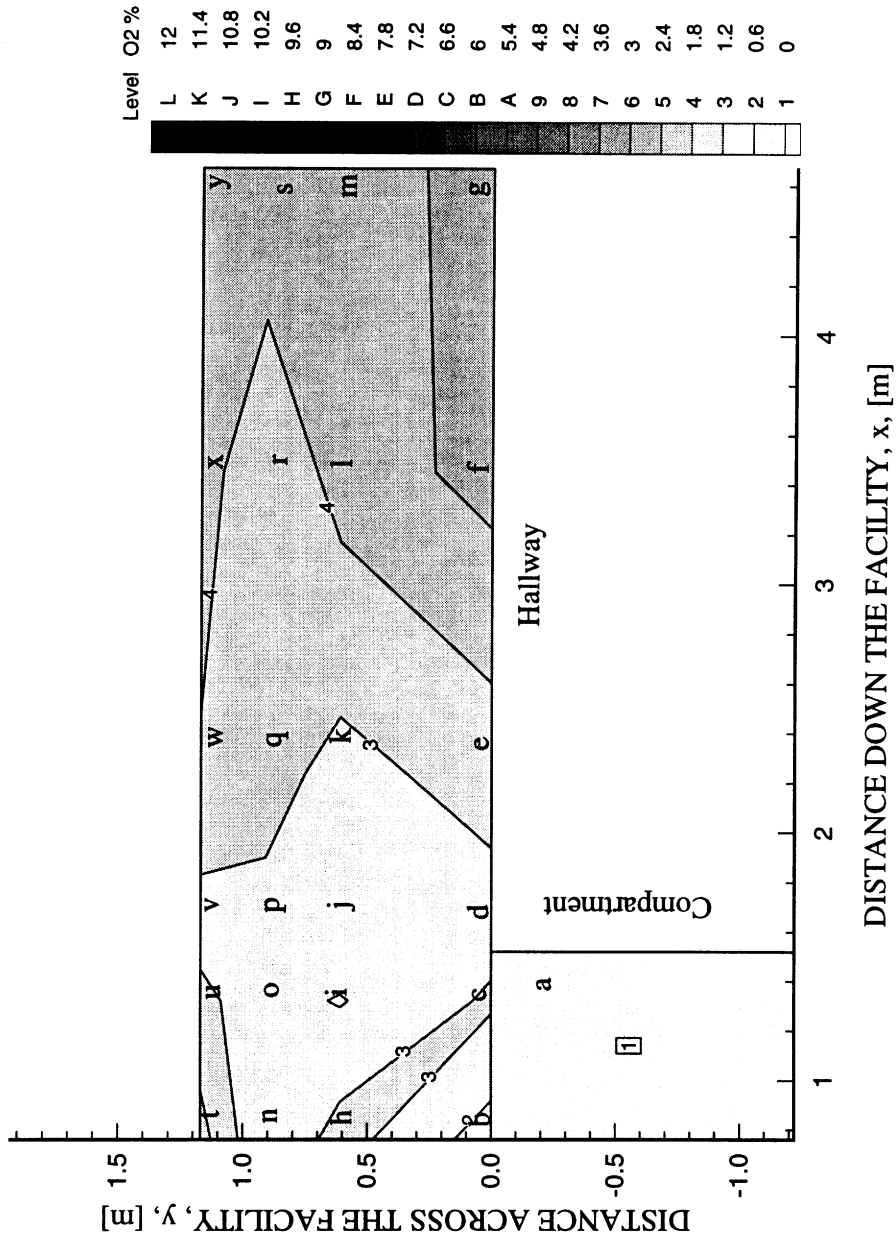


Figure 4.42 The wet O₂ concentration distribution 0.05 m below the ceiling 96-100 seconds after flashover in *n*-hexane fire experiments with a 0.12 m² opening, 0.20 m inlet soffit, 0.60 m exit soffit and external burning.

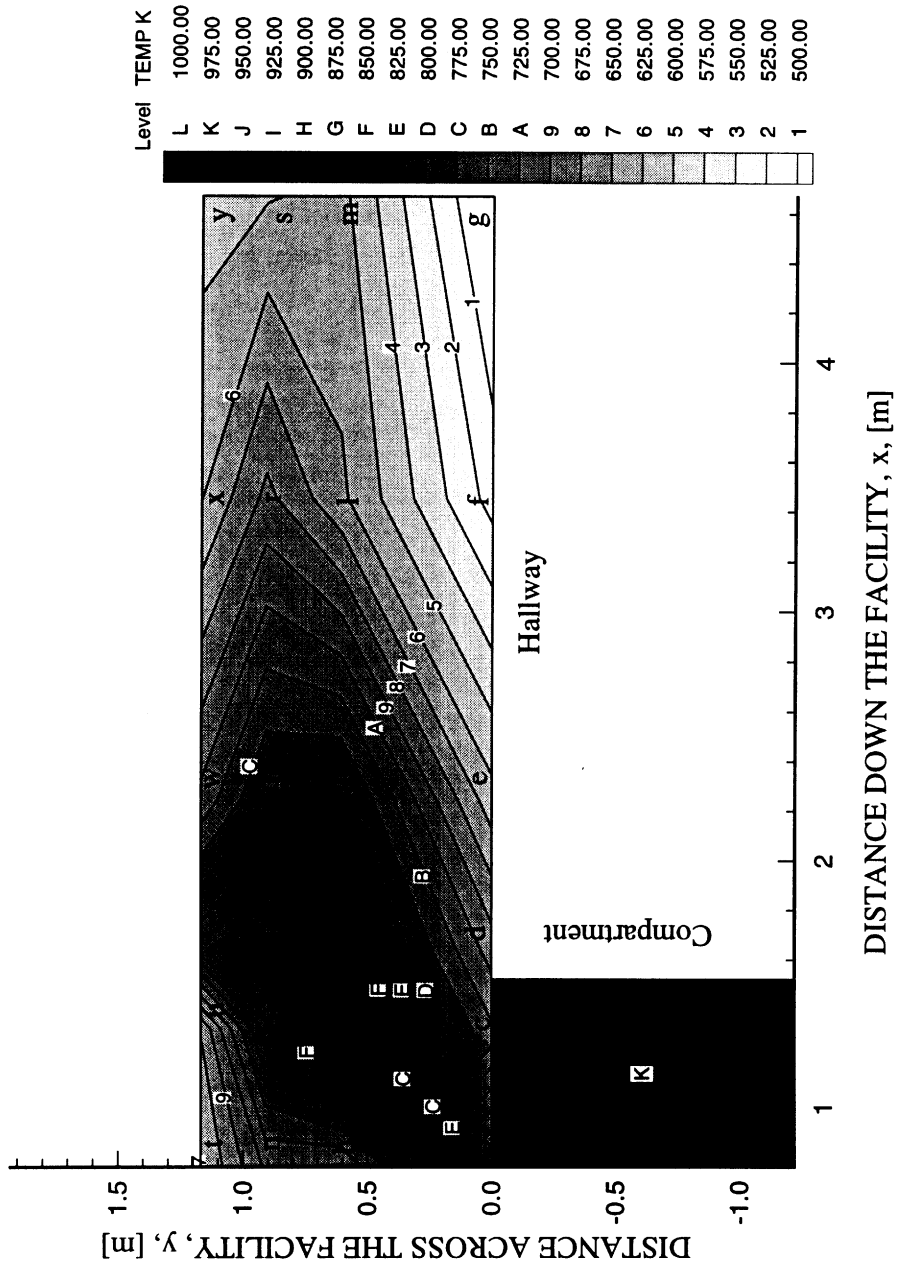


Figure 4.43 The temperature distribution 0.05 m below the ceiling 96-100 seconds after flashover in *n*-hexane fire experiments with a 0.12 m² opening, 0.20 m inlet soffit, 0.60 m exit soffit and external burning.

the fume hood. As a result, the species concentrations were not measured to reach a steady-state concentration until the end of the post-flashover period. Effects of external burning on species concentrations and temperature were also measured. The location of the sampling, previously noted in Fig. 2.10, is denoted by the lower case letters on the contour plots.

The fire growth parameter was used to align the compartment fire post-flashover period of 23 experiments. The alignment was verified using the temperature 0.05 m below the ceiling inside the compartment from ten experiments. The compartment temperatures are shown in Fig. 4.44 to coincide with one another during the steady-state period. With the experiments aligned, the temporal and spatial variation in the species concentrations and temperatures measured in the hallway are described in the paragraphs to follow.

The gases entering the hallway were measured to contain 2.4% CO and 3.9% UHC approximately 12-16 seconds after the onset flashover inside the compartment, see Fig. 4.45 and Fig. 4.46. The flow of gases across the hallway diluted CO and UHC to less than 1.0 %. With no external burning in the hallway, CO₂ concentrations were measured remain low at 6.5-7.5% as shown in the plot in Fig. 4.47. A plot of the O₂ concentration is seen in Fig. 4.48. Approximately 9.8% O₂ was measured downstream of the compartment. Figures 4.47 and 4.48 show a region ($y=0.9$ and $x=1.4-4.6$ m) of low CO₂ concentration and high O₂ concentration not present in the two cases discussed previously. This is attributed to the presence of a more shallow upper-layer ($\delta \approx 0.45$ m) in these experiments compared with the previous two cases ($\delta \approx 0.60$ m). It is believed that lower layer gases containing high (18-21%) O₂ concentrations were being pulled into the upper-layer by the vortical structure traveling along the corner of the wall (opposite the compartment) and the ceiling, see Fig. 4.1. The addition of the lower-layer gases in this region dilute the upper-layer gases resulting in lower CO₂ concentrations. The high O₂ concentrations at the bottom right corner of the hallway are attributed to ambient air

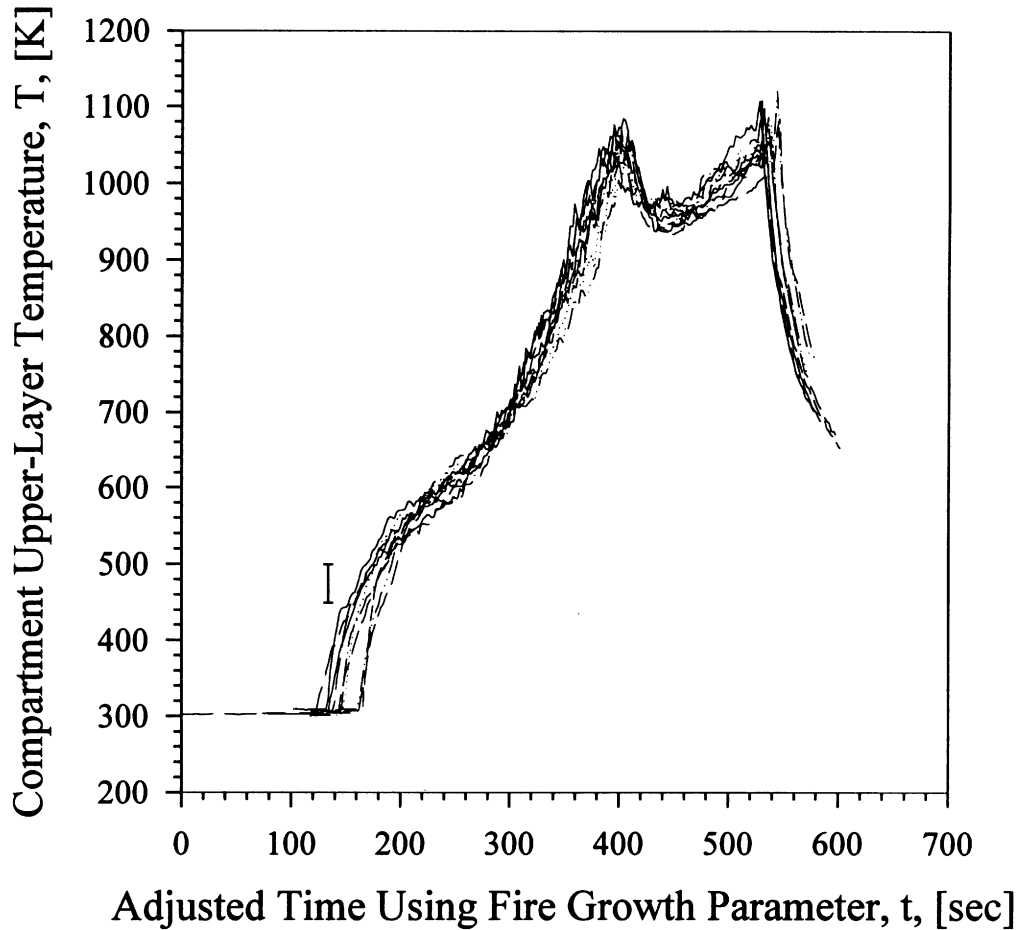


Figure 4.44 The temperature 0.05 m below the ceiling inside the compartment in 10 different *n*-hexane fire experiments with external burning, a 0.04 m² opening, and the exit of the hallway blocked leaving a 0.20 m high, 1.22 m wide opening. The experiments were aligned with one another in time using the fire growth parameter.

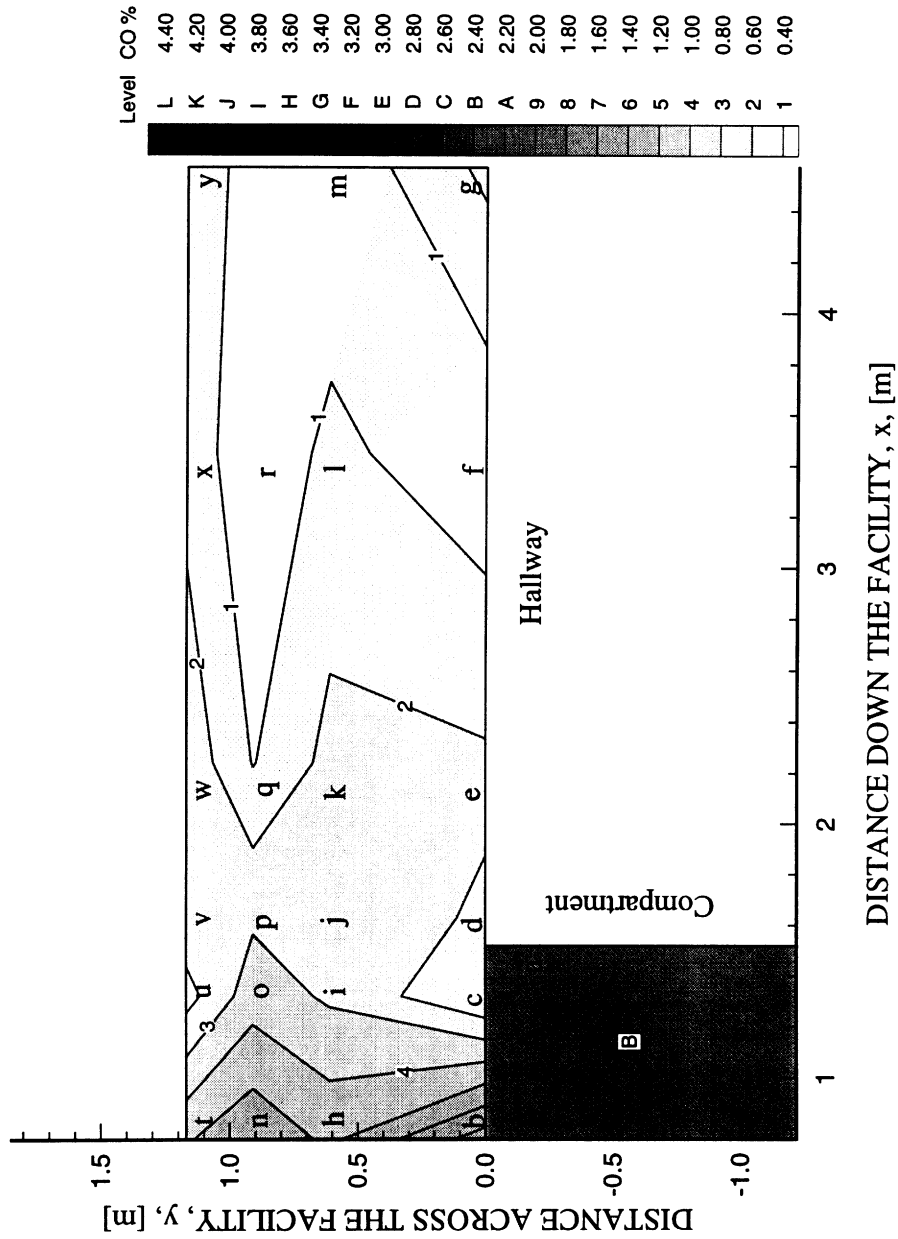


Figure 4.45 The wet CO concentration distribution 0.05 m below the ceiling 12-16 seconds after flashover in *n*-hexane fire experiments with a 0.04 m² opening, 0.20 m inlet soffit, 0.20 m high 1.22 m wide opening at top of hallway exit and external burning.

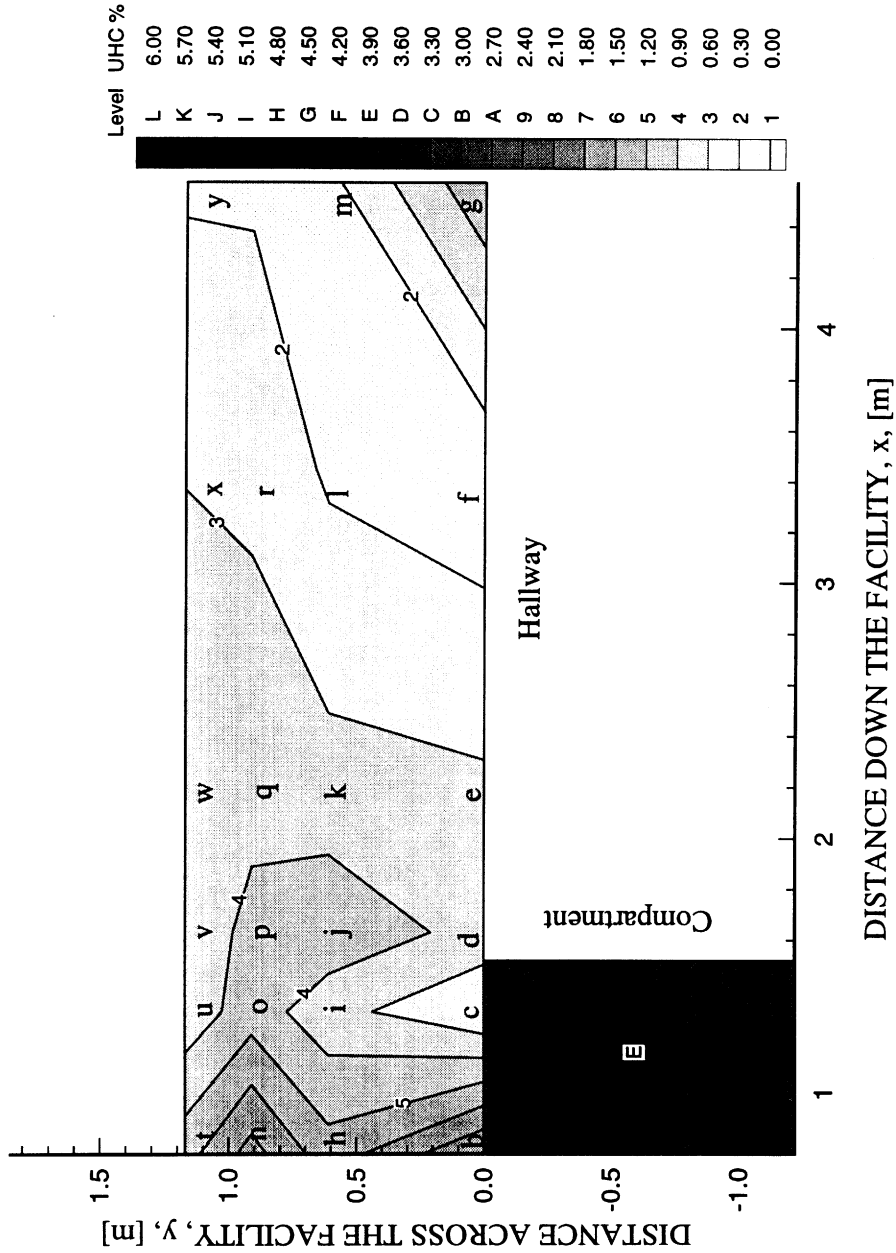


Figure 4.46 The wet UHC concentration distribution 0.05 m below the ceiling 12-16 seconds after flashover in *n*-hexane fire experiments with a 0.04 m² opening, 0.20 m inlet soffit, 0.20 m high 1.22 m wide opening at top of hallway exit and external burning.

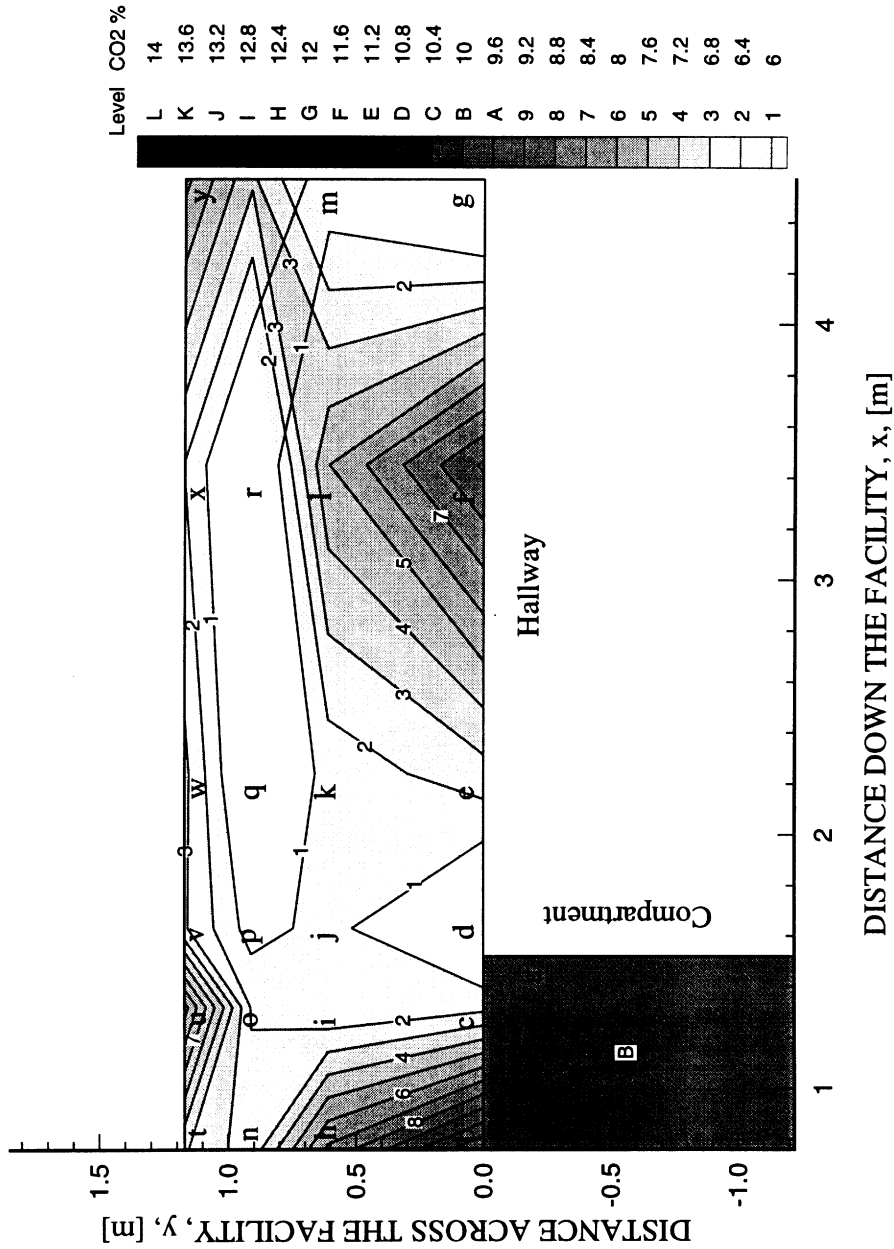


Figure 4.47 The wet CO₂ concentration distribution 0.05 m below the ceiling 12-16 seconds after flashover in *n*-hexane fire experiments with a 0.04 m² opening, 0.20 m inlet soffit, 0.20 m high 1.22 m wide opening at top of hallway exit and external burning.

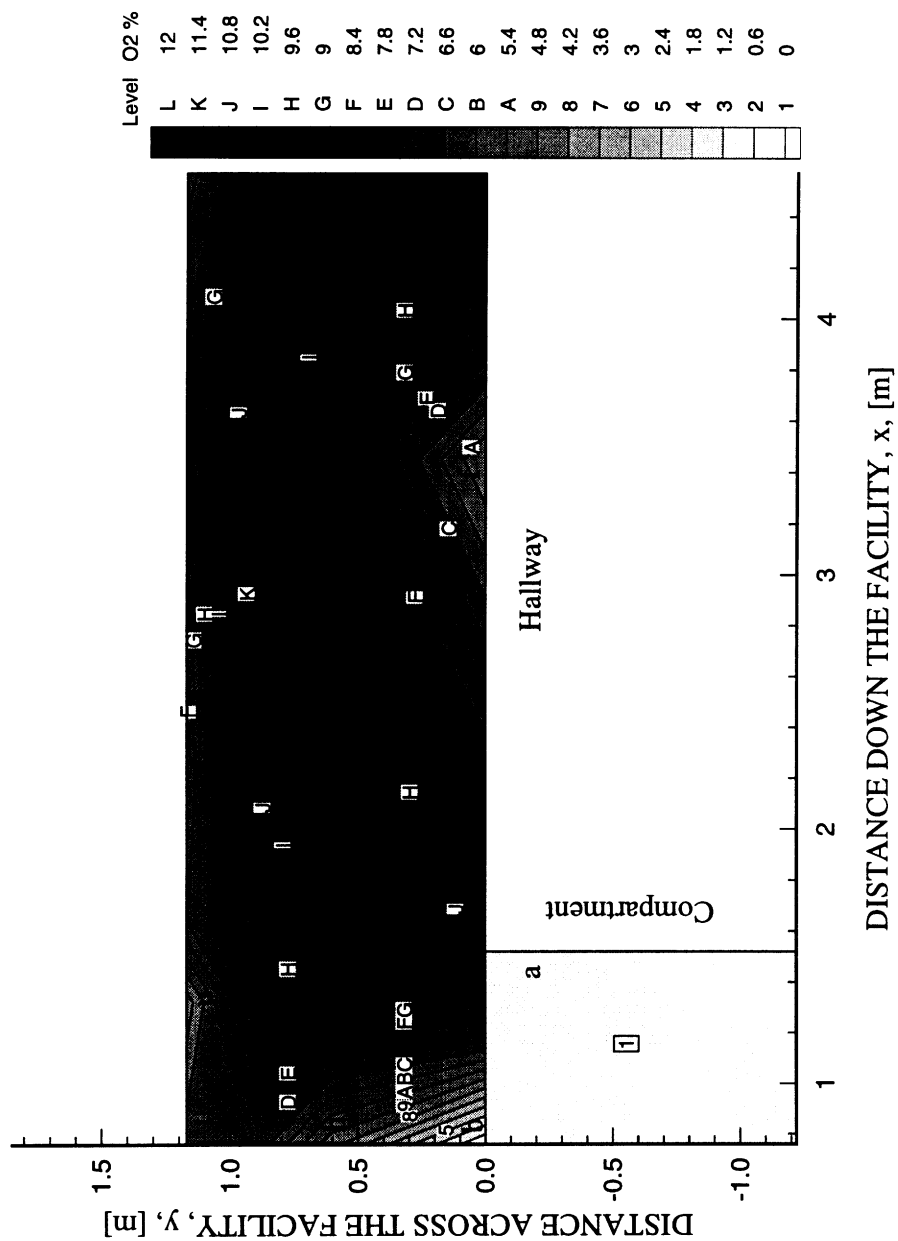


Figure 4.48 The wet O₂ concentration distribution 0.05 m below the ceiling 12-16 seconds after flashover in *n*-hexane fire experiments with a 0.04 m² opening, 0.20 m inlet soffit, 0.20 m high 1.22 m wide opening at top of hallway exit and external burning.

entering the hallway through the exit opening. The temperatures were measured to be approximately 500 K throughout the hallway, see Fig. 4.49. This is expected since no external burning was observed to be occurring in the hallway at this point in the fire.

External burning was observed to occur in the hallway for these experiments 20-24 seconds after flashover. The external burning in the hallway was not attached to the compartment window, but instead burning was observed to begin after the gases had traveled approximately half way across the hallway. This type of burning, where the flame is not attached to the window, was previously observed in the experiments performed by Gottuk (1992a). The downstream yields were measured to be higher in the experiments with external burning unattached to the opening compared with experiments with burning attached to the opening (Gottuk, 1992a). The burning gases impinged upon the wall opposite the compartment and traveled in a clockwise swirling motion along the corner of the ceiling and the side wall, see Fig. 4.1. The flame was visually observed to extend down the hallway approximately 2.5-3.0 m, slightly further than observed in the previous cases.

Approximately 48-52 seconds after flashover with external burning in the hallway, gases traveling along the side of the hallway opposite the compartment were measured to contain 1.7% CO, see Fig. 4.50. Only 0.8% CO was measured in the gases on the compartment side of the hallway. The UHC were measured to be oxidized from 3.9% to 1.5% after the gases flowed from the opening to the opposite side of the hallway as shown in the plot in Fig. 4.51. External burning resulted in an increase in CO₂ concentration to approximately 10.5%, see Fig. 4.52. The O₂ concentrations were measured to fall to 1-2% range, see Fig. 4.53, another indication that external burning was occurring in the hallway. Gas temperatures were measured to rise significantly to approximately 850 K at the compartment, see Fig. 4.54. The temperature was measured

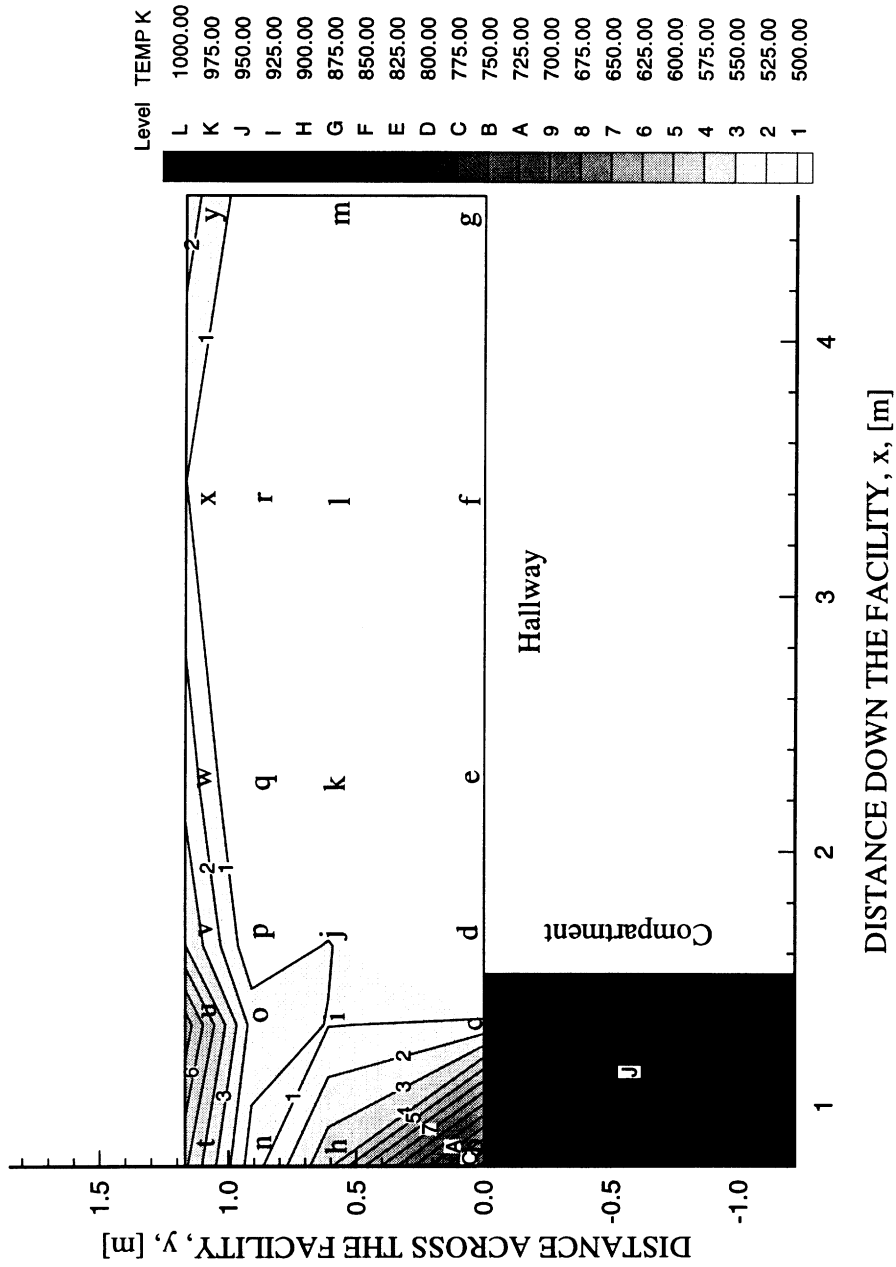


Figure 4.49 The temperature distribution 0.05 m below the ceiling 12-16 seconds after flashover in *n*-hexane fire experiments with a 0.04 m² opening, 0.20 m inlet soffit, 0.20 m high 1.22 m wide opening at top of hallway exit and external burning.

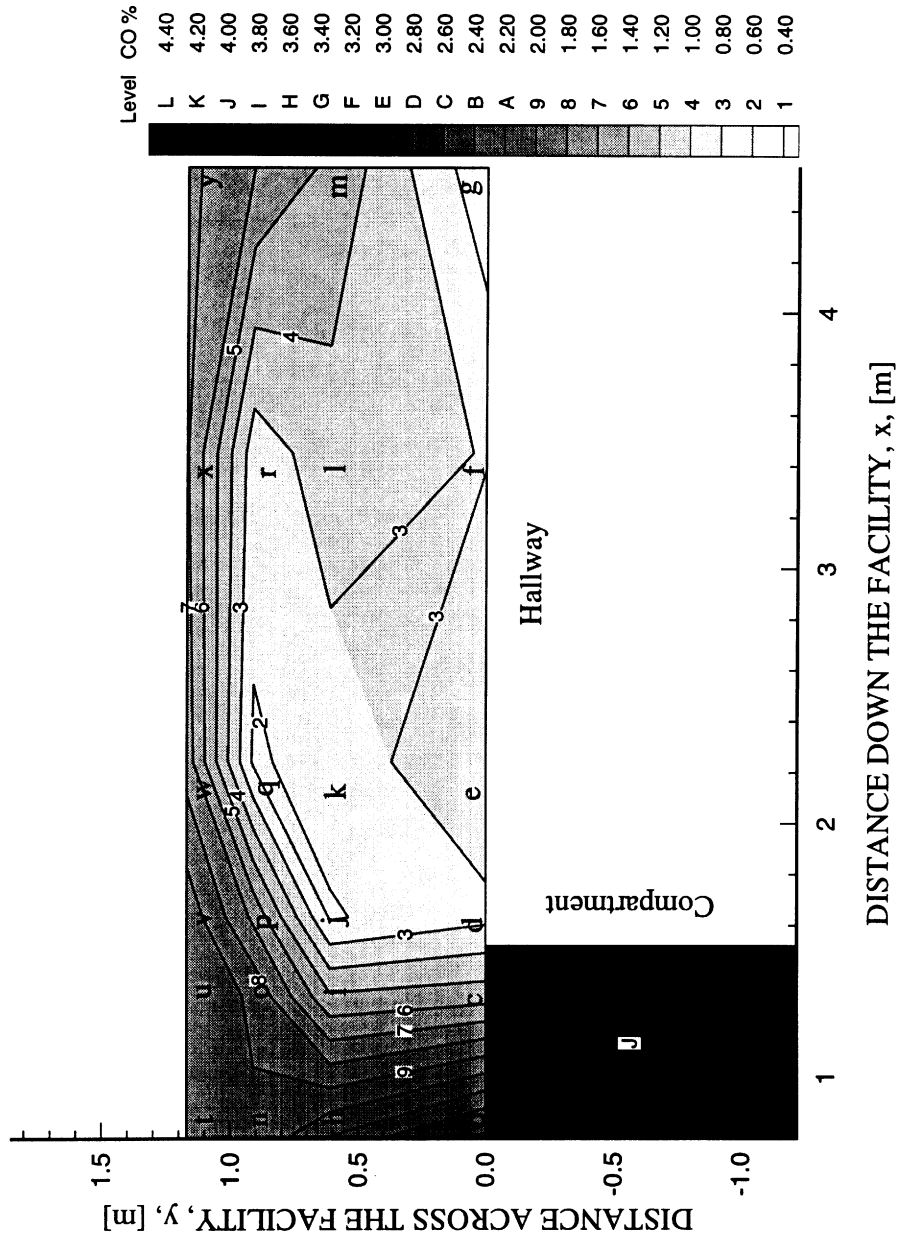


Figure 4.50 The wet CO concentration distribution 0.05 m below the ceiling 48-52 seconds after flashover in *n*-hexane fire experiments with a 0.04 m² opening, 0.20 m inlet soffit, 0.20 m high 1.22 m wide opening at top of hallway exit and external burning.

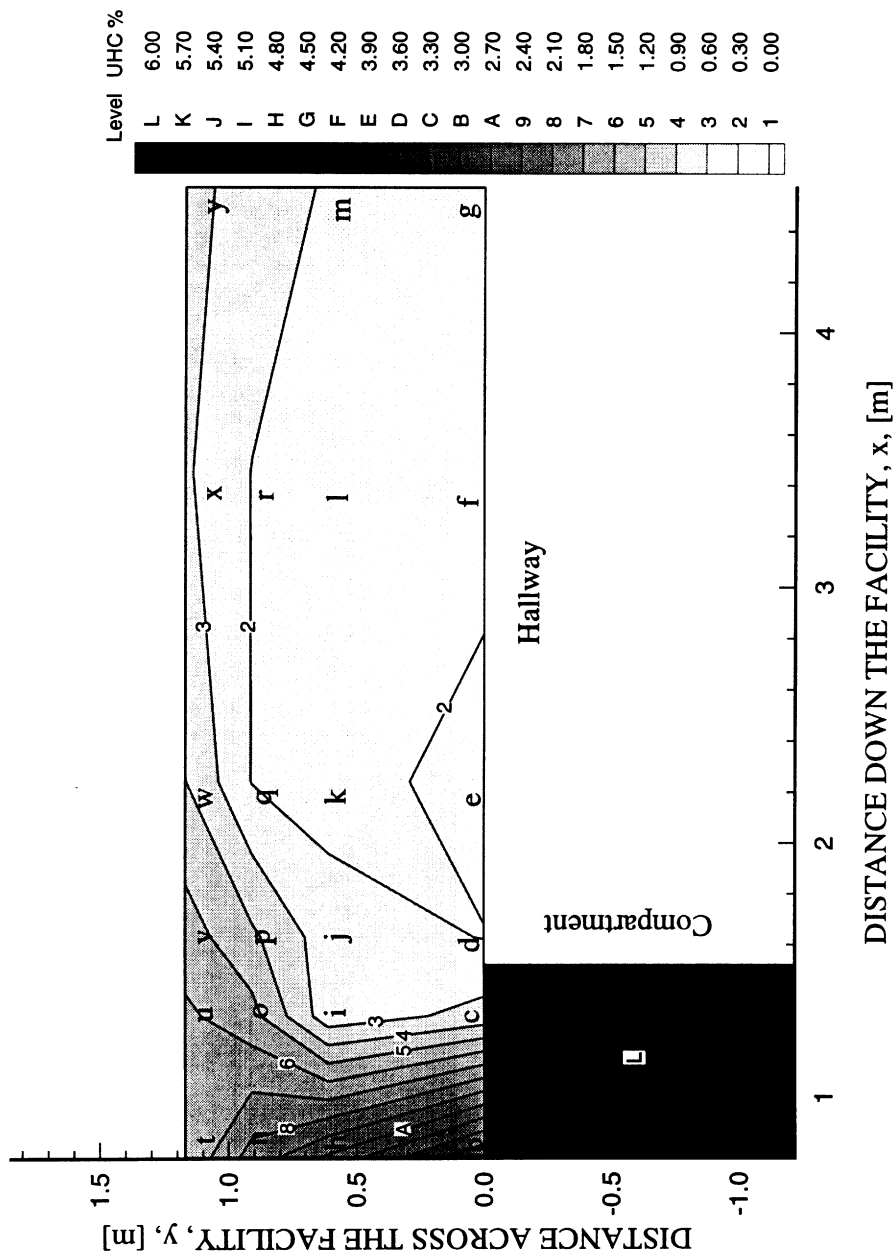


Figure 4.51 The wet UHC concentration distribution 0.05 m below the ceiling 48-52 seconds after flashover in *n*-hexane fire experiments with a 0.04 m² opening, 0.20 m inlet soffit, 0.20 m high 1.22 m wide opening at top of hallway exit and external burning.

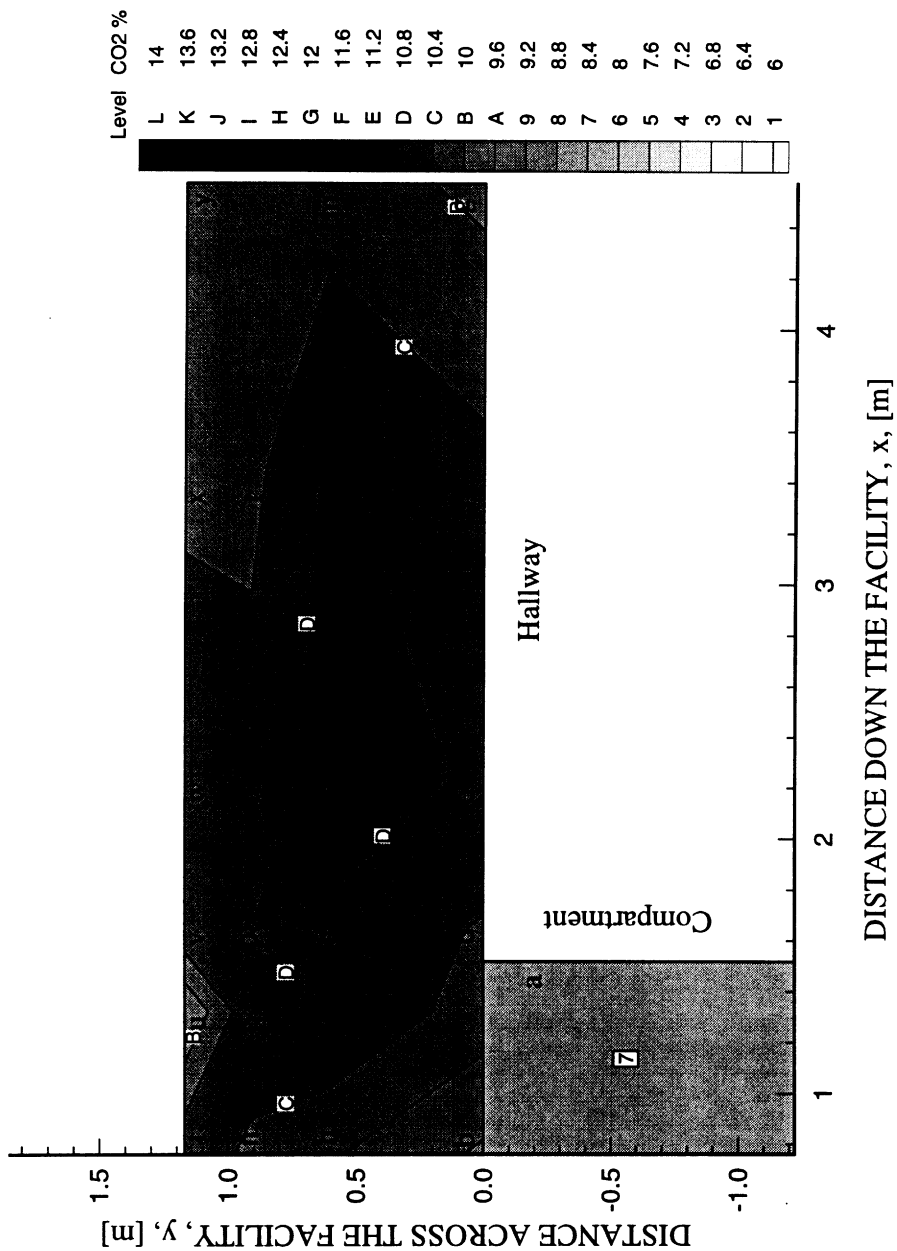


Figure 4.52 The wet CO₂ concentration distribution 0.05 m below the ceiling 48-52 seconds after flashover in *n*-hexane fire experiments with a 0.04 m² opening, 0.20 m inlet soffit, 0.20 m high 1.22 m wide opening at top of hallway exit and external burning.

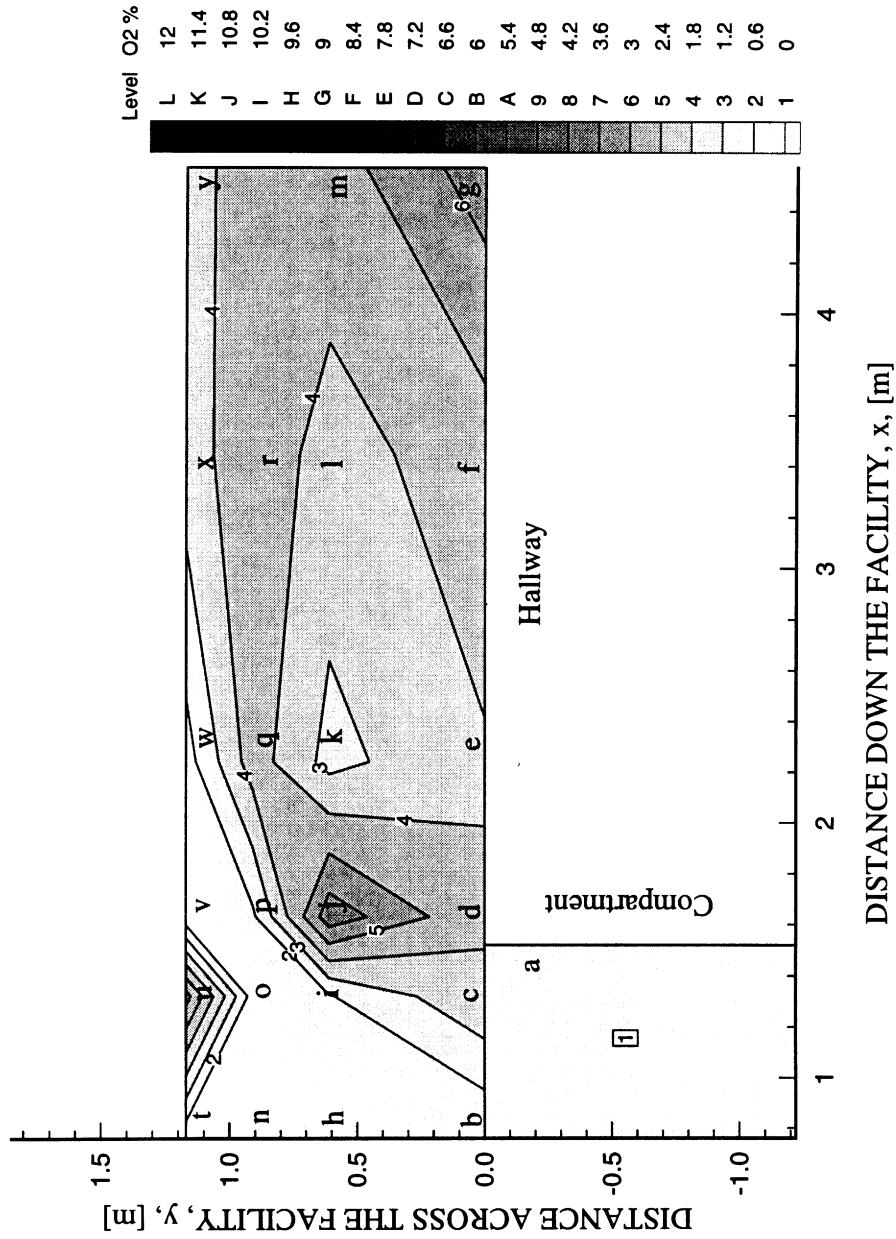


Figure 4.53 The wet O₂ concentration distribution 0.05 m below the ceiling 48-52 seconds after flashover in *n*-hexane fire experiments with a 0.04 m² opening, 0.20 m inlet soffit, 0.20 m high 1.22 m wide opening at top of hallway exit and external burning.

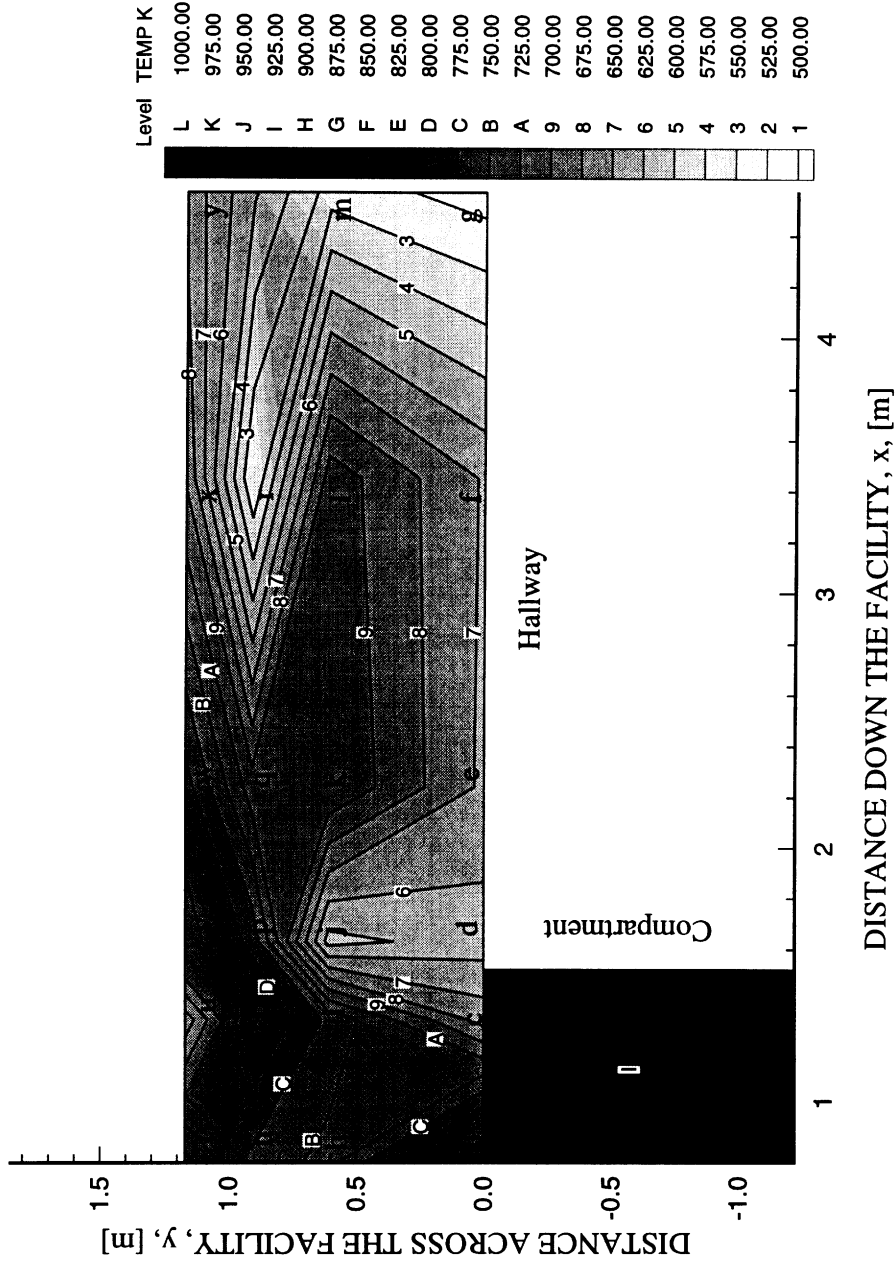


Figure 4.54 The temperature distribution 0.05 m below the ceiling 48-52 seconds after flashover in *n*-hexane fire experiments with a 0.04 m² opening, 0.20 m inlet soffit, 0.20 m high 1.22 m wide opening at top of hallway exit and external burning.

to rapidly fall with distance away from the compartment to 650 K by the end of the hallway.

Concentrations of 1.9% CO were measured in the gases traveling along the side of the hallway opposite the compartment 64-68 seconds after flashover despite the presence of external burning in the hallway, see Fig. 4.55. The CO concentration on the compartment side of the hallway was measured to be approximately 1.0%, nearly half of the concentration present on the opposite side of the hallway. The UHC, however, concentration was measured to be reduced from 3.0% at the opening to 1.2% at the wall opposite the compartment, see Fig. 4.56. As described in the previous section, the rate of reaction of UHC and radicals is higher than that of CO and radicals (Westbrook and Dryer, 1984). The UHC are therefore oxidized more readily than CO. The CO concentration in the present experiments was measured to be slightly less than in experiments described in section 4.3.3. The difference is attributed to the less deep upper-layer in these experiments. The more shallow upper-layer allows additional O₂ to mix with the hot gases promoting the production radicals for oxidation. Concentrations of 10.5% CO₂ and 1.2% O₂ were measured to be uniform in the hallway upper-layer, see Fig. 4.57 and Fig. 4.58. The high temperatures in the hallway (greater than 750 K) were measured at locations where external burning was observed to be present, see Fig. 4.59.

An area of low CO concentration was measured to be present 2.0 to 4.0 m down and 0.7-1.0 m across the hallway 80-84 seconds after flashover, see Fig. 4.60. The area of low concentration is at the same location where low CO₂ and high O₂ concentrations were measured 12-16 seconds after flashover, see Figs. 4.47 and 4.48. The gases on the side of the hallway opposite the compartment were measured to still contain 1.9% CO. The concentration of CO in gases on the compartment side of the hallway increased to 1.2%. The increase was attributed to gases being forced to circulate back toward the compartment. The distribution in the UHC concentration within the hallway is similar to that measured 64-68 seconds after flashover. The gases entered the hallway containing

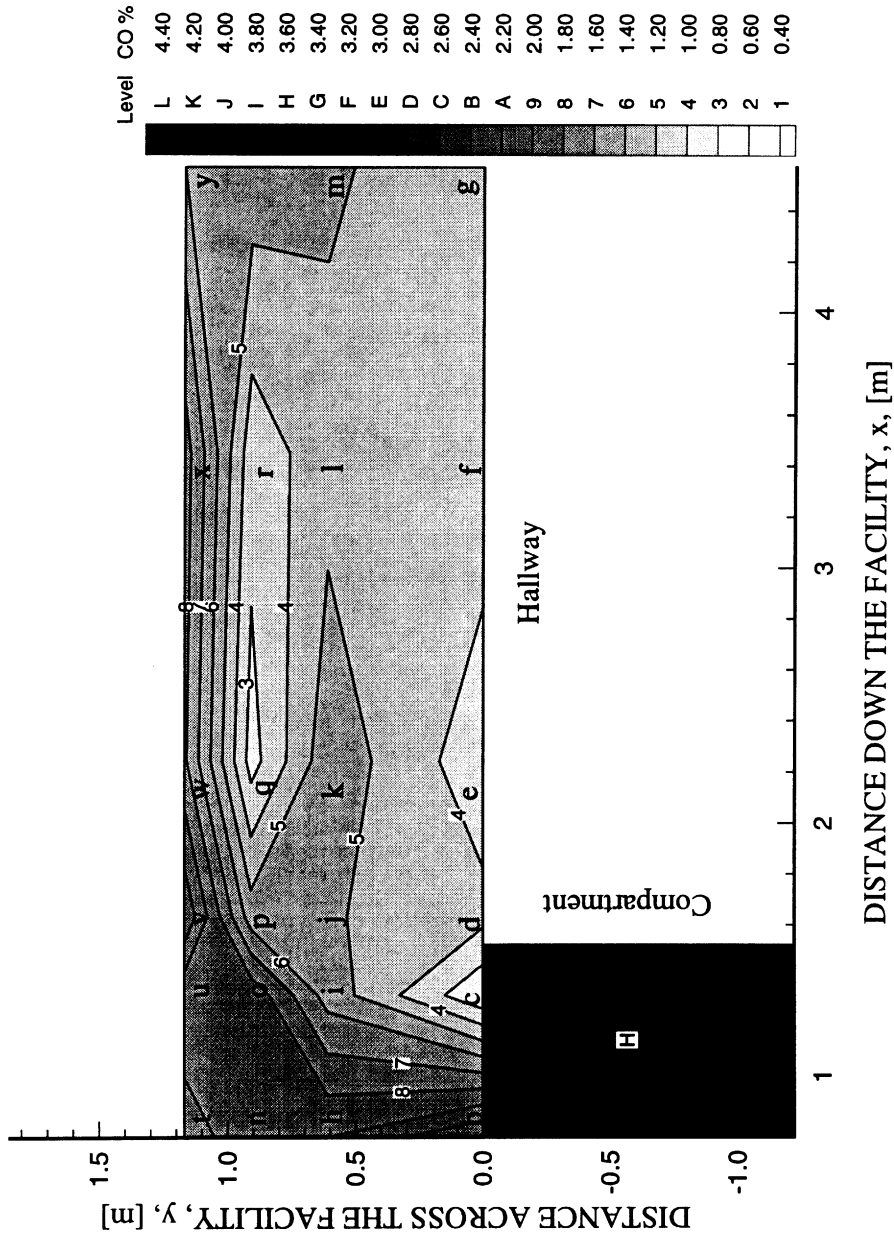


Figure 4.55 The wet CO concentration distribution 0.05 m below the ceiling 64-68 seconds after flashover in *n*-hexane fire experiments with a 0.04 m² opening, 0.20 m inlet soffit, 0.20 m high 1.22 m wide opening at top of hallway exit and external burning.

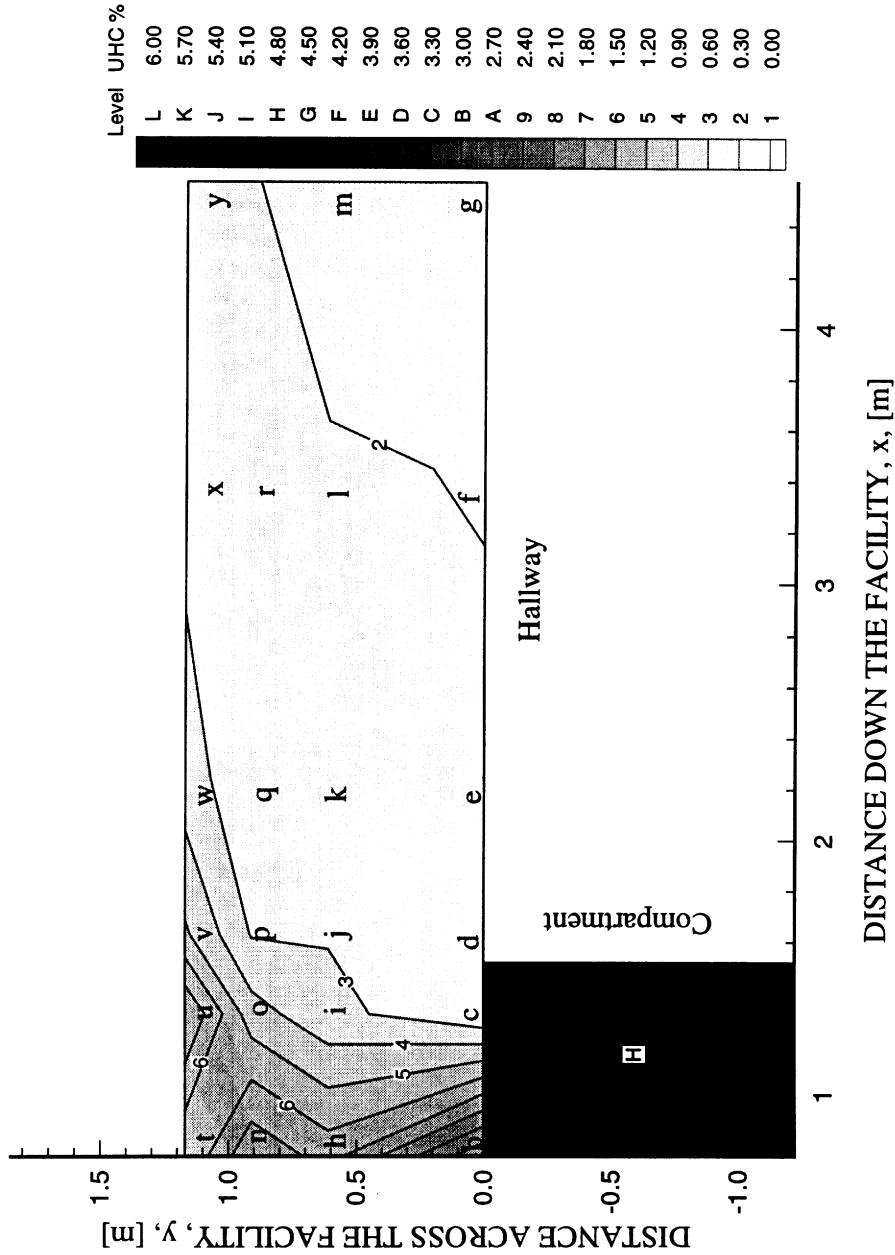


Figure 4.56 The wet UHC concentration distribution 0.05 m below the ceiling 64-68 seconds after flashover in *n*-hexane fire experiments with a 0.04 m² opening, 0.20 m inlet soffit, 0.20 m high 1.22 m wide opening at top of hallway exit and external burning.

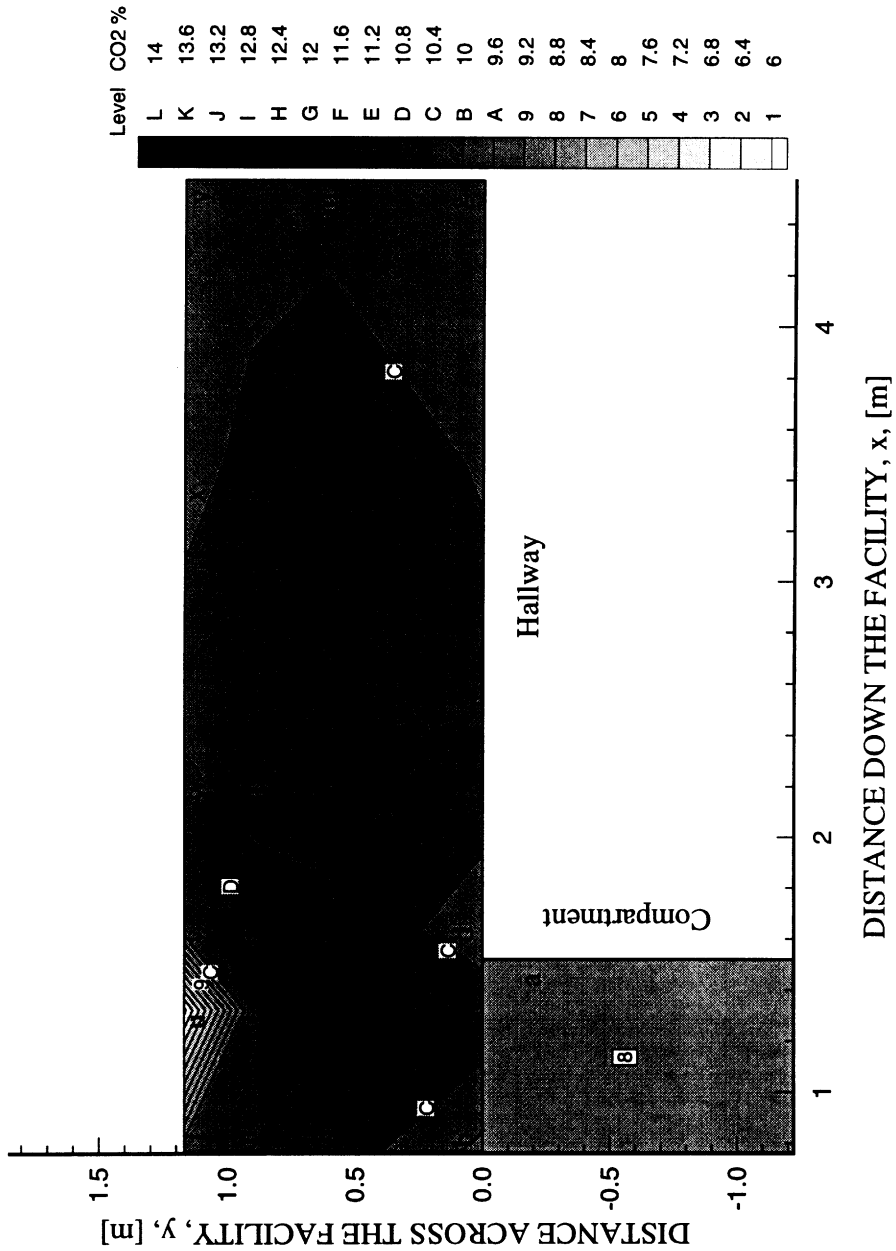


Figure 4.57 The wet CO₂ concentration distribution 0.05 m below the ceiling 64-68 seconds after flashover in *n*-hexane fire experiments with a 0.04 m² opening, 0.20 m inlet soffit, 0.20 m high 1.22 m wide opening at top of hallway exit and external burning.

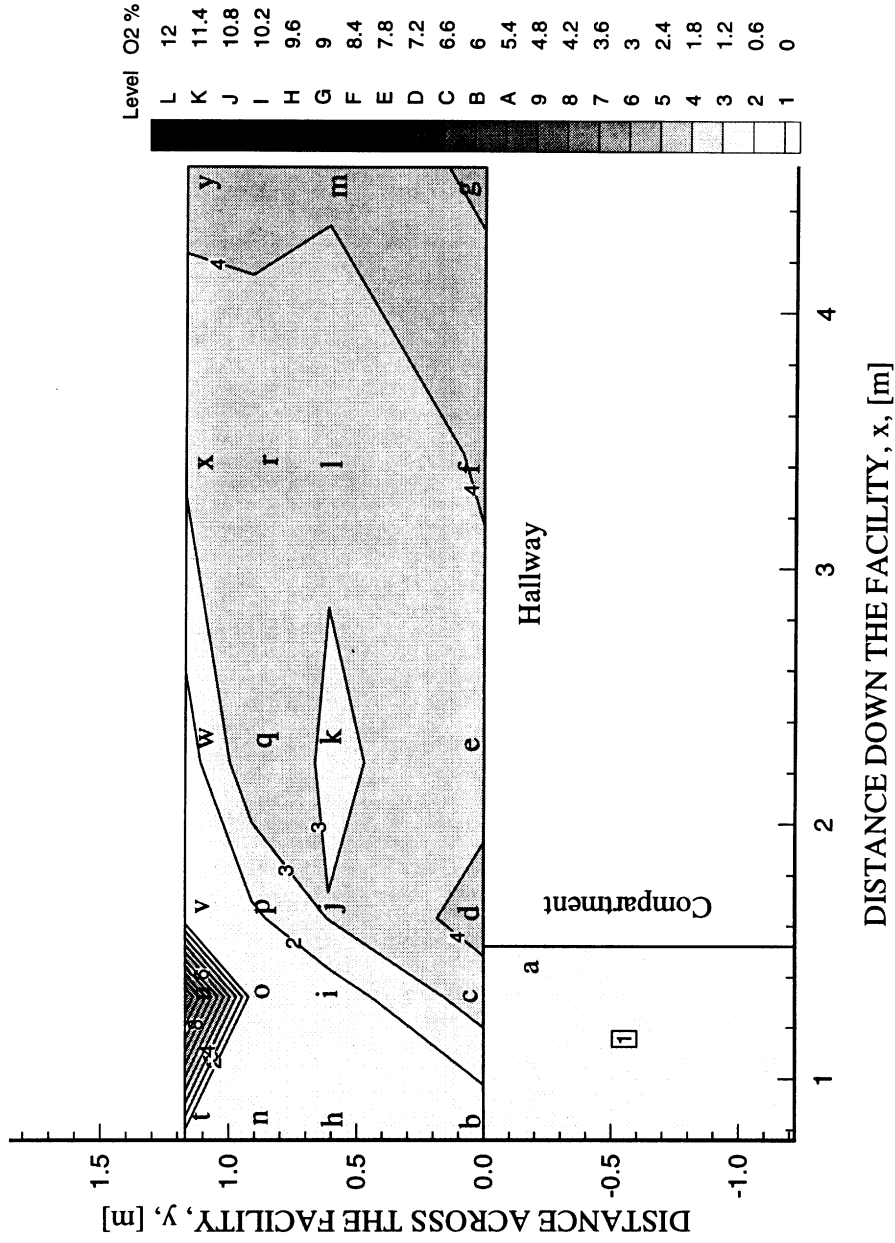


Figure 4.58 The wet O₂ concentration distribution 0.05 m below the ceiling 64-68 seconds after flashover in *n*-hexane fire experiments with a 0.04 m² opening, 0.20 m inlet soffit, 0.20 m high 1.22 m wide opening at top of hallway exit and external burning.

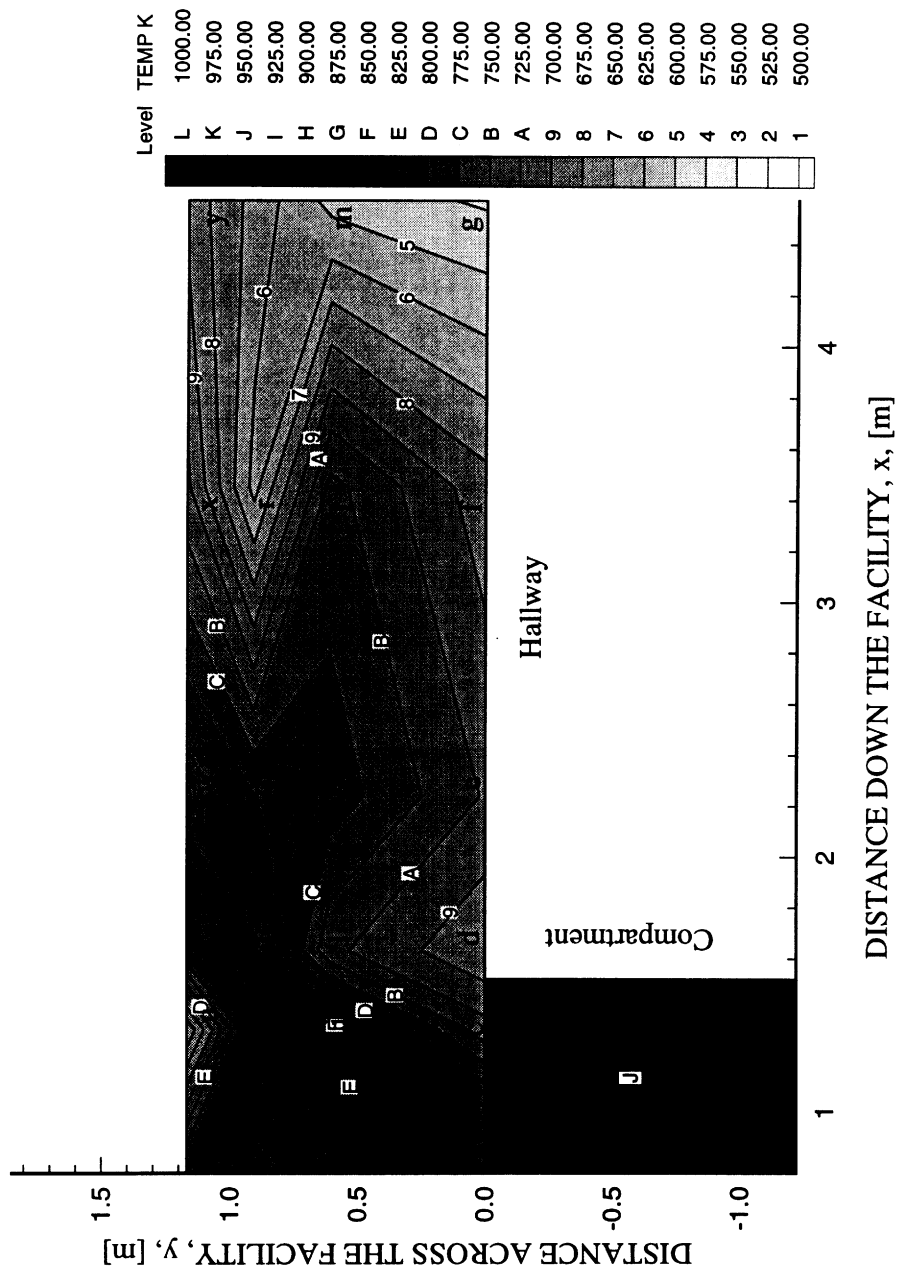


Figure 4.59 The temperature distribution 0.05 m below the ceiling 64-68 seconds after flashover in *n*-hexane fire experiments with a 0.04 m² opening, 0.20 m inlet soffit, 0.20 m high 1.22 m wide opening at top of hallway exit and external burning.

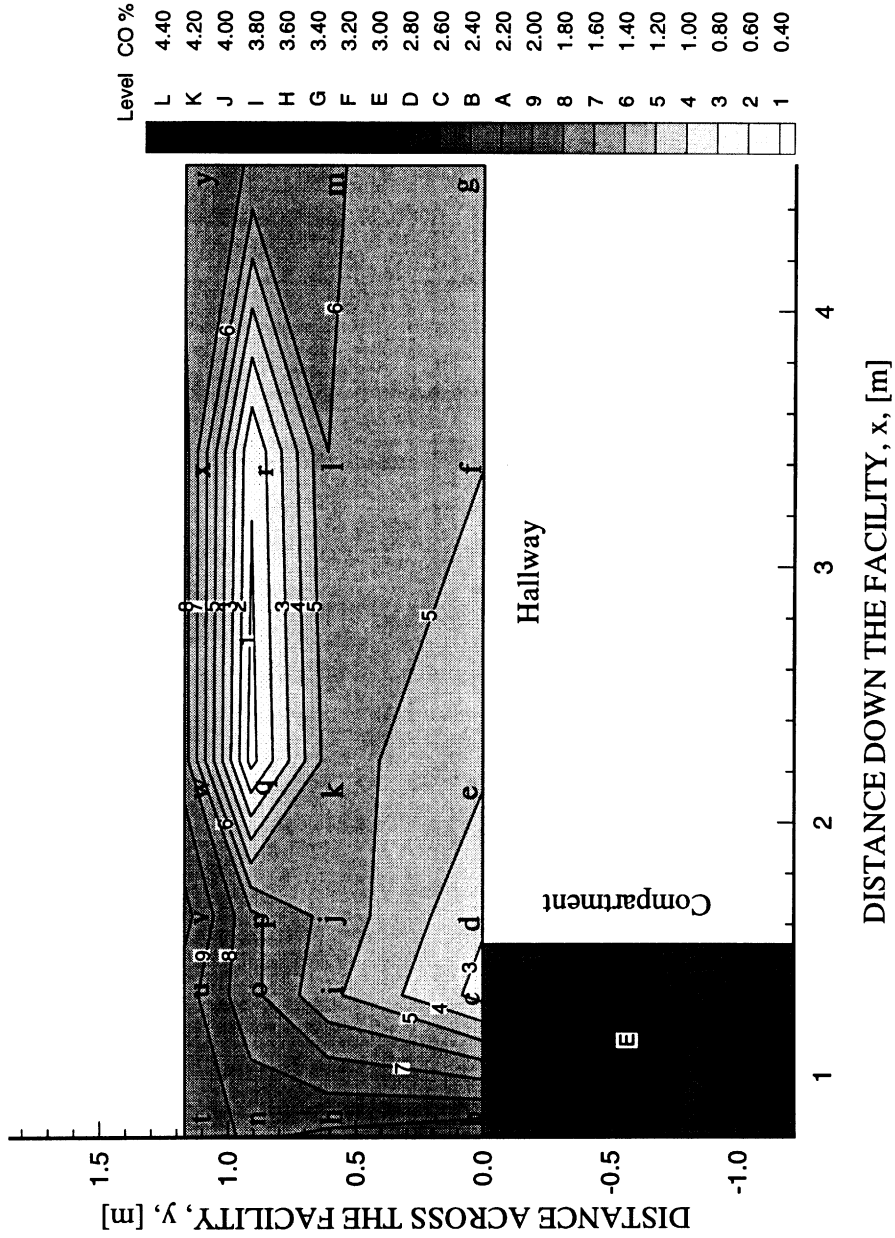


Figure 4.60 The wet CO concentration distribution 0.05 m below the ceiling 80-84 seconds after flashover in *n*-hexane fire experiments with a 0.04 m² opening, 0.20 m inlet soffit, 0.20 m high 1.22 m wide opening at top of hallway exit and external burning.

2.3 % UHC, but contained only 1.2% UHC after flowing across the hallway, see Fig 4.61. The gases flowing along the side of the hallway opposite the compartment were measured to contain UHC concentrations of nearly 10 times lower than the UHC concentration in the gases entering the hallway. The external burning continued to deplete the hallway gases of UHC, but the CO concentration in the hallway continued to rise. The upper-layer of the hallway was measured to contain a uniform distribution of approximately 10.5% CO₂ and 1.5% O₂, see Fig. 4.62 and Fig. 4.63 respectively. The temperatures were measured to be greater than approximately 775 K, see Fig. 4.64, and corresponded to where the external burning was visually observed in the hallway. The species concentrations were measured to reach a steady-state shortly after this period at approximately 96 seconds after flashover.

Approximately 108-112 seconds after flashover, external burning was no longer occurring in the hallway. The low concentration cell of CO in the upper-layer was measured to still be present, see Fig. 4.65. Slightly lower levels of CO (1.5%) were measured in the gases along the side of the hallway opposite the compartment. This was attributed to the fire entering the decay period. The CO concentration on the compartment side of the hallway was measured to be 1.4% CO, see Fig. 4.65. The UHC concentration was measured to increase slightly to 0.6% downstream of the compartment, see Fig. 4.66. The absence of external burning was also apparent by the lower levels of CO₂ (8-9%) and higher levels of O₂ (4-5%) measured in the upper layer gases, see Figs. 4.67 and 4.68, respectively. The temperatures in the hallway were measured to be approximately 50 K lower in magnitude after external burning has ceased in the hallway, see Fig. 4.69.

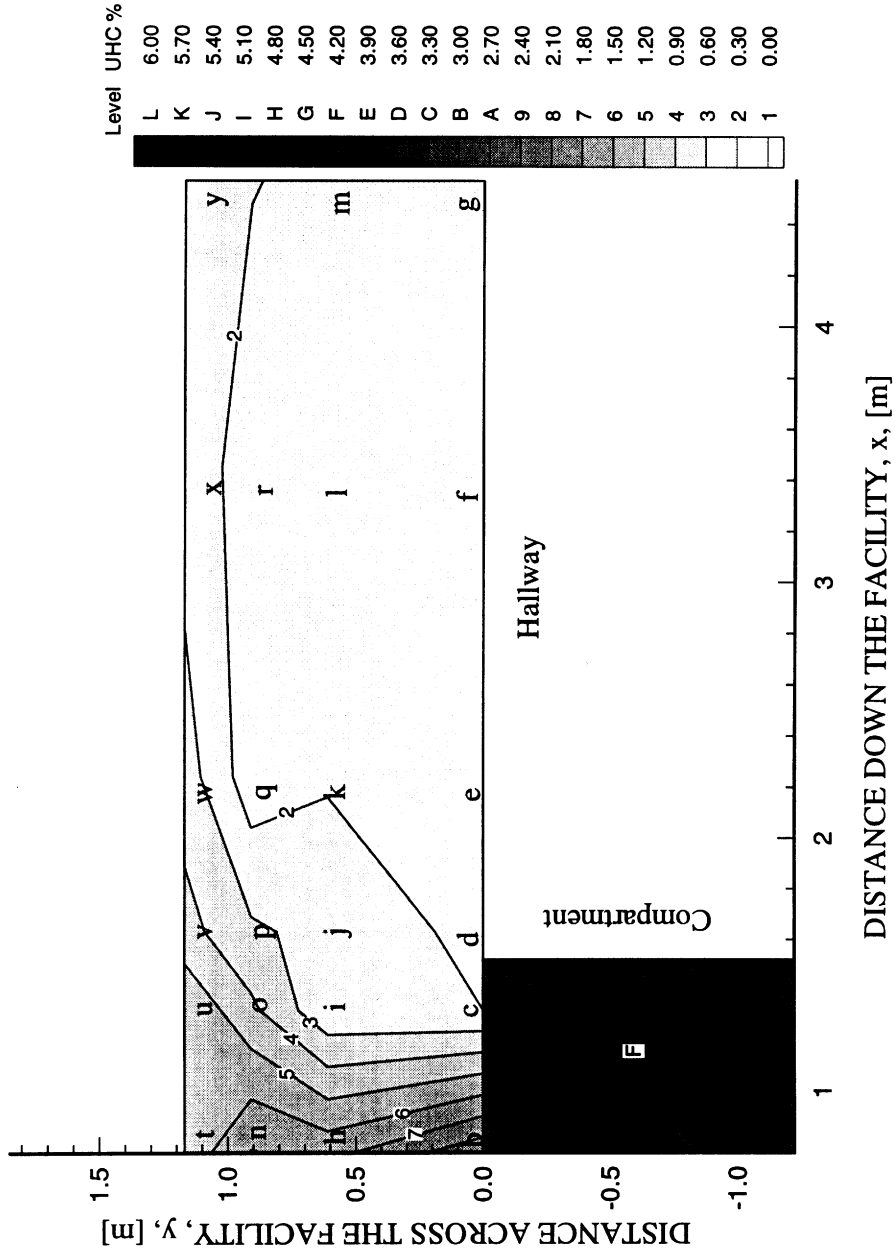


Figure 4.61 The wet UHC concentration distribution 0.05 m below the ceiling 80-84 seconds after flashover in *n*-hexane fire experiments with a 0.04 m² opening, 0.20 m inlet soffit, 0.20 m high 1.22 m wide opening at top of hallway exit and external burning.

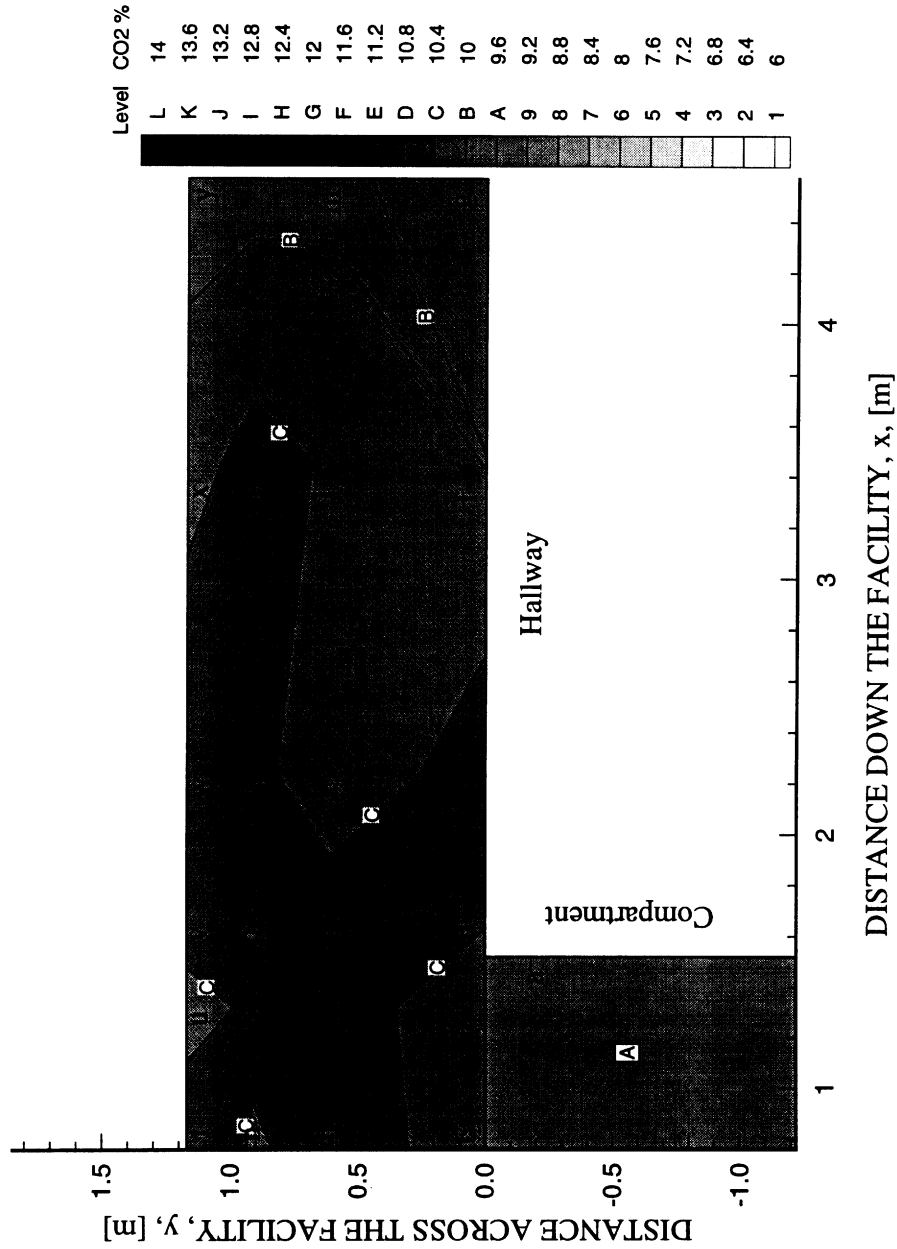


Figure 4.62 The wet CO₂ concentration distribution 0.05 m below the ceiling 80-84 seconds after flashover in *n*-hexane fire experiments with a 0.04 m² opening, 0.20 m inlet soffit, 0.20 m high 1.22 m wide opening at top of hallway exit and external burning.

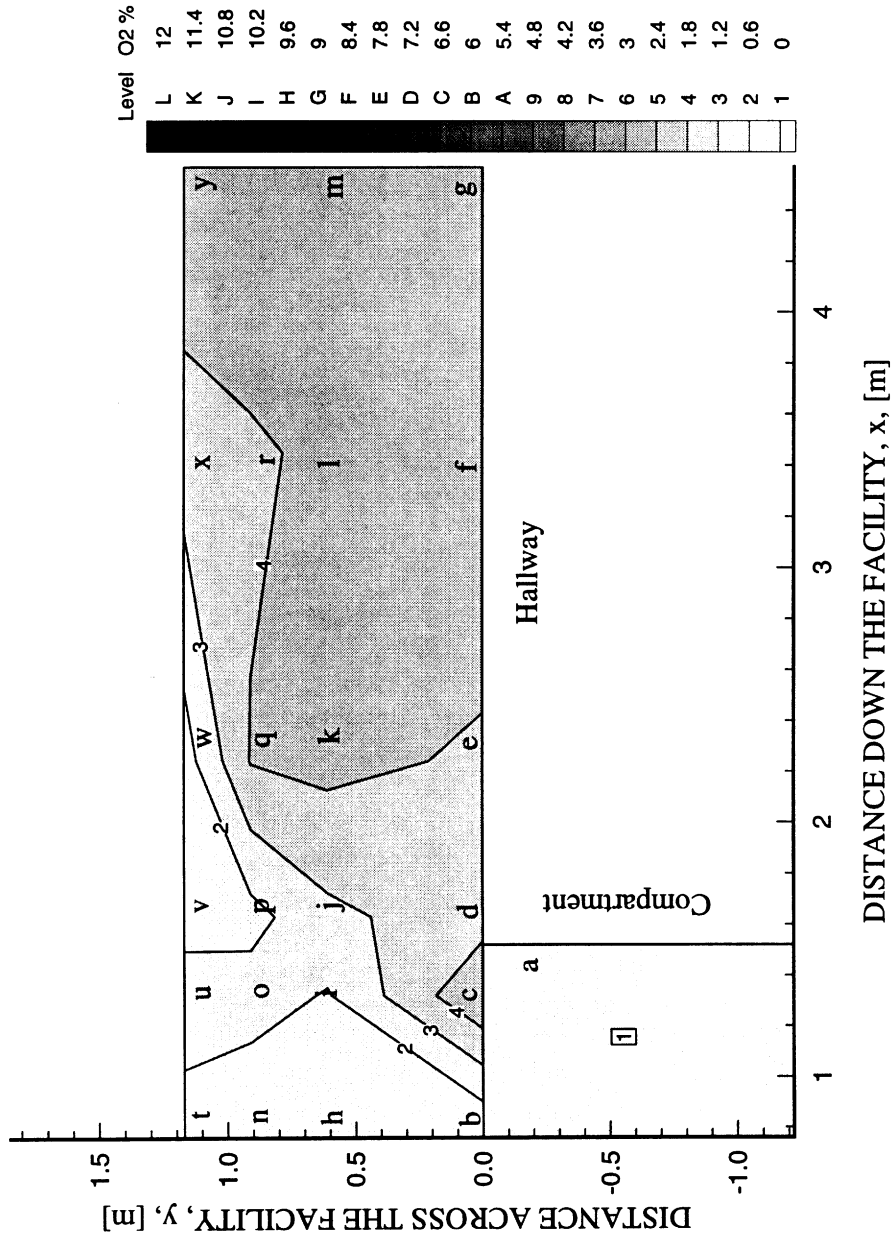


Figure 4.63 The wet O₂ concentration distribution 0.05 m below the ceiling 80-84 seconds after flashover in *n*-hexane fire experiments with a 0.04 m² opening, 0.20 m inlet soffit, 0.20 m high 1.22 m wide opening at top of hallway exit and external burning.

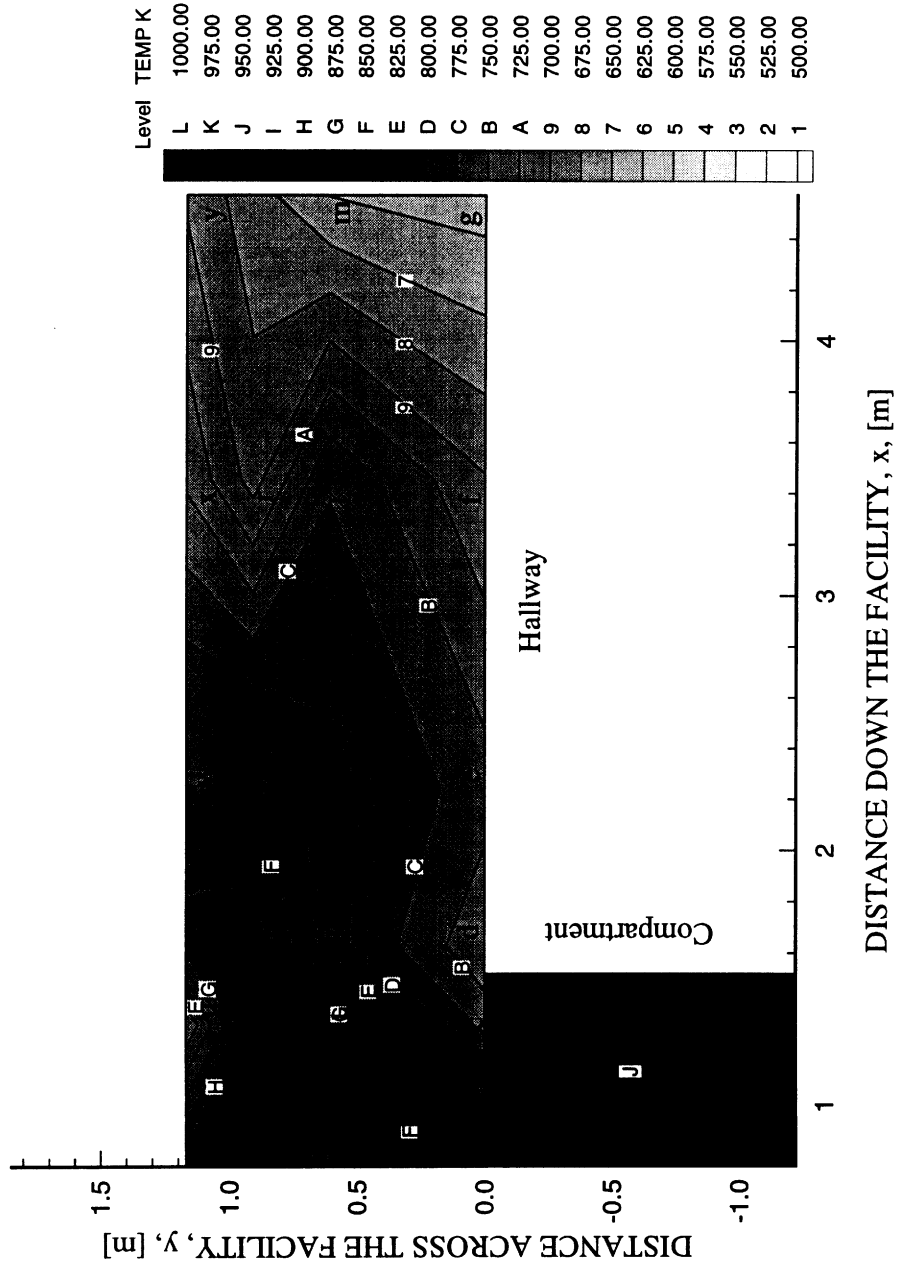


Figure 4.64 The temperature distribution 0.05 m below the ceiling 80-84 seconds after flashover in *n*-hexane fire experiments with a 0.04 m² opening, 0.20 m inlet soffit, 0.20 m high 1.22 m wide opening at top of hallway exit and external burning.

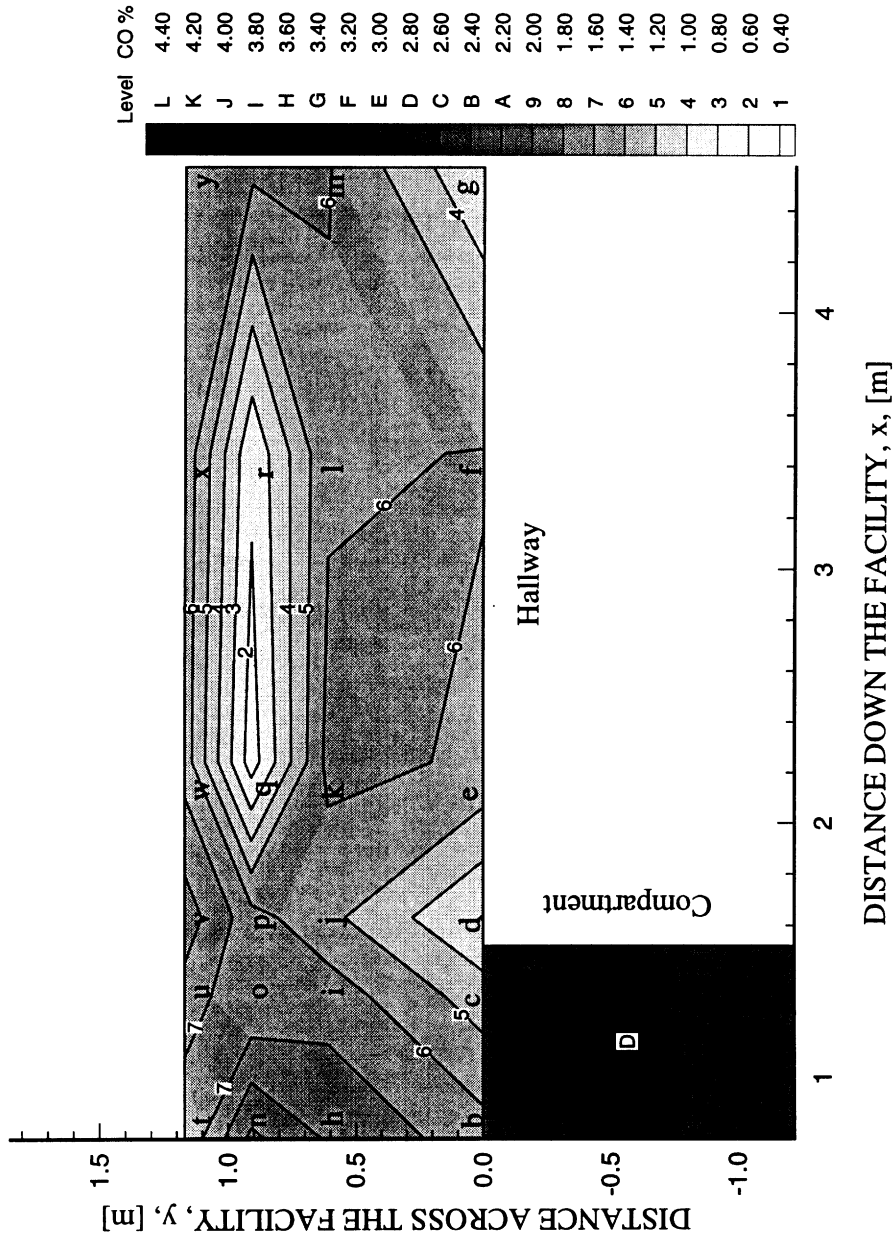


Figure 4.65 The wet CO concentration distribution 0.05 m below the ceiling 108-112 seconds after flashover in *n*-hexane fire experiments with a 0.04 m² opening, 0.20 m inlet soffit, 0.20 m high 1.22 m wide opening at top of hallway exit and external burning.

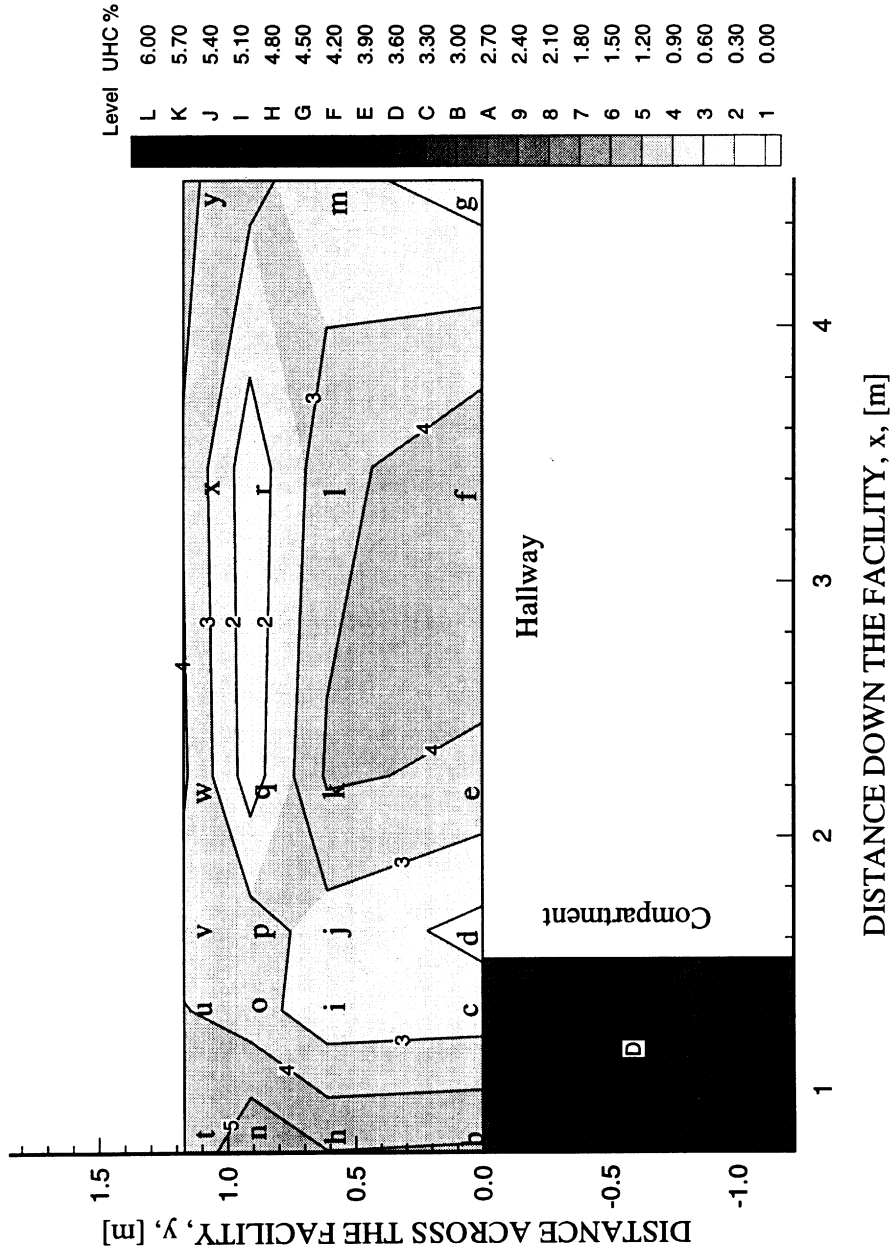


Figure 4.66 The wet UHC concentration distribution 0.05 m below the ceiling 108-112 seconds after flashover in *n*-hexane fire experiments with a 0.04 m² opening, 0.20 m inlet soffit, 0.20 m high 1.22 m wide opening at top of hallway exit and external burning.

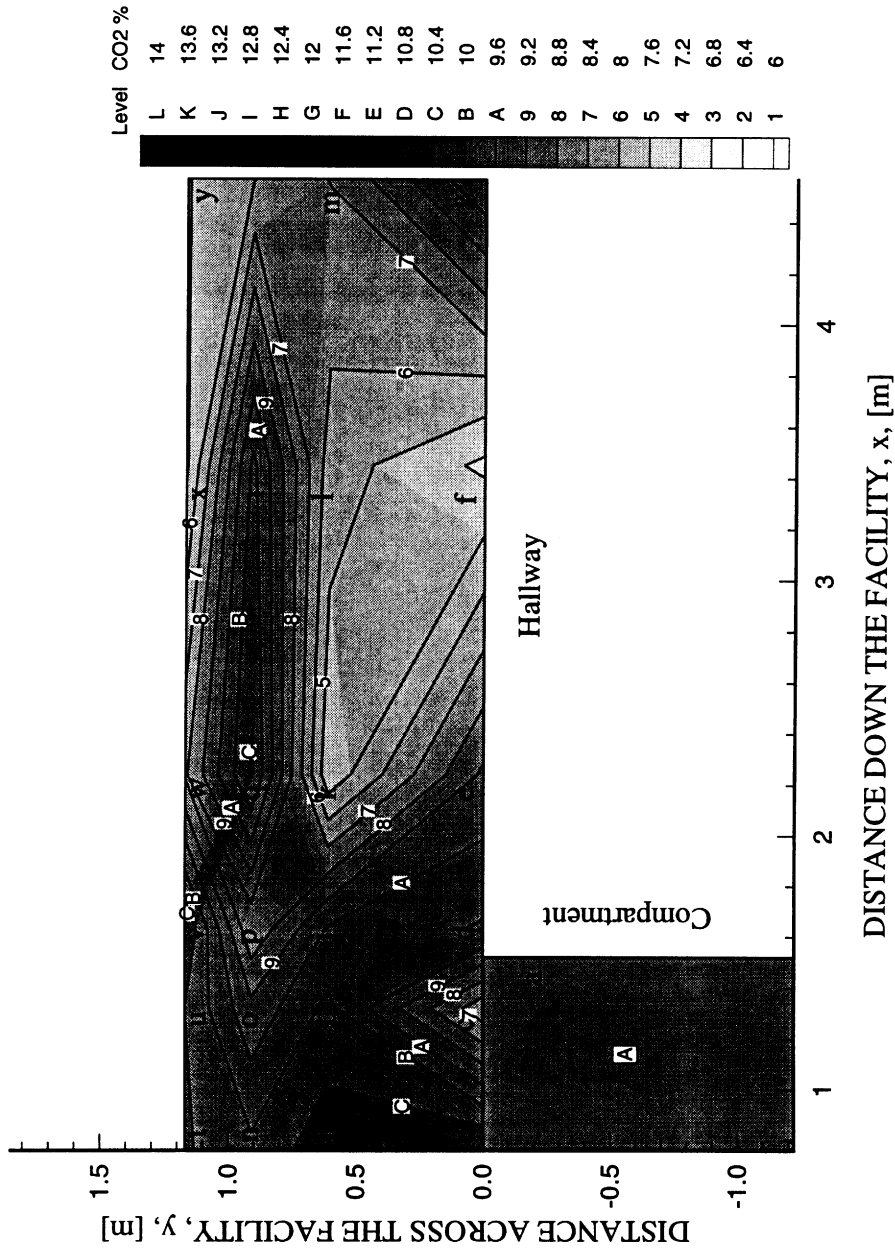


Figure 4.67 The wet CO₂ concentration distribution 0.05 m below the ceiling 108-112 seconds after flashover in *n*-hexane fire experiments with a 0.04 m² opening, 0.20 m inlet soffit, 0.20 m high 1.22 m wide opening at top of hallway exit and external burning.

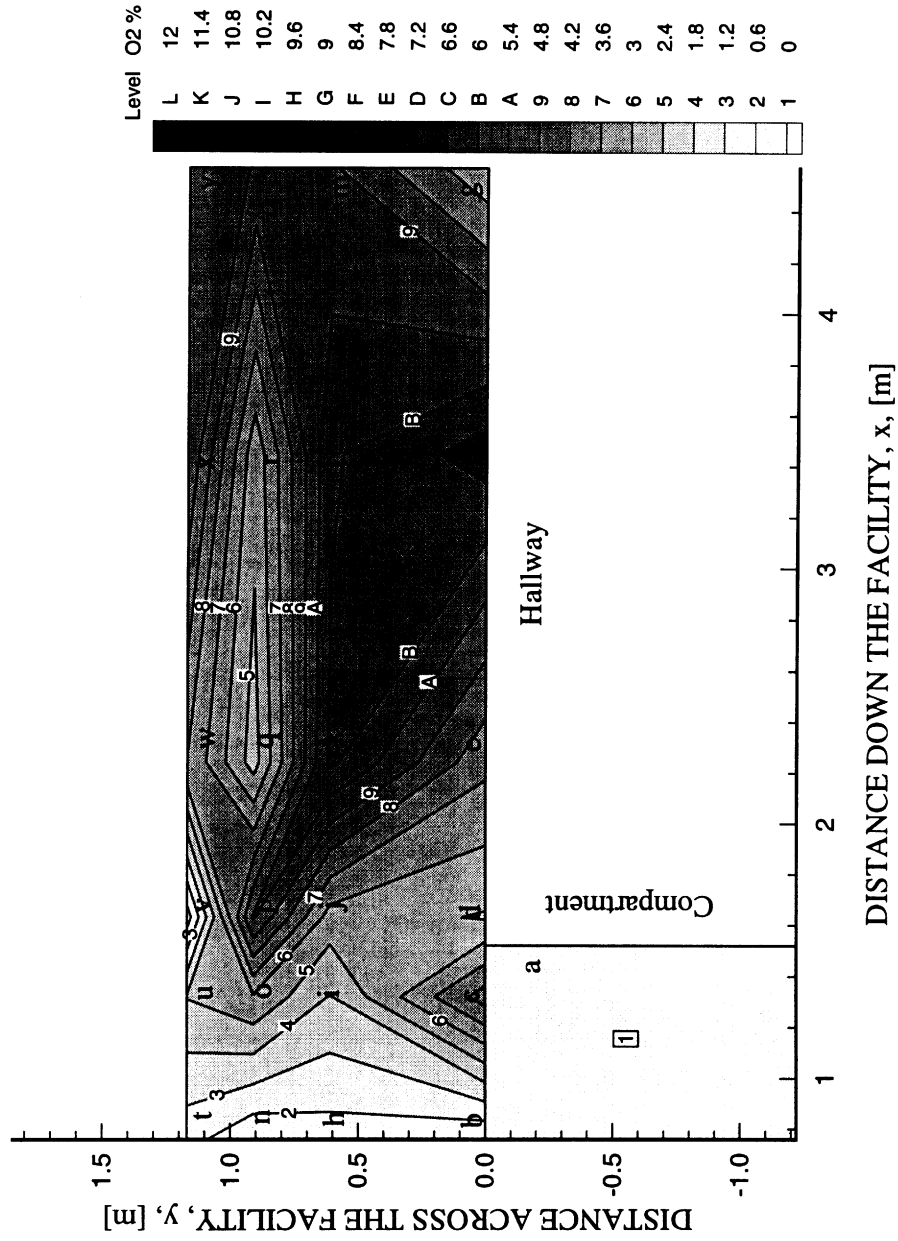


Figure 4.68 The wet O₂ concentration distribution 0.05 m below the ceiling 108-112 seconds after flashover in *n*-hexane fire experiments with a 0.04 m² opening, 0.20 m inlet soffit, 0.20 m high 1.22 m wide opening at top of hallway exit and external burning.

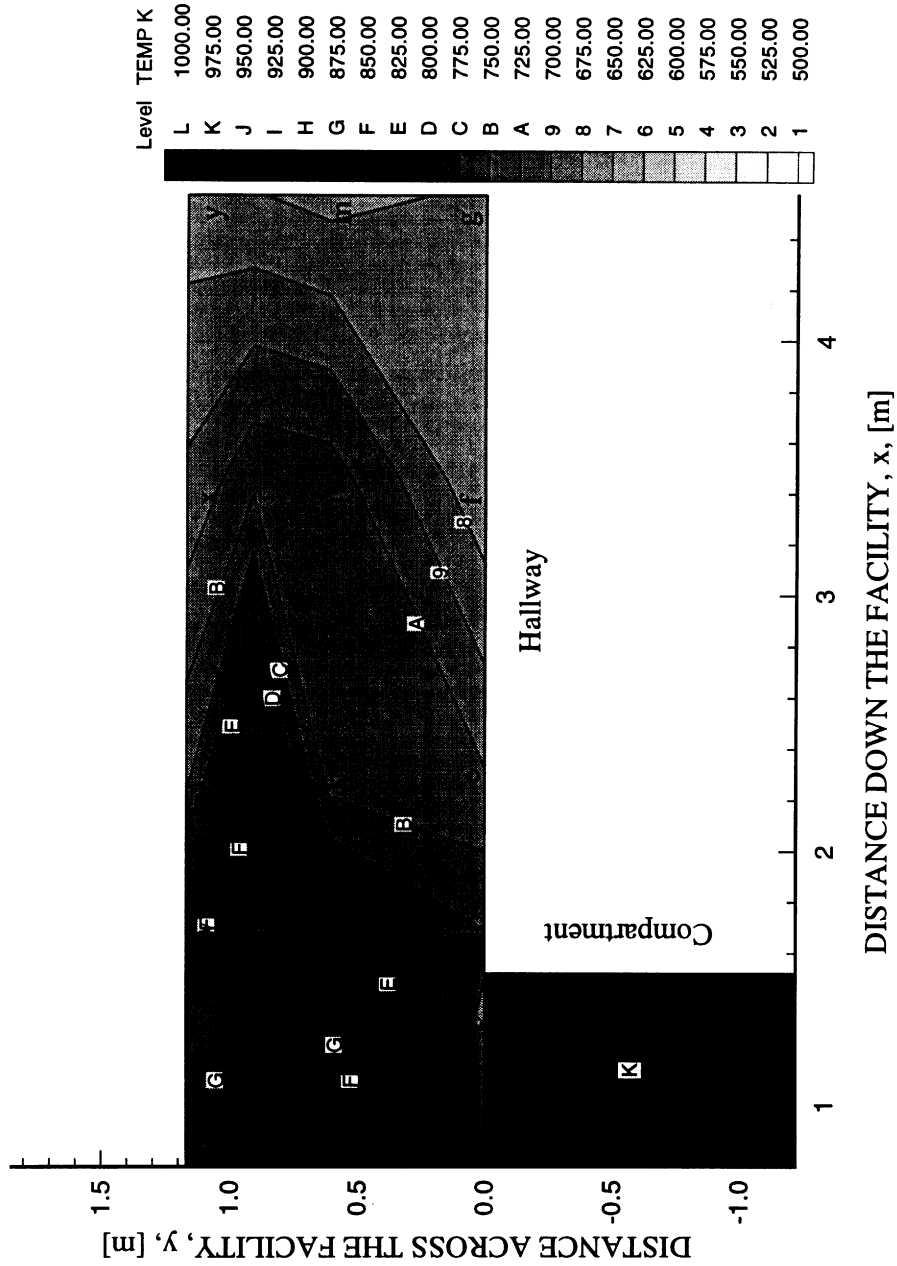


Figure 4.69 The temperature distribution 0.05 m below the ceiling 108-112 seconds after flashover in *n*-hexane fire experiments with a 0.04 m² opening, 0.20 m inlet soffit, 0.20 m high 1.22 m wide opening at top of hallway exit and external burning.

4.4 EVOLUTION IN POLYURETHANE FOAM COMPARTMENT FIRES

4.4.1 Short Transient Time with No External Burning

Compartment fire experiments with polyurethane foam as fuel were performed to investigate the effects of burning a fuel more commonly found in health care facilities and office buildings (i.e. upholstered furniture and bedding). Experiments were conducted with a 0.04 m² opening and a 0.60 deep hallway upper-layer. This corresponds to a nondimensional upper-layer depth of $\gamma=1.7$. As stated in section 3.4, no external burning was visibly apparent in these experiments. The compartment global equivalence ratios were, on average, 2.10 ± 0.07 .

The fire growth parameter was also used in these experiments to align the post-flashover period of the 11 experiments performed in this study, see Fig. 2.11. The compartment temperatures of the experiments are shown in Fig. 4.70 to be aligned with one another. Note that the time scale on Fig. 4.70 is different than that of Fig. 4.2, Fig. 4.18 and Fig. 4.44. The post-flashover period in these experiments was nearly twice as long as the post-flashover in the *n*-hexane experiments. The location of the sampling, previously noted in Fig. 2.11, is denoted by the lower case letters over top of the contour plots to follow.

With no external burning in the hallway during these experiments, the variation in the combustion gases, both spatially and temporally, is expected to be similar to the *n*-hexane experiments with no external burning discussed in section 4.3.1. The presence of the 0.60 m exit soffit, as previously seen in section 4.3.1 and 4.3.2, resulted in a short transient time for the species concentrations in the hallway upper-layer.

At 32-36 seconds after the onset of flashover inside the compartment, the concentration of CO was measured to be 1.9% in the compartment, see Fig. 4.71. As shown in the plot of CO concentrations in Fig. 4.71, the CO concentration was diluted rapidly to less than 0.5% by the time the gases had traveled across the hallway. High

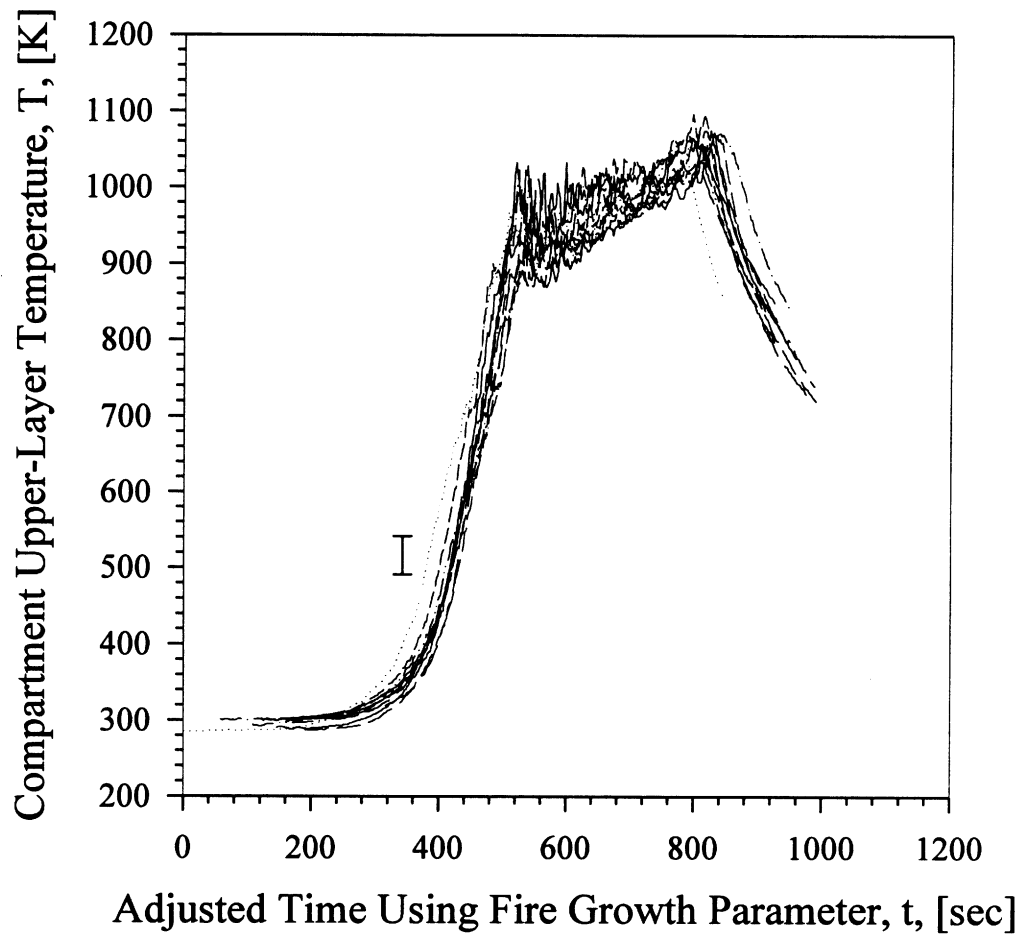


Figure 4.70 The temperature 0.05 m below the ceiling inside the compartment in 10 different polyurethane foam fire experiments with no external burning, a 0.04 m^2 opening, and a 0.60 m exit soffit. The experiments were aligned with one another in time using the fire growth parameter.

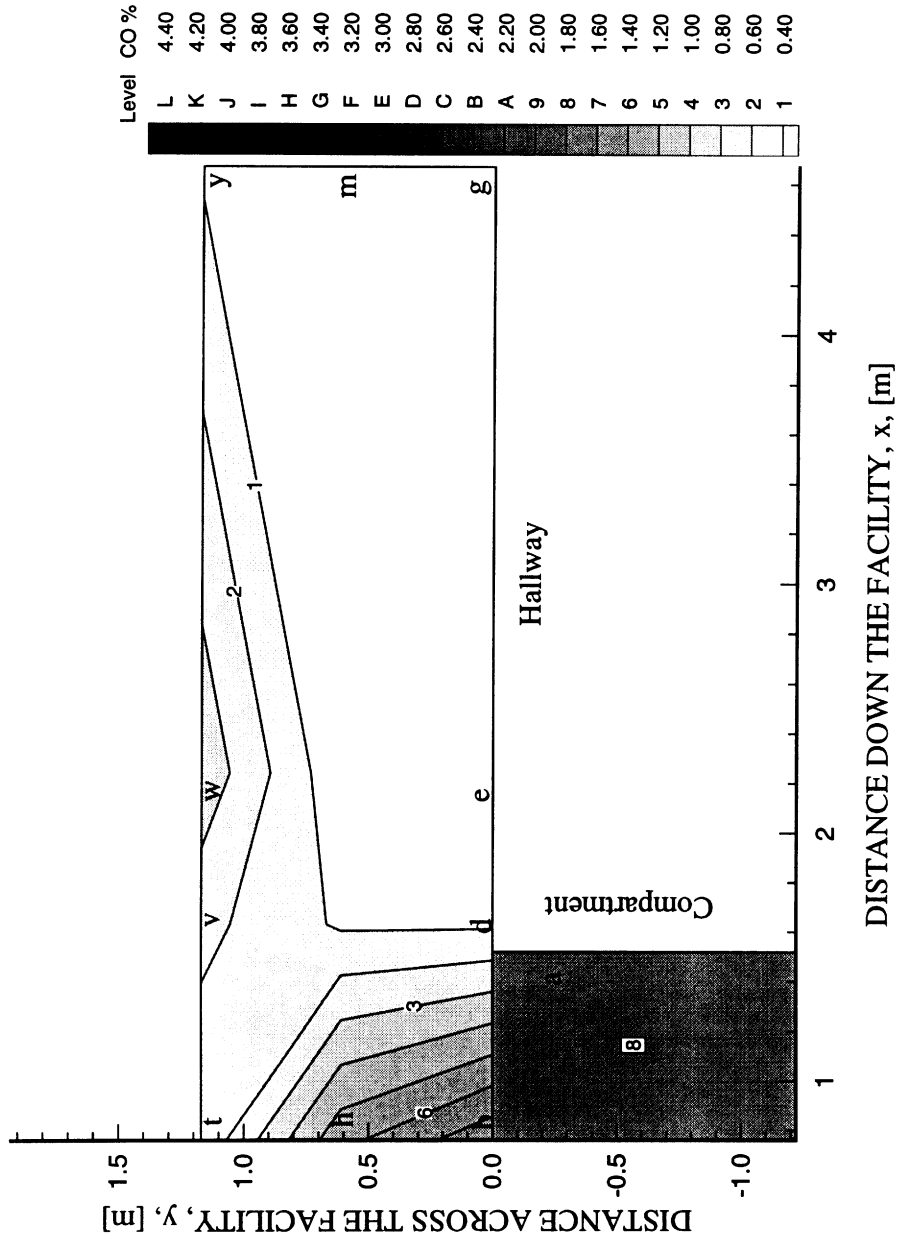


Figure 4.71 The wet CO concentration distribution 0.05 m below the ceiling 32-36 seconds after flashover in polyurethane foam fire experiments with a 0.04 m² opening, 0.20 m inlet soffit, 0.60 m exit soffit and no external burning.

concentrations of CO₂ (11%) were measured in the gases entering the hallway, see Fig. 4.72. These high concentrations were also measured in the gases flowing across the hallway and down the side of the hallway opposite the compartment. Similarly, lower levels of O₂ were measured in gases traveling across the hallway and down the side of the hallway opposite the compartment, see Fig. 4.73. The temperatures in the hallway just downstream of the compartment remained less than 525K as shown in Fig. 4.74.

At 64-68 seconds after flashover in the compartment, 1.7% CO was measured in the gases across the hallway from the compartment, see Fig. 4.75. The CO concentration in the gases along the compartment side of the hallway, however, was measured to be 1.0%, approximately half the level on the opposite side of the compartment. The CO₂ concentrations were measured to be uniform at a level of 6.7 %, see Fig. 4.76. The O₂ concentrations in the gases near the compartment were measured to be approximately 7.2% near the compartment and gradually increased in concentration as the gases flowed down the hallway, see Fig. 4.77. Temperatures were measured in Fig. 4.78 to remain low at levels less than or equal to 500 K downstream of the compartment.

The species concentrations in the hallway reached a steady-state at approximately 92-96 seconds after post-flashover inside the compartment. This is approximately 60 seconds after 1% CO was measured entering the hallway. The concentration of CO in the upper-layer was measured to be uniform in the upper-layer at approximately 1.8%, see Fig. 4.79. The CO₂ concentration was measured to be 7.0% within the upper-layer as shown in Fig. 4.80. Oxygen concentration in the hallway was measured to remain uniform at approximately 7.0%, see Fig. 4.81. The gas temperature also remained low at temperatures of approximately 500 K or less throughout the hallway upper-layer, see Fig. 4.82.

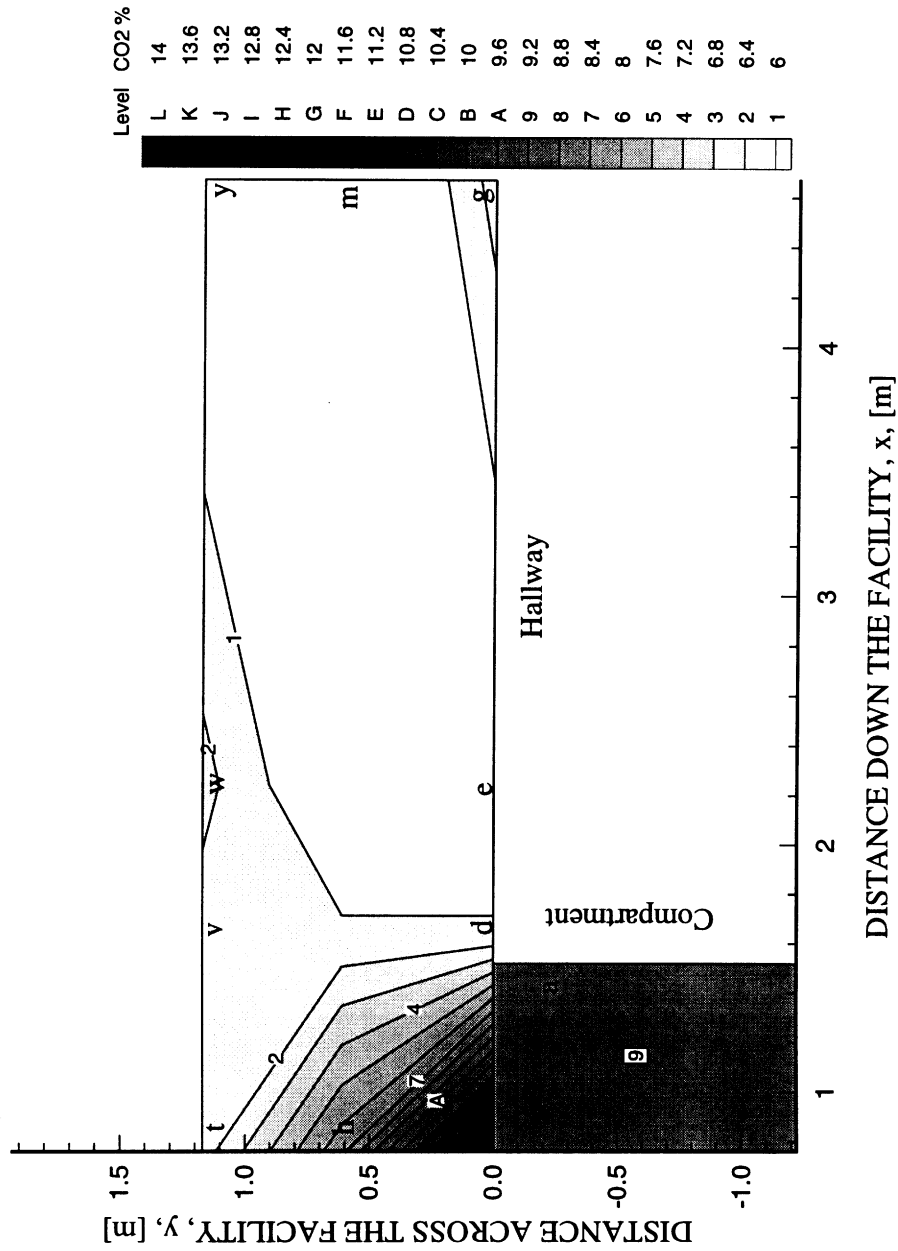


Figure 4.72 The wet CO₂ concentration distribution 0.05 m below the ceiling 32-36 seconds after flashover in polyurethane foam fire experiments with a 0.04 m² opening, 0.20 m inlet soffit, 0.60 m exit soffit and no external burning.

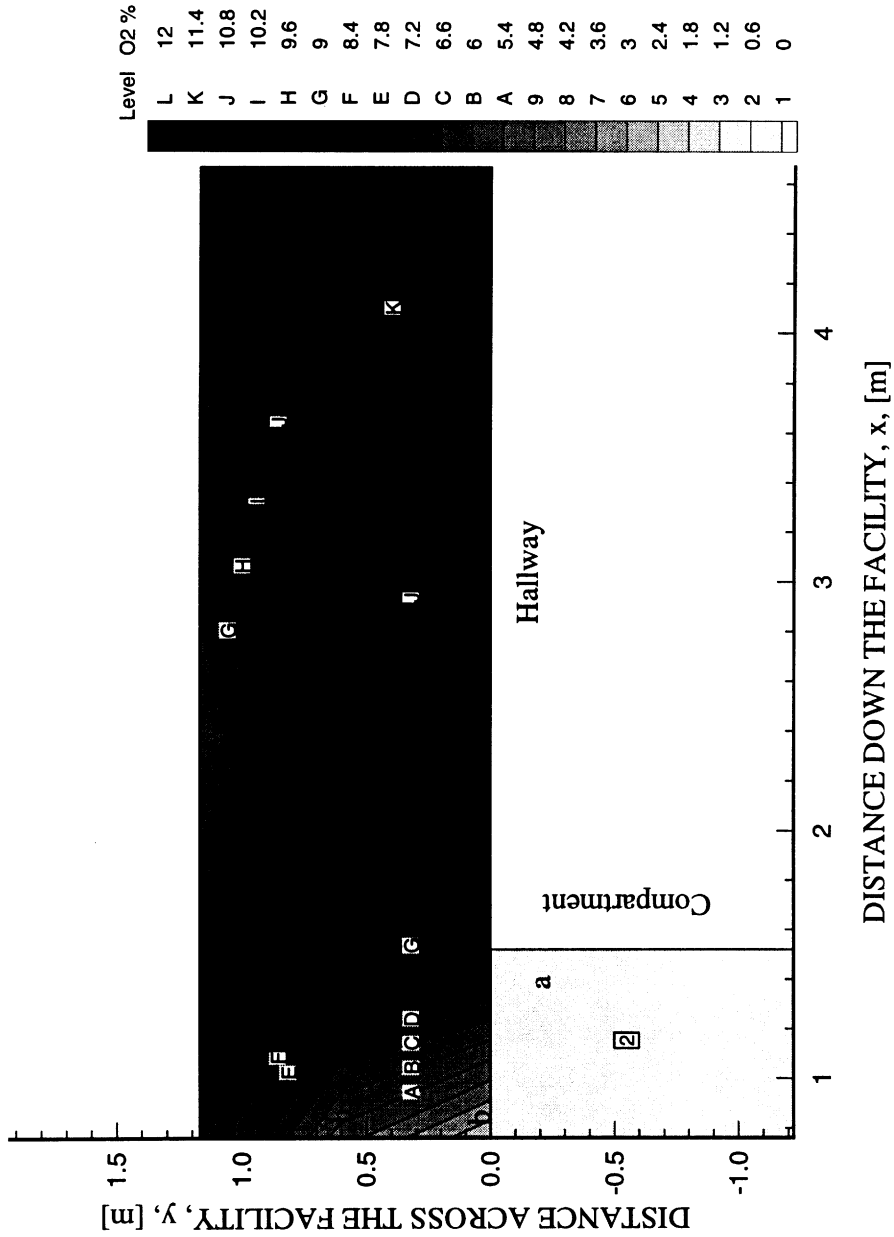


Figure 4.73 The wet O₂ concentration distribution 0.05 m below the ceiling 32-36 seconds after flashover in polyurethane foam fire experiments with a 0.04 m² opening, 0.20 m inlet soffit, 0.60 m exit soffit and no external burning.

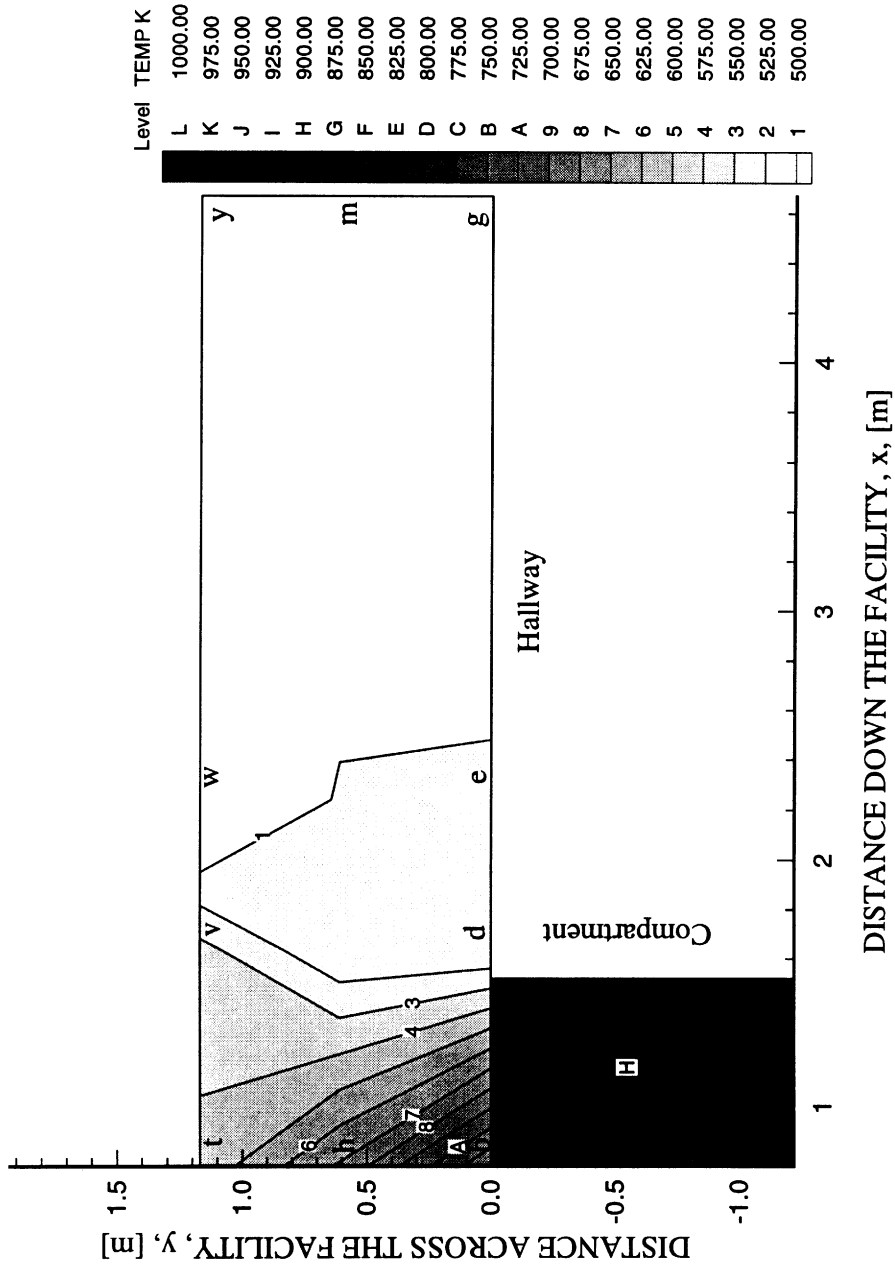


Figure 4.74 The temperature distribution 0.05 m below the ceiling 32-36 seconds after flashover in polyurethane foam fire experiments with a 0.04 m² opening, 0.20 m inlet soffit, 0.60 m exit soffit and no external burning.

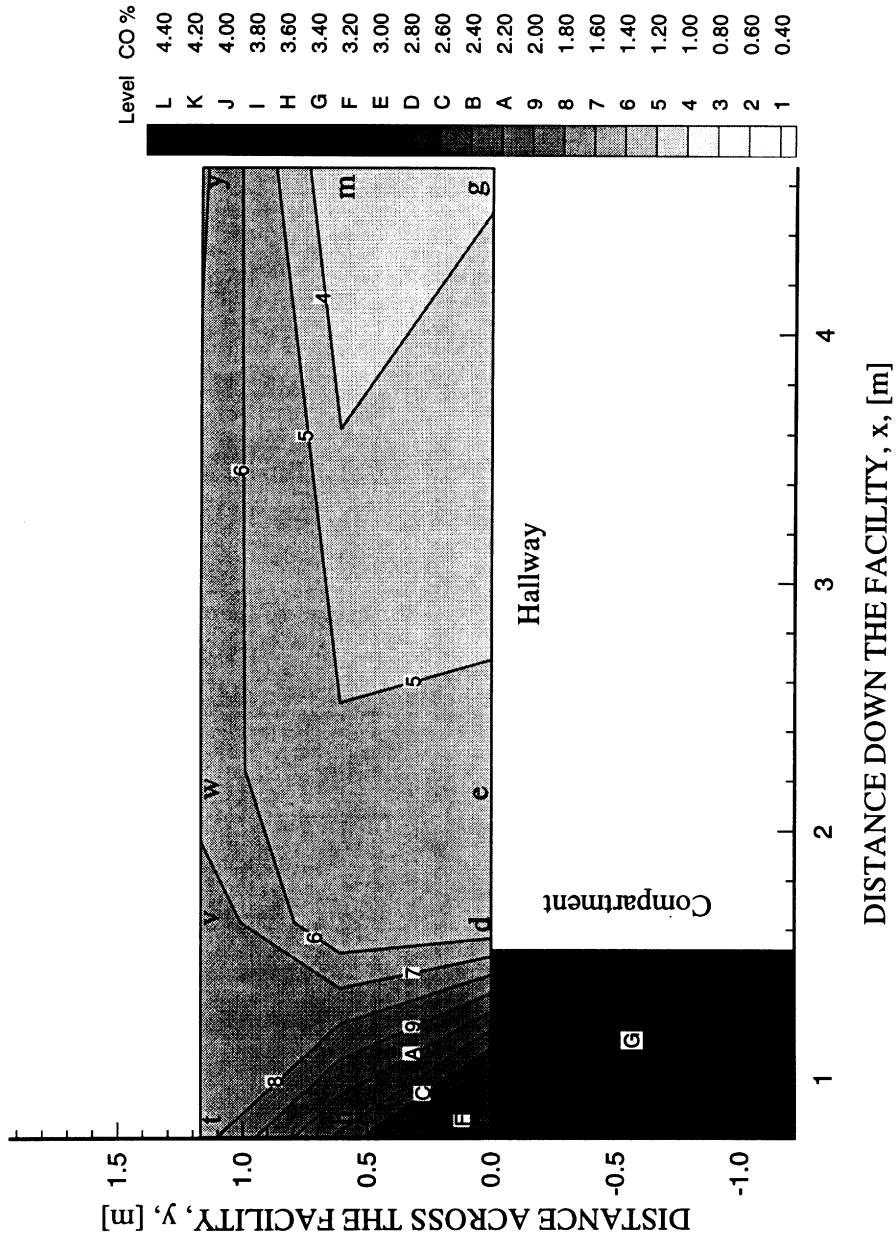


Figure 4.75 The wet CO concentration distribution 0.05 m below the ceiling 64-68 seconds after flashover in polyurethane foam fire experiments with a 0.04 m² opening, 0.20 m inlet soffit, 0.60 m exit soffit and no external burning.

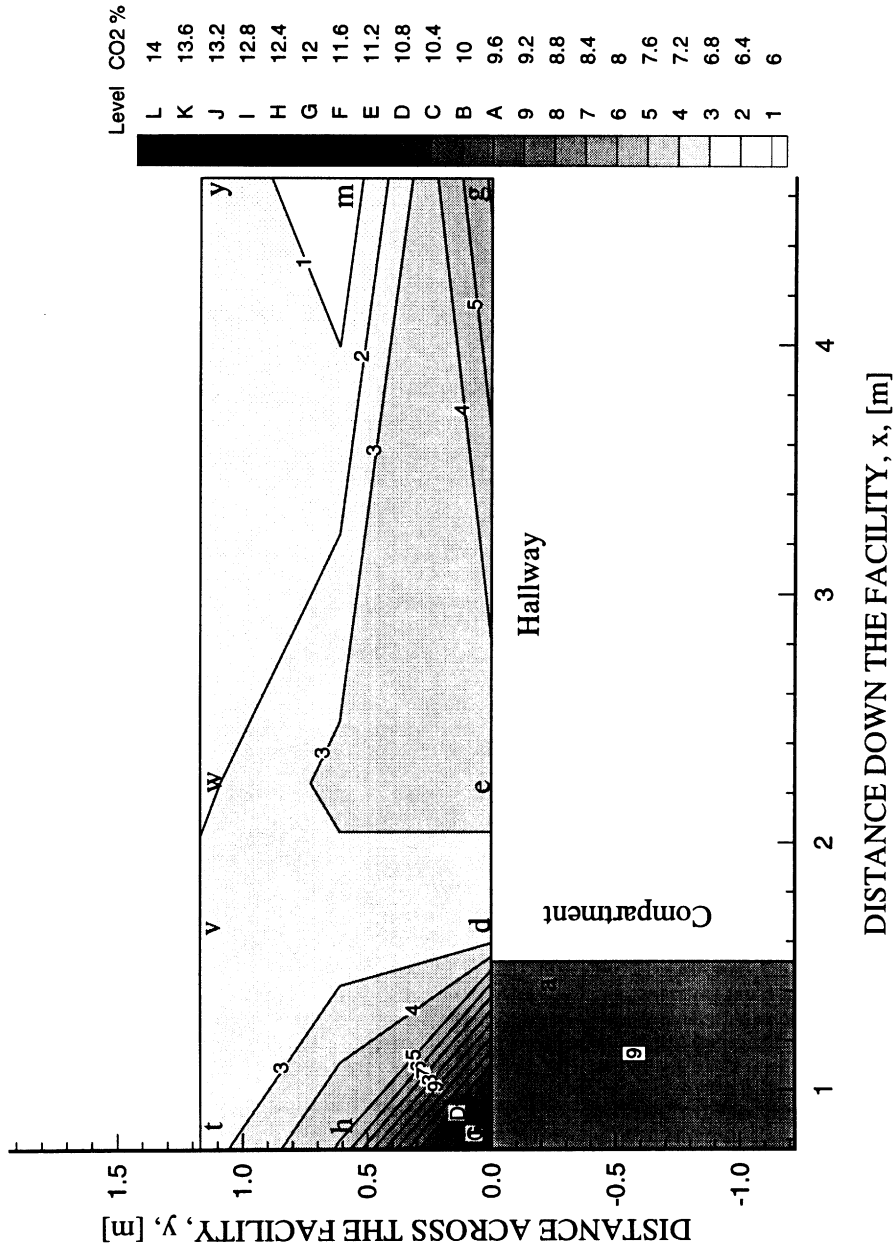


Figure 4.76 The wet CO₂ concentration distribution 0.05 m below the ceiling 64-68 seconds after flashover in polyurethane foam fire experiments with a 0.04 m² opening, 0.20 m inlet soffit, 0.60 m exit soffit and no external burning.

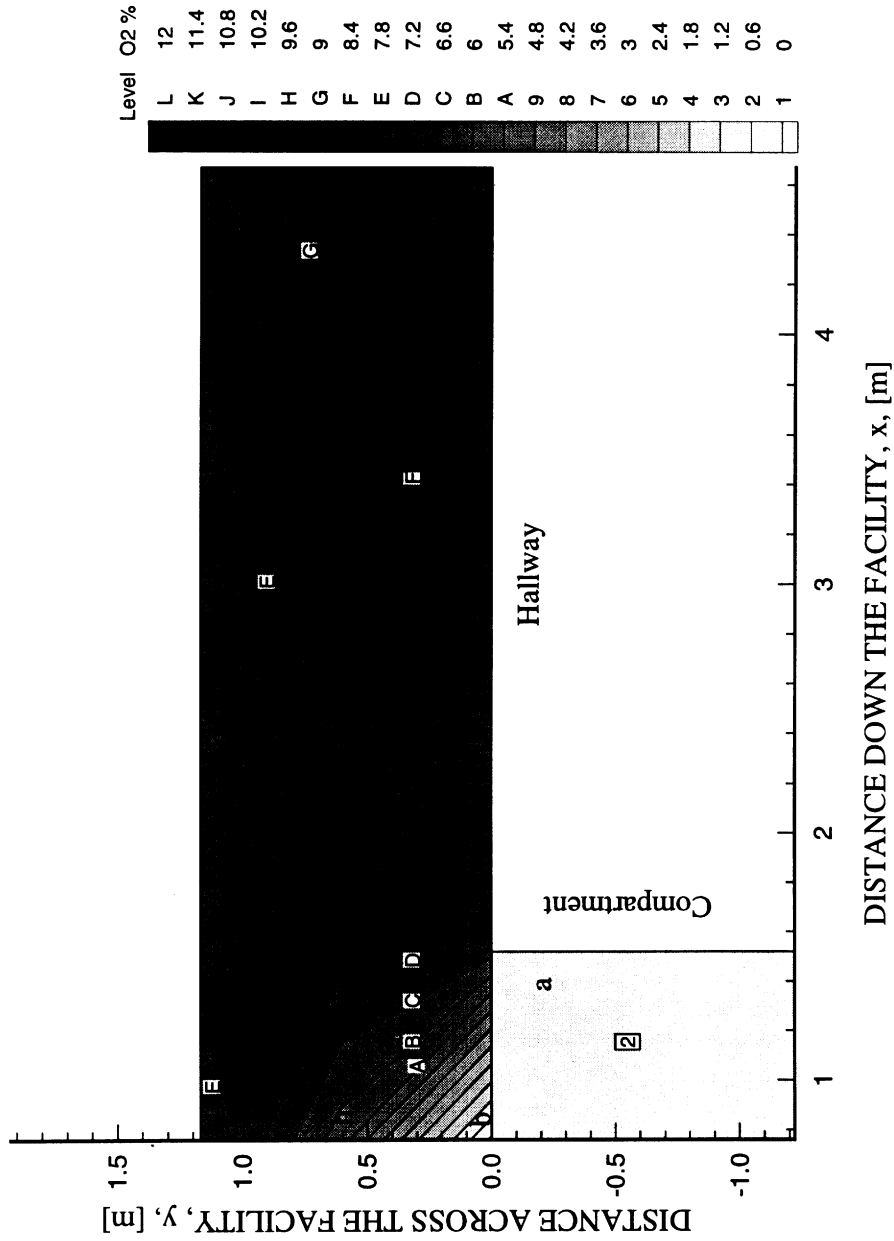


Figure 4.77 The wet O₂ concentration distribution 0.05 m below the ceiling 64-68 seconds after flashover in polyurethane foam fire experiments with a 0.04 m² opening, 0.20 m inlet soffit, 0.60 m exit soffit and no external burning.

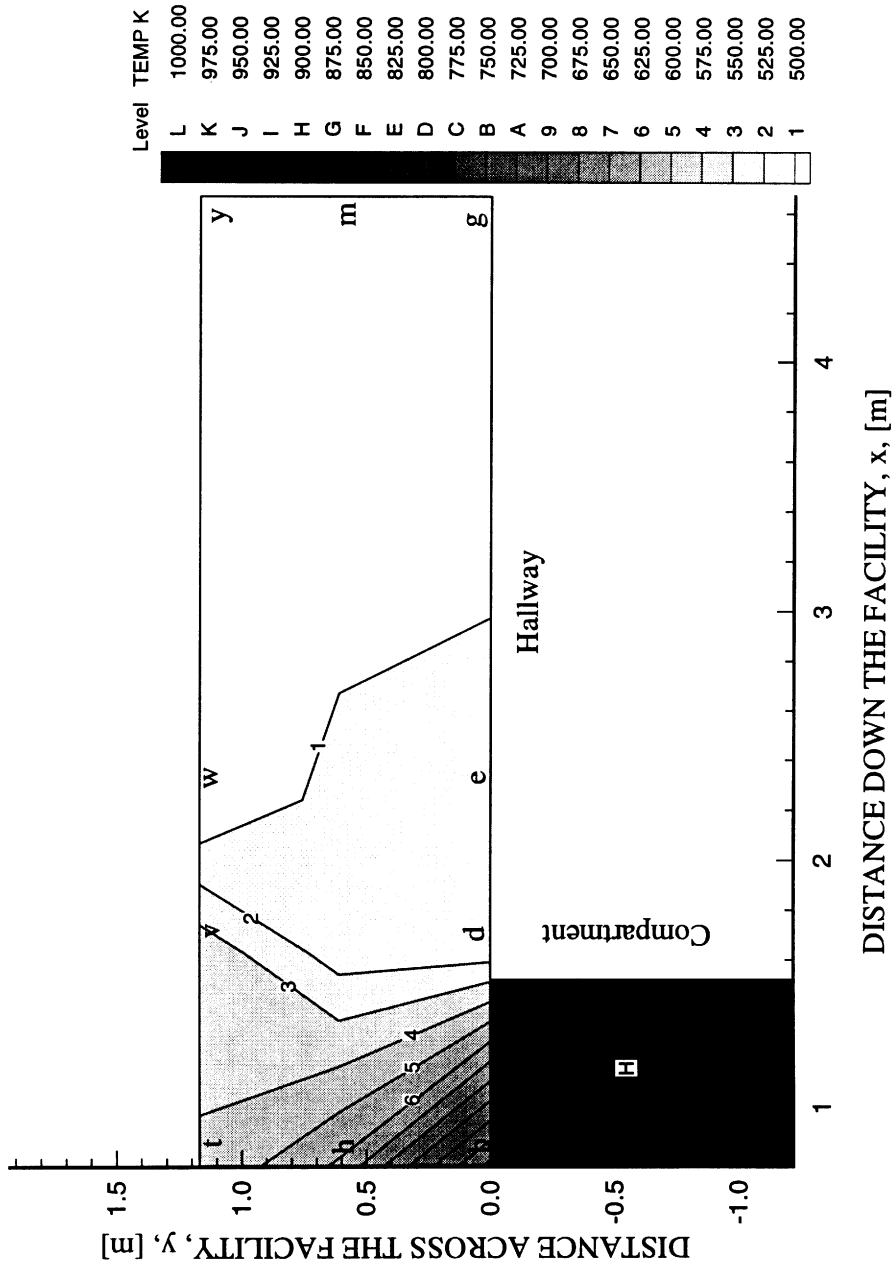


Figure 4.78 The temperature distribution 0.05 m below the ceiling 64-68 seconds after flashover in polyurethane foam fire experiments with a 0.04 m² opening, 0.20 m inlet soffit, 0.60 m exit soffit and no external burning.

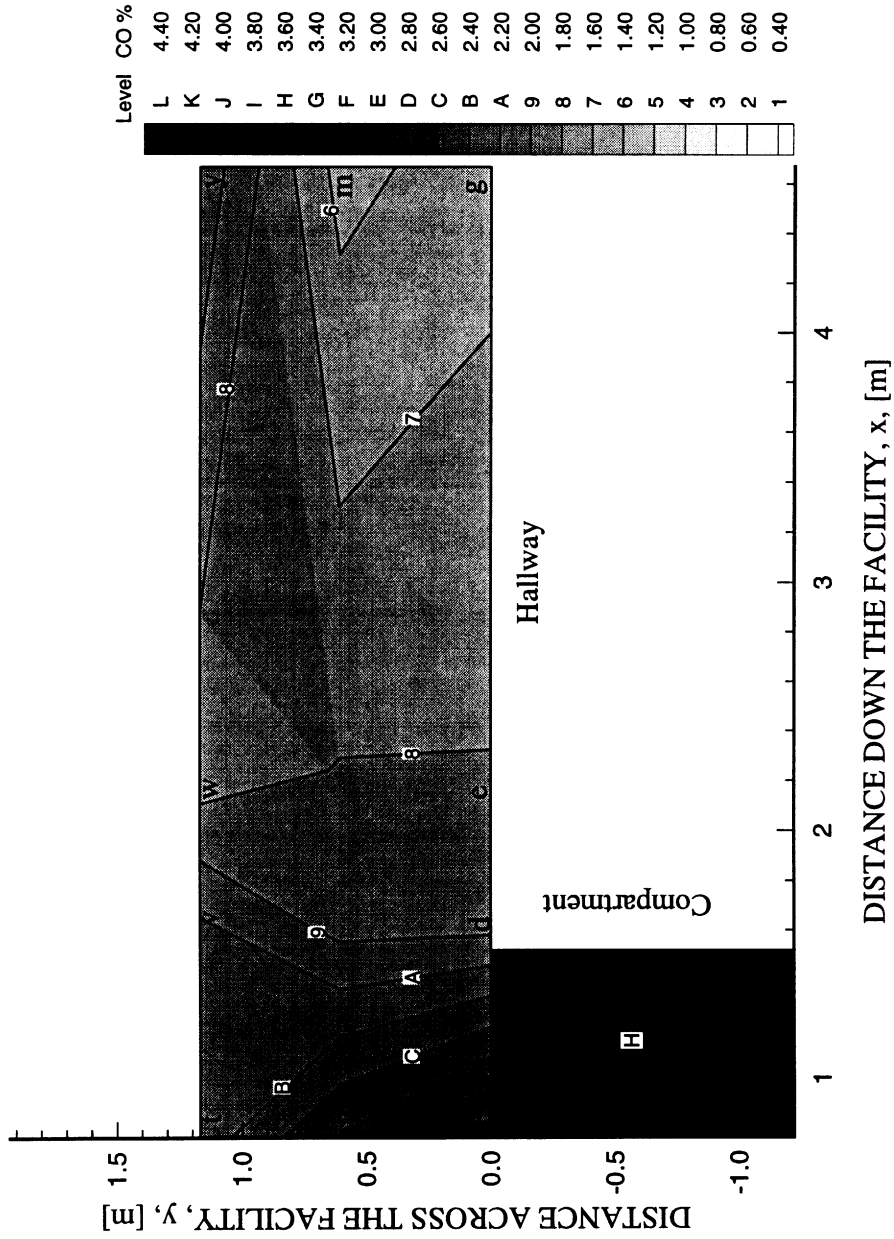


Figure 4.79 The wet CO concentration distribution 0.05 m below the ceiling 92-96 seconds after flashover in polyurethane foam fire experiments with a 0.04 m² opening, 0.20 m inlet soffit, 0.60 m exit soffit and no external burning.

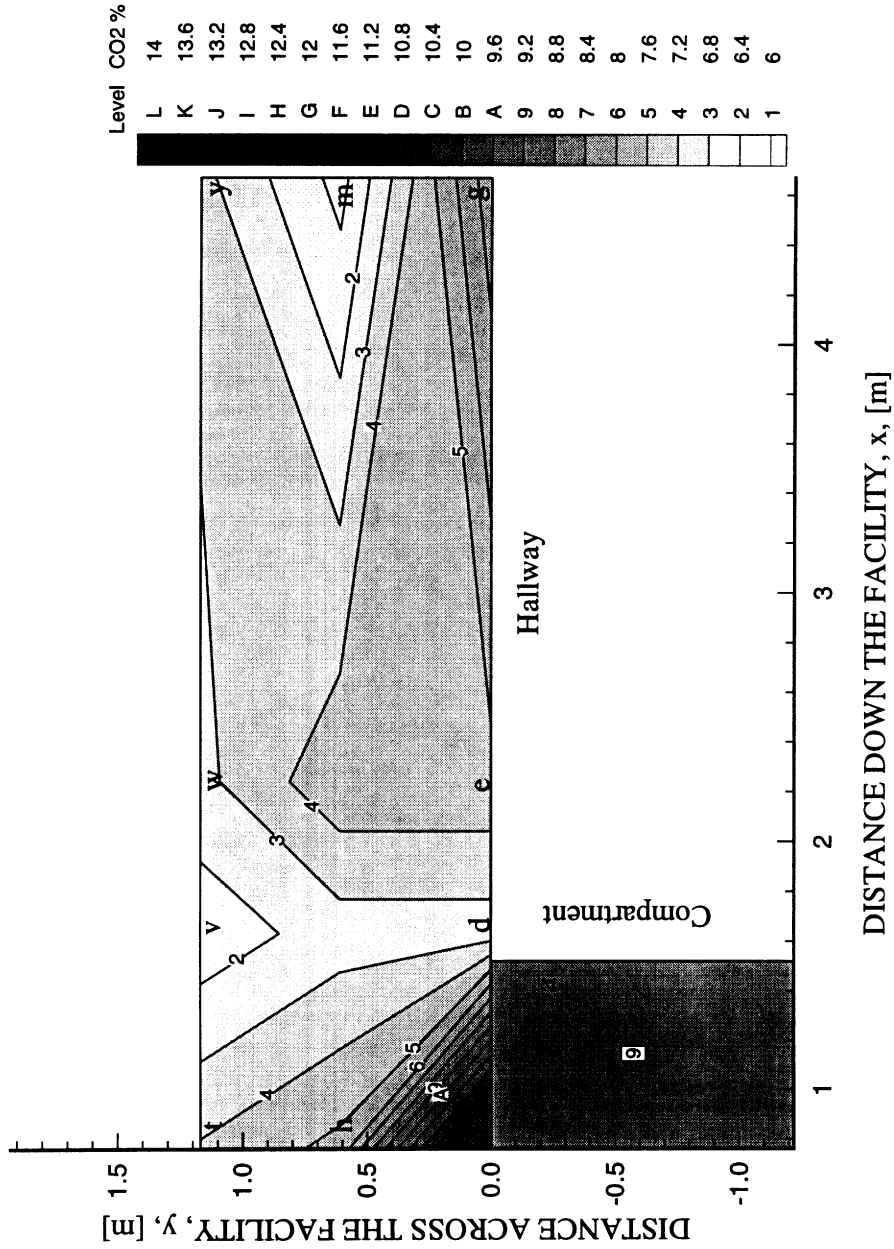


Figure 4.80 The wet CO₂ concentration distribution 0.05 m below the ceiling 92-96 seconds after flashover in polyurethane foam fire experiments with a 0.04 m² opening, 0.20 m inlet soffit, 0.60 m exit soffit and no external burning.

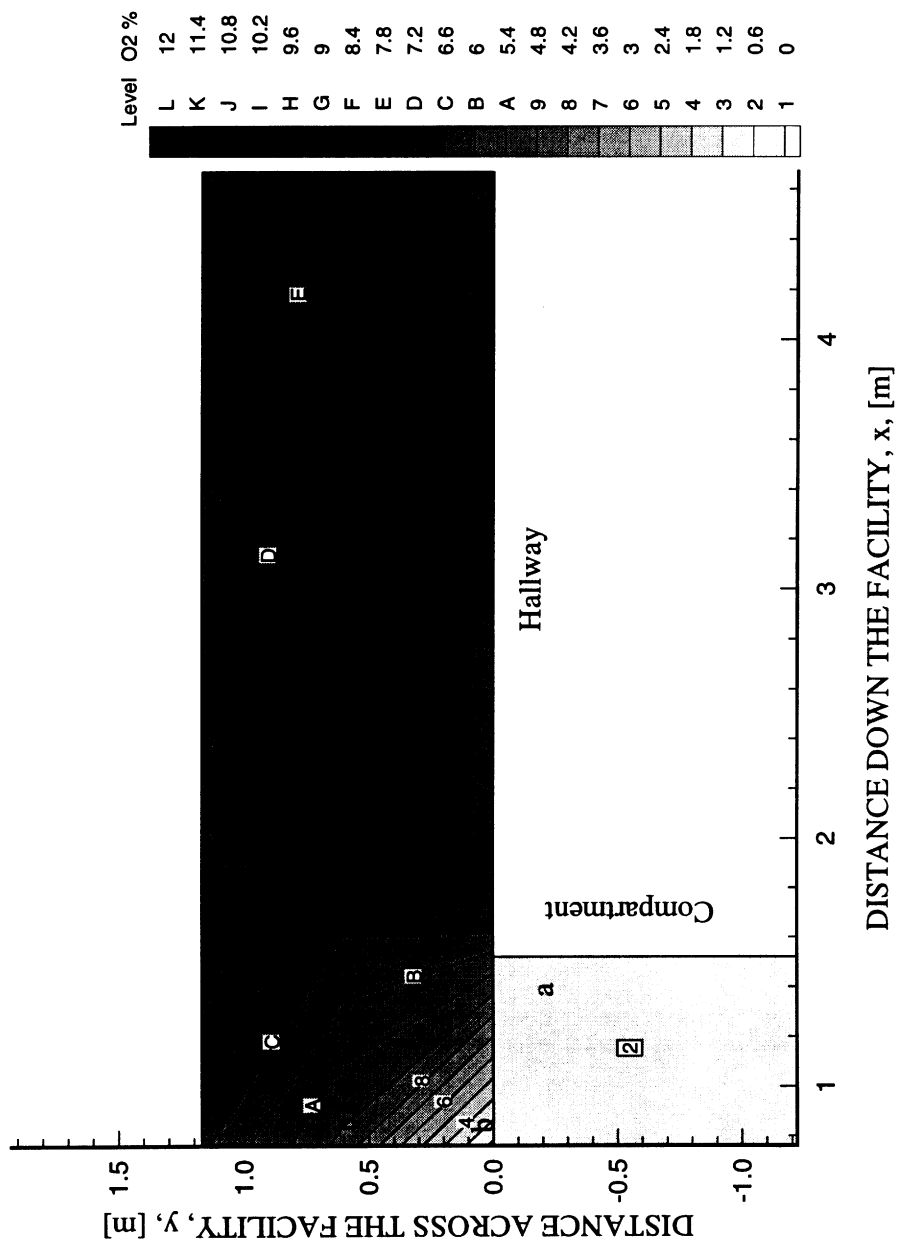


Figure 4.81 The wet O₂ concentration distribution 0.05 m below the ceiling 92-96 seconds after flashover in polyurethane foam fire experiments with a 0.04 m² opening, 0.20 m inlet soffit, 0.60 m exit soffit and no external burning.

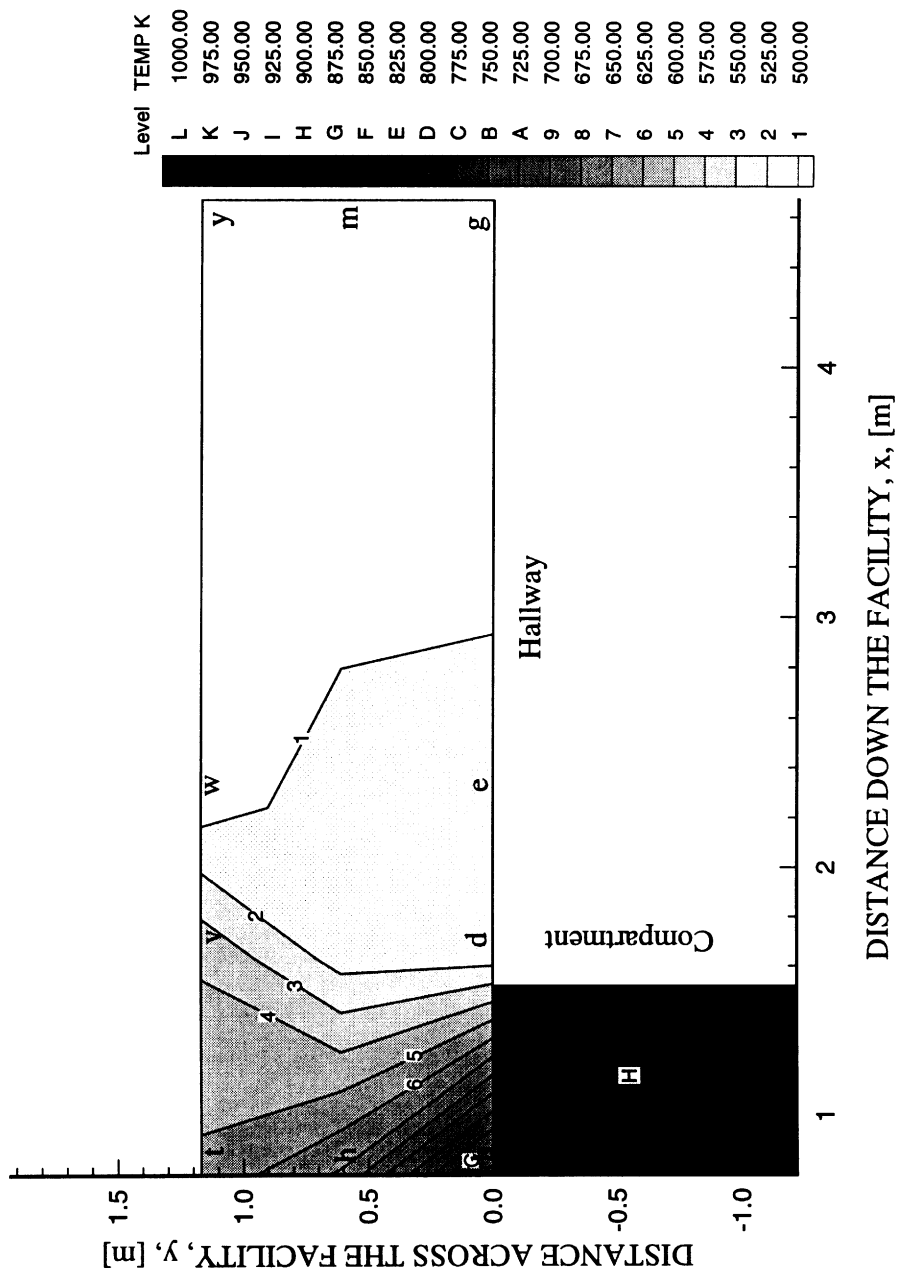


Figure 4.82 The temperature distribution 0.05 m below the ceiling 92-96 seconds after flashover in polyurethane foam fire experiments with a 0.04 m² opening, 0.20 m inlet soffit, 0.60 m exit soffit and no external burning.

4.5 SUMMARY OF SPECIES CONCENTRATION EVOLUTION RESULTS

The temporal and spatial evolution of CO, UHC, CO₂ and O₂ concentrations and temperatures in the hallway were measured for experimental situations where high CO post-hallway yields were measured. The experiments were conducted to determine the effect of external burning, species concentration transient time and fuel type.

In all experiments with the compartment on the side of the hallway, the movement of fire exhaust gases away from the compartment was non-uniform in the hallway. Gases first flowed across the hallway until they impinged on the wall opposite the compartment. The impingement of the hot gases on the wall resulted in the development of a large vortex on the side of the hallway opposite the compartment. The majority of the gases were visually (through observation of external burning) observed and measured to travel down the side of the hallway opposite the compartment.

External burning was measured to have a significant effect on the UHC, CO₂ and O₂ concentrations, but a minimal effect on CO concentrations in the hallway. With external burning in the hallway, 1.9-2.1 % CO were measured in the upper-layer of the hallway. The UHC were, however, measured to decrease to 25% of the UHC concentration exiting the compartment. The decrease in the UHC concentration more rapidly than CO concentration agrees with the results reported by Westbrook and Dryer (1984).

The time before the species concentrations reach a steady-state (transient time) in the hallway varied depending on the blockage present at the exit of the hallway. With a 0.60 m soffit, the transient time was approximately 60 seconds. Longer transient times were achieved by blocking the bottom portion of the hallway. This resulted in a transient time of 96 seconds. Once a steady-state was reached in the hallway, CO levels were approximately 2.0%, a level which could result in death with about 3 minutes of exposure.

Both *n*-hexane and polyurethane foam fires were burned inside the compartment. The amount of CO transported to remote locations was measured to be independent of the type of fuel burned in the compartment.

CHAPTER 5

DISCUSSION: ANALYSIS OF RESULTS AND MODEL DEVELOPMENT

5.1 INTRODUCTION

The goal of this research is to provide fire safety engineers with a procedure to estimate CO levels in building fires. Four major variables have been identified through this research as being critical to the prediction of CO at a location downstream of the burning compartment. The variables are: the stoichiometry of the compartment fire, the oxygen entrainment into the gases entering the hallway, the occurrence of external burning, and the transient time of species concentration in the hallway. In this chapter, models which predict the occurrence of external burning and the transient time of species concentrations in the hallway are developed and verified using experimental data. The stoichiometry and the oxygen entrainment are used in developing models for the prediction of post-hallway yields. A procedure is then given to determine the hazards (i.e. flame spread, toxic gas levels) which are present during a building fire upon the onset of flashover inside the burning compartment.

5.2 PREDICTION OF EXTERNAL BURNING

The occurrence of external burning in the hallway has been shown in Chapters 3 and 4 to have a significant effect on the amount of CO transported away from the burning room. The absence of external burning resulted in post-hallway yields equal to the levels measured inside the compartment. The prediction of external burning within the hallway was attempted using the ignition index, given as Eqn. (2.16), defined by Beyler (1984).

When the ignition index rises above 1.0, the amount of energy available for ignition exceeds the amount of energy necessary for ignition. Ignition is, therefore, predicted to occur when $I.I. > 1.0$ assuming a pilot ignition source exists.

In chapter 3, experimental results were presented where an ignitable mixture was produced by a compartment fire, but ignition did not occur in the hallway. The absence of external burning was attributed to the presence of a deep oxygen deficient upper-layer in the hallway. The ignition of hallway combustion gases was determined to be a function of the nondimensional upper-layer depth, $\gamma = \delta/z$. With a nondimensional upper-layer depth less than 1.7, it was experimentally determined that a pilot ignition source was present to ignite the hallway gases. Above a value of 1.7, the oxygen deficient upper-layer in the hallway was deep enough to prevent the entrainment oxygen into the compartment fire exhaust gas jet. This was hypothesized to inhibit the promotion of oxidative radicals and to prevent the ignition of the hallway gases.

The proposed method for the predicting the ignition of gases entering the hallway has two parts. First, determine whether a pilot ignition source is present by calculating whether the nondimensional upper-layer depth is less than 1.7. If a pilot source is present, calculate the ignition index (I.I.). If I.I. is greater than 1.0, then the ignition is predicted to occur.

The method is verified using numerous experimental results which contained various nondimensional upper-layer depths. The gases for the calculation of the I.I. were sampled in the middle of the compartment opening, at location "b" in Fig. 2.10.

The results of the application of the model to predict external burning in an experiment is tabulated in Table 5.1. The temporal variation in the ignition index for an experiment $\gamma < 1.7$ and one with $\gamma > 1.7$ are shown in Fig. 5.1 and 5.2, respectively. These plots are a representative sample of the data presented in Table 5.1. The experiment where external burning occurred contained a 0.12 m^2 opening,

Table 5.1 The use of the ignition index and the nondimensional upper-layer depth to predict the occurrence of external burning in the hallway.

Opening Size, m ²	Upper-Layer Depth, δ , m	Distance to Bottom of Opening, z, m	$\gamma=\delta/z$	Start of External Burning, t, sec	I.I. at Start of External Burning
0.04	0.30	0.36	0.83	313	1.24
0.12	0.60	0.44	1.36	371	1.37
0.08	0.25	0.16	1.56	319	1.08
0.04	0.25	0.16	1.56	317	1.16
0.12	0.25	0.24	1.04	307	1.10
0.04	0.60	0.36	1.67	N/A	N/A*
0.04	0.30	0.16	1.88	N/A	N/A*
0.04	0.35	0.16	2.19	N/A	N/A**
0.12	0.45	0.24	1.88	N/A	N/A**
Average					1.19

*I.I.>1.0 but no ignition occurred since $\gamma>1.7$.

**I.I.<1.0 and no ignition occurred.

$\phi=2.70$ and $\gamma=1.04$. The experiment where no external burning occurred in the hallway contained a 0.04 m² opening, $\phi=3.0$ and $\gamma=1.88$.

In the experiment with external burning, the ignition index predicted the ignition of the hallway gases at 307 seconds, see Fig. 5.1. The value of γ was also determined to be less than 1.7, signifying the existence of a pilot source to ignite the hallway gases. As predicted, external burning occurred in the hallway at approximately 307 seconds.

The experiment without external burning had a $\gamma=1.88$. A pilot source for ignition was, therefore, predicted not to exist. The magnitude of the ignition index is seen in

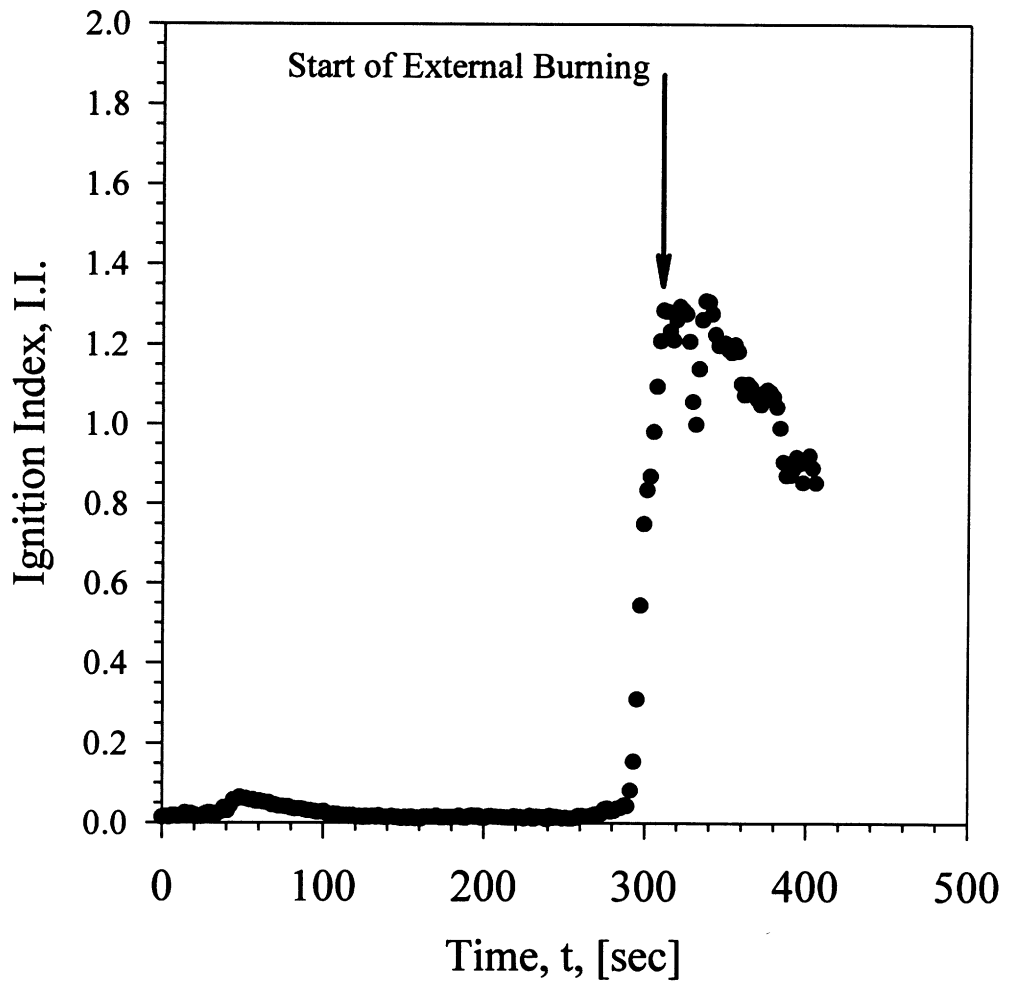


Figure 5.1 The ignition index for an experiment with external burning in the hallway.

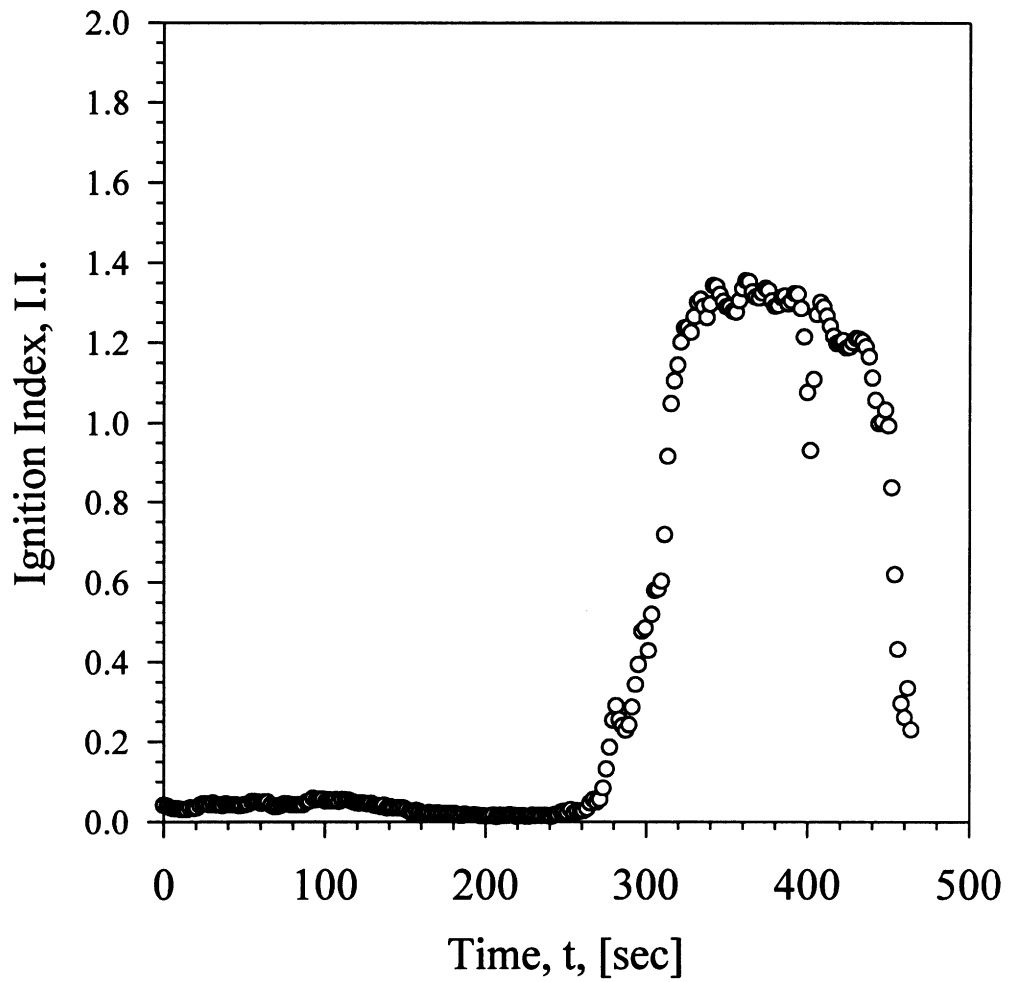


Figure 5.2 The ignition index for an experiment with no external burning.

Fig. 5.2 to rise above 1.0 at approximately 300 seconds. As predicted by γ , no ignition source was present and external burning did not occur in the hallway.

This analysis suggests that the ignition index should, therefore, be used in combination with the nondimensional upper-layer depth, γ , to predict the occurrence of external burning. External burning is expected occur when

- the nondimensional upper-layer depth, γ , is less than 1.7 and
- the ignition index, I.I., rises above 1.0.

No external burning is expected occur in the hallway with $\gamma \geq 1.7$. This is attributed to the production of oxidative radicals being inhibited by the extremely deep oxygen deficient upper-layer present in the hallway. The ignition index in this case gives information on whether (I.I.>1.0) or not (I.I.<1.0) the gases entering the hallway are ignitable.

5.3 PREDICTION OF SPECIES CONCENTRATION TRANSIENT TIME

The yield of species formed inside the compartment was found to correlate well with the global equivalence ratio of the compartment fire (Beyler, 1984, Tewarson, 1984 and Gottuk, 1992). Correlations for the estimation of species levels in the space adjacent to the compartment are formulated in section 5.4 and are based on the post-hallway species yields. The limitation of using a correlation based on the post-hallway yields is that the species levels need to be uniform within the hallway upper-layer. The results in Chapter 4 suggest that yield correlations are valid after the gases have reached a steady-state concentration in the hallway. A well-stirred model is developed in this section to provide an estimate the transient time for the gas concentrations in the hallway upper-layer.

The hallway is modeled as a well-stirred volume as seen in Fig. 5.3. Gases containing high CO concentrations are assumed to enter the volume and instantaneously mix within the volume. From the assumption of instantaneous mixing, the concentration

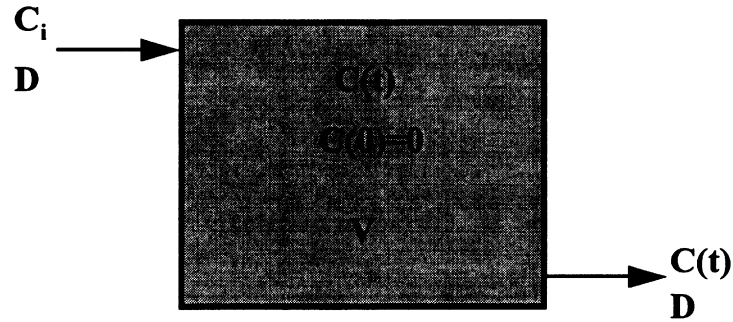


Figure 5.3 The well-stirred volume model for the estimation of species concentration transient time in the hallway.

of the gases exiting the volume is equal to the gas concentration within the volume. The variation in the concentration of CO, $C(t)$, inside the volume with time is,

$$\frac{dC(t)}{dt} + \frac{D}{V} C(t) = \frac{D}{V} C_i, \quad (5.1)$$

with the initial condition being,

$$C(0) = 0. \quad (5.2)$$

The volumetric flow rate of the gases into the volume, D , the volume, V , and the initial concentration of CO in the volume, C_i , are all assumed to be known.

The concentration of CO as a function of time is therefore:

$$C(t) = C_i \left(1 - \exp\left(-\frac{D}{V} t\right) \right). \quad (5.3)$$

Solving Eqn. (5.3) for t ,

$$t_{tran} = \frac{-A_{hall}\delta}{D(\bar{T}_{hall}/T_{comp})} \ln\left(\frac{C_i - C(t)}{C_i}\right), \quad (5.4)$$

and substituting the volume of the hallway upper-layer for V , an expression to estimate

Table 5.2 The conditions in experiments with both short and long steady-state times in the hallway.

Transient Time, t_{tran} , sec	Transient Time (from experiment), t_{exp} , sec	Area of Hallway, A_{hall} , m ²	Depth of Layer in Hallway, δ , m	D , m ³ /s	T_{comp} , K	\bar{T}_{hall} , K
48	60*	6.32	0.60	0.115	950	550
82	96**	16.85***	0.45	0.136	950	550

*Exit soffit at end of hallway.

**Bottom blockage at end of hallway.

***Determined using effective hallway length.

the transient time of the gas concentrations in the hallway is given. The flow rate of the high temperature compartment fire gases entering the hallway is known. A density correction factor for the flow rate in the hallway is added in the denominator of Eqn. (5.4) so that the flow rate is representative of the average flow rate in the hallway.

The transient time of experiments reported in Chapter 4 is estimated using Eqn. (5.4). The calculations assume that the gases entering the hallway contain 3.5% CO ($C_i=3.5\%$), and that the upper-layer gases at steady-state contain 2.0% CO ($C(t)=2.0\%$). All times are referenced from flashover (i.e. 60 seconds is 60 seconds after flashover).

A transient time of 48 seconds was calculated using the conditions present in experiments with an exit soffit connected to the hallway shown in Table 5.2. This is within 20% of the transient time determined from the experimental data.

The experiments with a blockage at the bottom the hallway exit simulated toxic gas movement in a hallway longer than 5.18 m. The effective length of the hallway was determined using the time required for gases containing 1.0% CO to circulate back to the compartment opening after traveling down the hallway. Approximately 24 seconds was

required for gases to circulate in experiments with an exit soffit (5.18 m long hallway). With the blockage at the bottom of the hallway exit, approximately 64 seconds was required for the gases to circulate back to the opening. The effective length of the hallway was determined by multiplying the actual length of the hallway (5.18 m) by the ratio of the bottom blockage circulation time and the exit soffit circulation time. The assumption here is that the velocity of the gases in the two cases is approximately the same. The effective hallway length was determined to be 13.81 m. Using the effective hallway length, the transient time was calculated to be 82 seconds. The calculated time is within 15% of the experimental time of 96 seconds.

The transient time of the species concentrations in the upper-layer was calculated to within 20% of the experimentally determined value. The transient time calculation provides a method for determining when the species concentrations in the hallway have reached a steady-state. After such time, post-hallway species yield correlations can accurately be used to determine the species levels transported away from the compartment.

5.4 CORRELATIONS FOR THE PREDICTION OF CO

The post-hallway combustion product yields were shown in Chapter 3 to be strongly dependent on the occurrence of external burning in the hallway, the oxygen entrainment into the jet exiting the compartment and the stoichiometry of the compartment fire. As mentioned in Section 5.2, the absence of external burning results in post-hallway yields equal to compartment yields. Therefore, the post-hallway yields in these cases can be predicted using correlations based on the compartment global equivalence ratio. With external burning occurring in the hallway, post-hallway yields were shown in Chapter 3 to be highly dependent on oxygen entrainment into the gases entering the hallway and the stoichiometry of these gases. A relationship between the post-hallway yields and the

oxygen entrainment into the gases entering the hallway is developed. To account for the stoichiometry in the experiments, a global equivalence ratio is developed for the compartment-hallway system. The global equivalence ratio is then used to predict post-hallway yields.

5.4.1 Oxygen Entrainment into Gases Entering the Hallway

The data in Chapter 3 showed the inlet soffit height, the compartment opening size and the upper-layer depth all had a significant effect on the post-hallway CO yields with external burning in the hallway. Variation in the soffit height and opening size was shown to alter the type of jet entering the hallway (i.e. ceiling or buoyant) and the jet flow characteristics (i.e. shape and velocity). This resulted in a variation in the mass flow of gases entrained into the jet. The magnitude of the entrainment was quantified using the entrainment function, E . The upper-layer depth in the hallway determined the concentration of oxygen present in the gases being entrained into the jet. The degree to which the jet was surrounded by hallway upper-layer gases was quantified by the nondimensional upper-layer depth, γ (defined as the upper-layer depth divided by the distance between the ceiling and the bottom of the opening). A relationship accounting for the effect of these parameters on the oxygen entrainment into the compartment fire gases is developed. The relationship is then correlated to the post-hallway CO and UHC yield data.

In experiments with external burning, the CO and UHC yields were shown in Fig. 3.13-3.15 to rise nearly exponentially with nondimensional upper-layer depth for a particular opening size. Assuming the oxygen entrainment was the cause of the rise, the oxygen entrained into the hallway gases was assumed to decrease exponentially with the

nondimensional upper-layer depth. The oxygen entrainment parameter,

$$\varepsilon = E[X_{O_2,amb}(\exp(-\delta/z))]100, \quad (5.5)$$

was developed to account for both the entrainment into the jet and the level of oxygen entrained into the jet.

The data from Fig. 3.13, Fig. 3.14 and Fig. 3.15 where external burning occurred and the values of E shown in Table 3.4 for all three opening sizes were used to verify the model. The post-hallway CO yields are shown in Fig. 5.4 plotted against the oxygen entrainment parameter. The curve fit to the data is given by the following equation:

$$Y_{CO} = 0.42 \exp(-1.5\varepsilon) \quad (5.6)$$

From Eqn. (5.6), a decrease in the entrainment into the jet or an increase in the nondimensional upper-layer depth results in higher CO yields. This trend can also be seen in Fig. 5.4.

The UHC yields are plotted against the oxygen entrainment parameter in Fig. 5.5. A curve fit to the data was determined to be

$$Y_{UHC} = 0.38 \exp(-2.0\varepsilon) \quad (5.7)$$

As expected from the results in Chapter 3, the trend in the data is similar to that observed for CO yields.

The oxygen entrainment parameter does not account for the amount of fuel entering the hallway. This is governed by the compartment equivalence ratio. The yield of CO and UHC produced in the compartment was shown in the study of Gottuk (1992a) to be constant at a compartment global equivalence ratio greater than 1.8. All experiments considered in this section having a compartment global equivalence ratio of 3.0 ± 0.5 . Therefore, the yield of CO and UHC entering the hallway was assumed to be equal in all

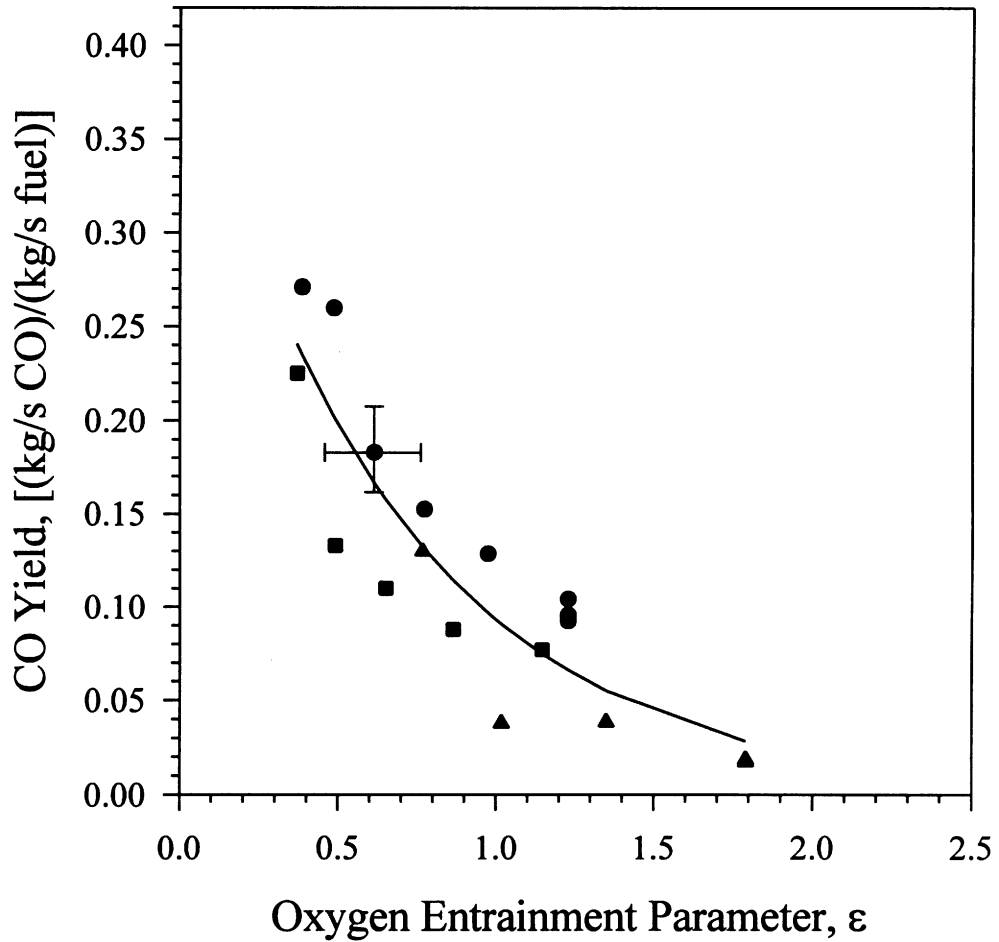


Figure 5.4 The use of the oxygen entrainment parameter, Eqn. (5.5), to predict the hallway exit CO yield with external burning occurring in the hallway. Data from opening sizes of ●-0.12 m², ▲-0.08 m², and ■-0.04 m². The solid line is a curve fit to the data.

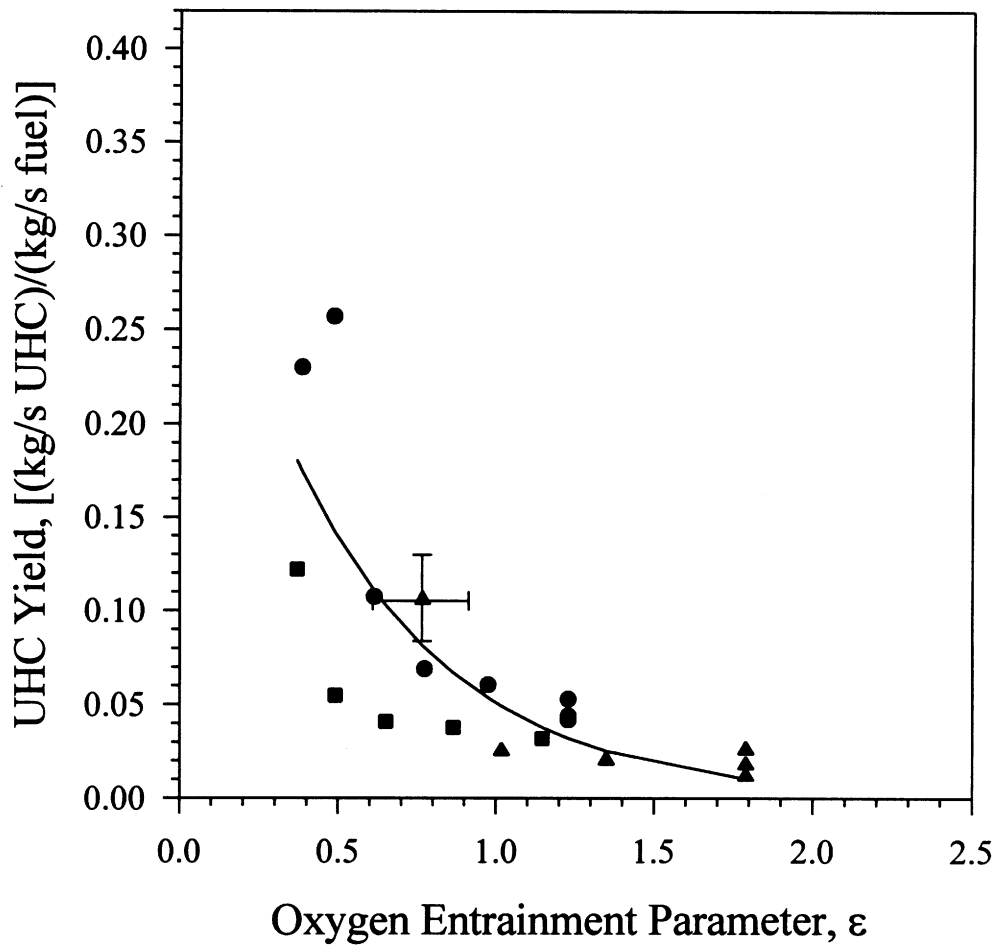


Figure 5.5 The use of the oxygen entrainment parameter, Eqn. (5.5), to predict the hallway exit UHC yield with external burning occurring in the hallway. Data from opening sizes of ●-0.12 m², ▲-0.08 m², and ■-0.04 m². The solid line is a curve fit to the data.

experiments. A more general approach is taken in the next section to account for the stoichiometry.

5.4.2 Global Equivalence Ratio of the Compartment-Hallway System

The formation compartment fire products has been shown to be related to the compartment global equivalence ratio in the studies of Beyler (1983), Gottuk (1992a) and others. A global equivalence ratio for the compartment and hallway is developed in this section. The system global equivalence ratio is then used to predict post-hallway yields.

The system global equivalence ratio,

$$\phi_{sys} = \frac{\left(\frac{\dot{m}_{fuel}}{\dot{m}_{air,comp} + \dot{m}_{air,hall}} \right)}{\left(\frac{\dot{m}_{fuel}}{\dot{m}_{air}} \right)_{st}}, \quad (5.8)$$

is of the same form as the global equivalence ratio calculated for the compartment. The difference in the two is the air entrained into the flaming portion of the hallway gases, $\dot{m}_{air,hall}$. The air entrained into the flaming portion of the hallway gases is believed to control the oxidation of combustion products in the hallway. The rest of the air entering the hallway is merely diluting the upper-layer gases, and has no effect on post-hallway yields.

The measurement of the exact amount of air being entrained into the flaming portion of the gases is very difficult. As a first order approximation, the measurements of the mass flow rate of air entrained into overventilated gases entering the hallway, see Table 3.2 and 3.4, are used in the analysis. The air entrainment mass flow rate given in the tables is the air entrainment which had occurred after the compartment fire gases had flowed 0.60 m across the hallway. The entrainment over the entire flaming region was

determined by first estimating the flame extension from the compartment. The flame length under the ceiling was estimated using the correlation of Gross (1989)

$$F = L \left(1 - 0.3 \left(1 - \frac{H}{L} \right) \right) - F_{comp}, \quad (5.9)$$

where F is the flame extension, L is the free flame height, H is the height of the ceiling above the pool fire (height of the compartment), and F_{comp} is the portion of the flame extension which occurs inside the compartment (0.61 m). The free flame height was determined using the correlation of Heskestad (1983)

$$L = -1.02d + 0.23Q^{2/5}, \quad (5.10)$$

where d is the diameter of the pool fire and Q is the fire size. Using the calculated flame lengths, the air entrainment into the flaming portion of the hallway,

$$\dot{m}_{air,hall} = \dot{m}_e \left(\frac{L}{0.6} \right) \left(\frac{T_{OV}}{T_{UV}} \right), \quad (5.11)$$

was determined by multiplying the measured air entrainment into the overventilated compartment fire gases by the ratio of the flame length and 0.6 m and a density correction factor.

The model was verified using the data of Ewens (1994b) where the effects of the upper-layer depth on the oxygen entrainment were considered to be minimal. The post-hallway CO yield is plotted against the compartment equivalence ratio in Fig. 5.6. The compartment CO yield data from the study of Gottuk is also shown in the figure. The post-hallway data is completely uncorrelated to the compartment equivalence ratio. A correlation is, however, seen to exist between the post-hallway CO yield and the system global equivalence ratio, see Fig. 5.7. In fact, the majority of the data collapses to the data of Gottuk (1992a). This is expected since the system global equivalence ratio in the study of Gottuk was the compartment equivalence ratio. A small portion of the data

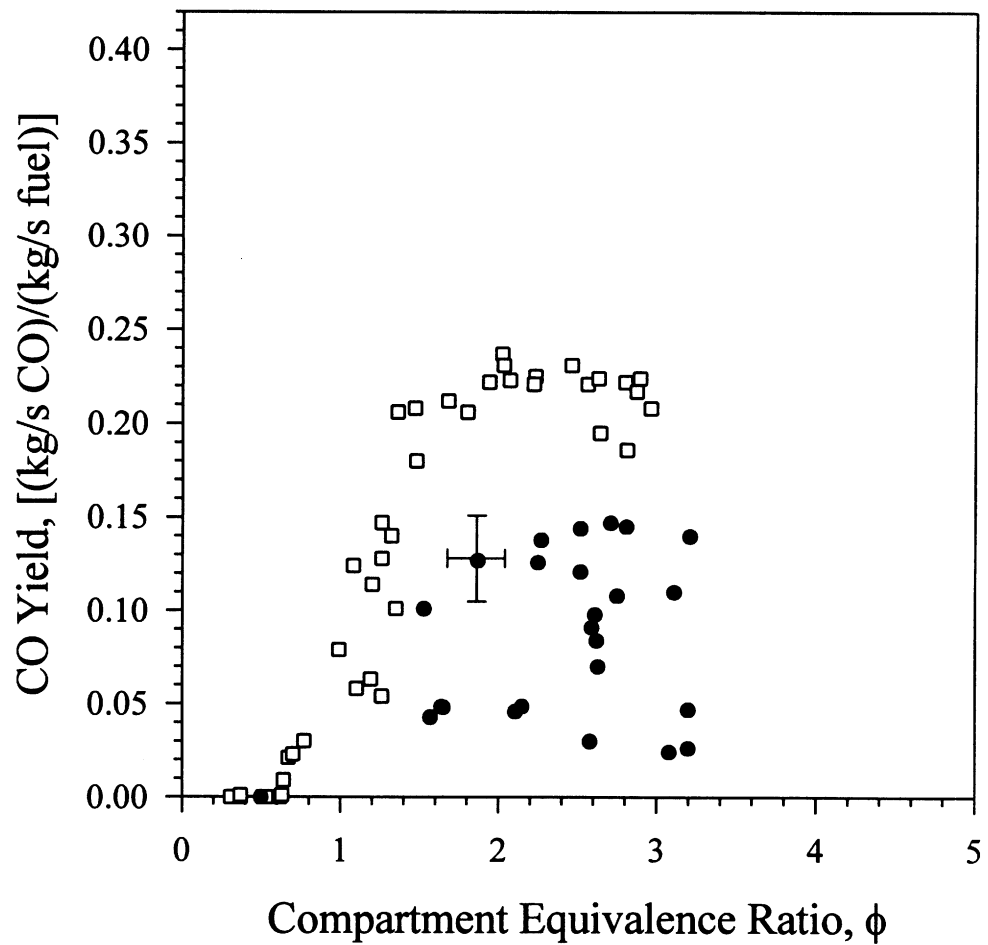


Figure 5.6. The post-hallway CO yields (●) plotted against the compartment equivalence ratio. The compartment yields (□) from the study of Gottuk (1992a) are also shown.

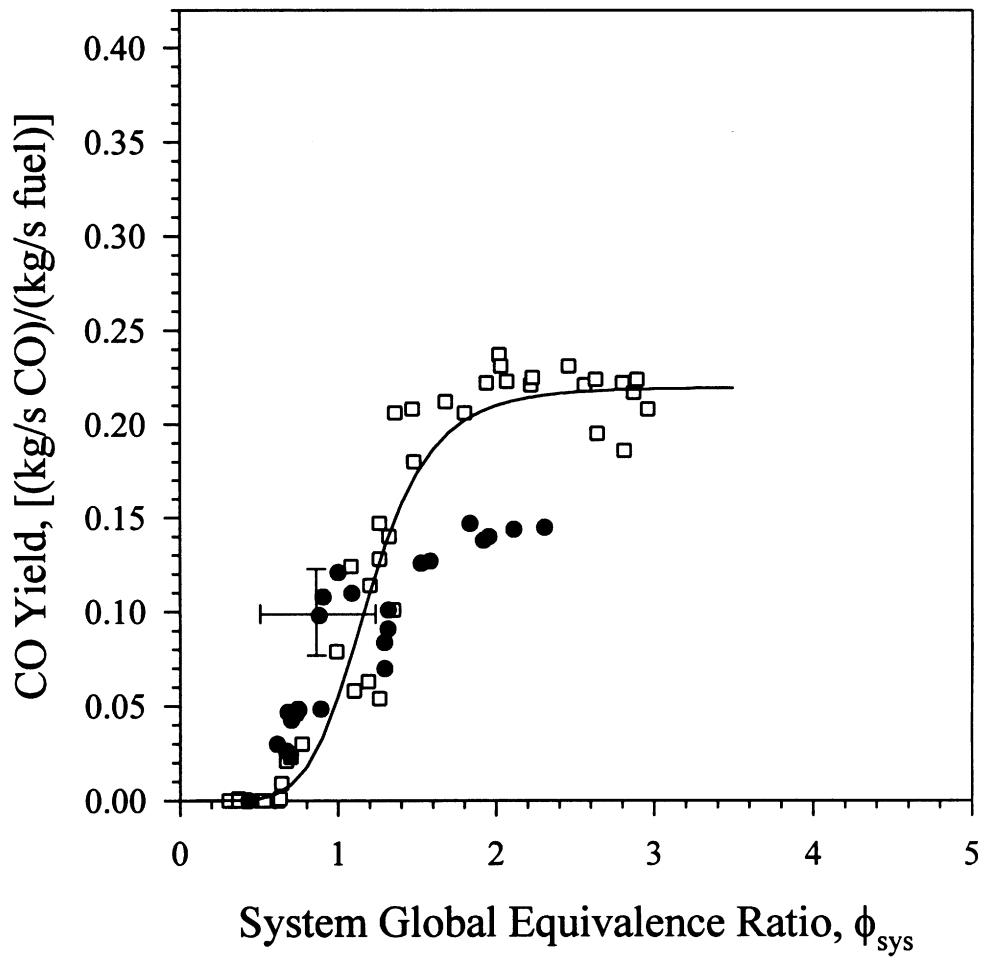


Figure 5.7 The post-hallway CO yields (●) plotted against the system global equivalence ratio. The compartment yields (□) from the study of Gottuk (1992a) are also shown. The solid line is a curve fit to the data of Gottuk.

did not collapse to the data of Gottuk. This may be attributed to an error in the estimation of air entrainment into the flaming portion of the gases. These points may also indicate that post-hallway yields are not well described by compartment data at higher global equivalence ratios. Assuming the error is due to a poor estimation of entrainment, the CO yield can be predicted from using the global equivalence ratio for the system and the curve fit to Gottuk's data,

$$Y_{CO} = \frac{0.22}{\left[1 + \left(\frac{\phi}{1.2} \right)^{-6} \right]} \quad (5.12)$$

The system global equivalence ratio is accurate for $\gamma < 1.4$. With $\gamma > 1.4$, CO yields were measured to rise above in-compartment yields making the correlation invalid.

5.5 PROCEDURE FOR PREDICTING CO LEVELS IN BUILDING FIRES

Using the models developed in this chapter, a procedure for estimating the CO levels in building fires is now possible. The procedure, see Fig. 5.8, is as follows:

1. Determine the transient time of the gas concentrations in the adjacent space.
2. Determine whether external burning occurs in the adjacent space.
3. If no external burning occurs and the time after flashover is greater than the transient time, use the compartment yield correlations to estimate CO yields.
4. If external burning occurs and the time after flashover is greater than the transient time, predict the CO yields in the hallway using:
 - a) the oxygen entrainment parameter model; valid for upper-layers with $\gamma < 1.7$ and compartment global equivalence ratio greater than 1.8, or

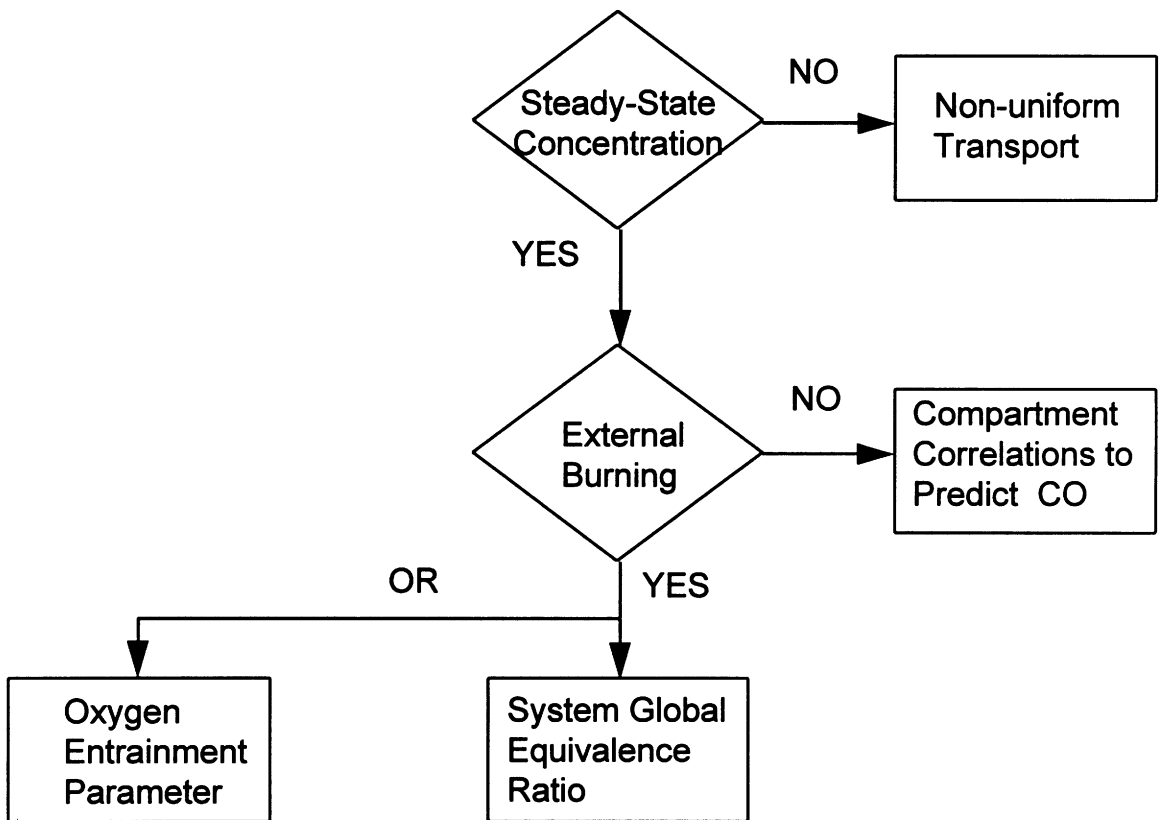


Figure 5.8 The proposed procedure for estimating CO levels in building fires.

- b) the system global equivalence ratio model; valid for any compartment global equivalence ratio, but for $\gamma < 1.4$.

5.6 APPLICATION OF RESULTS TO FULL-SCALE SITUATIONS

The post-hallway CO yield has been shown here to be strongly related to the entrainment into the gases entering the hallway. These fluid mechanics are sensitive to the scale of the experiment. Suggestions of how the results of the 1/4 scale experiments presented in this thesis can be used in full scale situations are given below.

The scaling laws for transport of gases away from the hallway are mainly taken from the study performed by Steckler et al. (1986), with similar relationships developed by Emori and Saito (1979) and Daikou and Saito (1995). Steckler et al. (1986) investigated smoke movement from a burning room on the side of a hallway using salt-water experiments. Dimensions were scaled using the height of the room, while the compartment fire was scaled using the Froude number,

$$Fr = \frac{V_s^2}{2gH} \frac{\rho_s}{(\rho_e - \rho_s)} \quad (5.13)$$

which is simply the inverse of the Richardson number, Ri. The term ρ_s is the density of the gas at the source.

It should be noted that the Ri number used in the entrainment correlation, Eqn. (3.3), uses a different form of the densimetric term, $\rho_e/(\rho_i - \rho_e)$, compared to $\rho_s/(\rho_e - \rho_s)$ shown in Eqn. (5.13). The reasoning for the difference is to account for the physics driving the process. The physics driving the fire plume rising to the ceiling in the compartment is the inertia of the plume and the buoyancy induced by the density difference in the hot plume and the surrounding gases. The physics driving the entrainment into the gases entering

the hallway is the gravitational potential of the gases, the kinetic potential of the gases, and the density of the hot gases relative to the entraining gases (density defect).

To scale the present results, the dimensions of the compartment, the hallway, the layer-depth, the distance between the bottom of the opening and any other physical distance should be scaled to the distance between floor and ceiling inside the compartment, h . Born out of these relationships is the nondimensional upper-layer depth ($\gamma = \delta/z$) which was previously used to correlate downstream results with the O_2 entrainment into the gases entering the hallway. The compartment fire should be scaled relative to the Froude number. The opening size should be scaled to $A_{\text{open}} h^{1/2}$ to ensure the flow into the hallway is similar (Kawogoe, 1959).

These scaling laws are suggested, but no experiments were performed to validate them. In addition, no experimental data was available to determine whether these laws would give similar CO yields in full scale situations. The laws should be experimentally tested to determine their range of validity.

CHAPTER 6

ENGINEERING TOOLS FOR THE ESTIMATION OF CO LEVELS IN BUILDING FIRES

6.1 INTRODUCTION

The development of engineering tools to predict the formation, oxidation and transport of CO in building fires is essential for designing a more fire safe building. A chemical kinetic model was developed to estimate species concentrations formed inside the compartment. The compartment is modeled as a homogeneous reactor using the FORTRAN version of *SENKIN*. The initial species mole fractions are determined utilizing the conditions present inside the compartment before the onset of flashover. Mechanisms for both *n*-hexane ($n\text{-C}_6\text{H}_{14}$) and methane were utilized in the study. Results of the model were compared to experimental measurements from *n*-hexane and methane compartment fires.

6.2 PROGRAMS AND CHEMICAL KINETIC MECHANISMS

6.2.1 CHEMKIN, STANJAN and SENKIN

The FORTRAN programs *CHEMKIN*, developed by Kee et al. (1994) at Sandia National Laboratory, and *SENKIN*, developed by Lutz et al. (1994) also at Sandia, were used to perform the chemical kinetic modeling. The program *STANJAN* was also used in the modeling process. The programs were run on a UNIX based Hewlett-Packard workstation.

CHEMKIN organizes the thermodynamic and chemical kinetic data to be input into *STANJAN* and *SENKIN*. *STANJAN* is used to determine the chemical equilibrium of a

mixture of gases. The program *SENKIN* is used to determine species mole fractions in a homogeneous reactor at a given condition. With a given temperature and pressure, *SENKIN* solves the equations for the species conservation,

$$\frac{dmf_j}{dt} = \frac{\dot{\omega}_j MW_j}{\rho}, \quad (6.1)$$

to determine the temporal variation in the species mass fractions in the reactor. The values for $\dot{\omega}_j$ are determined from the rate of destruction and formation for a species j . The rate equations of destruction and formation of species are determined using the law of mass action and the modified Arrhenius rate coefficients,

$$k = A_r T^\alpha \exp\left(\frac{-E_a}{RT}\right) \quad (6.2)$$

Constants for equation (6.2) are given for each reaction in the mechanism.

6.2.2 Chemical Kinetic Mechanisms for *n*-Hexane and Methane

A detailed chemical mechanism for *n*-hexane, in addition to the thermodynamic data for all species involved, was obtained from Lawrence Livermore National Laboratories (LLNL), Curran and Westbrook (1996), and was then adapted to *CHEMKIN* format. The mechanism contains 398 chemical species and 1910 chemical reactions, and is valid in the low to middle temperature range, 300 K to 1600 K.

Since the mechanism only considered gaseous species, the energy necessary for the conversion of the liquid hexane to the gaseous state was accounted for by determining the difference in the adiabatic flame temperature for liquid hexane and gaseous hexane. The temperature difference, approximately 15 K, was accounted for in the calculations by setting the initial conditions in the *STANJAN* calculations, which model the plume, to 285 K instead of 300 K.

A propane mechanism was used to model the methane compartment fire chemical kinetics. This mechanism was used so higher order hydrocarbons reactions could be considered.

6.3 ESTIMATION OF SPECIES PRODUCTION IN COMPARTMENT FIRES

6.3.1 Background

Most of the knowledge of species production and behavior in the upper-layer of a compartment fire has come from experimental investigations. Hood experiments performed by Beyler (1986a., 1986b.), Toner et al. (1987) and Morehart et al. (1990) experimentally modeled the upper-layer environment of the compartment, and correlated the species produced to the global equivalence ratio (GER).

The temperatures measured in the hood experiments were lower than those measured in actual compartment fires. Compartment fire experimental investigations were, therefore, conducted by Gottuk (1992a) and Bryner, et al. (1994) to verify the species levels measured in hood experiments. These investigations were also used to test the validity of the GER concept for predicting species levels at higher temperatures (Pitts, 1994a).

The success of estimating the species levels measured in the compartment upper-layer with chemical kinetic modeling has been limited. In the study by Morehart (1990, 1991), the qualitative effect of temperature on the production of species in the upper-layer of the hood experiments was determined, and compared with his data. The chemical kinetic modeling of Pitts (1992) used the species levels from Morehart's experiments to investigate the effects of temperature and GER on the species levels in the upper-layer environment. The study by Pitts (1992) showed a drastic increase in the level of CO at

elevated temperatures (1300 K), and related this rise to a shift in the water-gas shift reaction:



toward chemical kinetic equilibrium at high temperatures. The prediction of species levels in a compartment upper-layer with a GER less than 1.5 was performed by Gottuk(1992a) using *CHEMKIN* and *SENKIN*. Gottuk modeled the compartment upper-layer as a constant pressure, constant temperature homogeneous reactor. The reactor temperature was equal to his experimentally measured compartment fire upper-layer temperatures, and the initial species levels were taken from the experiments of Beyler (1983). The model accurately predicted the species levels for overventilated compartment fires ($\phi < 1.1$), but over-predicted CO levels by as much as 400% for underventilated compartment fires ($\phi > 1.1$). In a later publication, Gottuk et al. (1995) attributed the discrepancy in the CO levels in underventilated compartment fires to the oxidation which occurs in the plume. Better agreement with experimental results was achieved when the initial species compositions were adjusted to account for more complete oxidation in the plume. This was done by oxidizing all the unburned hydrocarbons (in this case C_2H_4) to CO_2 and H_2O . The initial O_2 concentration was also reduced to 1%. The results of both modeling cases and of the experimental results of Gottuk (1992a) and Beyler (1986b) are shown in Fig. 6.1.

The production of CO in compartment fires is now believed to occur within the fire plume which rises to the ceiling (Pitts, 1995, Gottuk, et al., 1995). The vortical structures of the fire are hypothesized to entrain pockets of air. This entrained air is subsequently carried into the upper-layer of the compartment fire to burn in an extremely underventilated environment. Modeling the fluid mechanics and chemical kinetics occurring in this process is extremely complex and, hence, is not attempted here. A

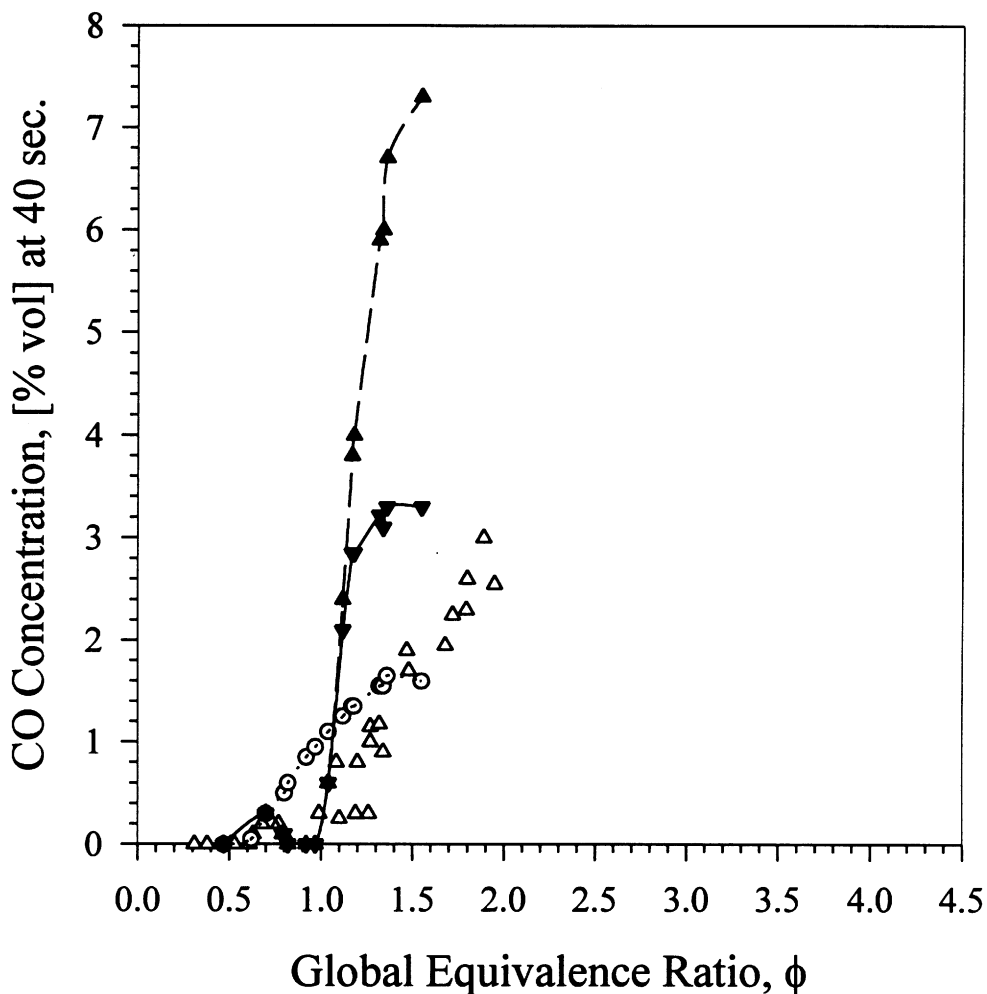


Figure 6.1 The CO experimental results of \circ -Beyler and Δ -Gottuk compared with the modeling results of Gottuk. Using \circ -Beyler's data as the initial concentrations in the model, the dotted line is the result using the upper-layer temperature of Beyler and the \blacktriangle -dashed line is the result using the upper-layer temperature of Gottuk. The \blacktriangledown -solid line corresponds to CO levels where all of the UHC was assumed to be consumed in the plume.

simple method which provides an estimate of the upper-layer species concentrations expected to be present in a compartment fire during post-flashover is developed.

The basis of the method is to use the conditions in the compartment just prior to flashover as initial conditions in a homogeneous reactor to estimate the species concentrations expected after flashover. The GER of the compartment fire and upper-layer temperature are the two input parameters for the model. Hexane compartment fire modeling results were compared with the experimental measurements of Gottuk (1992a). Modeling results of methane fires were compared with the species concentration measurements in natural gas compartment fires conducted by Bryner et al. (1994, 1995). The effects of temperature on species levels is also investigated.

6.3.2 Description of the Compartment Fire Model

Two approaches were considered when modeling the combustion products in the upper-layer of the compartment. The compartment upper-layer temperature and GER are the necessary inputs in both approaches.

Equilibrium calculations performed using *STANJAN* were determined to be adequate to model overventilated ($GER < 0.9$) compartment fires. *STANJAN* was run with the constant pressure and constant enthalpy conditions invoked (in other words a constant pressure, adiabatic system).

A homogeneous reactor was used to estimate species concentrations in an underventilated ($GER > 0.9$) compartment fire upper-layer. The assignment of the initial species mass fractions in the homogeneous reactor was critical. The initial species levels were determined using a model of the fire structure inside the compartment present just prior to the onset of flashover, see Fig. 6.2.

A compartment fire, as seen in Fig. 6.2, was considered to consist of two distinct parts: a fire plume and an accumulated upper-layer. The plume was assumed to be divided into two zones, an external flame sheet and a pure fuel core. Since the plume was

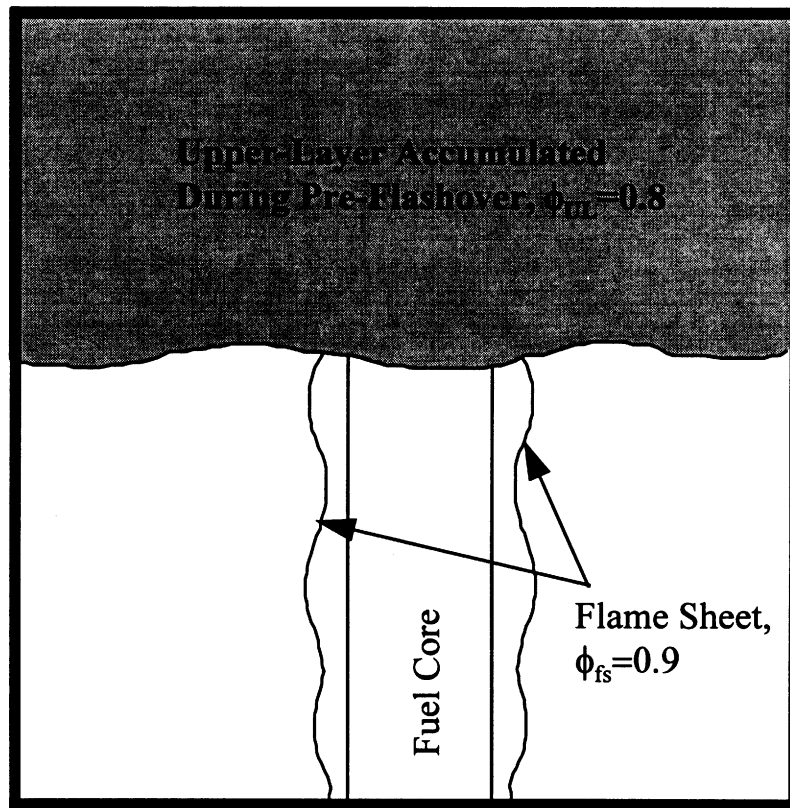


Figure 6.2 A phenomenological representation of the conditions present inside an idealized compartment fire just prior to the onset of flashover.

considered to rise to the upper-layer in an overventilated environment, the flame sheet was considered to have an equilibrium composition with an initial equivalence ratio of $\phi_{fs}=0.9$. The remainder of the fuel in the compartment was assumed to be convected into the upper-layer through the core.

Experimental data was utilized to develop a basis for the general estimation of species concentrations accumulated in the compartment upper-layer before flashover. The O_2 and CO_2 concentrations present in the compartment upper-layer just prior to the onset of flashover were measured in *n*-hexane fires to be approximately 4 % and 10%, respectively. These levels are consistent with O_2 and CO_2 concentrations measured in the upper-layer by Gottuk (1992a) at a GER of approximately 0.8. Hence, the upper-layer prior to flashover was modeled as an equilibrium mixture with an initial equivalence ratio of $\phi_{UL}=0.8$.

To predict the species concentrations in the upper-layer during the steady-state period (i.e. post-flashover) of the compartment fire, the upper-layer was modeled as a homogeneous isothermal reactor. The initial composition in the reactor was obtained by adding the moles of products from the flame sheet, the moles of fuel in the plume core and the moles of species accumulated in the upper-layer prior to flashover.

The detailed steps for modeling underventilated compartment fire upper-layers are listed below.

1. Simulate upper-layer accumulated during pre-flashover by running *STANJAN* at $\phi_{ul}=0.8$ with the constant pressure and enthalpy conditions invoked.
2. Simulate the burning portion of plume (the flame sheet) rising into upper-layer by running *STANJAN* at $\phi_{fs}=0.9$ with the constant pressure and the constant enthalpy conditions invoked.

3. Subtract the moles of fuel burned in step 2 from the global equivalence ratio of the upper-layer during the steady-state, and add this amount of fuel (in moles) to the result of step 2. This simulates the species in the plume entering the upper-layer.
4. Add the result of step 1 and step 3 and use this mixture as the initial condition in *SENKIN* with the constant pressure and constant temperature (steady-state gas temperature) conditions invoked.

The code was run until the species concentrations came to a steady state. This was assumed to occur when a less than 0.05% change in the CO level was observed, approximately 15 seconds of computer run time.

The simulations considered both highly overventilated (GER=0.1) and underventilated (GER=4.0) compartment fires. The initial molar concentrations in the homogeneous reactor was determined using the procedure previously described. The *SENKIN* calculations were performed at various upper-layer temperatures to include the conditions of all available experimental data. In particular, temperatures of 900 , 1000 and 1100 K were used in the computations to model the reduced-scale *n*-hexane compartment fires. Temperatures of 1000 K and 1300 K were used to model the reduced-scale methane fires.

6.3.3 *n*-Hexane Compartment Fire Modeling Results

In the experiments performed by Gottuk (1992a), the average upper-layer temperature inside the compartment during steady-state was approximately 1000 K with a variation of ± 100 K. Measurements of CO, CO₂ and O₂ concentrations in the compartment upper-layer were made for a GER ranging from 0.3 to 3.0.

The CO concentration data of Gottuk (1992a) is shown in Fig. 6.3 plotted against the GER. Also shown in Fig. 6.3 are the predictions of the current model and the modeling results of Gottuk (1992a). Using a 1000 K as the upper-layer

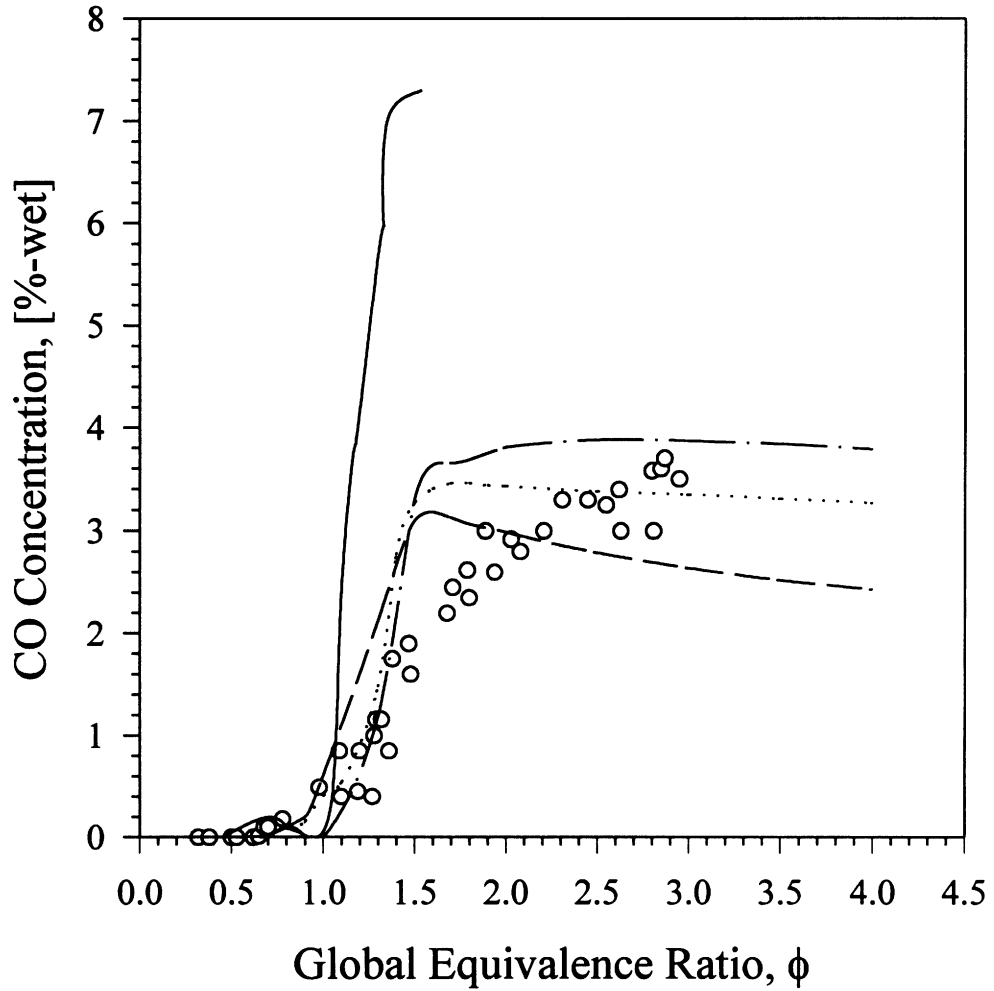


Figure 6.3 Comparison of the \circ -experimental and —modeling results of Gottuk(1992a) with the proposed model estimations of CO concentrations for *n*-hexane fires during the steady-state time with temperatures of ----900K, ••• 1000 K, and -•- 1100 K.

temperature, the proposed model estimated the data within $\pm 10\%$ for GER greater than 1.8 and less than 1.4. With the GER between 1.4 and 1.8, the model over-predicted the experimental results by as much as 50 %. Though this error seems high, the estimations of CO concentration using the model of Gottuk is seen in Fig. 6.3 to be in error by as much as 700% in this range.

The model estimations of the CO_2 and O_2 concentrations are plotted in Fig. 6.4 and Fig. 6.5, respectively. The model estimates the experimental data to within $\pm 10\%$ over the entire range of GER.

The model estimations of other species concentrations formed in a compartment fire at 1000 K are plotted in Fig. 6.6 versus the global equivalence ratio. The ignition index calculations assumed the H_2 concentration was half the concentration of CO. The modeling results verify this assumption to be accurate to within $\pm 20\%$ over all GER. The concentration of different UHC in the upper-layer is plotted in Fig. 6.7. The UHC with the highest concentration was ethylene. This verifies the assumption made when using ethylene as a calibration gas for the FID analyzer.

6.3.4 Methane Compartment Fire Modeling Results

Species concentration measurements in natural gas compartment fire experiments were performed by Bryner et al. (1994). Measurements were performed in both the rear of the compartment (near the wall on the opposite end of the room from the doorway) and in the front of the compartment (by the wall containing the doorway). Temperatures of approximately 1000 K were measured in the rear while temperatures of 1300 K were measured in the front. The CO concentrations estimated using the model at the temperatures in the rear (1000 K) are seen in Fig. 6.8 to be within $\pm 25\%$ of the compartment rear experimental data. The CO concentrations estimated for the front of the compartment (1300 K) are seen in Fig. 6.8 within $\pm 30\%$. The model consistently under-predicted the experimental data from a GER of 0.6 to 1.2.

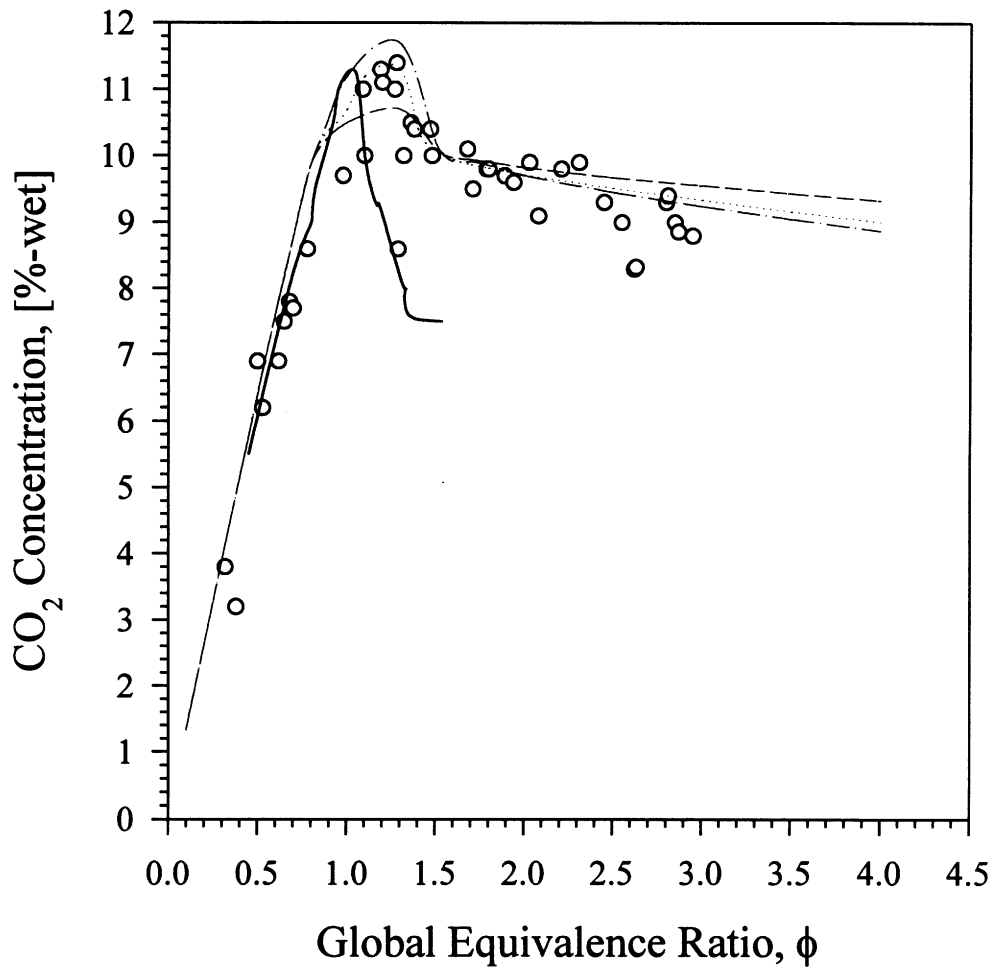


Figure 6.4 Comparison of the O-experimental and — modeling results of Gottuk (1992a) with the proposed model estimations of CO₂ concentrations for *n*-hexane fires during the steady-state time with temperatures of ----900K, ••• 1000 K, and -•- 1100 K.

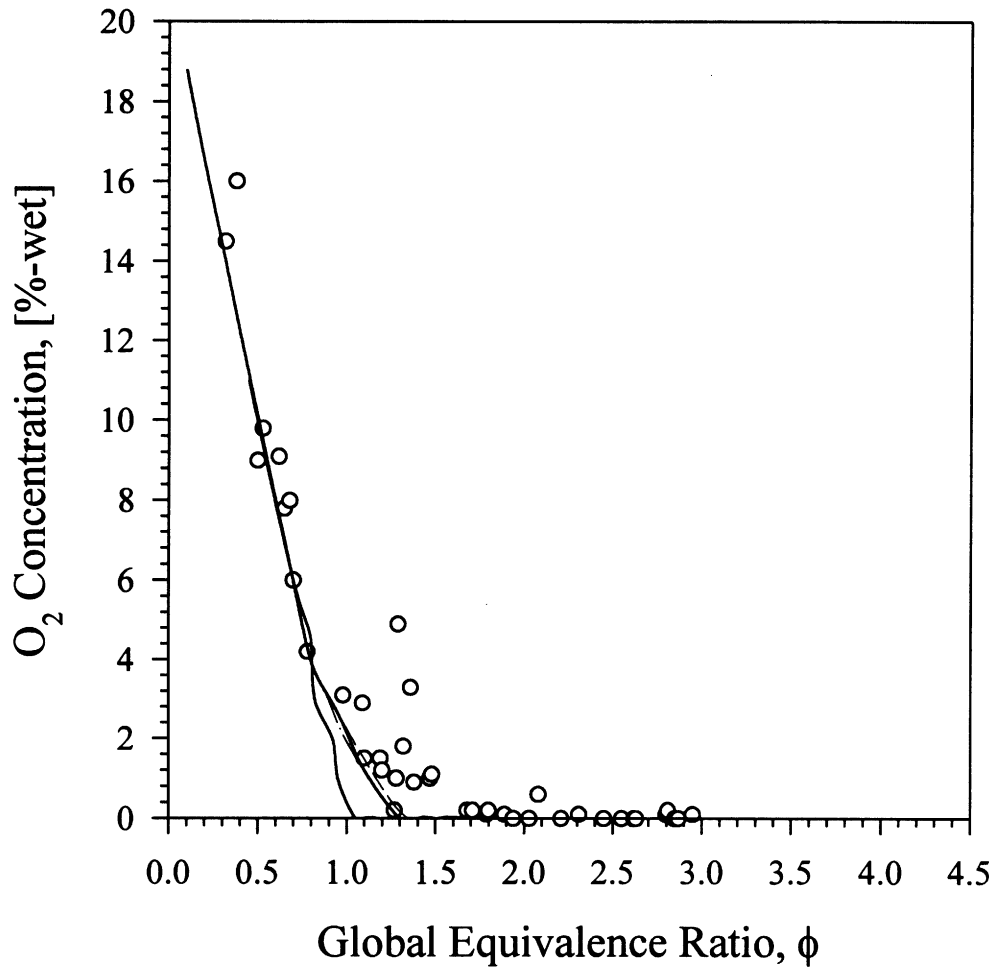


Figure 6.5 Comparison of the \circ -experimental and — modeling results of Gottuk (1992a) with the proposed model estimations of O₂ concentrations for *n*-hexane fires during the steady-state time with temperatures of ----900K, ••• 1000 K, and -•- 1100 K.

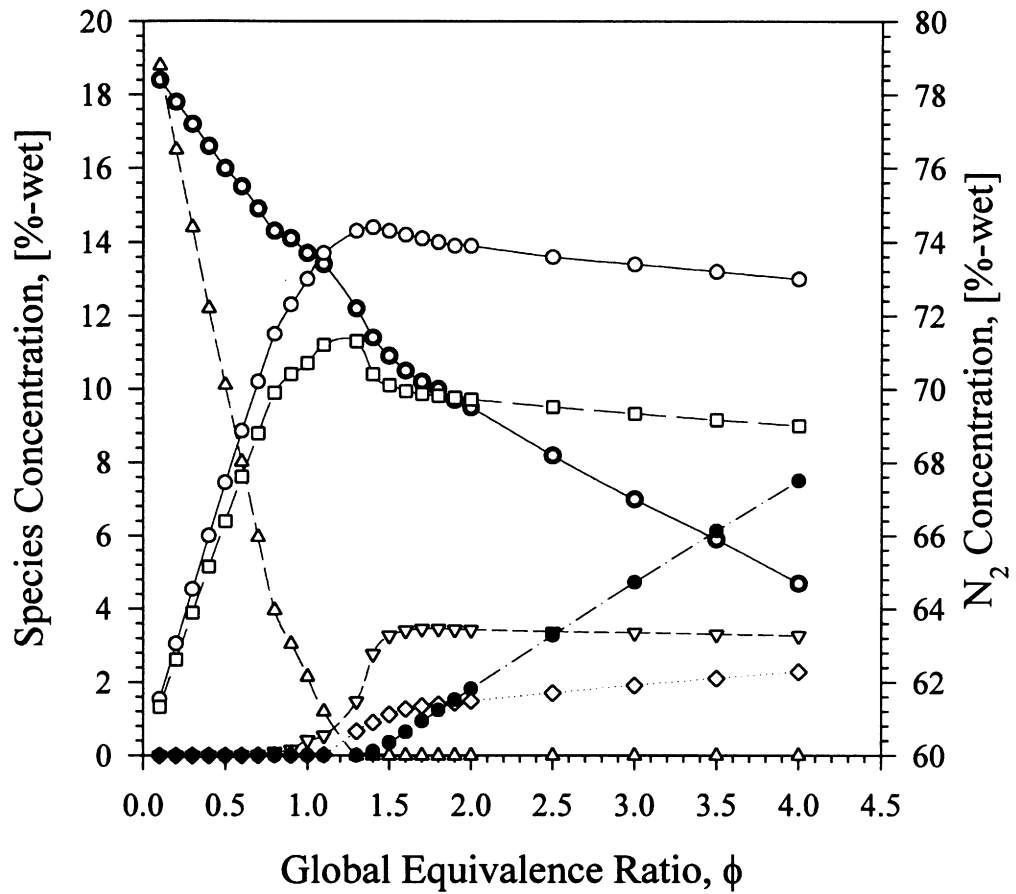


Figure 6.6 Model estimation of the major species concentrations present in the 1000 K compartment upper-layer during the steady-state time of a *n*-hexane fire. Symbols: ●- N_2 , ○- H_2O , □- CO_2 , △- O_2 , ▽- CO , ◇- H_2 and ●-UHC.

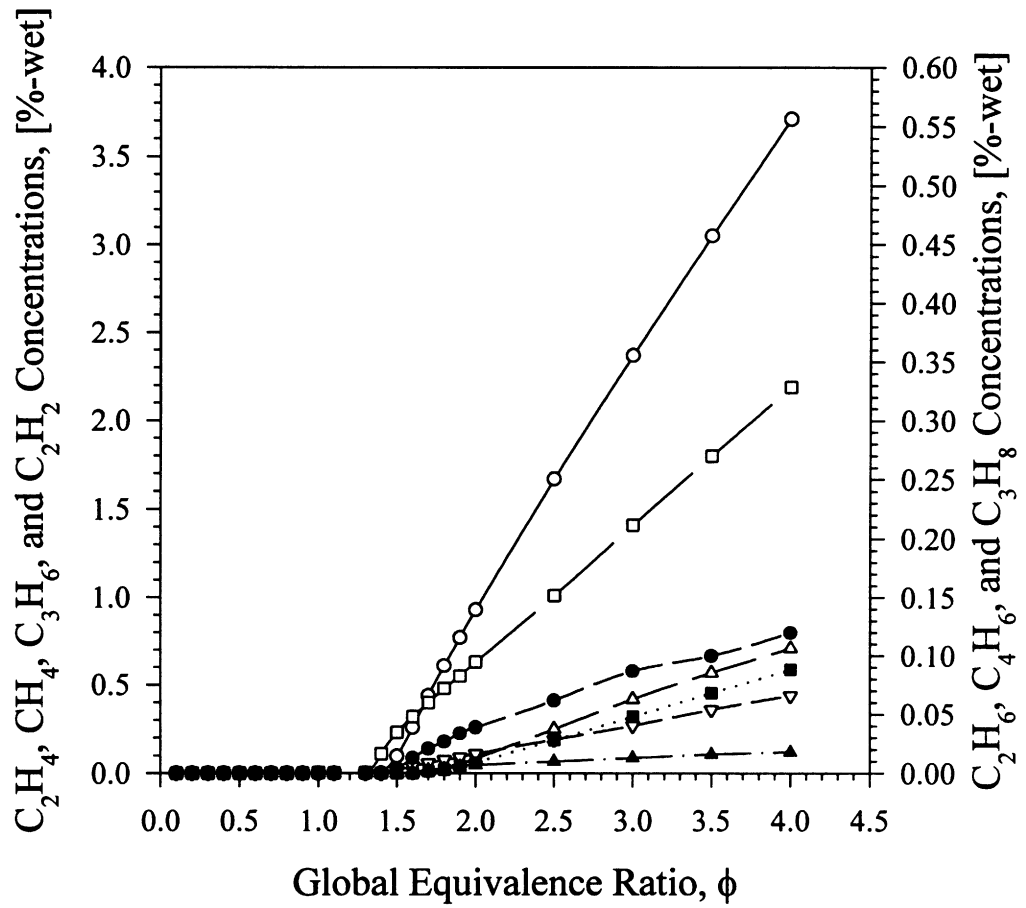


Figure 6.7 Model estimation of the UHC concentrations present in the 1000 K compartment upper-layer during the steady-state time of a *n*-hexane fire. Open symbols, O- C_2H_4 , \square - CH_4 , Δ - C_3H_6 , and ∇ - C_2H_2 , correspond to the left y-axis while closed symbols, \bullet - C_2H_6 , \blacksquare - C_4H_6 and \blacktriangle - C_3H_8 correspond to the right y-axis.

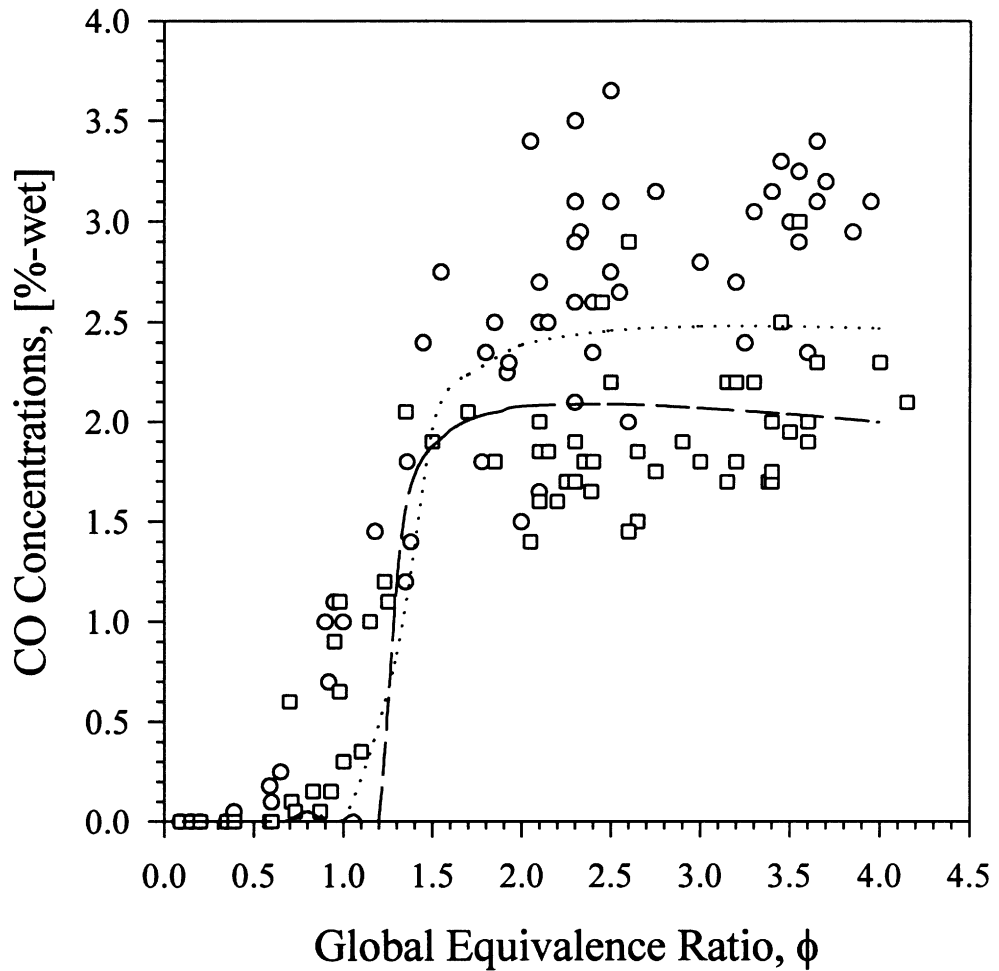


Figure 6.8 Comparison of the experimental results of Bryner, et al. (1994), in both the O-front (1300 K) and the \square -back (1000 K) of their compartment, with the proposed model estimations of CO concentrations for methane compartment fires during the steady-state time with temperatures of ---1000K and •••1300 K.

The estimations of CO_2 and O_2 concentrations in the upper-layer are plotted in Fig. 6.9 and 6.10, respectively. The model estimated the CO_2 and O_2 concentrations to within $\pm 10\%$ of the experimental data over the entire range of GER study.

The model estimations of other species concentrations in a compartment upper-layer at 1000 K are shown in Fig. 6.11. The H_2 concentrations were measured to be nearly equal to the concentration of CO. The difference in CO- H_2 ratio between the methane experiments and the *n*-hexane experiments was attributed to the carbon-hydrogen ratio in the fuel. Methane has a 1:4 carbon-hydrogen ratio while *n*-hexane has a 1:2.3 carbon-hydrogen ratio. The estimations of the concentrations of different unburned hydrocarbons in the upper-layer is plotted in Fig. 6.12. Methane is the dominant hydrocarbon in these compartment fires.

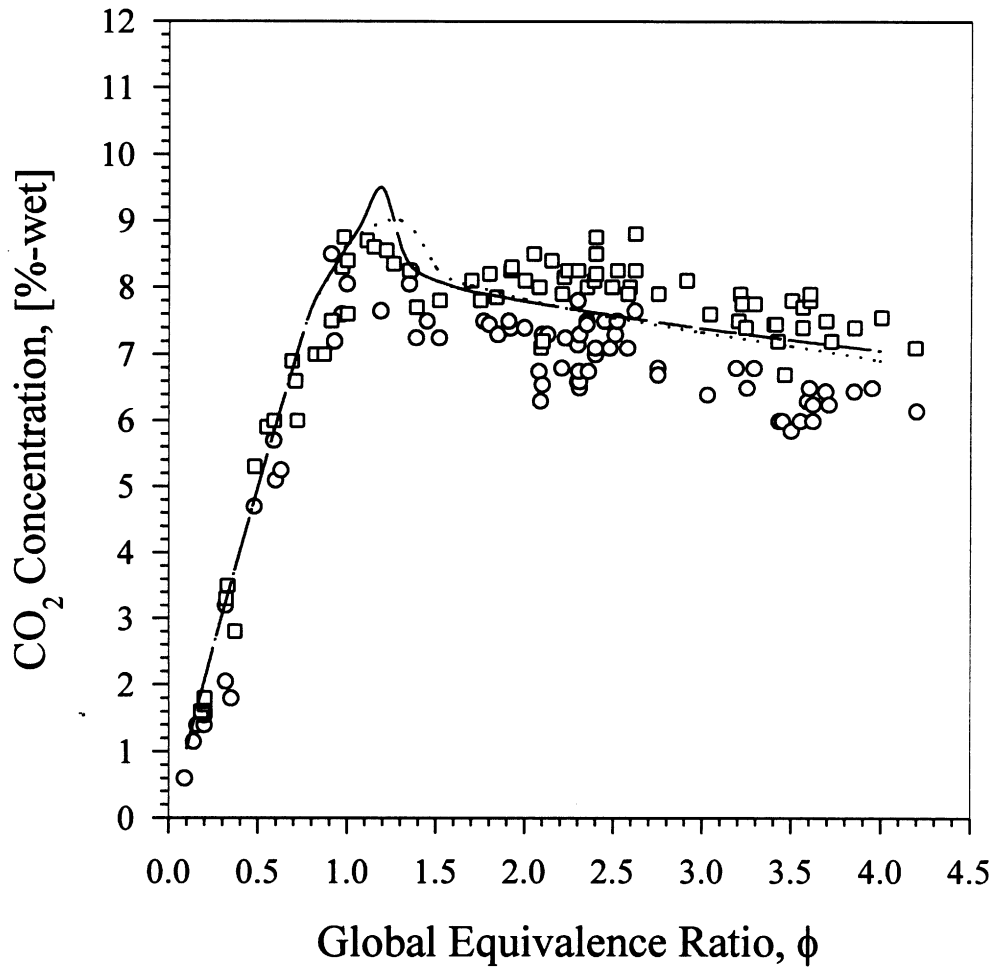


Figure 6.9 Comparison of the experimental results of Bryner, et al. (1994), in both the O-front (1300 K) and the \square -back (1000 K) of their compartment, with the proposed model estimations of CO₂ concentrations for methane compartment fires during the steady-state time with temperatures of ---1000K and •••1300 K.

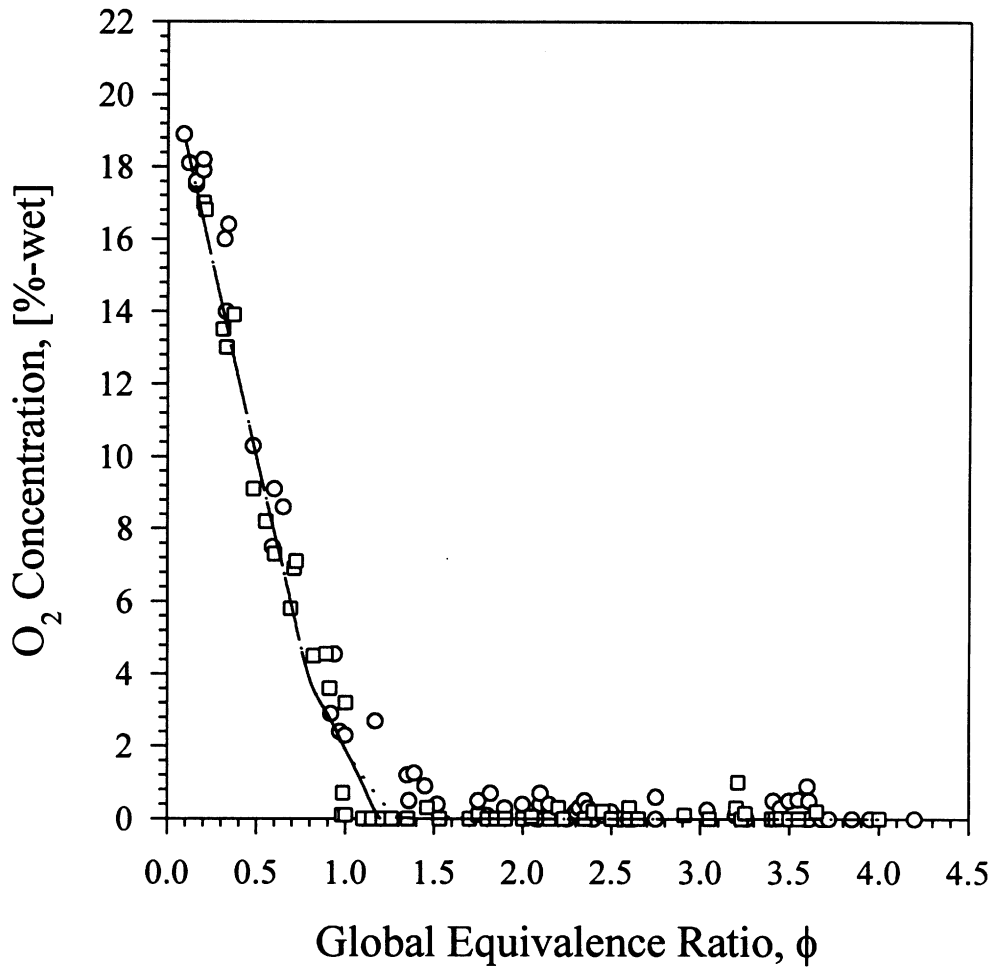


Figure 6.10 Comparison of the experimental results of Bryner, et al. (1994), in both the O-front (1300 K) and the □-back (1000 K) of their compartment, with the proposed model estimations of O₂ concentrations for methane compartment fires during the steady-state time with temperatures of ----1000K and •••1300 K.

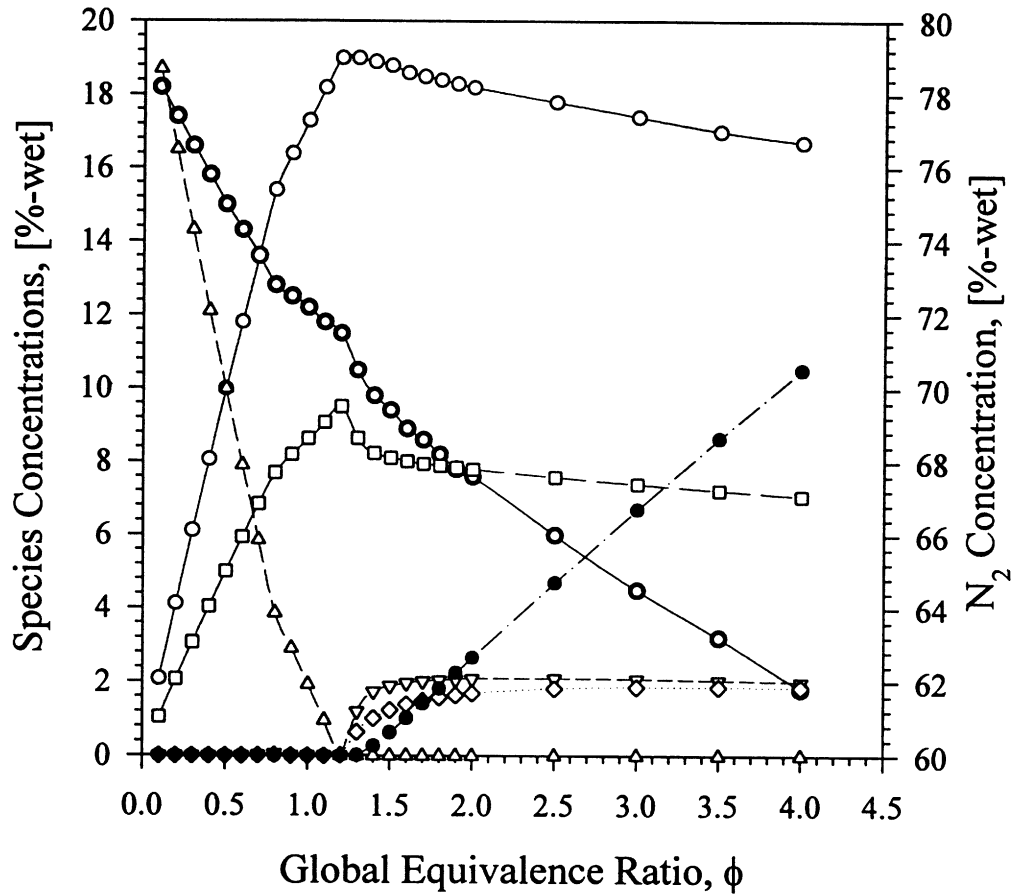


Figure 6.11 Model estimation of the major species concentrations present in the 1000 K compartment upper-layer during the steady-state time of a methane fire. Symbols: ●-N₂, ○-H₂O, □-CO₂, △-O₂, ▽-CO, ◇-H₂ and ●-UHC.

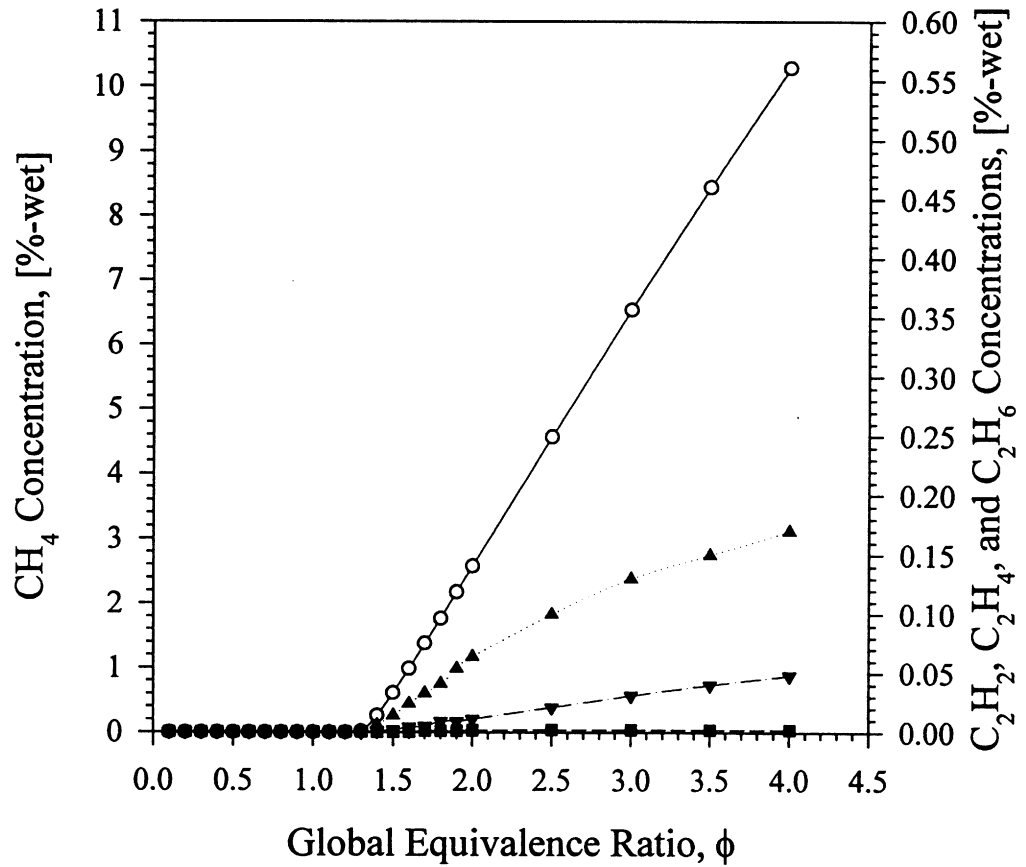


Figure 6.12 Model estimation of the UHC concentrations present in the 1000 K compartment upper-layer during the steady-state time of a methane fire. The open symbol, O- CH_4 , corresponds to the left y-axis while closed symbols, ■- C_2H_2 , ▲- C_2H_4 , and ▼- C_2H_6 correspond to the right y-axis.

CHAPTER 7

CONCLUSIONS AND RECOMMENDATIONS

7.1 SUMMARY

Smoke inhalation accounted for 76% of the deaths in building fires during 1990. Two-thirds of these victims were found at locations remote from the burning room. Carbon monoxide (CO) has been determined by numerous studies to be the major toxicant in the fire gases, and has been deemed responsible for the majority of the smoke inhalation deaths in building fires.

The level of CO transported to remote locations from a burning compartment is a function of the

- global equivalence ratio in the compartment,
- oxygen entrainment into gases burning in the hallway, and
- heat transfer.

The entrainment into the gases entering the hallway strongly affects the last two variables. Therefore, it was hypothesized that this entrainment strongly controls the CO level transported to remote areas. This experimental study focused on the effects of entrainment into the compartment fire gases entering the hallway on the CO levels at locations remote from the burning compartment.

The results of the experimental investigation were discussed in Chapters 3-5. The level of CO exiting the hallway (termed post-hallway yields) was measured for different experimental conditions. The transport of CO away from a burning compartment on the side of a hallway was characterized by sampling in the hallway. Experimental data was

used to identify the key parameters controlling the transport of high CO concentrations. Correlations were developed using the experimental data to estimate CO levels transported to remote locations. Models which identify when these correlations can accurately be applied to building fires were also developed. A general procedure was proposed for the estimation of CO levels transported in building fires. A chemical kinetic model was also developed to estimate the species concentrations present in a compartment fire upper-layer after the onset of flashover.

Through the research, the following parameters were identified to most significantly affect the level of CO transported to remote locations.

1. entrainment rate of surrounding gases into compartment fire gases,
2. oxygen level in the surrounding gases being entrained,
3. presence or absence of external burning in the hallway,
4. stoichiometry of the gases entering the hallway, and
5. the transient time of the species concentrations in the hallway.

Overventilated *n*-hexane compartment fire experiments were performed to measure the entrainment rate under different experimental conditions. The entrainment rate was most drastically affected by the compartment-hallway opening size and the soffit height above the opening. A reduction in the opening size resulted in an increase in the entrainment. The entrainment was measured to exponentially increase with a decrease in the Richardson number of the flow entering the hallway. An increase in the entrainment rate was also measured when the soffit height was increased. This was attributed to the presence of the soffit allowing the gases to enter the hallway as a buoyant plume instead of a ceiling jet.

During a building fire, a deep upper-layer of oxygen deficient combustion gases develops in the space adjacent to the burning room. The depth of this upper-layer was

hypothesized to significantly affect the O₂ level entrained into compartment fire gases entering the space. Underventilated *n*-hexane experiments were conducted to study the effect of gradually increasing the depth of the upper-layer in the hallway on the post-hallway species yields. The degree to which the hallway upper-layer surrounds the jet of compartment gases entering the hallway was defined by the nondimensional upper-layer depth ($\gamma = \delta/z$, where δ is the upper-layer depth and z is the distance between the bottom of the opening and the ceiling). The post-hallway CO and UHC yields were measured to increase with an increase in γ (by increasing the upper-layer depth). This was attributed to less oxygen being entrained into the compartment fire gases entering the hallway. The study of Westbrook and Dryer (1984) noted that a decrease in O₂ levels at the flame front results in limited radicals being formed to oxidize CO and UHC. The CO yield was actually measured to increase to levels 6-25% greater than measured compartment yields. This was measured in experiments with a 0.12 and 0.08 m² opening sizes, γ between 1.4 and 1.7, and external burning occurring in the hallway. The jets associated with these opening sizes were measured to have the lowest entrainment rates of experimentally tested jets. From the results of Westbrook and Dryer (1984), the low entrainment rate coupled with the low oxygen level being entrained is believed to have resulted in a limited pool of radicals. It is hypothesized that the majority of these radicals were used to oxidize UHC thus forming additional CO in the process (Westbrook and Dryer, 1984). The increase in CO yields is attributed to limited radicals being able to react with the CO before the oxidation reactions were frozen (Westbrook and Dryer, 1984). With $\gamma > 1.7$, no external burning was observed to occur in the hallway. Post-hallway CO yields were measured to be equal to those measured inside the compartment.

No external burning was observed to occur when polyurethane foam slabs were burned in the compartment. The yields downstream were, therefore, always nearly equal to the species yields measured inside the compartment (0.19 for CO) regardless of the hallway upper-layer depth.

With the compartment on the side of the hallway, the fluid mechanics in the hallway are highly 3-dimensional. Flow visualization of the hallway fluid mechanics was performed by observing the external burning occurring in the hallway. The burning was observed at the open end of the hallway. The gases were observed to flow initially across the hallway and were then seen to impinge on the wall opposite the compartment. The impingement resulted in large clockwise rotating vortical structure. The vortical structure swirled down the hallway along the corner of the ceiling and the wall opposite the compartment. From the size of the structure, the majority of the gases flowing away from the room appeared to be transported down the hallway within the structure.

The temporal and spatial variation in species concentrations and temperature in the hallway was investigated for experiments where high post-hallway CO yields were measured. Concentrations of CO exceeding 1.8% were measured in gases flowing across the hallway and down the side of the hallway opposite the compartment shortly after compartment flashover. This is precisely the flow pattern observed from the flow visualization. The concentration of CO measured in the gases on the compartment side of the hallway at this period of the fire was less than 0.8%. The non-uniformity of CO concentration in the hallway persisted until the hallway species concentrations were measured to reach a steady-state in the hallway. This was approximately 60 seconds after flashover in experiments with a 0.60 m exit soffit and 96 seconds in experiments with the bottom of the hallway exit blocked. The CO concentrations during the steady-state period were measured to be approximately 2.0% within the upper-layer despite the occurrence of external burning. The burning was measured to reduce UHC levels to approximately 1.0%. Compartment fire exhaust gas temperatures cooled to less than 800 K approximately 4 seconds after entering the hallway with temperatures never measured in excess of 1000 K. The CO oxidation was, therefore, believed to occur at or near the flame front where temperatures greater than 1200 K exist.

The effects of fuel type in the compartment was studied by conducting a series of 11 polyurethane foam fire experiments. The variation in the species concentrations and temperatures were measured in the hallway 0.05 m below the ceiling. No external burning occurred in these experiments. The flow of gases containing high concentrations of CO was measured to be nearly equivalent to that measured in the *n*-hexane fire experiments. The species concentrations were measured to equilibrated approximately 60 seconds after compartment flashover. Approximately 1.8% CO was measured to be uniform within the upper-layer gases 0.05 m below the ceiling.

External burning in the hallway was measured to have significant effect on the post-hallway yields. A model to determine the occurrence of external burning was developed. The model uses the ignition index and the nondimensional upper-layer depth to predict external burning. The ignition index was used to determine whether the mixture entering the hallway was ignitable. The nondimensional upper-layer depth determined whether a pilot ignition source (in the form of oxidative radicals) was available. Ignition was determined to occur in the hallway when the ignition index exceeded approximately 1.0 and the nondimensional upper-layer depth was less than 1.7.

Correlations to predict CO levels transported to remote locations are most conveniently expressed in terms of yields. For the post-hallway yields to accurately predict the level of species in the hallway, the concentration of the species must be uniform within the hallway. A perfectly stirred reactor model was developed to estimate the time necessary for the species concentrations to reach a steady-state (termed the transient time). The transient time from the model was determined to be within $\pm 15\%$ of the experimentally determined transient times.

Post-hallway yields were measured to be equal to compartment yields when no external burning occurred in the hallway. In this case, correlations based on the compartment global equivalence ratio can be used to predict post-hallway CO yields.

The occurrence of external burning in the hallway led to the oxidation of species in the hallway. Post-hallway yields were determined to no longer be correlated with the compartment global equivalence ratio when external burning occurred .

Two models are proposed to predict post-hallway CO yields with external burning occurring in the hallway. The first model relates the oxygen entrained into the compartment fire gases entering the hallway to the post-hallway yields of CO and UHC. The model accounts for the entrainment rate of the jet and the concentration of oxygen entrained by the oxygen entrainment parameter. The model is accurate for a compartment global equivalence ratio greater than 1.8 and for hallway upper-layer depths less than $\gamma=1.7$. A second model relates the post-hallway yields to a global equivalence ratio for the hallway and compartment. The oxidation of CO in the hallway is most significantly affected by the air entrained into the burning gases in the hallway. This entrainment was approximated using the air entrainment measurements and a estimation of the flame extension in the hallway. The data was determined to collapse to the compartment data of Gottuk (1992). This was expected since the system global equivalence ratio in the study performed by Gottuk was the compartment global equivalence ratio. The model is accurate for all compartment global equivalence ratios, but is only valid for upper-layers with $\gamma<1.4$.

A phenomenological model which considers only chemical kinetics was developed to provide an estimation of species concentrations inside the compartment during post-flashover. Previous models have relied on available experimental data to set the initial conditions in a reactor. The proposed model requires knowledge of the compartment global equivalence ratio and upper-layer temperature to provide estimations of species concentrations in the compartment upper-layer. The model was able to estimate CO, CO₂, and O₂ concentrations to within $\pm 25\%$ for both *n*-hexane and methane compartment fire data. The model was also able to estimate higher levels of CO measured in the full-

scale methane fire experiments conducted by Bryner, et al.(1995). With validation of the models agreement with available experimental data, the model verified several approximations and assumptions which have been used in the study. The model confirms H_2 levels being half of the CO level in the 900-1100K temperature range, in addition to confirming that ethylene, C_2H_4 , is the major unburned hydrocarbon produced in the *n*-hexane fires.

7.2 CONCLUSIONS

The goal of the experimental study was to provide fire protection engineers with correlations to predict CO levels transported to remote locations. The experiments were conducted with the compartment on the side of the hallway. The research identified the parameters most significantly affecting the post-hallway CO yields. The temporal and spatial variation of the CO concentration in the hallway upper-layer was measured with the burning compartment on the side of the hallway. A procedure was developed to provide engineers with a sound method for predicting CO yields in building fires. An engineering tool was also developed to predict species formation in a compartment fire after flashover.

The experimental investigation has determined that

- the existence of a deep oxygen deficient upper-layer in the adjacent space contributes significantly to the transport of fatally high levels of CO in building fires, and
- with the burning room on the side of the hallway, fire gases are transported non-uniformly down the hallway.

Both of these conditions were present in the unfortunate fire which took place in the Hillhaven Nursing Home in Norfolk, Virginia during October of 1989. In this fire, 13 people died with 10 people perishing on the wing of the floor containing the room with

the fire. Nine of the fatalities were located in rooms across the hallway from the burning room while only one occurred on the side of the hallway containing the burning room. The gas distributions in the hallway adjacent to the burning room are believed to be similar to the experiments with a long transient time. Disturbingly, incidents such as these are not isolated and occur several times annually.

Present fire protection engineering computer models would not have predicted such a hazard to the Hillhaven patients on the side of the hallway opposite the burning room since these codes use zonal models. Zonal models assume a spatially uniform CO yield in the upper-layer along the entire length of the hallway. With the burning room located on the side of the hallway, results show the transport of gases containing high levels of CO are transported to remote locations is highly non-uniform. The duration of time which the non-uniformity in the hallway exists depends on the characteristics of the adjacent space (i.e. hallway length, number of rooms connected to the hallway). Field models allow spatial and temporal variation in the species within the space applied. These models can be used to accurately predict the toxic gas flow away from a room on the side of a hallway at all times during the fire. However, field models are expensive and time consuming.

Some situations may not require field models to provide good estimates of the toxic gas flow. The species concentrations in the adjacent space were measured in this study to be uniform after the species concentrations had reached a steady-state. The transient time can be estimated using the perfectly stirred volume model. With species concentrations uniform in the adjacent space hallway, zonal models may be used to predict the toxic gas hazard in the space.

An engineering tool was also developed to provide a more detailed estimate of the concentrations present in a compartment fire upper-layer after post-flashover. The model

requires the upper-layer temperature and the global equivalence ratio of the compartment as inputs.

7.3 RECOMMENDATIONS

The research included in this thesis has addressed the effects of oxygen entrainment on the transport of CO to remote locations when the burning compartment is on the side of the hallway. Additional experiments need to be performed to measure the effects of heat loss, a door connecting the hallway and compartment, and the compartment-hallway orientation on the CO yields and in-hallway concentrations. The effects of these parameters on the CO yields need to be compensated for in the correlations developed in this work. An engineering tool needs to be developed to estimate species levels in the hallway.

Heat losses in the hallway are responsible for the gases cooling to a point where oxidative reactions no longer occur. To gain a full understanding of the phenomena controlling the transport of high levels of CO, measurements of heat losses in the hallway need to be performed. Specifically, the heat transfer losses to the surroundings (i.e. the walls, the area below the upper-layer) and the heat transfer effects of the air entrainment need to be determined.

Experiments measuring the entrainment into the burning hallway gases need to be performed. Besides the measurements made in this study, very little data is available on the entrainment of air into ceiling jet flows. Measurements made in this study provided a good approximation for these levels, but improved measurements are suggested.

Experiments need to be conducted with the compartment shifted from the end of the hallway to the middle of the hallway forming a T shape. In this scenario, the gases would split off into two directions after impinging on the wall opposite the compartment. In one

direction, the gases would flow toward the open end of the hallway where the fume hood is located, possibly leaving the hallway. The gases moving in the other direction are forced to circulate within the dead end of the hallway. The dead end of the hallway has been speculated by many to be an area where high levels of CO are produced because of the long residence times of the gases in this area (Nelson, 1996). The temporal and spatial evolution of hallway CO concentrations in this compartment-hallway scenario would be particularly interesting.

The burning room is typically connected to the adjacent space by a door. From the results in Appendix C, a doorway connecting the compartment and the hallway has an effect on both the level of species produced inside the compartment and the oxidation of gases within the hallway. Further experiments should be conducted with a door (where a bi-directional flow of cool air entering the room and hot combustion gases exiting the room is present) to quantify the effects of deep hallway upper-layers on CO levels. The application of the nondimensional upper-layer depth for doorway scenarios should be tested. The distance between the neutral plane of the doorway and the ceiling (instead of the distance between the bottom of the opening and the ceiling) should be investigated. The neutral plane is typically 1.44 m below a 2.44 m high ceiling. External burning will most likely occur in all experiments since a maximum value of γ is slightly less than 1.7. External burning was observed not to occur when $\gamma > 1.7$ in experiments with a uni-directional flow opening.

A simple plug flow reactor model is desired for the estimation of species oxidation in the hallway. With no plug flow reactor code available, assumptions were applied to the governing equations in Appendix D to allow the momentum equation to be disregarded. This leaves just the species conservation equations to be solved; a task which can be accomplished using a code such as *SENKIN*. Since *SENKIN* solves such equations with time and all the data is in spatial coordinates, the transformations necessary to convert the

spatial results to a temporal coordinate system, and vice versa, are also developed in Appendix D. The plug flow reactor model developed in Appendix D. would use the results of the compartment fire model as the species mole fractions initially entering the reactor. Experimentally determined temperatures and air entrainment into the upper-layer gases would be used to apply the model.

REFERENCES

Alpert, R.L., 1972, "Fire Induced Turbulent Ceiling-Jet," Technical Report 19722-2, Factory Mutual Research Corporation, Norwood, Mass, 91 p.

Alpert, R.L., 1980, "Turbulent Ceiling-Jet Induced by Large-Scale Fires," *Combustion Science and Technology*, **11**, pp. 197-213.

ASME, (1971), Fluid Meters: Their Theory and Application, Report of A.S.M.E. Research Committee on Fluid Meters, Sixth Edition, Ed. H.S. Bean, New York.

Babrauskas, V., 1980, "Flame Lengths Under Ceilings," *Fire and Materials*, **4**(3), pp. 119-126.

Bakke, P., 1957, *Journal Fluid Mechanics*, **2**, p. 467.

Beyler, C.L., 1983, "Development and Burning of a Layer of Products of Incomplete Combustion Generated by a Buoyant Diffusion Flame," Ph.D. Thesis, Harvard University, 162 p.

Beyler, C.L., 1984, "Ignition and Burning of a Layer of Incomplete Combustion Products," *Combustion Science and Technology*, **39**, pp. 287-303.

Beyler, C.L., 1986a, "Major Species Production by Solid Fuels in a Two Layer Compartment Fire Environment," *Fire Safety Journal*, **10**, pp. 47-56.

Beyler, C.L., 1986b, *Fire Safety Science-Proceedings First Int. Symposium*, Hemisphere, Washington, D.C., pp. 431-440.

Bryner, N.P., Johnsson, E.L., and Pitts, W.M., 1994, "Carbon Monoxide Production in Compartment Fires--Reduced-Scale Enclosure Test Facility," NISTIR 5568.

Bryner, N.P., Johnsson, E.L., and Pitts, W.M., 1995, "Scaling Compartment Fires-Reduced and Full-Scale Enclosure Burns," *Proceedings of the International Conference on Fire Research and Engineering Proceedings*, September 10-15, Orlando, Florida, pp. 9-14.

Cetegen, B.M., Zukoski, E.E., Kubota, T., 1982, "Entrainment and flame geometry of fire plumes," NBS Report, GCR-82-402, April, 222 p.

Colket, M.B., Naegeli, D.W., Dryer, F.L., and Glassman, I., 1974, "Flame Ionization Detection of Carbon Oxides and Hydrocarbon Oxygenates," *Environmental Science and Technology*, **8**(1), pp.43-46.

Curran, H. and Westbrook, C.K., 1996, *n*-hexane mechanism, LLNL.

Daikoku, M. and Saito, K., 1995, "A Study on Thermal Characteristics of Vertical Corner Wall in Room Fire," *Proceedings of ASME/JSME Thermal Engineering*, Fletcher, L.S. and Aihara, T. eds., Book No. H0933C.

Deal, S. and Beyler, C., 1990, "Correlating Pre-flashover Room Fire Temperature," *Journal of Fire Protection Engineering*, **2**(2), pp. 33-48.

Drysdale, D., 1985, An Introduction to Fire Dynamics, John Wiley and Sons, New York.

Ellison, T.H. and Turner, J.S., 1959, "Turbulent Entrainment in Stratified Flows," *Journal of Fluid Mechanics*, **6**, pp. 423-446.

Emori, R.I. and Saito, K., 1979, "Model Rules of Motion of Smoke and Gases in Building Fires," **29**(2), pp. 41-49.

Ewens, D.S., 1994a, "The Transport and Remote Oxidation of Compartment Fire Exhaust Gases", Master of Science Thesis, Department of Mechanical Engineering, Virginia Polytechnic Institute and State University, 134 p.

Ewens, D.S., 1994b, Unpublished Data.

Fardell, P.J., Murell, J.M. and Murell, J.V., 1986, "Chemical 'Fingerprint' Studies of Fire Atmospheres," *Fire and Materials*, **10**, pp. 21-28.

Gann, R.J., Babrauskas, V., and Peacock, R.D., 1994, "Fire Conditions for Smoke Toxicity Measurements," *Fire and Materials*, **18** (3), (May/June), pp. 193-199.

Gottuk, D.T., 1992a, "The Generation of Carbon Monoxide in Compartment Fires," Ph.D. Thesis, Virginia Polytechnic Institute and State University, Department of Mechanical Engineering, 245 p.

- Gottuk, D.T., Roby, R.J., Peatross, M.J. and Beyler, C.L., 1992b, "Carbon Monoxide Production in Compartment Fires,:" *Journal of Fire Protection Engineering*, **4**, pp. 133-150.
- Gottuk, D.T., Roby, R.J., and Beyler, C.L., 1992c, "A Study of Carbon Monoxide and Smoke Yields from Compartment Fires with External Burning," *Twenty-Fourth Symposium (International) on Combustion*, The Combustion Institute, Pittsburgh, PA, pp. 1729-1735.
- Gottuk, D.T., Roby, R.J., and Beyler, C.L., 1995, "The Role of Temperature on Carbon Monoxide Production in Compartment Fires," *Fire Safety Journal*, **24**, pp. 315-331.
- Gross, D., 1989, "Measurements of Flame Lengths Under Ceilings," *Fire Safety Journal*, **15**, pp. 31-44.
- Hall, J.R. and Harwood, B., 1995, "Smoke or Burns-Which is Deadlier?," *NFPA Journal*, January/February, pp. 38-43.
- Harland, W.A. and Anderson, R.A., 1982, "Causes of Death in Fires," *Proceedings of Smoke and Toxic Gases from Burning Plastics*, London, England, pp. 15.1-15.19.
- Heskestad, G., 1983, "Luminous Heights of Turbulent Diffusion Flames," *Fire Safety Journal*, **5**, p.103.
- Heskestad, G. and Hill, J.P., 1987, "Propagation of Fire Smoke in a Corridor," *Proceedings of the 1987 ASME-JSME Thermal Engineering Joint Conference*, Honolulu, Hawaii, pp. 371-379.
- Hinkley, P.L., Wraight, H.G.H. and Theobald, C.R., 1984, "The Contribution of Flames Under Ceilings to Fire Spread in Compartments," *Fire Safety Journal*, **7**, pp. 227-242.
- Janssen, M. and Tran, H., 1992, "Data Reduction of Room Tests for Zone Model Validation," *Journal of Fire Science*, **10**, pp. 528-555.
- Jones, A.R., 1979, "Scattering of Electromagnetic Radiation in Particulate Laden Fluids," *JPECS*, **5**, pp.73-96.

- Karter, M.J., 1995, "Fire Loss in the United States in 1994", *NFPA Journal*, September/October, pp. 93-100.
- Kawogoe, K., 1985, "Fire Behavior in Room," Report of the Building Research Institute (Japan), September.
- Kee, R.J., Rupley, F.M. and Miller, J.A., 1994, Sandia Report SAND89-8009B, April.
- Levine, R.S. and Nelson, H.E., 1990, "Full Scale Simulation of a Fatal Fire and Comparison of Results with Two Multiroom Models," National Institute of Standards and Technology Internal Report NISTR 90-4268, August, 101 p.
- Lutz, A.E., Kee, R.J. and Miller, J.A., 1994, Sandia Report SAND87-8248, May.
- McCaffery, B., Quintiere, J., Harkleroad, M., 1981, "Estimating Room Fire Temperatures and the Likelihood of Flashover using Fire Test Correlations," *Fire Technology*, 17(2), pp. 98-119.
- Morehart, J.H., Zukoski, E.E. and Kubota, T., 1990, "Species Produced in Fires Burning in Two Layered and Homogeneous Vitiated Environments," National Institute of Standards and Technology, Center for Fire Research, Report NBS-GCR-90-585.
- Morehart, J.H., Zukoski, E.E., Kubota, T., 1991, "Characteristics of Large Diffusion Flames Burning in a Vitiated Atmosphere," Cox, G. and Langford, B. eds., *Fire Safety Science--Proceedings of the Third International Symposium*, New York, NY, Elsevier, pp. 575-583.
- Morehart, J.H., Zukoski, E.E., Kubota, T., "Chemical Species Produced in Fires Near the Limit of Flammability," *Fire Safety Journal*, 19 (2,3), pp. 177-188.
- Morikawa T., Yanai, E., Watanabe, T., Okada, T. and Sato, T., 1990, "Toxic Gases from House Fires of Natural Polymers or Both Synthetic and Natural Polymers Under Different Conditions," *Proceedings of Interflam 1990*, pp. 249-255.
- Morikawa, T., Yanai, E., Okada, T. and Sato, K., 1993, "Toxicity of the Atmosphere in an Upstairs Room Caused by Inflow of Fire Effluent Gases Rising from a Burning Room," *Journal of Fire Sciences*, 11, pp. 195-209.
- Nelson, H.E., 1988, "Engineering Analysis of Fire Development in the Hospice of Southern Michigan, December 15, 1989," *Fire Safety Science Proceedings from the Second International Symposium*, pp. 927-938.

- Nelson, H.E. and Tu, K.M., 1991, "Engineering Analysis of the Fire Development in the Hillhaven Nursing Home Fire, October 5, 1989," NISTIR 4664, 51 p.
- Nelson, H.E., 1996, Personal Communication.
- Newman, J.S. and Steciak, J., 1987, "Characterization of Particulates from Diffusion Flames," *Combustion and Flame*, **67**, pp. 55-64.
- Peterson, J.E. and Stewart, R.D., 1970, "Absorption and Elimination of Carbon Monoxide by Inactive Young Men," *Arch. Environ. Health*, **21**, August.
- Pitts, W.M., 1992, "Reactivity of Product Gases Generated in Idealized Enclosure Fire Environments," *Twenty-Fourth Symposium (International) on Combustion*, The Combustion Institute, Pittsburgh, PA, pp. 1737-1746.
- Pitts, W.M., Johnsson, E.L. and Bryner, N.P., 1994, "Carbon Monoxide Formation in Fires by High-Temperature Anaerobic Wood Pyrolysis," *Twenty-Fifth Symposium (International) on Combustion*, The Combustion Institute, pp. 1455-1462.
- Pitts, W.M., 1994a, "The Global Equivalence Ratio Concept and the Prediction of Carbon Monoxide Formation in Enclosure Fires," NIST Monograph 179.
- Pitts, W.M., 1994b, "An Engineering Algorithm for the Estimation of Carbon Monoxide Generation in Enclosure Fires," *1994 Fire Research Conference*, Gaithersburg, MD.
- Pitts, W.M., 1994c, "Application of Thermodynamic and Detailed Chemical Kinetic Modeling to Understanding Combustion Product Generation in Enclosure Fires," *Fire Safety Journal*, **23**, pp. 271-303.
- Poreh, M., Tsuei, Y.G., and Cermak, J.E., 1967, *Journal of Applied Mechanics*, Paper No. 67-APM-10.
- Sivanthanu, Y.R. and Faeth, G.M., 1990, "Soot Volume Fraction in the Overfire Region of Turbulent Diffusion Flames," *Combustion and Flame*, **81**, pp. 133-149.
- Steckler, K.D., Baum, H.R., and Quintiere, J.G., 1986, "Salt Water Modeling of Fire Induced Flows in Multicompartment Enclosures," *Twenty-First Symposium (International) on Combustion*, The Combustion Institute, pp. 143-149.

- Tewarson, A., 1984, "Fully Developed Enclosure Fires of Wood Cribs," *Twentieth Symposium (International) on Combustion*, The Combustion Institute, Pittsburgh, PA, pp. 1555-1566.
- Tewarson, A., 1988, "Generation of Heat and Chemical Compounds in Fires," contained in The SFPE Handbook of Fire Protection Engineering, (P.J. DiNenno, Ed.), National Fire Protection Association, Quincy, Mass, pp. 1-194-1-198.
- Toner S.J., Zukoski, E.E. and Kubota, T., 1987, "Entrainment, Chemistry and Structure of Fire Plumes," National Institute of Standards and Technology, Center for Fire Research, Report NBS-GCR-87-528, 259 p.
- Turner, J.S., 1973, Buoyancy Effects in Fluids, Cambridge University Press, Great Britain.
- Van Wylan, G.J. and Sonntag, R.E., 1986, Fundamentals of Classical Thermodynamics, 3rd Edition, John Wiley & Sons, Inc., New York.
- Westbrook, C.K. and Dryer, F.L., 1984, "Chemical Kinetic Modeling of Hydrocarbon Combustion," *Progress in Energy and Combustion Science*, **10**, pp. 1-57.
- Woods, G., 1982, Flexible Polyurethane Foams Chemistry and Technology, Applied Science Publishers, London.
- Yetter, R.A., Dryer, F.L. and Rabitz, H., 1991, "A Comprehensive Reaction Mechanism for Carbon Monoxide / Hydrogen / Oxygen Kinetics," *Combustion Science and Technology*, **79**, pp. 97-128.
- Zukoski, E.E., Kubota, T., Lim, C., 1985, "Experimental Study of Environment and Heat Transfer in a Room Fire. Mixing in Doorway Flows and Entrainment in Fire Plumes," NBS Report, GCR-85-493, May, 119 p.
- Zukoski, E.E., Morehart, J.H., Kubota, T., and Toner, S.J., 1991, *Combustion and Flame*, **83**, pp. 324-332.

APPENDIX A.

EFFECT OF ORIFICE DIAMETER ON AIR INLET DUCT VELOCITY PROFILES

Different size orifices were attached to the end of the air inlet duct to vary the air entrainment rate into the compartment. The velocity profiles in the duct were measured using a hot film probe for the four different orifice diameters used in the study: no orifice (0.30 m), 0.25 m, 0.20 m and 0.15 m. The velocity profiles were used to determine the radial location of the probe to measure the average velocity in the duct.

The velocity profile was measured by moving the hot film probe along the height of the air inlet duct in 0.025 m increments. Data was recorded for 150 seconds. Each data point is the result of averaging over a 90 second time window.

Shown in Fig. A.1 are the velocity profiles generated with each air inlet condition listed above. As can be seen in Fig. A.1, the shape of the velocity profiles are very similar for all of the orifice diameters used in the study. The position of the average velocity of the profiles, therefore, does not change significantly, and was set at 0.044 m (1.75 inches) below the top of the duct.

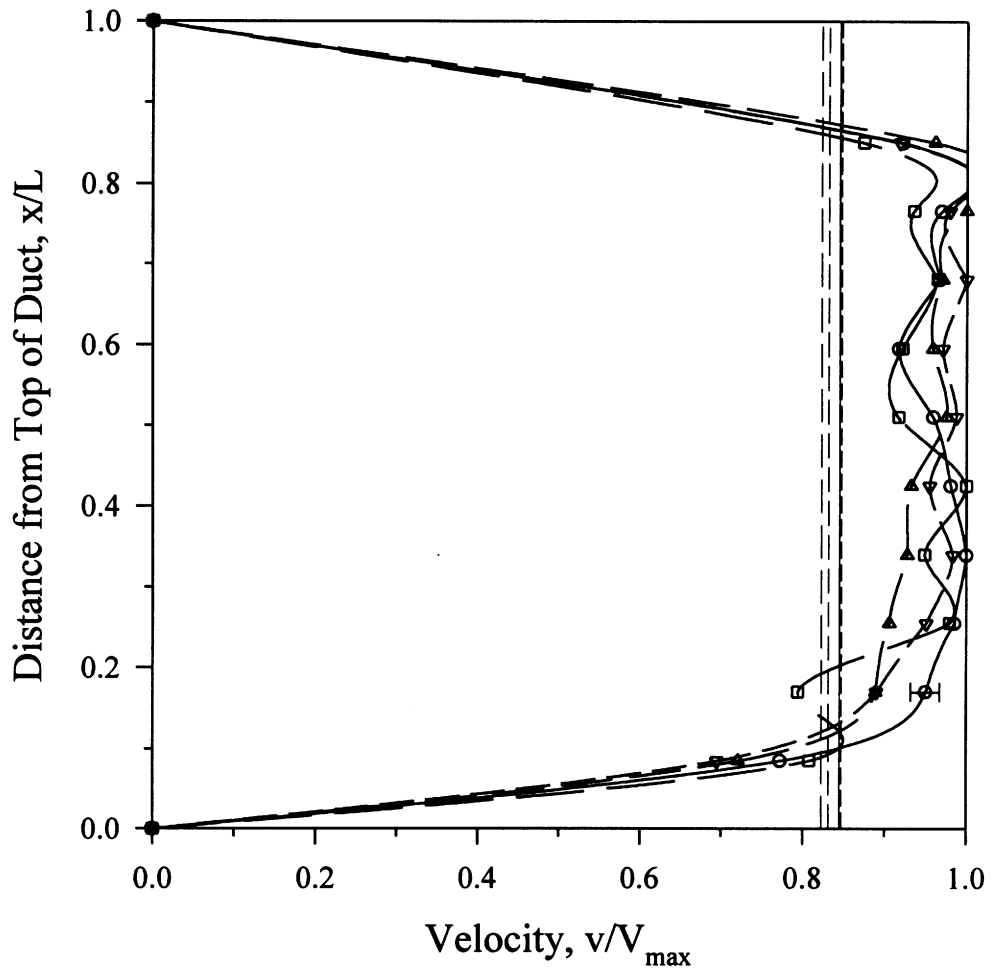


Figure A.1 The velocity profiles in the air inlet duct for with ●-no orifice (0.30 m), ■-0.25 m, ▲-0.20 m and ▼-0.15 m diameter orifices attached to the duct. The vertical lines represent average velocities of the profiles.

APPENDIX B.**DATA REDUCTION PROGRAMS*****FIRERED3.FOR***

```

C MODIFIED BY: BRIAN LATTIMER   LAST UPDATE: 8/25/94
C PREVIOUS VERSION: FIRERED2.FOR  LAST VERSION BY: DAVID EWENS, 11/6/93
C PREVIOUS VERSION: FIREDATA.FOR  LAST VERSION BY: DAN GOTTUK, 7/31/92
C
C PURPOSE:
C THIS PROGRAM REDUCES THE EXPERIMENTAL DATA FROM THE RAW DATA FILE
C CREATED BY PROGRAM FIRES5.BAS.
C THIS PROGRAM COMPENSATES FOR ANALYZER AND FLOW LAG TIME (FID,CO,CO2,O2).
C DATA FILE CAN (SHOULD) INCLUDE DATA PAST END OF FIRE, AT LEAST 15 SECS.
C THE REDUCED DATA MAY BE AVERAGED USING FIREAVG3.FOR
C
C VARIABLES:
C
C AIRRAT   - INLET DUCT AIR MASS FLOW RATE [Kg AIR/S]
C AIRVEL(I) - INLET DUCT AIR VELOCITY [M/S]
C AREA     - AREA OF AIR INLET DUCT [M^2]
C CCT      - CARBON COUNT, # C ATOMS IN FUEL MOLECULE [#]
C CERROR   - RELATIVE CARBON ERROR [%] (Cout-Cin)/Cin
C CMOLIN   - # OF CARBON MOLES IN FROM FUEL [KMOLES]
C CMOLOT   - # OF CARBON MOLES OUT FROM CO, CO2 AND THC [KMOLES]
C COAMB    - AVG AMBIENT ATMOSPHERE CO MOLE FRACTION [KMOL CO/KMOL AIR]
C COCST    - TO ADJUST CO [MOLE FRACTION/CONC.(ppm OR %)]
C CORNG    - RANGE OF CO ANALYZER [ppm OR %]
C COYLD    - CO YIELD [KG CO PRODUCED/KG FUEL BURNED]
C CO2AMB   - AVG AMBIENT ATMOSPHERE CO2 MOLE FRACTION [KMOL CO2/KMOL AIR]
C CO2CST   - TO ADJUST CO2 [MOLE FRACTION/CONC.(ppm OR %)]
C CO2RNG   - RANGE OF CO2 ANALYZER [ppm OR %]
C CO2YLD   - CO2 YIELD [KG CO2 PRODUCED/KG FUEL BURNED]
C DATE     - DATE OF EXPERIMENT [TEXT]
C DELHC    - HEAT OF COMBUSTION OF FUEL [KJ/Kg]
C DTIME    - INTERMEDIATE VALUE TO CALCULATE FUEL RATE [S]
C DTIME2   - INTERMEDIATE VALUE TO CALCULATE FUEL RATE [S]
C D2FUEL   - 2nd DERIVATIVE OF FUEL W.R.T. TIME [KG/S^2]
C DENOM    - DENOMINATOR OF DRY TO WET CONC CONVERSION [UNITLESS]
C DENSTY   - INLET DUCT AIR DENSITY [KG/M^3]
C DRYCO(I) - DRY CO CONCENTRATION [ppm OR %]
C DRYCO2(I) - DRY CO2 CONCENTRATION [%]
C DRYO2(I) - DRY O2 CONCENTRATION [%]
C DCTFLW   - EXHAUST DUCT VOLUME FLOW RATE [M^3/S]

```

Appendix B. Data Reduction Programs

C EQUIV - PLUME EQUIVALENCE RATIO [UNITLESS]
 C EXMOLS - TOTAL NUMBER OF MOLES IN COMPARTMENT [KMOL EXHAUST/S]
 C ASSUMES EXHAUST HAS AVG MOLE WT OF AIR !!!
 C EXCOEF - EXTINCTION COEFFICIENT FROM BEER'S LAW [1/m]
 C EXTDAT - REDUCED DATA FILE EXTENSION [TEXT] (ie. '.DTA')
 C EXTRAW - RAW DATA FILE EXTENSION [TEXT] (ie. '.RAW')
 C F0WT - BEGINNING WEIGHT OF FUEL [Kg]
 C FID(I) - SIGNAL FROM FID [mV*FIDRANGE]
 C FIDCAL - FID SPAN GAS READING [mV * FIDRANGE]
 C FIDCST - TO ADJUST THC [MOLE FRACTION/ppm C2H4]
 C FIDRNG - FID RANGE [MULT FACTOR]
 C FIDSPN - FID SPAN GAS CONCENTRATION [ppm C2H4]
 C FIDZER - FID ZERO (ATMOSPHEREIC SAMPLE) READING [mV * FIDRANGE]
 C FNAME - DATA FILE NAME [7 CHAR'S, ie. HALL001]
 C FNAMEX - TOTAL NAME FOR OPENING ALL FILES [TEXT] (ie. 'HALL001 .RAW')
 C FTOA - MEASURED MASS FUEL TO MASS AIR RATIO [KG FUEL/KG AIR]
 C FUEL(I) - FUEL MASS [KG]
 C FUELRT - FUEL MASS BURN RATE [KG FUEL/S]
 C GF - FUEL VOLATILIZATION RATE [g FUEL/S]
 C HTOC - H TO C RATIO OF FUEL [# H/# C, UNITLESS]
 C I - TOTAL NUMBER OF RECORDEDD DATA POINTS [#]
 C ICORG - CO RANGE (1, 2, OR 3) [#]
 C ICO2RG - CO2 RANGE (1, 2, OR 3) [#]
 C IFIDRG - FID RANGE [POWER OF 100]
 C IFUELTYPE - FUEL TYPE [#]
 C = 1 HEXANE
 C = 2 PMMA
 C = 3 WOOD
 C = 4 POLYURETHANE
 C IPROBE - PROBE LOCATION [#]
 C = 1 IF COMPARTMENT SAMPLED
 C = 2 IF EXHAUST DUCT SAMPLED
 C = 3 IF HALLWAY SAMPLED
 C IRUNNO - RUN NUMBER [#]
 C ISTEP - DATA POINT USED STEP SIZE [#] (1 = USE ALL)
 C IQUIT - DUMMY ABORT REDUCTION FLAG VARIABLE [NONE]
 C J,JJ - DUMMY COUNTER INTEGER [#]
 C K - DATA POINT COUNTER [#]
 C K1 - SPECIES ANALYZER LAG COMPENSATED TIME DATA POINT COUNTER [#]
 C K2 - FID LAG COMPENSATED TIME DATA POINT COUNTER [#]
 C LASPTH - EXHAUST DUCT SMOKE LASER PATH LENGTH [m]
 C MASODL - MASS OPTICAL DENSITY OF SMOKE PER UNIT PATH LENGTH [m²/g]
 C MOLWT - MOLECULAR WEIGHT OF FUEL [KG FUEL/KMOLE FUEL]
 C N - DUMMY INTEGER COUNTER [#]
 C NOTE1 - ANY NOTE ON EXPERIMENT RUN [TEXT] (60 CHAR'S MAX)
 C NOTE2 - ANY NOTE ON EXPERIMENT RUN [TEXT] (60 CHAR'S MAX)
 C NOTE3 - ANY NOTE ON EXPERIMENT RUN [TEXT] (60 CHAR'S MAX)
 C NOTE4 - ANY NOTE ON EXPERIMENT RUN [TEXT] (60 CHAR'S MAX)
 C ODL - OPTICAL DENSITY OF SMOKE PER UNIT PATH LENGTH (1/m)

Appendix B. Data Reduction Programs

C O2AMB - AVG AMBIENT ATMOSPHERE O2 MASS FRACTION [Kg O2/Kg AIR]
 C O2CST - TO ADJUST O2 [MOLE FRACTION/CONC.(ppm OR %)]
 C O2RNG - MAXIMUM MEASURABLE O2 CONCENTRATION [%]
 C O2YLD - O2 YIELD [KG O2 USED/KG FUEL BURNED]
 C PA - AMBIENT PRESSURE [mm Hg] (TYP. 710 mmHg)
 C PBELOC - DESCRIPTION OF PROBE LOCATION IN HALLWAY [TEXT]
 C PRESS - EXHAUST DUCT ORIFACE PRESSURE DROP [mmHg=Torr] (TYP. 15.8)
 C PROBE - PROBE LOCATED DESCRIPTION [TEXT]
 C PNSIZE - FUEL PAN SIZE [inches]
 C PNWT - WEIGHT OF FUEL PAN [Kg]
 C PTSPST - # OF DATA POINTS PAST END OF FIRE [#]
 C PTSTRT - LAG TIME AS # OF DATA POINTS [#] (FUNC. OF PROBE LOCATION)
 C Q - HEAT RELEASE RATE [KW]
 C RESTIM - RESIDENCE TIME OF GASSES IN COMPARTMENT [S]
 C RUNTIM - TOTAL RUN TIME [S]
 C SEC - SPECIFIC EXTINCTION COEFFICIENT FOR SMOKE [m²/g]
 C SMK10 - SMOKE0 CALCULATED FROM 1ST 5 SMOKE1 DATA POINTS
 C [RELATIVE LIGHT INTENSITY]
 C SMKMAX - MAX SMOKE VOLUME (MOLE) FRACTION DURING FIRE [ppb]
 C SMKYLD - SMOKE YIELD [KG SMOKE PRODUCED/KG FUEL BURNED]
 C SMOKE0(I) - MEASURED I0 FOR BEER'S LAW (NOT WORKING/NOT USED)
 C [RELATIVE LIGHT INTENSITY]
 C SMOKE1(I) - I FOR BEER'S LAW [RELATIVE LIGHT INTENSITY]
 C SMKVF - SMOKE VOLUME FRACTION IN DUCT [ppm]
 C SOFF1 - HEIGHT OF SOFFIT FROM COMPARTMENT TO HALLWAY [inches]
 C ALSO CEILING HEIGHT ABOVE TOP OF COMPARTMENT VENT
 C SOFF2 - HEIGHT OF SOFFIT AT EXIT OF HALLWAY [inches]
 C SSTIME - RATIO OF RESIDENCE TIME TO D2FUEL [UNITLESS]
 C STOIC - STOICHIOMETRIC AIR TO FUEL RATIO BY MASS [KG AIR/KG FUEL]
 C TAMBA - AMBIENT ATMOSPHERIC TEMPERATURE INPUT BY USER [K]
 C TAMBC - AMBIENT COMPARTMENT TEMPERATURE INPUT BY USER [K]
 C AVERAGE THE TOP 3 COMPARTMENT TC RAKE THERMOCOUPLES
 C TCC(1) - COMPARTMENT THERMOCOUPLE TREE TEMPERATURES [K] (1 = TOP)
 C - TCC(8)
 C TCC3 - 3RD TC OF COMPARTMENT TC TREE TEMPERATURE [K]
 C TCH(1) - HALLWAY THERMOCOUPLE TREE TEMPERATURES [K] (1 = TOP)
 C - TCH(9)
 C TCEV - EXHAUST VENT THERMOCOUPLE [K]
 C TCED - EXHAUST DUCT THERMOCOUPLE [K]
 C TCID - AIR INLET DUCT THERMOCOUPLE [K]
 C TDMOLS - TOTAL NUMBER OF MOLES IN EXHAUST DUCT [KMOL EXHAUST/S]
 C TFUEL - FUEL TYPE NAME [TEXT]
 C THC - UNBURNED HYDROCARBONS [KMOLES UHC/KMOLES TOTAL]
 C TIME - TIME FROM START OF FIRE [S]
 C TMEPST - TIME PAST END OF FIRE THAT DATA WAS COLLECTED [S]
 C VENT - VENT SIZE [TEXT: inches]
 C VOLC - AVG VOLUME OF UPPER LAYER [M³]
 C WETCO - WET CO CONCENTRATION [ppm OR %]
 C WETCO2 - WET CO2 CONCENTRATION [%]

```

C WETO2      - WET O2 CONCENTRATION [%]
C
C
C FILES ACCESSED:
C ( HALL####.* , WHERE #### IS THE RUN NUMBER, ie. HALL0001 )
C
C READ:
C
C HALL####.RAW - RAW EXPERIMENTAL SERIAL DATA FILE CREATED BY FIRE3.BAS
C
C WRITTEN:
C
C HALL####.DTI - EXPERIMENTAL INFORMATION DATA FILE (CONTAINS: FILE NAME
C      TEST DATE, AMBIENT CONDITIONS, ANALYZER SETTINGS, ETC)
C HALL####.DTA - EXPERIMENTAL CHRONOLOGICAL DATA FILE (CONTAINS: TIME,
C      WET CONC'S, YIELDS)
C HALL####.DTB - EXPERIMENTAL CHRONOLOGICAL DATA FILE (CONTAINS: TIME,
C      FUEL & INLET AIR DATA, CARBON ERROR, EQUIVALENCE RATIO)
C HALL####.DTC - EXPERIMENTAL CHRONOLOGICAL DATA FILE (CONTAINS: TIME,
C      TIME SCALES, DRY CONC'S, THC, HEAT RELEASE, DILUTION)
C HALL####.DTD - EXPERIMENTAL CHRONOLOGICAL DATA FILE (CONTAINS: TIME,
C      SMOKE DATA, WET H2O & H2 CONC'S)
C HALL####.DTE - EXPERIMENTAL CHRONOLOGICAL DATA FILE (CONTAINS: TIME,
C      HALLWAY THERMOCOUPLE DATA)
C HALL####.DTF - EXPERIMENTAL CHRONOLOGICAL DATA FILE (CONTAINS: TIME,
C      COMPARTMENT THERMOCOUPLE DATA, INLET AIR & EXHAUST
C      THERMOCOUPLE DATA)
C
C
C
C2345-7-901234567890123456789012345678901234567890123456789 72
C * INITIALIZATION
  IMPLICIT DOUBLE PRECISION (A-H,O-Z)
  DIMENSION TIME(1300),DRYCO(1300),DRYCO2(1300),DRYO2(1300)
  DIMENSION FUEL(1300),AIRVEL(1300),TCC(8),TCH(9),TCC3(1300)
  DIMENSION FUELRT(1300),AIRRAT(1300),RESTIM(1300),Q(1300),Q2(1300)
  DIMENSION D2FUEL(1300),SMOKE1(1300),FULRT2(1300),FUEL2(1300)
  DIMENSION FID(1300),FTOA(1300),TCEV(1300),TCED(1300),TCID(1300)
  DIMENSION TOTRT(1300)
  INTEGER PTSTRT,PTSPST,PNSIZE,SOFF1,SOFF2
  DOUBLE PRECISION MASODL,MOLWT
  REAL LASPTH
  CHARACTER*4 EXTDAT,EXTRA W
  CHARACTER*8 FNAME
  CHARACTER*9 DATE
  CHARACTER*12 FNAMEX
  CHARACTER*20 TFUEL
  CHARACTER*30 VENT,PROBE
  CHARACTER*60 PBELOC

```

C-----7-----72

```

C * INITIALIZE VARIABLES
  IQUIT = 1
  FIDRNG = 1.0E-11
  ISTEP = 1
  IWOOD = 0
  IAFUEL = 0
  SMKVF = 0.0
  EXCOEF = 0.0
  SMK10 = 0.0
  DO 10 N=1,1300
    TCC3(N) = 0.0
    SMOKE1(N) = 0.0
    FID(N) = 0.0
    FUELRT(N) = 0.0
    FULRT2(N) = 0.0
    RESTIM(N) = 0.0
    Q2(N) = 0.0
10 CONTINUE
  WETH2O = 0.000
  WETH2 = 0.000
C * INITIALIZE CONSTANTS
  AREA = 0.0699573
  FIDSPN= 615.0
  PA=713.0
  PRESS=14.3
  VOLC=1.137
  COAMB=0.000000
  CO2AMB=0.000400
  O2AMB=0.232
C-----7-----72
C * INPUT RUN PARAMETERS
  WRITE(*,*)'ENTER FILE NAME W/O EXT, 8 CHARACTORS (i.e. HALL0001)'
  READ(*,21)FNAME
21 FORMAT(A8)
  WRITE(*,*) ' ENTER RUN #'
  READ(*,*) IRUNNO
  WRITE(*,*) ' ENTER DATE (ie. "12-23-93")'
  READ(*,21) DATE
  WRITE(*,*) 'HEXANE (1), PMMA (2), WOOD (3) OR POLYURETHANE (4) FIR
  $E?'
  READ(*,*)IFUELT
40 GOTO(41,42,43,44)IFUELT
41 TFUEL='HEXANE'
  ISTEP=1
  DELHC=44735.0
  HTOC=2.333
  STOIC=15.2010
  MOLWT=86.18
  CCT=6.0

```

```

GOTO 45
42 TFUEL='PMMA'
WRITE(*,*)' DO YOU WISH TO KEEP EVERY 1st, 2nd OR 3rd POINT?'
WRITE(*,*)' ENTER 1, 2, OR 3 RESPECTIVELY'
READ(*,*)ISTEP
DELHC=25200.0
HTOC=1.6
STOIC=8.2824
MOLWT=100.0
CCT=5.0
GOTO 45
43 TFUEL='WOOD'
ISTEP=1
DELHC=17900.0
HTOC=3.584
C STOICOMETRIC RATIO ASSUMES 15% CHAR
STOIC=3.823
MOLWT=40.428
CCT=1.0
GOTO 45
44 TFUEL='POLYURETHANE'
ISTEP=1
DELHC=26570.0
HTOC =1.74
C STOICOMETRIC RATIO ASSUMES NO CHAR
STOIC=8.83
MOLWT=19.91
CCT=1.0
C * END OF FUEL SELECTION
45 WRITE(*,*)TFUEL
WRITE(*,*)' ENTER PAN SIZE (6, 8, 9, 11) [inches]'
READ(*,22) PNSIZE
22 FORMAT(I2)
23 FORMAT(A13)
WRITE(*,*)' ENTER FUEL PAN WEIGHT [Kg]'
READ(*,*) PNWT
WRITE(*,*)' ENTER BEGINNING WEIGHT OF FUEL ONLY [Kg]'
READ(*,*) F0WT
C** ADDITIONAL FUELS
C*** WOODEN CEILING INSIDE COMPARTMENT
WRITE(*,*)' WAS A WOODEN CEILING PRESENT INSIDE THE COMPARTMENT?'
WRITE(*,*)' YES(ENTER 1) AND NO(ENTER 2)'
READ(*,*) IANS1
IF (IANS1 .EQ. 1) THEN
WRITE(*,*)' ENTER THE INITIAL WEIGHT OF THE WOODEN CEILING',
+ ' [kg]'
READ(*,*) F02WT
IWOOD = 1
HCWOOD = 26656.9

```

```

ENDIF
C*** AUTOMATED FUEL SUPPLY ACTIVATED
WRITE(*,*) ' WAS THE AUTOMATED FUEL SUPPLY USED?'
WRITE(*,*) ' YES(ENTER 1) AND NO(ENTER 2)'
READ(*,*) IANS2
IF (IANS2 .EQ. 1) THEN
  WRITE(*,*) ' ENTER THE INITIAL WEIGHT OF THE RESERVOIR FUEL',
+ ' [kg]'
  READ(*,*) F02WT
  IAFUEL = 1
ENDIF

WRITE(*,*) ' ENTER EXHAUST VENT SIZE (ie. 20 X 6.25) [inches]'
READ(*,23) VENT
WRITE(*,*) ' ENTER COMPARTMENT/HALLWAY SOFFIT HEIGHT or'
WRITE(*,*) ' HALL CEILING HEIGHT FROM TOP OF COMPARTMENT EXH VENT'
WRITE(*,*) ' (0, 4, 8) [inches]'
READ(*,22) SOFF1
WRITE(*,*) ' ENTER HALLWAY EXIT SOFFIT HEIGHT (0, 4, 8) [inches]'
READ(*,22) SOFF2

WRITE(*,*) ' ENTER CO RANGE 1 (1000 ppm), 2 (1%) or 3 (10%)'
READ(*,*) ICORG
WRITE(*,*) ' ENTER CO2 RANGE 1 (5000 ppm), 2 (2%), 3 (15%) or',
+ ' 4 (20%)'
READ(*,*) ICO2RG
30 WRITE(*,*) ' (1) COMPARTMENT, (2) EXHAUST DUCT, OR (3) HALLWAY'
WRITE(*,*) ' ENTER 1, 2 or 3'
READ(*,*) IPROBE
GOTO(31,32,33)IPROBE
GOTO 30
C COMPARTMENT SAMPLED
31 PROBE='COMPARTMENT'
PTSTRT=4
GOTO 34
C EXHAUST DUCT SAMPLED
32 PROBE='EXHAUST'
C EXHAUST DUCT
PTSTRT=14
GOTO 34
C HALLWAY SAMPLED
33 PROBE='HALLWAY'
PTSTRT=4
34 WRITE(*,*)PROBE
WRITE(*,*) ' ENTER PROBE LOCATION (60 CHARACTORS)'
WRITE(*,*) ' ( ie. EXH DUCT: L=132, H=2, W=0 IN., -OR-'
WRITE(*,*) ' HALL: L=72, H=2(6), W=-1(1) IN. RAKE (SAMPLE) )'
READ(*,24) PBELOC
24 FORMAT(A60)

```

```

WRITE(*,*) ' ENTER AMBIENT ATMOSPHERIC TEMPERATURE [°C]'
READ(*,*)TAMBA
TAMBA = TAMBA + 273.15
WRITE(*,*) ' ENTER AMBIENT COMPARTMENT TEMPERATURE [°C]'
WRITE(*,*) ' AVERAGE THE TOP 3 COMPARTMENT TC RAKE THERMOCOUPLES'
READ(*,*)TAMBC
TAMBC = TAMBC + 273.15
WRITE(*,*) ' ENTER AMBIENT PRESSURE [mm Hg]'
WRITE(*,*) ' DEFAULT IS 713.0 mm Hg'
READ(*,*)PA
WRITE(*,*) ' ENTER THE FID SPAN GAS CONCENTRATION [ppm C2H4]'
READ(*,*)FIDSPN
FIDCST=1000000.0
WRITE(*,*) ' ENTER THE FID OPERATING RANGE (for 1E-10, enter 10)'
READ(*,*)IFIDRG
FIDRNG=10.0**(-IFIDRG)
WRITE(*,*) ' ENTER THE FID ZERO GAS READING AS [mV]'
READ(*,*)FIDZER
FIDZER=FIDZER*FIDRNG
WRITE(*,*) ' ENTER THE FID SPAN GAS READING AS [mV]'
READ(*,*)FIDCAL
FIDCAL=FIDCAL*FIDRNG
WRITE(*,*) ' USES A RUN TIME PAST END OF FIRE = 30 sec'
TMEPST=30.0D0
WRITE(*,*) ' CONTINUE WITH REDUCTION ? ENTER "0" TO QUIT'
READ(*,*) IQUIT
IF (IQUIT.EQ.0)GOTO 9999
WRITE(*,*) ' OK, HERE WE GO...'

C-----7-----72
C * CALCULATIONS BEGIN
C * ASSIGN THE APPROPRIATE MAXIMUM VALUE FOR CHOSEN ANALYZER RANGE
C ** O2 ANALYZER
  O2RNG=22.0
  O2CST=100.0
C ** CO ANALYZER
  GOTO(50,51,52)ICORG
50 CORNG=1000.0
  COCST=1.000E+6
  GOTO 53
51 CORNG=1.
  COCST=100.
  GOTO 53
52 CORNG=10.
  COCST=100.
C ** CO2 ANALYZER
53 GOTO(54,55,56,57)ICO2RG
54 CO2RNG = 5000.0
  CO2CST = 1.000E+6
  GOTO 58

```

```

55 CO2RNG=2.
   CO2CST=100.
   GOTO 58
56 CO2RNG=15.
   CO2CST=100.
   GOTO 58
57 CO2RNG=20.
   CO2CST=100.
C-----7-----72
C * READ DATA AND CREATE AN ARRAY FOR EACH CHANNEL
C * WRITE TEMPERATURE DATA FILES E AND F
C # NOTE: I IS THE NUMBER OF DATA POINTS PER CHANNEL
C OPEN *.RAW DATA FILE
58 EXTRAW='.RAW'
   FNAMEX=FNAME
   FNAMEX(9:12)=EXTRA(1:4)
   OPEN(15,FILE=FNAMEX)
   WRITE(*,*) '
   WRITE(*,*) 'READING DATA FILE ',FNAMEX
C OPEN NEW *.DTE AND *.DTF DATA FILES
   EXTDAT='.DTE'
   FNAMEX(9:12)=EXTDAT(1:4)
   DO 59 JJ=1,2
     FNAMEX(12:12) = CHAR(68+JJ)
     OPEN(UNIT=24+JJ, FILE=FNAMEX, STATUS='NEW')
     WRITE(*,*) ' AND WRITING DATA FILE ',FNAMEX
59 CONTINUE
   I=1
C BEGINNING OF READING DO LOOP (CURRENTLY 29 DATA BITS / TIME STEP)
60 READ(15,*,END=65) TIME(I)
   RUNTIM=TIME(I)
   READ(15,*) DRYCO(I)
   READ(15,*) DRYCO2(I)
   READ(15,*) DRYO2(I)
   READ(15,*) FUEL(I)
   READ(15,*) AIRVEL(I)
   READ(15,*) FID(I)
   READ(15,*) FUEL2(I)
   READ(15,*) SMOKE1(I)
   READ(15,*) TCH(1)
   READ(15,*) TCH(2)
   READ(15,*) TCH(3)
   READ(15,*) TCH(4)
   READ(15,*) TCH(5)
   READ(15,*) TCH(6)
   READ(15,*) TCH(7)
   READ(15,*) TCH(8)
   READ(15,*) TCH(9)
   READ(15,*) TCC(1)

```

```

READ(15,*) TCC(2)
READ(15,*) TCC(3)
READ(15,*) TCC(4)
READ(15,*) TCC(5)
READ(15,*) TCC(6)
READ(15,*) TCC(7)
READ(15,*) TCC(8)
READ(15,*) TCEV(I)
READ(15,*) TCED(I)
READ(15,*) TCID(I)
C TEMPERATURE REDUCTION - CONVERT TEMPERATURES TO KELVIN
DO 63 JJ=1,8
  TCH(JJ)=TCH(JJ)+273.15
  TCC(JJ)=TCC(JJ)+273.15
63 CONTINUE
  TCH(9)=TCH(9)+273.15
  TCEV(I)=TCEV(I)+273.15
  TCED(I)=TCED(I)+273.15
  TCID(I)=TCID(I)+273.15
  TCC3(I)=TCC(3)
C WRITE TEMPERATURE DATA TO FILES
  WRITE(25,2005)TIME(I),TCH(1),TCH(2),TCH(3),TCH(4),TCH(5),TCH(6),
  $TCH(7),TCH(8),TCH(9)
  WRITE(26,2006)TIME(I),TCC(1),TCC(2),TCC(3),TCC(4),TCC(5),TCC(6),
  $TCC(7),TCC(8),TCEV(I),TCED(I),TCID(I)
2005 FORMAT(F7.1,9F6.0)
2006 FORMAT(F7.1,11F6.0)
  I=I+1
  GOTO 60
65 I=I-1
  CLOSE (15)
  CLOSE (25)
  CLOSE (26)
  WRITE(*,3001)FNAME,'.RAW READ! '
3001 FORMAT(1X,A8,A14)
  WRITE(*,*) '
  WRITE(*,3001)FNAME,'.DTE WRITTEN!'
  WRITE(*,3001)FNAME,'.DTF WRITTEN!'
  WRITE(*,*) '
  WRITE(*,*)' TEMPERATURE DATA REDUCED!'
C-----7-----72
C * CREATE EXPERIMENT INFORMATION FILE
  EXTDAT='.DTI'
  FNAMEX(9:12)=EXTDAT(1:4)
  OPEN(UNIT=20, FILE=FNAMEX, STATUS='NEW')
C * WRITE TO INFO FILE
  WRITE(20,1001)FNAME
  WRITE(20,1002)DATE,IRUNNO,ICORG,ICO2RG,IProbe,TMEPST
  WRITE(20,1003)PROBE

```

```

WRITE(20,1004)PA,TAMBA,TAMBC
WRITE(20,1005)TFUEL
WRITE(20,1006)IFUEL,ISTEP,DELHC,HTOC,STOIC,MOLWT,CCT
WRITE(20,1007)FIDSPN,FIDRNG,FIDZER,FIDCAL
WRITE(20,1008)RUNTIM,F0WT,PNSIZE,VENT,SOFF1,SOFF2
WRITE(20,1009)PBELOC
IF (IWOOD .EQ. 1) THEN
  WRITE(20,1010) F02WT
ENDIF
IF (IAFUEL .EQ. 1) THEN
  WRITE(20,1011) F02WT
ENDIF
1001 FORMAT(1X,A8)
1002 FORMAT(1X,A8,I5,3I2,F9.3)
1003 FORMAT(1X,A30)
1004 FORMAT(1X,3F9.3)
1005 FORMAT(1X,A20)
1006 FORMAT(1X,2I3,F10.1,F8.3,F10.4,F10.3,F6.1)
1007 FORMAT(1X,F12.1,E11.1,2E15.4)
1008 FORMAT(1X,F7.1,F8.3,I3,A14,2I3)
1009 FORMAT(1X,A60)
1010 FORMAT(1X,'A 1/4 INCH THICK, DOUGLAS FIR WOODEN CEILING WAS',/,
  + 'PRESENT IN THE COMPARTMENT WITH AN INITIAL WEIGHT OF',F6.3,
  + ' kg.')
1011 FORMAT(1X,'THE AUTOMATED FUEL SUPPLY WAS USED WITH AN INITIAL',
  +/, 'FUEL WEIGHT IN THE RESERVOIR OF',F6.3,' kg.')
CLOSE(20)
WRITE(*,3001)FNAME,'.DTI WRITTEN!'
C-----7-----72
C * DATA MANIPULATION FOR EACH CHANNEL LOOP J=1 to I
WRITE(*,*) '
WRITE(*,*) PLEASE WAIT -- I AM DIGESTING THE DATA'
PTSPST=NINT(TMEPST/1.97)
C BEGINING OF ANALYZER DATA CONVERSION DO LOOP
DO 77 J=1,I-PTSPST
  K1=J+PTSTRT-1
C ** CONVERT INSTRUMENT MEASUREMENTS FROM VOLTS TO CONCENTRATIONS
C *** CO ANALYZER [mole fraction]
IF(DRYCO(K1).LT.0.0)THEN
  DRYCO(K1)=0.0
ENDIF
DRYCO(J)=(DRYCO(K1)/5.0)*CORNG/CO2CST
C *** CO2 ANALYZER [mole fraction]
IF(DRYCO2(K1).LT.0.0)THEN
  DRYCO2(K1)=0.0
ENDIF
DRYCO2(J)=(DRYCO2(K1)/5.0)*CO2RNG/CO2CST
C *** O2 ANALZER [mole fraction]
IF(DRYO2(K1).LT.0.0)THEN

```

```

    DRYO2(K1)=0.0
  ENDIF
  DRYO2(J)=(DRYO2(K1)/5.08)*O2RNG/O2CST
C *** THC [mole fraction]
  K2 = J + PTSTRT
74 FID(J)=FID(K2)
  IF (FID(J).LT.0.0)THEN
    FID(J)=0.000
  ENDIF
  FID(J)=FID(J)*1000.0*FIDRNG
77 CONTINUE
  WRITE(*,*) ANALYZER DATA CONVERTED AND COMPENSATED FOR LAG!
  DO 80 J=1,I
C *** FUEL WEIGHT [kg]
  FUEL(J)=(FUEL(J)-1.0)*10.0/4.0
  IF (IWOOD .EQ. 1) THEN
    FUEL2(J)=(FUEL2(J)-1.0)*10.0/4.0
  ENDIF
C *** INLET AIR VELOCITY [m/s]
C SHOWN TO BE IDEAL LINEAR TO WITHIN 5% (IE. V=VEL*AREA)
C EQUATION FROM AIRVEL = (VOLTS*2M/S)/5VOLTS MAX*(760/PA)*(TCID/298)
  AIRVEL(J)=(AIRVEL(J)/5.0D0)*5.098D0*TCID(J)/PA
  ENDIF
80 CONTINUE
  WRITE(*,*) FUEL AND AIR DATA CONVERTED AND COMPENSATED FOR LAG!
C *** ELIMINATE INCORRECT FUEL DATA POINTS
  DO 85 J=2,I-2
    IF(FUEL(J+1).GT.FUEL(J)) THEN
      FUEL(J+1)=FUEL(J)
    ENDIF
85 CONTINUE
  IF (IWOOD .EQ. 1) THEN
    DO 86 J=2,I-2
      IF(FUEL2(J+1).GT.FUEL2(J)) THEN
        FUEL2(J+1)=FUEL2(J)
      ENDIF
86 CONTINUE
  ENDIF
C *** CALCULATE FUEL BURN RATE USING AVERAGING SMOOTHING [kg/sec]
  DO 90 J=6,(I-5)
    FUELRT(J)=(FUEL(J-5)-FUEL(J+5))/(TIME(J+5)-TIME(J-5))
90 CONTINUE
  IF (IWOOD .EQ. 1) THEN
    DO 92 J=6,(I-5)
      FULRT2(J)=(FUEL2(J-5)-FUEL2(J+5))/(TIME(J+5)-TIME(J-5))
92 CONTINUE
  ENDIF
C *** ESTIMATE INITIAL FUEL BURN RATES [kg/sec]
  DO 95 J=1,5

```

```

    FUELRT(J)=FUELRT(8)
95 CONTINUE
    IF (IWOOD .EQ. 1) THEN
        DO 96 J=1,5
            FULRT2(J)=FULRT2(8)
96 CONTINUE
        ENDIF
C *** ESTIMATE LAST FUEL BURN RATES [kg/sec]
    DO 97 J=(I-4),(I-2)
        FUELRT(J)=(FUEL(J-2)-FUEL(J+2))/(TIME(J+2)-TIME(J-2))
97 CONTINUE
    IF (IWOOD .EQ. 1) THEN
        DO 98 J=(I-4),(I-2)
            FULRT2(J)=(FUEL2(J-2)-FUEL2(J+2))/(TIME(J+2)-TIME(J-2))
98 CONTINUE
        ENDIF
        DTIME=TIME(I)-TIME(I-2)
        FUELRT(I-1)=(FUEL(I-2)-FUEL(I))/DTIME
        IF (IWOOD .EQ. 1) THEN
            FULRT2(I-1)=(FUEL2(I-2)-FUEL2(I))/DTIME
        ENDIF
        DTIME2=TIME(I)-TIME(I-1)
        FUELRT(I)=(FUEL(I-1)-FUEL(I))/DTIME2
        IF (IWOOD .EQ. 1) THEN
            FULRT2(I)=(FUEL2(I-1)-FUEL2(I))/DTIME2
        ENDIF
        DO 100 J=(I-PTSPST+1),I
            FUELRT(J)=0.0
            IF (IWOOD .EQ. 1) THEN
                FULRT2(J)=0.0
            ENDIF
100 CONTINUE
        WRITE(*,*) 'BURN RATE CALCULATIONS COMPLETE'
C CALCULATE SMK10 FROM 1ST 5 SMOKE1'S SINCE SMOKE0 NOT WORKING
        SMK10=0.000
        DO 110 J=1,5
            SMK10 = SMK10 + SMOKE1(J)/5.
110 CONTINUE
C-----7-----72
C * CREATE OUTPUT FILES
        EXTDAT='.DTA'
        FNAMEX(9:12)=EXTDAT(1:4)
        DO 140 J=1,4
            FNAMEX(12:12) = CHAR(64+J)
            OPEN(UNIT=20+J, FILE=FNAMEX, STATUS='NEW')
140 CONTINUE
C-----7-----72
C 1 TIME INITIALIZATIONS BEFORE LOOP (150)
        SMKMAX = 0.0

```

```

DO 150 K=1,I-PTSPST,ISTEP
C-----7-----72
C * CALCULATE HEAT RELEASE RATE (kW)
  Q(K) = FUELRT(K)*DELHC
  IF (IWOOD .EQ. 1) THEN
    Q2(K) = FULRT2(K)*HCWOOD
  ENDIF
C-----7-----72
C * CALCULATE AIR FLOWRATE (kg/sec)
C   AND RESIDENCE TIME (sec)
  DENSTY=(PA/TCID(K)/0.287)*0.1333
  IF (AIRVEL(K).LE. 0.0) THEN
    WRITE(*,*) AIR VELOCITY ERROR ! (AIRVEL < 0)
    RESTIM(K)=999.
  ELSE
    RESTIM(K)=VOLC/(AIRVEL(K)*AREA*TCC3(K)/TCID(K))
  ENDIF
  AIRRAT(K)=AIRVEL(K)*DENSTY*AREA
C-----7-----72
C * CALCULATE FUEL/AIR RATIO
  IF (AIRRAT(K).LE.0.0) THEN
    FTOA(K) = 0.0
  ELSE
    IF (IWOOD .EQ. 1) THEN
      TOTRT(K)=FUELRT(K)+FULRT2(K)
    ELSE
      TOTRT(K)=FUELRT(K)
    ENDIF
    FTOA(K)=TOTRT(K)/AIRRAT(K)
  ENDIF
C-----7-----72
C *** CALCULATE WET CONCENTRATIONS, YIELDS AND STORE DATA IN FILES
C-----7-----72
C * VOLUMETRIC FLOWRATE (m^3/s) IN EXHAUST DUCT
C EXMOLES ASSUMES AVG MOLECULAR WEIGHT EXHAUSTED IS SAME AS AIR
  EXMOLS = (AIRRAT(K)+FUELRT(K))/28.97
  DCTFLW = 1.2099*DSQRT(PRESS*TCED(K)/PA)
  TDMOLS = DCTFLW*PA*0.1333/(8.3144*TCED(K))
C-----7-----72
C * FOR EXHAUST DUCT SAMPLED FIRES
  IF (IPROBE.EQ.2) THEN
    WETCO=DRYCO(K)
    WETCO2=DRYCO2(K)
    WETO2=DRYO2(K)
  ELSE
C * FOR (UNDILUTED) HALLWAY AND COMPARTMENT SAMPLED FIRES
    DENOM = 1.0+((HTOC/2.0)*DRYCO2(K))
    WETCO=DRYCO(K)/DENOM
    WETCO2=DRYCO2(K)/DENOM

```

```

      WETO2=DRYO2(K)/DENOM
    ENDIF
C-----7-----72
C SET YIELDS TO 0 IF FUELRATE = 0
C OR IF HALLWAY SAMPLED
  IF (FUELRT(K).EQ.0.0.OR.IPROBE.EQ.3) THEN
    COYLD=0.0
    CO2YLD=0.0
    O2YLD=0.0
  ELSE IF (IPROBE.EQ.2) THEN
C EXHAUST DUCT SAMPLED
    COYLD=(WETCO-COAMB)*TDMOLS*28.01/FUELRT(K)
    CO2YLD=(WETCO2-CO2AMB)*TDMOLS*44.01/FUELRT(K)
    O2YLD=0.0
  ELSE
C COMPARTMENT SAMPLED
    COYLD=(WETCO-COAMB)*EXMOLS*28.01/FUELRT(K)
    CO2YLD=(WETCO2-CO2AMB)*EXMOLS*44.01/FUELRT(K)
    O2YLD=((O2AMB*AIRRAT(K))-(WETO2*EXMOLS*32.00))/FUELRT(K)
  ENDIF
C-----7-----72
C CHECK FOR YIELD ERRORS
  IF (CO2YLD.GT.100.0) THEN
    WRITE(*,*) 'ERROR IN CO2 YIELD! > 100'
  ENDIF
  IF (COYLD.GT.100.0) THEN
    WRITE(*,*) 'ERROR IN CO YIELD! > 100'
  ENDIF
  IF (O2YLD.GT.100.0) THEN
    WRITE(*,*) 'ERROR IN O2 YIELD! > 100'
  END IF
C  WRITE(*,*) 'WET CONCENTRATIONS AND YIELDS COMPLETE'
C-----7-----72
C * CALCULATE SMOKE VOLUME FRACTION IN [ppb]
  IF (SMOKE1(K).EQ.0.)THEN
    WRITE(*,*) 'ERROR IN SMOKE VOLUME FRACTION CALCULATION !'
    WRITE(*,*) 'SMOKE1 SIGNAL = 0 !'
    EXCOEF= 999.
    SMKVF = 999.
    SMKYLD= 999.
  ELSE
    LASPTH = 0.4572
    IF (SMOKE1(K).GE.SMK10) THEN
      EXCOEF = 0.000
    ELSE
      EXCOEF = DLOG(SMK10/SMOKE1(K))/LASPTH
    ENDIF
    SMKVF = 1.3697E-07*EXCOEF*1.0E+9
    IF (SMKVF.LT.0.0)THEN

```

```

    SMKVF = 0.0
    ENDIF
C-----7-----72
C * CALCULATE SMOKE YIELD ACCORDING TO TEWARSON
  IF (FUELRT(K).LE.0.0)THEN
    WRITE(*,*)' ERROR IN SMOKE YIELD CALCULATION !'
    WRITE(*,*)'FUELRATE = 0 =',FUELRT(K),'AT TIME = ',TIME(K)
    SMKYLD = 999.
  ELSE
    GF = FUELRT(K)*1000.
    ODL = EXCOEF/2.303
    MASODL = ODL * DCTFLW / GF
    SEC = 3.213/(0.67*1.1)
    SMKYLD = MASODL / SEC
  ENDIF
ENDIF
C  WRITE(*,*)' SMOKE CALCULATIONS COMPLETE'
C-----7-----72
C * EQUIVALENCE RATIO
  EQUIV=FTOA(K)*STOIC
  IF (EQUIV.LE.0.0)THEN
    EQUIV=0.0
  ENDIF
C-----7-----72
C * CALCULATE DERIVATIVE OF FUEL BURN RATE
  IF (K.LE.5.OR.K.GE.I-PTSPST-4) THEN
    D2FUEL(K)=0.0
  ELSE
    D2FUEL(K)=(FUELRT(K+5)-FUELRT(K-5))/(TIME(K+5)-TIME(K-5))
  ENDIF
C-----7-----72
C * STEADY STATE TIME RATIO
  IF (FUELRT(K) .EQ. 0.0) THEN
    FUELRT(K) = 0.00001
  ENDIF
  SSTIME=RESTIM(K)*D2FUEL(K)/FUELRT(K)
  IF (ABS(SSTIME).GT.10.0) THEN
    SSTIME = 10.0
  ENDIF
C-----7-----72
C * CALCULATE UNBURNED HYDROCARBON CONCENTRATIONS AND YIELDS
  IF (FID(K).LE.0.0)THEN
    THC=0.0
    THCYLD=0.0
  ELSE
    THC=(FIDSPN/FIDCST)*(FID(K)-FIDZER)/(FIDCAL-FIDZER)
    IF (IPROBE.EQ.1)THEN
      THCYLD=(THC*(EXMOLS)*28.05)/FUELRT(K)
    ELSE IF (IPROBE.EQ.2) THEN

```

```

      THCYLD=(THC*(TDMOLS)*28.05)/FUELRT(K)
    ELSE
      THCYLD=0.0
    ENDIF
  ENDIF
C-----7-----72
C * CARBON BALANCE ERROR CHECK
  IF (IPROBE.EQ.3) THEN
C   WRITE(*,*)' OR SAMPLED IN HALLWAY'
    CERROR=999.0
    GOTO 145
  ENDIF
  IF (FUELRT(K).LE.0.0) THEN
    WRITE(*,*)' ERROR IN CARBON BALANCE CHECK!'
    WRITE(*,*)' FUELRATE = 0 AT TIME = ',TIME(K)
    CERROR=999.0
    GOTO 145
  ENDIF
C-----7-----72
C * MOLES OF CARBON IN FROM FUEL
  CMOLIN=CCT*FUELRT(K)/MOLWT
  IF (CMOLIN.LE.0.0)THEN
    WRITE(*,*)' ERROR IN CARBON BALANCE CHECK W/ CMOLIN !'
    CERROR=999.0
    GOTO 145
  ENDIF
C-----7-----72
C * MOLES ACCOUNTED FOR BY MEASUREMENTS
C IF COMPARTMENT SAMPLED
  IF (IPROBE.EQ.1) THEN
    CMOLOT=(WETCO+WETCO2+2.0*THC)*EXMOLS
  ELSE
C IF EXHAUST DUCT SAMPLED
    CMOLOT=(WETCO-COAMB+WETCO2-CO2AMB+2.*THC)*TDMOLS
  ENDIF
  CERROR=(CMOLOT-CMOLIN)*100.0/CMOLIN
145 IF (ABS(CERROR).GT.999.1) THEN
  CERROR=999.0
  ENDIF
C   WRITE(*,*)' CARBON ERROR CALCULATIONS COMPLETE'
C-----7-----72
C * STORE DATA (80 CHARACTORS / LINE MAX)
  WRITE(21,2001)TIME(K),WETCO,WETCO2,WETO2,COYLD,CO2YLD,O2YLD,
  $$SMKYLD,THCYLD
  WRITE(22,2002)TIME(K),FUEL(K),FUELRT(K),AIRVEL(K),AIRRAT(K),
  $$D2FUEL(K),CERROR,EQUIV
  WRITE(23,2003)TIME(K),RESTIM(K),SSTIME,DRYCO(K),DRYCO2(K),
  $$DRYO2(K),THC,Q(K),TDMOLS/EXMOLS
  WRITE(24,2004)TIME(K),SMKVF,SMOKE1(K),EXCOEF,WETH2O,WETH2,

```

```
$FUEL2(K),FULRT2(K),Q2(K)
2001 FORMAT(F6.1,3E10.3,F7.4,2F10.4,F9.3,F7.4)
2002 FORMAT(F6.1,F10.3,F10.4,F10.2,F10.3,F9.5,F11.2,F8.3)
2003 FORMAT(F6.1,F7.1,F7.2,3E10.3,F10.6,F8.2,F8.1)
2004 FORMAT(F6.1,F8.2,6F9.3,F10.2)
150 CONTINUE
    CLOSE (21)
    CLOSE (22)
    CLOSE (23)
    CLOSE (24)
    WRITE(*,*) 'DATA REDUCTION COMPLETED!'
    WRITE(*,*) ' '
    WRITE(*,*) ' '
    WRITE(*,*) 'FILES WRITTEN:'
    WRITE(*,*) ' '
    WRITE(*,3000)FNAME,'.DTI'
    WRITE(*,3000)FNAME,'.DTA'
    WRITE(*,3000)FNAME,'.DTB'
    WRITE(*,3000)FNAME,'.DTC'
    WRITE(*,3000)FNAME,'.DTD'
    WRITE(*,3000)FNAME,'.DTE'
    WRITE(*,3000)FNAME,'.DTF'
3000 FORMAT(1X,A8,A4)
9999 STOP
    END
```

FIREAVG3.FOR

```

C PROGRAM: *** FIREAVG3.FOR ***
C REVISED BY: BRIAN LATTIMER   LAST UPDATE: 08/31/94
C WRITTEN BY: DAVID EWENS     LAST UPDATE: 11/17/93
C
C PURPOSE:
C THIS PROGRAM FINDS THE AVERAGE VALUES FOR THE VARIABLES OVER A GIVEN
C TIME RANGE IN THE DATA FILES CREATED BY PROGRAM FIRERED2.FOR.
C THIS PROGRAM ALSO CALCULATES 95% C.I. FOR EACH VARIABLE (+/- 2 SIGMA)
C OUTPUTS AVG, % ERROR BAND (FROM C.I.), 95% C.I. BAND
C
C VARIABLES:
C
C FILES ACCESSED:
C ( HALL####.*, WHERE #### IS THE RUN NUMBER, ie. HALL0001 )
C
C READ:
C
C HALL####.DTA - EXPERIMENTAL CHRONOLOGICAL DATA FILE (CONTAINS: TIME,
C           WET CONC'S, YIELDS)
C HALL####.DTB - EXPERIMENTAL CHRONOLOGICAL DATA FILE (CONTAINS: TIME,
C           FUEL & INLET AIR DATA, CARBON ERROR, EQUIVALENCE RATIO)
C HALL####.DTC - EXPERIMENTAL CHRONOLOGICAL DATA FILE (CONTAINS: TIME,
C           TIME SCALES, DRY CONC'S, THC, HEAT RELEASE, DILUTION)
C HALL####.DTD - EXPERIMENTAL CHRONOLOGICAL DATA FILE (CONTAINS: TIME,
C           SMOKE DATA, WET H2O & H2 CONC'S)
C HALL####.DTE - EXPERIMENTAL CHRONOLOGICAL DATA FILE (CONTAINS: TIME,
C           HALLWAY THERMOCOUPLE DATA)
C HALL####.DTF - EXPERIMENTAL CHRONOLOGICAL DATA FILE (CONTAINS: TIME,
C           COMPARTMENT THERMOCOUPLE DATA, INLET AIR & EXHAUST
C           THERMOCOUPLE DATA)
C WRITTEN:
C
C TO PRINTER - AVG AND 95% C.I. FOR ALL FILES ABOVE
C
C2345-7-9012345678901234567890123456789012345678901234567890123456789 72
C * INITIALIZATION
  IMPLICIT DOUBLE PRECISION (A-H,O-Z)
  DOUBLE PRECISION AVG(15),A(15,200),A2SIG(15),APER(15)
  CHARACTER*4 EXTDAT
  CHARACTER*8 FNAME
  CHARACTER*10 CNAME(12)
  CHARACTER*12 FNAMEX
C   CHARACTER*12 FDAT
  CHARACTER*27 PATHNM

C * INPUT FILE NAME
C   WRITE(*,*) ' IS THE FOLLOWING PATH TO DATA FILES CORRECT ?'
C   WRITE(*,*) ' YES = ENTER ANY NUM, NO = CHANGE PATHNM IN PROGRAM '

```

```

C MAX 15 CHAR'S, USE ALL 15, PUT BLANKS AS FRONT CHAR'S, NOT LAST CHAR'S!
C >>>>>>>>123456789012345<<<<<<<<
  PATHNM=' '
C WRITE(*,*)PATHNM
C READ(*,*)DUMMY
  WRITE(*,*)' ENTER THE FILE NAME TO AVERAGE'
  WRITE(*,*)' WITH OUT EXTENSION (ie. HALL0001)'
  READ(*,10)FNAME
C WRITE(*,*)PATHNM,FNAME
10 FORMAT(A8)
C WRITE(*,*)' ENTER THE TEST NUMBER'
C READ(*,*)ITEST
  WRITE(*,*)' ENTER START TIME FOR AVERAGE!'
  READ(*,*)START
  END=START+60.0D0
C WRITE(*,*)' ENTER END TIME FOR AVERAGE!'
C READ(*,*)END
C OPEN PRINTER FILE
  EXTDAT='.AVG'
  FNAMEX=FNAME
  FNAMEX(9:12)=EXTDAT(1:4)
C OPEN(UNIT=10, FILE=FNAMEX, STATUS='NEW')
  OPEN(UNIT=10, FILE='PRN')
C SET UP PRINTER PAPER
  WRITE(10,30)' AVERAGE TIME SPAN (SEC):',START,' - ',END
30 FORMAT(4X,A25,F7.1,A3,F7.1)
C SET UP FOR READ FILES
  EXTDAT='.DTA'
  FNAMEX(9:12)=EXTDAT(1:4)
  PATHNM(16:27)=FNAMEX(1:12)
  WRITE(*,*)FNAMEX,PATHNM
C-----7-----72
C * READ DATA
C * WRITE TEMPERATURE DATA FILES E AND F
C # NOTE: I IS THE NUMBER OF DATA POINTS PER CHANNEL
C OPEN *.RAW DATA FILE
  DO 400 I=1,6
    FNAMEX(12:12) = CHAR(64+I)
    PATHNM(27:27) = CHAR(64+I)
    WRITE(*,*)FNAMEX,PATHNM
    WRITE(*,*) '
    WRITE(*,*)' READING DATA FILE ',PATHNM
    WRITE(*,*) '
    OPEN(15,FILE=PATHNM)
  DO 40 KK=1,15
    AVG(KK)=0.0D0
    DO 39 KKK=1,50
      A(KK,KKK)=0.0D0
39 CONTINUE

```

```

40 CONTINUE
C   KOUNT=0
    K=1
C * READ DATA FROM CORRECT FILE
50 GOTO (51,52,53,54,55,56)I

C   51 READ(21,2001)TIME,WETCO,WETCO2,WETO2,COYLD,CO2YLD,O2YLD,
C   $SMKYLD,THCYLD
C-----7-----72
51  READ(15,2001,END=70)TIME,A(1,K),A(2,K),A(3,K),A(4,K),A(5,K),A(6,K)
    $,A(7,K),A(8,K)
    JJ=8
    CNAME(1)='WET CO'
    CNAME(2)='WET CO2'
    CNAME(3)='WET O2'
    CNAME(4)='CO YIELD'
    CNAME(5)='CO2 YIELD'
    CNAME(6)='O2 YIELD'
    CNAME(7)='SMK YIELD'
    CNAME(8)='THC YIELD'
    GOTO 57

C   52 READ(22,2002)TIME,FUEL,FUELRT,AIRVEL,AIRRT,
C   $D2FUEL,CERROR,EQUIV
C-----7-----72
52  READ(15,2002,END=70)TIME,A(1,K),A(2,K),A(3,K),A(4,K),A(5,K),A(6,K)
    $,A(7,K)
    JJ=8
    A(8,K)=A(2,K)+A(4,K)
    CNAME(1)='FUEL WT'
    CNAME(2)='FUEL RATE'
    CNAME(3)='AIR VEL'
    CNAME(4)='AIR RATE'
    CNAME(5)='D2FUEL'
    CNAME(6)='C ERROR'
    CNAME(7)='EQ. RATIO'
    CNAME(8)='VENT FLOW'
    GOTO 57

C   53 READ(23,2003)TIME,RESTIM,SSTIME,DRYCO,DRYCO2,
C   $DRYO2,THC,Q,TDMOLS/EXMOLS
C-----7-----72
53  READ(15,2003,END=70)TIME,A(1,K),A(2,K),A(3,K),A(4,K),A(5,K),A(6,K)
    $,A(7,K),A(8,K)
    JJ=8
    CNAME(1)='RES TIME'
    CNAME(2)='SS TIME'
    CNAME(3)='DRY CO'

```

```
CNAME(4)='DRY CO2'
CNAME(5)='DRY O2'
CNAME(6)='THC'
CNAME(7)='Q, HEAT'
CNAME(8)='DIL RATIO'
GOTO 57
```

```
C 54 READ(24,2004)TIME,SMKVF,SMOKE0,SMOKE1,EXCOEF,WETH2O,
C $WETH2
C-----7-----72
54 READ(15,2004,END=70)TIME,A(1,K),A(2,K),A(3,K),A(4,K),A(5,K),A(6,K)
$,A(7,K),A(8,K)
JJ=8
CNAME(1)='SMK VF'
CNAME(2)='SMOKE 1'
CNAME(3)='EXCOEF'
CNAME(4)='WET H2O'
CNAME(5)='WET H2'
CNAME(6)='FUEL WT2'
CNAME(7)='FUEL RATE2'
CNAME(8)='Q2, HEAT2'
GOTO 57
```

```
C 55 READ(25,2005)TIME(I),TCH(1),TCH(2),TCH(3),TCH(4),TCH(5),TCH(6),
C $TCH(7),TCH(8),TCH(9)
C-----7-----72
55 READ(15,2005,END=70)TIME,A(1,K),A(2,K),A(3,K),A(4,K),A(5,K),A(6,K)
$,A(7,K),A(8,K),A(9,K)
JJ=9
CNAME(1)='TC HALL 1'
CNAME(2)='TC HALL 2'
CNAME(3)='TC HALL 3'
CNAME(4)='TC HALL 4'
CNAME(5)='TC HALL 5'
CNAME(6)='TC HALL 6'
CNAME(7)='TC HALL 7'
CNAME(8)='TC HALL 8'
CNAME(9)='TC HALL 9'
GOTO 57
```

```
C 56 READ(26,2006)TIME(I),TCC(1),TCC(2),TCC(3),TCC(4),TCC(5),TCC(6),
C $TCC(7),TCC(8),TCEV(I),TCED(I),TCID(I)
C-----7-----72
56 READ(15,2006,END=70)TIME,A(1,K),A(2,K),A(3,K),A(4,K),A(5,K),A(6,K)
$,A(7,K),A(8,K),A(9,K),A(10,K),A(11,K)
JJ=11
CNAME(1)='TC COMP 1'
CNAME(2)='TC COMP 2'
```

```

CNAME(3)='TC COMP 3'
CNAME(4)='TC COMP 4'
CNAME(5)='TC COMP 5'
CNAME(6)='TC COMP 6'
CNAME(7)='TC COMP 7'
CNAME(8)='TC COMP 8'
CNAME(9)='TC EX VENT'
CNAME(10)='TC EX DUCT'
CNAME(11)='TC IN DUCT'

57 IF (TIME.LT.START) GOTO 50
   IF (TIME.GT.END) GOTO 70
C   KOUNT=KOUNT+1
   K=K+1
   DO 60 J=1,JJ
   AVG(J) = AVG(J)+A(J,K-1)
60 CONTINUE
   GOTO 50

C-----7-----72
70 WRITE(10,*)FNAMEX,'      AVERAGE +/- % ERROR +/- 95% C.I.
   $ % ERROR (2 SIGMA)'
   WRITE(*,*)FNAMEX,'      AVERAGE +/- % ERROR +/- 95% C.I.
   $ % ERROR (2 SIGMA)'
75 FORMAT(2X,A10,2X,I2,2X,F16.10,2X,F9.2,2X,D12.6)
   K=K-1
   DO 80 J=1,JJ
C CALCULATE AVG AND 2 SIGMA
   A2SIG(J)=0.0D0
   AVG(J)=AVG(J)/DBLE(FLOAT(K))
   DO 78 KS=1,K
   A2SIG(J)=A2SIG(J)+((A(J,KS)-AVG(J))**2)
78 CONTINUE
   A2SIG(J)=A2SIG(J)/DBLE(FLOAT(K-1))
   A2SIG(J)=2.0D0*SQRT(A2SIG(J))
   APER(J)=0.0D0
   IF (ABS(AVG(J)).GE.1.0D-9) THEN
   APER(J)=100.0D0*A2SIG(J)/AVG(J)
   ENDIF
C WRITE OUTPUT
   WRITE(10,75)CNAME(J),J,AVG(J),APER(J),A2SIG(J)
   WRITE(*,75)CNAME(J),J,AVG(J),APER(J),A2SIG(J)
80 CONTINUE
C   WRITE(10,*)' '
   CLOSE(15)

C~~~~~7*****72

400 CONTINUE

```

Appendix B. Data Reduction Programs

```
2001 FORMAT(F6.1,3E10.3,F7.4,2F10.4,F9.3,F7.4)
2002 FORMAT(F6.1,F10.3,F10.4,F10.2,F10.3,F9.5,F11.2,F8.3)
2003 FORMAT(F6.1,F7.1,F7.2,3E10.3,F10.6,F8.2,F8.1)
2004 FORMAT(F6.1,F8.2,6F9.3,F10.2)
2005 FORMAT(F7.1,9F6.0)
2006 FORMAT(F7.1,11F6.0)
```

```
WRITE(10,*) '
WRITE(*,*) '
WRITE(*,*) DATA REDUCTION COMPLETED!
WRITE(*,*) '
WRITE(*,*) FILE PRINTED!
WRITE(*,*) '
9999 STOP
END
```

APPENDIX C.

ENHANCED CO GENERATION IN THE COMPARTMENT

C.1 INTRODUCTION

Two experimental situations were investigated where CO levels inside the compartment were measured to be significantly higher than levels measured in the study by Gottuk (1992a). The effects of bi-directional flow opening (a door) connecting the compartment and hallway on CO levels in the compartment and hallway is initially discussed. The effect of a wood ceiling inside the compartment on the CO levels measured in the compartment and hallway is then discussed. Results of these two situations are compared with results from experiments containing a 0.12 m² opening with unidirectional flow.

C.2 DOORWAY EXPERIMENTS

C.2.1 Experimental Methodology

A study was performed to investigate the effect of the presence of a bi-directional flow opening on the species concentrations. To produce this using the current compartment, shown in Fig. 2.2, the plenum was blocked off from both the ambient air and the inside of the compartment, see Fig. C.1. Note that the compartment-hallway configuration is different than experiments previously discussed. This compartment-hallway orientation is the same as that used in the study by Ewens (1994a). The opening connecting the compartment and hallway was enlarged to its maximum dimensions of 0.50 m wide, 0.75 m high (0.38 m²). The experiments were conducted with a 0.20 m inlet soffit and a 0.23 m diameter fuel pan in the room. Comparisons are made with experiments having a 0.12 m² opening, a 0.20 m inlet soffit, and a 0.20 m diameter fuel

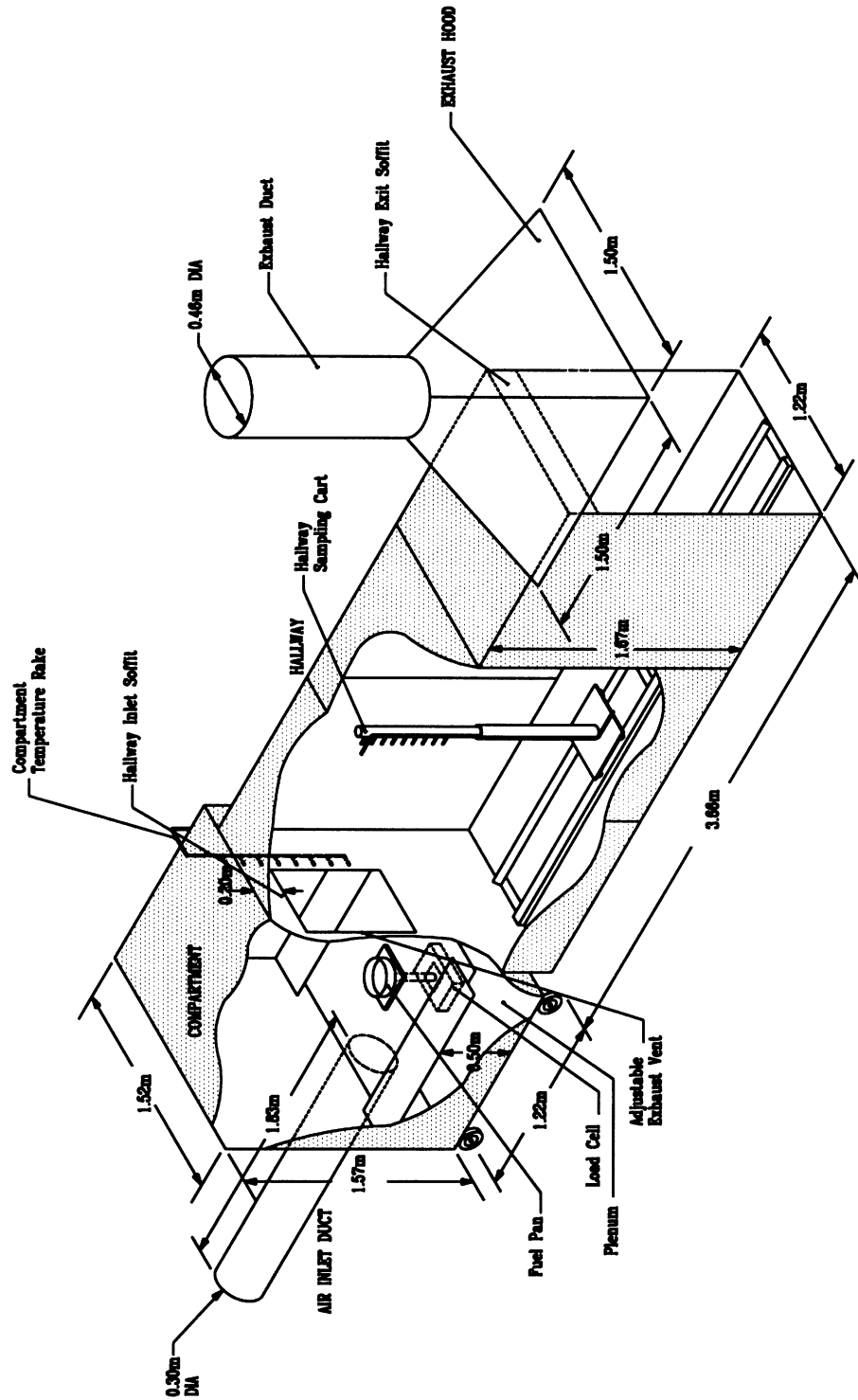


Figure C.1 The compartment on the end of the hallway with the plenum blocked forcing a bi-directional flow of air into and combustion gases out of the compartment through a door.

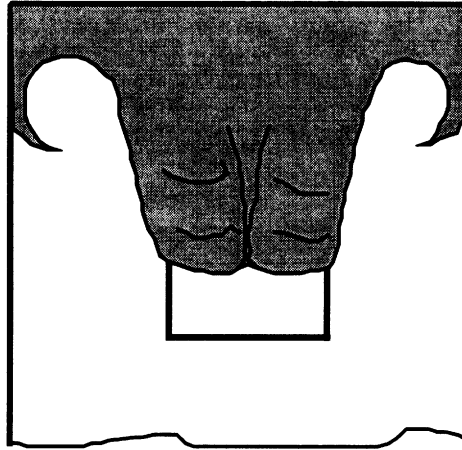
pan. A different fuel pan diameter was used so the experiments would have approximately the same fire size, 576 kW with a door and 542 kW with the 0.12 m² opening.

Sampling was conducted at two locations in the compartment and three locations along the hallway with all sampling being performed 0.05 m below the ceiling. The in-compartment sampling was performed 0.20 m from the wall containing the door on the temperature rake side of the compartment (termed the front), and 1.02 m from the wall containing the door on the same side of the compartment (termed the back). The in-hallway sampling locations were performed 0.45 m, 1.80 m and 3.20 m downstream of the compartment opening as shown in Fig. C.1. The door (or opening) is taken as the spatial origin in the hallway and is shown in the plots as 0.0 m.

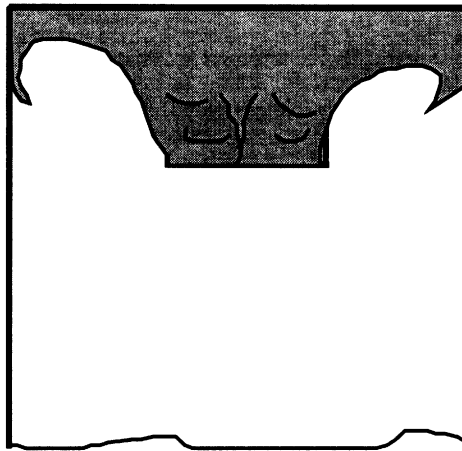
C.2.2 Flow Visualization

The differences in the flow of hallway gases in the experiments with a door and a 0.12 m² opening is expected to be significantly different. The external burning in the hallway was observed to determine the differences in the flow patterns.

With a door connecting the compartment and the hallway, two large vortical structures were present in the first half of the hallway as shown in Fig. C.2 (a). The vortical structures originated near the bottom of the door approximately 0.9 m below the ceiling. The structures were observed to rise nearly vertically in the corridor until the flame impinged on the ceiling. These vortical structures were also observed in the 0.12 m² opening experiments, but were much smaller, see Fig. C.2 (b). With the 0.12 m² opening, the gases were only permitted to rise 0.44 m before impinging upon the ceiling. In both cases, the gases were seen to travel down the hallway as a ceiling jet after impinging upon the ceiling. Vortical structures were also evident downstream of the compartment along the corner of the ceiling and the walls in both cases. The vortical



(a)



(b)

Figure C.2 The external burning *n*-hexane fire experiments with (a) a door and (b) a 0.12m^2 opening connecting the compartment to the hallway.

structures do not separate as observed by Hinkley et al. (1984), but are instead connected by a sheet of fire.

C.2.3 Results and Discussion

Axial profiles of the combustion gases from experiments with a door and with a 0.12 m^2 opening connecting the compartment to the hallway are shown in Fig. C.3 and Fig. C.4, respectively. The normalizing values are shown in parentheses beside the appropriate species in the caption. Negative axial locations indicate sampling inside the compartment.

The levels of CO inside the compartment with a door are seen in Fig. C.3 to be 6.4% in the back and 4.5% in the front. This is a significant increase over the levels measured inside the compartment with a 0.12 m^2 opening of 2.8% in the back and 3.7% in the front, see Fig. C.4. The difference in the two experiments is not only the path of the air entrainment into the compartment, but also the momentum of the air entering the compartment. When air is drawn into the compartment through the plenum from two sides of the plume, the plume (with a 0.12 m^2 opening) appears to be relatively undisturbed, and rises vertically in the compartment, see Fig. C.5 (a). With the air entering through the door, the momentum of the air is apparent by the flame from the pool fire being bent backward. The flame eventually was observed to impinge on the back wall of the compartment as shown in Fig. C.5 (b). It is believed that the air which does not get entrained into the plume impinges upon the back wall. The air is believed to then be drawn upward into the compartment upper-layer. This “injection” of air into the hot, fuel rich environment of the compartment upper-layer results in the oxidation of UHC leading directly to the formation of additional CO.

Concentrations of CO and UHC are both seen in Fig. C.3 as being oxidized rapidly in the first portion of the hallway, but the cool temperatures in the later 1.80 m of the hallway prevented further oxidation. Significant dilution of the gases was, however,

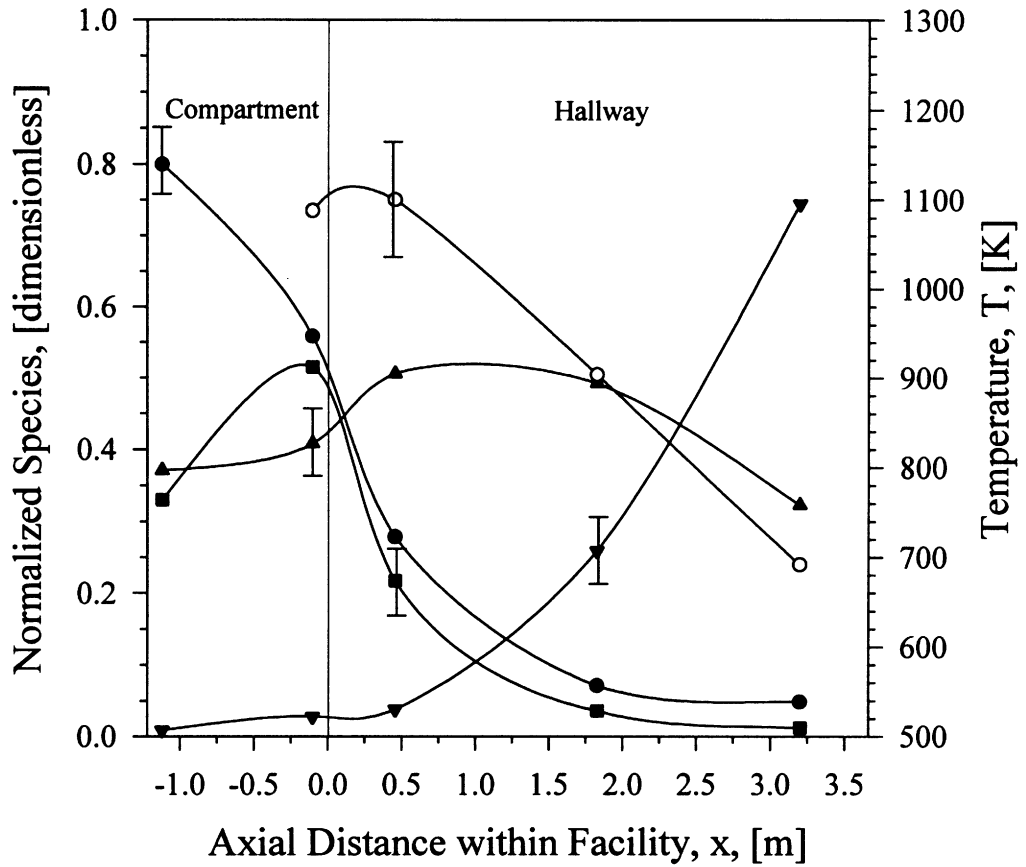


Figure C.3 The normalized species concentrations (wet) and temperatures within the compartment and hallway for *n*-hexane fire experiments with a door. Symbols and normalization values: ●-CO (8.0%), ■-UHC (10%), ▲-CO₂ (20%), ▼-O₂(10.5%), and ○-Temperature.

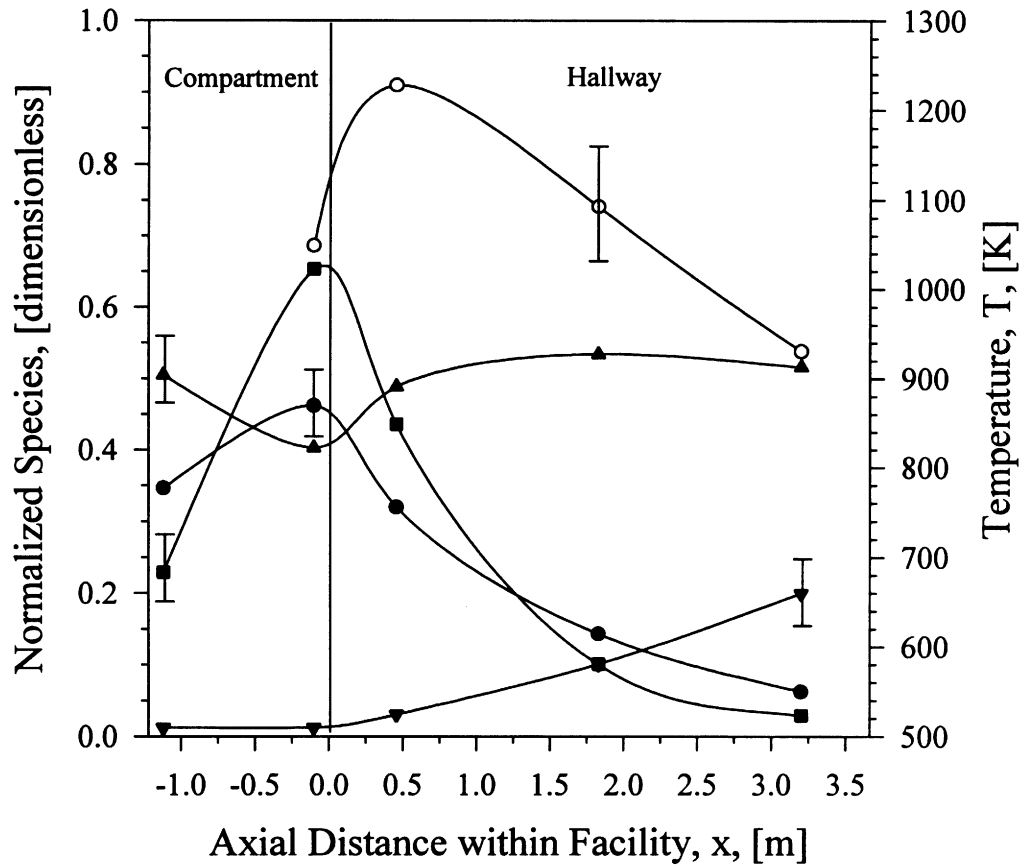
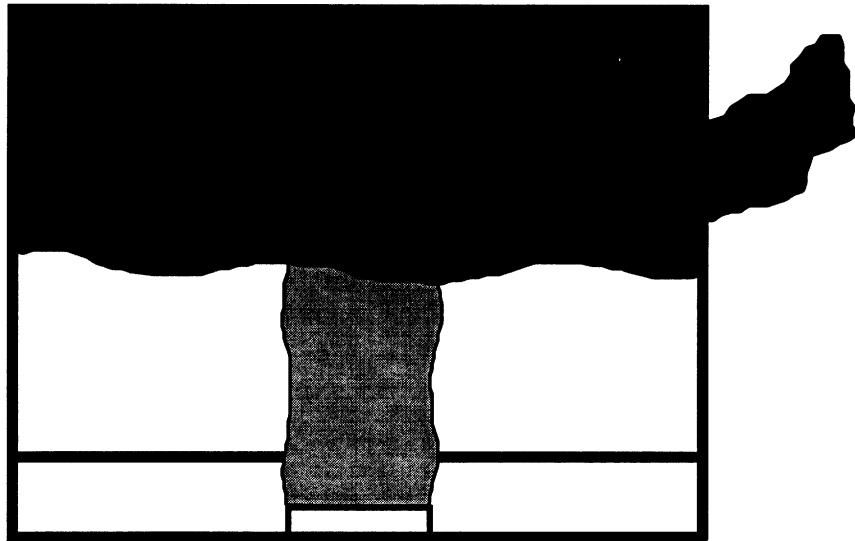


Figure C.4 The normalized species concentrations (wet) and temperatures within the compartment and hallway for *n*-hexane fire experiments with a 0.12 m² opening. Symbols and normalization values: ●-CO (8.0%), ■-UHC (10%), ▲-CO₂ (20%), ▼-O₂(10.5%), and ○-Temperature.



(a)



(b)

Figure C.5 The effect of air being entrained into the compartment through (a) the plenum and (b) the doorway on the fire plume inside the compartment.

measured to occur in the later portion of the hallway. This is evident by the rise in the O₂ concentrations to approximately 7.5% by the end of the hallway. Oxidation of CO and UHC is also significant in the first half of the hallway in experiments with a 0.12 m² opening, but CO oxidation was measured to be much slower than that measured in the door experiments. With a 0.12 m² opening, temperatures in the hallway were measured to remain above 900 K the entire length of the hallway. This allowed CO oxidation to occur for the majority of the length. The O₂ concentration of 2% in the upper-layer at the end of the hallway was measured to be considerably lower compared to the 7.5% measured in the experiments with a door.

The post-hallway yields of CO and UHC with a door were 0.10 and 0.029, respectively. In experiments with a 0.12 m² opening, the post-hallway yield of CO of 0.12 and UHC of 0.038 are slightly higher than those measured with a door present. The reduction in the concentration of CO and UHC at the end of the hallway was, however, higher in the experiments with a door. The concentration reduction

$$\eta_{red} = \left(1 - \frac{(X_i)_{hallexit}}{(X_i)_{comp}} \right) 100 \text{ [%]} \quad (\text{C.1})$$

in CO and UHC was 95% and 99%, respectively for experiments with a door and 85% and 96%, respectively, with a 0.12 m² opening. Noting that approximately the same amount of CO and UHC leave the hallway, the higher concentration reduction efficiency with a door present is the result of a dilution of the combustion gases via increased air entrainment into the upper-layer, which is unaccounted for in the yield data.

C.2.4 Summary and Conclusions

Experiments with a door resulted in approximately the same post-hallway CO and UHC yields compared with levels measured with a 0.12 m² opening. Experiments with a door resulted in 50% lower CO and UHC concentrations and 300% higher O₂ concentration exiting the hallway compared with measurements in experiments with a

0.12 m² opening. The higher dilution in the door case is attributed to more efficient entrainment into the compartment fire gases exiting the compartment and rising to the ceiling.

C.3 COMPARTMENT WITH A COMBUSTIBLE CEILING

C.3.1 Background

In 1987, three people died due to smoke inhalation in a townhouse in Sharon, Pennsylvania. Extremely high levels of carboxyhemoglobin, 91%, were present in one of the victim's bloodstream. This prompted an investigation by NIST/BFRL to simulate the townhouse fire (Levine and Nelson, 1990). The source of the fire was in the kitchen of the townhouse where a large amount of wood (wood paneling and cabinets) was located. The CO levels exiting the kitchen were found to be as high as 8.5%-dry, while the levels upstairs where the bedrooms were located was 5.0%-dry (Levine and Nelson, 1990). Experiments performed by Pitts et al. (1994a) in a reduced-scale compartment with the ceiling and the upper-portion of the walls lined with wood showed the CO concentrations were 6%-dry or greater in the front and 12%-dry in the rear of the compartment. This was a dramatic increase from the CO concentrations, approximately 4%-dry in the front and 3%-dry in the rear, measured in a compartment without combustible surfaces (Pitts, 1994a).

C.3.2 Experimental Methodology

The compartment and hallway were oriented in the same manner shown in Fig. C.1. A 0.20 m soffit was present at the hallway entrance while no soffit was present at the exit. Three sheets of 1.22 m long, 0.30 m wide, 6.35 mm thick Douglas fir plywood were suspended approximately 0.05 m below the ceiling of the compartment, see Fig. C.6. The mass loss rate of the wood was monitored using a A&D load cell located on the top of the

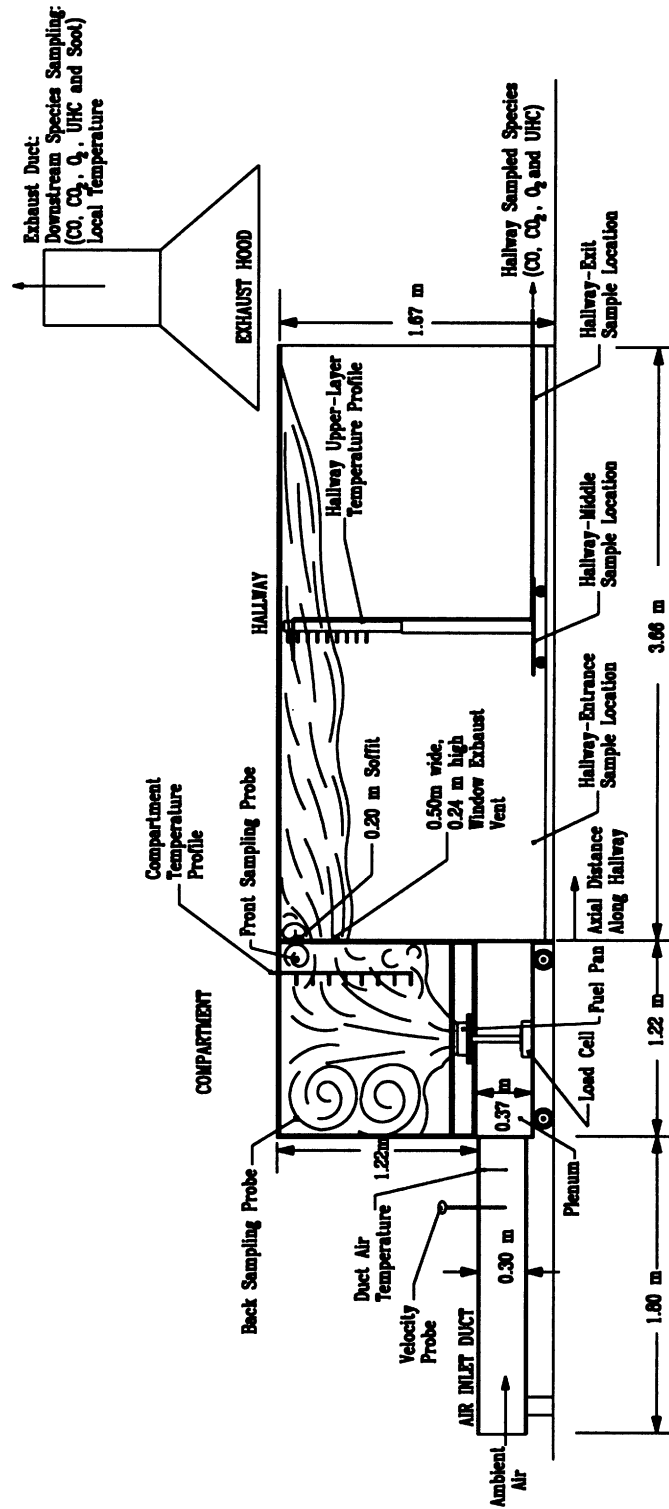


Figure C.6 A side view of the facility showing wood suspended from the ceiling of the compartment.

compartment. During the fire, both sides of the wood (total surface area of 2.20 m²) were exposed to the hot upper layer gases and were allowed to pyrolyze. This is less surface area than was used by in the experiments performed by Pitts, et al. (1994) where 3.19 m² of wood was pyrolyzing.

Experiments were performed with a 0.12 m² window, with and without a combustible ceiling in the compartment. Results from sampling inside the compartment and along the length of the hallway were compared for the two cases. Sampling inside the compartment was performed in the back (0.10 m away from the wall opposite the window) and in the front (0.10 m away from the wall containing the window). Both sampling probes were 0.10 m below the ceiling and 0.23 m from the side wall.

The sampling in the hallway was performed 0.46 m, 1.83 m and 3.20 m down the hallway from the window. The sampling was done 0.05 m below the ceiling at an equal distance from both side walls. The sampling locations and wood ceiling are shown in Fig. C.7.

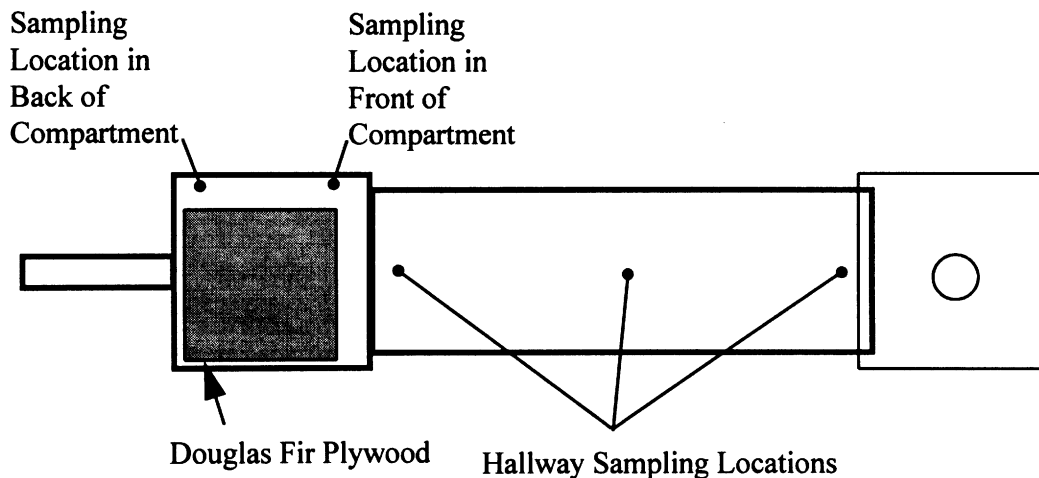


Figure C.7 A top view of the facility showing the orientation of the wood in the upper layer of the compartment and the gas sampling locations.

C.3.3 Results and Discussion

The mass loss rate of the wood ceiling was experimentally measured and compared with the estimation of the wood mass loss rate found using the oxygen depletion method as determined by Pitts, et al. (1994). The burning of the wood during flashover, shown in Fig. C.8, is seen to be divided into three regions: (1) gasification stage, (2) transition stage and (3) char stage. The first stage of gasification (volatiles escape) is indicated by the first peak of 13 g/s m^2 seen in Fig. C.8. During this stage, as noted by Pitts, et al. (1994), gases are formed directly from the wood. Char began forming on the wood during the transition stage causing a drop in the mass loss rate to an average value of 8 g/s m^2 . Eventually, enough energy was available in the system (i.e. high enough temperatures) to pyrolyze the char, and the mass loss rate was measured to rise to a peak value of 17 g/s m^2 . The mass loss rate of $10\text{-}15 \text{ g/s m}^2$ determined by Pitts, et al. (1994) is similar to these measured values. As previously noted by Pitts, et al. (1994), the pyrolysis of the wood is an endothermic process causing the upper-layer temperatures to be lower when a wood ceiling was present compared with results from a compartment with no combustible surfaces.

The species concentrations and the temperatures within the facility having a non-combustible ceiling are shown in Fig. C.9. The variations in species concentration and temperature for a compartment containing a wooden ceiling are shown in Fig. C.10. The CO and UHC concentrations in the experiments with a non-combustible ceiling were lower in the rear of the compartment compared with the levels in the front. This was attributed to the gases in the rear of the compartment having a longer residence time in the compartment. The species concentrations were fairly uniform in the upper-layer of the compartment with the wood ceiling. This uniformity is a result of the burning of the wood dominating the production of species in the upper-layer. The in-compartment

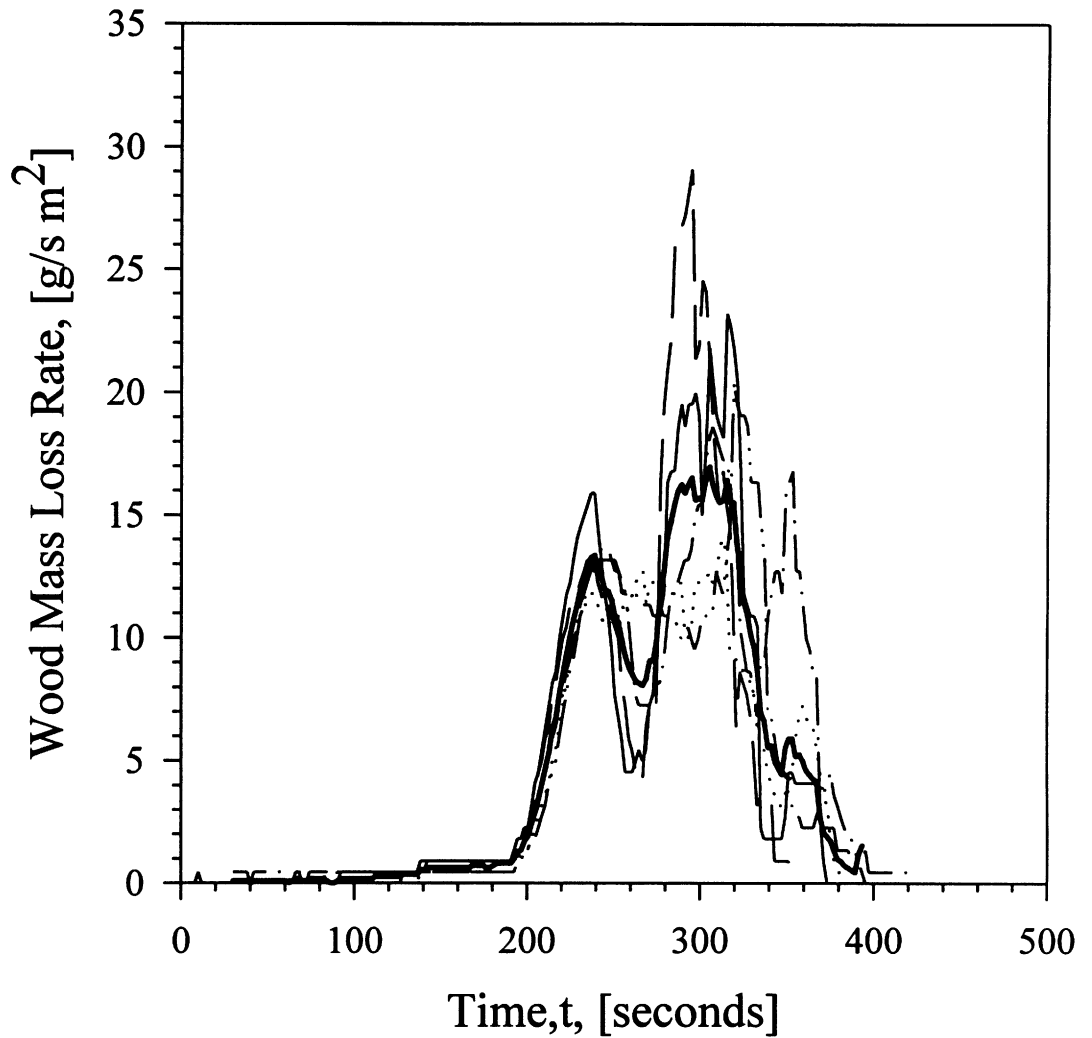


Figure C.8 The mass loss rate of the wooden ceiling as a function of time. The sampling locations of the five different experiments: Experimental sampling in the compartment: —Rear, ----Front, and down the hallway: ••0.46 m, -•- 1.83 m, -••- 3.20 m. —Average.

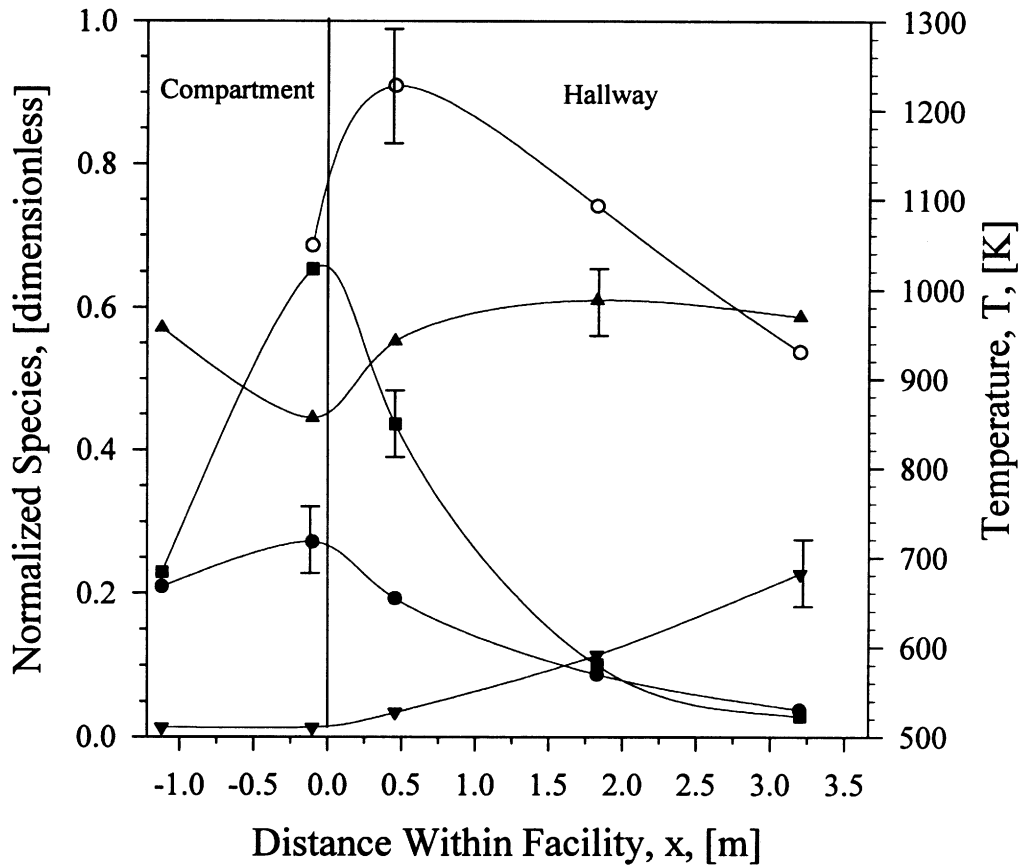


Figure C.9 The normalized species concentrations (dry) and temperatures within the compartment and hallway for *n*-hexane fire experiments with a 0.12 m² opening. Symbols and normalization values: ●-CO (15.0%), ■-UHC (10%), ▲-CO₂ (20%), ▼-O₂(10.5%), and ○-Temperature.

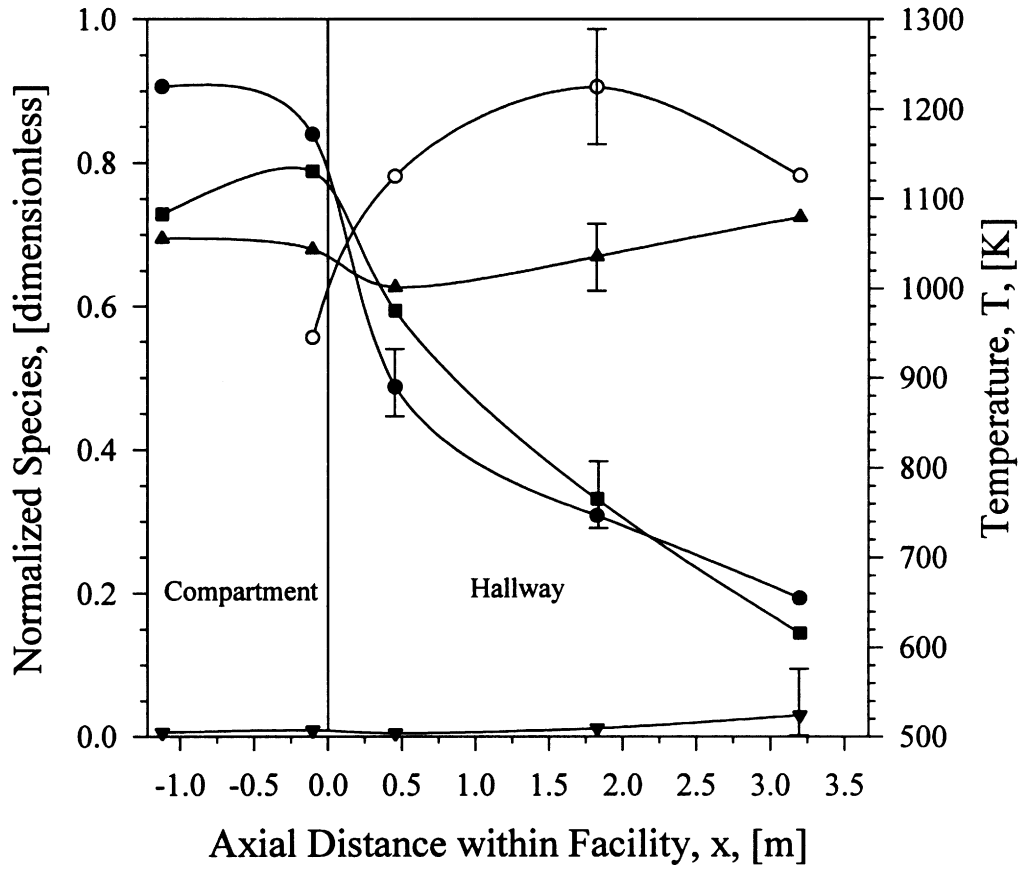


Figure C.10 The normalized species concentrations (dry) and temperatures within the compartment and hallway for *n*-hexane fire experiments containing a wood ceiling with a 0.12 m² opening . Symbols and normalization values: ●-CO (15.0%), ■-UHC (10%), ▲-CO₂ (20%), ▼-O₂(10.5%), and ○-Temperature.

levels of CO were found to drastically increase to 13.6% in the rear and 12.6% in the front compared to 3.1% and 4.1%, respectively, in a compartment without wood. The CO concentration produced in the combustible ceiling experiments are consistent with those measured in the experiments reported by Pitts, et al. (1994).

As the exhaust gases exited the compartment into the hallway, there was a competition between CO and UHC for the entrained air. The competition is explained through the application of the ‘law of mass action’

$$RR = k_{fuel}[C_{fuel}][O_2] \quad (C.2)$$

where RR is the rate of reaction, k_{fuel} is the reaction rate constant for the fuel and $[C_{fuel}]$ is the concentration of the fuel. In the non-combustible ceiling case, both the UHC concentration and the reaction rate constant are higher than those of CO resulting in a higher oxidation rate of UHC. This is evident in Fig. C.9 by the faster reduction in UHC relative to CO. When a wooden ceiling was present in the compartment, the concentration of CO was significantly higher than the UHC. This is believed to result in a higher CO oxidation rate of reaction compared with that of UHC. This is evident in the first part of the hallway as seen in Fig. C.9, by the CO being reduced more rapidly than UHC. As the concentrations of CO and UHC became equivalent, the reduction of UHC occurred at a higher rate. This was attributed to the competition between the oxidation of the two species becoming more a function of the reaction rate constant.

By the exit of the hallway, the highest in-compartment levels of CO had been reduced by 86% in the non-combustible ceiling case and by 79% in the wood ceiling case. The UHC exhibited a similar trend with a measured reduction of 96% in the non-combustible ceiling case and 82% in the wood ceiling case. The presence of the wood ceiling in the compartment led to higher concentrations of CO and UHC entering the hallway. The air entrained into the gases flowing in the hallway was, therefore, not

sufficient to reduce the CO and UHC as effectively as that measured in experiments with no combustible ceiling.

C.3.4 Summary

The presence of a Douglas fir plywood ceiling in the compartment had a dramatic effect on the level of CO in both the compartment and the hallway, while the UHC showed a slight change in their in-compartment levels but a dramatic change in the hallway. The CO concentration in the compartment was seen to increase to levels in excess of 12%. This is 3-5 times higher (depending on the sampling location) than that measured in a compartment without combustible surfaces. The oxidation of the compartment fires gases in the hallway in the two cases is also different, and was explained through the application of the “law of mass action”. The high concentrations of CO generated in the compartment caused the CO to initially be oxidized at a faster rate (compared with the UHC) until the concentrations became nearly equivalent. Afterward, the UHC were oxidized at faster rate. For the non-combustible ceiling case, the UHC levels were always measured to be reduced at a faster rate than CO. Most important, the presence of the wood ceiling allowed the CO to leave the hallway at 2.5% which is lethal after approximately 2 minutes of exposure.

APPENDIX D.

CHEMICAL KINETIC MODELING OF THE HALLWAY GASES

D.1 INTRODUCTION

A plug flow reactor model for the oxidation and transport of compartment fire gases entering and traveling down the hallway is developed in this section. The equations describing the fluid mechanic, thermodynamic and chemical behavior of the species in a plug flow reactor are derived from basic principles. Application of assumptions reduces the set of equations to only the equation for species conservation. Finally, transformations for converting spatial experimental data to time data, and vice versa, is given.

D.2 DERIVATION OF GOVERNING EQUATIONS

In the following derivations, consider a plug flow reactor in steady-state and steady-flow, see Fig. D.1. One-dimensional (1-D) flow is considered with uniform properties

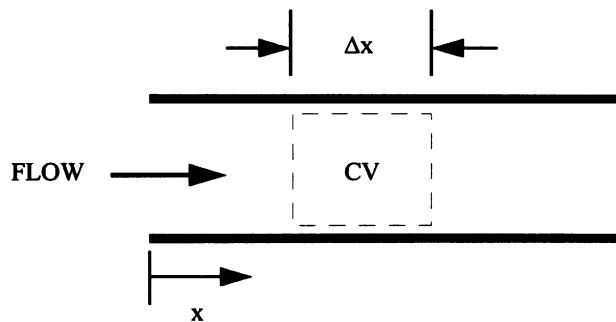


Figure D.1 The plug flow reactor being used to model the hallway gases.

present at each cross section. No mixing is assumed to occur in the axial direction (x -direction), and the flow is assumed to be frictionless. The gases within the reactor are assumed to behave as ideal gases.

Figure D.2 shows a control volume of gases in the plug flow reactor of length dx . Summing the mass flowing into and out of the control volume, the law of mass conservation yields:

$$\rho u A + \frac{d(\rho u A)}{dx} dx - \rho u A = 0 \quad (\text{D.1})$$

and reduces to

$$\frac{d}{dx}(\rho u A) = 0 \quad (\text{D.2})$$

The momentum of the gases entering and exiting the control volume shown in Fig. D.2 is equivalent to the forces acting upon the control volume. Assuming no body forces,

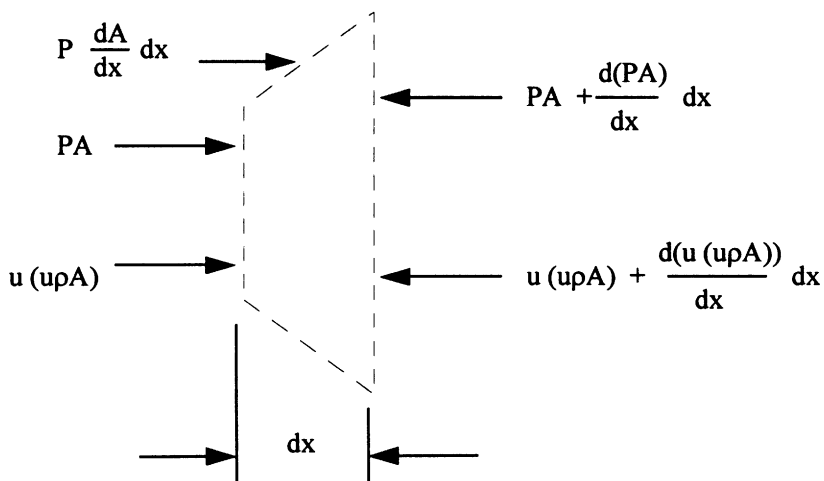


Figure D.2 The control volume showing the fluxes of momentum.

$$u^2 \rho A + \frac{d(u^2 \rho A)}{dx} dx - u^2 \rho A = PA + P \frac{dA}{dx} dx - PA - \frac{d(PA)}{dx} dx \quad (\text{D.3})$$

which is equivalent to

$$\frac{d(u^2 \rho A)}{dx} = P \frac{dA}{dx} - \frac{d(PA)}{dx} \quad (\text{D.4})$$

Expanding the first term on the left hand side and the second term on the right hand side using the chain rule,

$$u \frac{d(u \rho A)}{dx} + u \rho A \frac{du}{dx} = P \frac{dA}{dx} - P \frac{dA}{dx} - A \frac{dP}{dx} \quad (\text{D.5})$$

Applying continuity, Eqn. (D.2), and a little algebra transforms Eqn. (D.5) into

$$u \rho \frac{du}{dx} = - \frac{dP}{dx} \quad (\text{D.6})$$

To derive the energy and species equations, consider the control volume shown in Fig. D.3.

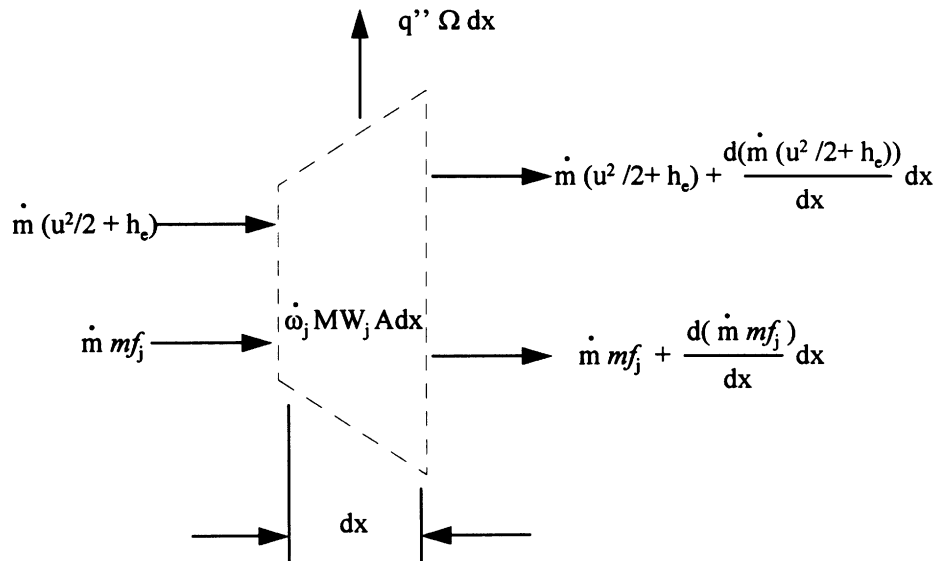


Figure D.3 The control volume showing the fluxes of energy and species.

By summing the energy into, out of and stored within the control volume

$$\rho u A (h_e + u^2/2) + \frac{d(\rho u A (h_e + u^2/2))}{dx} dx - \rho u A (h_e + u^2/2) = -q'' \Omega dx \quad (\text{D.7})$$

After canceling terms one and three on the left side and using the chain rule to expand the second term on the same side, the application of continuity reduces Eqn. (D.7) to

$$\rho u A \frac{d(h_e + u^2/2)}{dx} = -q'' \Omega \quad (\text{D.8})$$

Similarly, the summation of the species into, out of and stored within the control volume yields the following relation

$$\rho u A m f_j + \frac{d(\rho u A m f_j)}{dx} dx - \rho u A m f_j = \dot{\omega}_j M W_j A dx \quad (\text{D.9})$$

Through the cancellation of terms, the expansion of the second term on the left side, and the application of continuity, Eqn. (D.9) is reduced to

$$\frac{d m f_j}{dx} = \frac{\dot{\omega}_j M W_j}{\rho u} \quad (\text{D.10})$$

To model the 1-D system of equations, Eqns. (D.2), (D.6), (D.8) and (D.10), a computational fluid dynamics (CFD) code must be written. Instead, further manipulation was performed on Eqn. (D.6) to reduce the complexity of the problem. If the plug flow reactor is consider to have a constant cross sectional area, then the (ρu) term in equation (D.6) is constant. This allows Eqn. (D.6) to be integrated,

$$(\rho u) \int_0^l du = - \int_0^l dP, \quad (\text{D.11})$$

yielding the following expression

$$(\rho u)(u_l - u_o) = P_o - P_l \quad (\text{D.12})$$

Applying continuity with the constant cross sectional area assumption invoked, Eqn. (D.11) is transformed to

$$(\rho u)^2 = -\frac{P_1 - P_o}{\left[\frac{1}{\rho_1} - \frac{1}{\rho_o}\right]} \quad (\text{D.13})$$

Equation (D.13) represents the equation of the negatively sloped Rayleigh line. If q'' is considered to be zero, then Eqn. (D.8) can be integrated and yields the following relationship

$$h_1 - h_o = \left[\frac{u_o^2}{2} - \frac{u_1^2}{2} \right] \quad (\text{D.14})$$

If the velocity is put in terms of mass flow again and the mass flow from Eqn. (D.13) is substituted into the equation, the Eqn. (D.14) becomes

$$h_1 - h_o = -\frac{P_1 - P_o}{2} \left[\frac{1}{\rho_1} - \frac{1}{\rho_o} \right] \quad (\text{D.15})$$

the Hugoniot equation. For a deflagration wave, the density variation is responsible for the majority of the rise in enthalpy and the pressure difference is considered small. By assuming no pressure drop, Eqn. (D.6) is no longer a function of x .

Though the energy equation could be solved to determine the temperature along the reactor, a temperature will be specified along the length of the reactor from experimental results. Thus, the energy equation need not be solved.

From this additional analysis and consideration of the problem, the number of fundamental equations is reduced down to the species conservation Eqn. (D.10). The number of ordinary differential equations which must be solved is actually equivalent to the number of species, j , considered.

D.3 METHODOLOGY OF MODELING

D.3.1 Transformation of Experimental Results to a Temporal Coordinate System

Figure D.4 shows the location of the sampling points in the hallway and the spatial transformation of the L-shaped path.

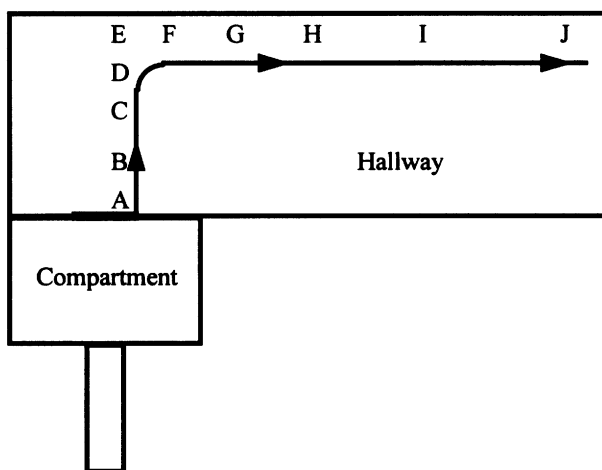


Figure D.4 The bulk flow path of the compartment fire gases. The letters denote locations where temperature and air entrainment measurements were performed.

Assuming that the gases behave as ideal gases, the density can be determined from

$$\rho = \frac{P}{RT} \quad (\text{D.16})$$

A discretized form equation of the velocity,

$$\bar{u} = \frac{\Delta x}{\Delta t}, \quad (\text{D.17})$$

defines the gas velocity between two points in the hallway. Since velocity measurements are not made, the conservation of mass is applied

$$\bar{u} = \frac{(\bar{m}/A)}{\rho} \quad (\text{D.18})$$

to determine the velocity in terms of known values. From the continuity equation applied in the plug flow reactor derivation, the value of (\bar{m}/A) in Eqn. (D.18) is constant. A value for \bar{m} and A can be arbitrarily chosen at any location along the length of the hallway. The \bar{m} is, therefore, the mass flow rate exiting the compartment while A is the area of the opening. Substituting the right hand side of Eqn. (D.16) for ρ into Eqn. (D.18), an expression containing previously measured values is generated

$$\bar{u} = \frac{(\bar{m}/A)RT}{P} \quad (\text{D.19})$$

Solving Eqn. (D.17) for Δt and substituting Eqn. (D.19) in for the velocity term, a discretized expression for the transformation of the spatial coordinates into temporal coordinates

$$\Delta t = \frac{P\Delta x}{(\bar{m}/A)RT} \quad (\text{D.20})$$

is formed. The value for P is equivalent to the ambient pressure, while Δx is the distance between sampling positions. The ideal gas constant is divided by the molecular weight of the upper-layer gases (assumed to be equivalent to that of air) to determine R , and T is the temperature of the gases in the upper-layer of the hallway.

To determine the temperature distribution in the plug flow reactor, the reactor is divided into 10 sections with the center of each section containing a sampling point, as seen in Fig. D.5. Each section takes on the temperature which is measured at each point and the velocity is determined from the temperature using Eqn. (D.19). Based on the velocity and Δx of the section, a Δt for each section is calculated using Eqn. (D.20).

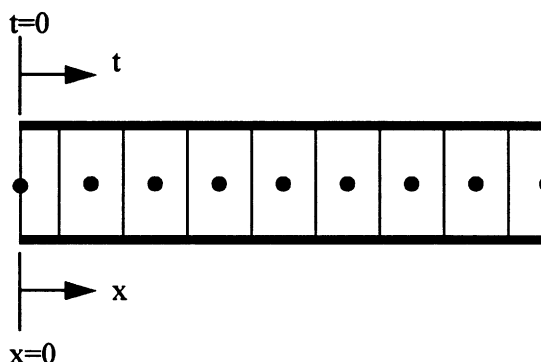


Figure D.5 The location of the data points within the plug flow reactor.

The time at each point after gases enter the reactor was determined through linear interpolation between values of x and t . The air entrainment data, taken at the locations where the temperatures were measured, was transformed into the temporal coordinate system using the same analysis performed to convert the spatial temperature data to a temporal temperature data.

D.3.2 Transformation of Plug Flow Reactor Results to Spatial Coordinate System

To compare experimental results with *SENKIN* results, the data from *SENKIN* is transformed from a temporal coordinate system to a spatial coordinate system. To do this, consider the differential form of the velocity,

$$v = \frac{dx}{dt} \quad (\text{D.21})$$

Converting the velocity to mass flow and integrating the left side from 0 to x and the right side from 0 to t , Eqn. (D.21) becomes

$$\int_0^x dx = (\bar{m}/A) \int_0^t (1/\rho) dt \quad (\text{D.22})$$

By assuming a steady state process, the cross sectional area of the plug flow reactor and the mass flow rate are constant with time. The cross sectional area of the plug flow reactor and the mass flow can be taken outside of the integrand. Applying the ideal gas law to Eqn. (D.22) to rewrite the density in terms of temperature, the following formulation is obtained:

$$\int_0^x dx = \frac{(\bar{m}/A)R}{P} \int_0^t T dt \quad (\text{D.23})$$

Note that Eqn. (D.20) is simply the integrated form of Eqn. (D.23), having assumed constant temperature across the integrated area. Assuming constant pressure and integrating the left hand side of the equation, the following transformation from spatial to temporal coordinates is derived

$$x = \frac{(\bar{m}/A)R}{P} \int_0^t T dt \quad (\text{D.24})$$

APPENDIX E.

EXPERIMENTAL ERROR ANALYSIS

E.1 INTRODUCTION

The experimental error of the measured and calculated values in the research is determined in the following sections. The error into parameters measured directly is addressed first. Error in the parameters calculated using the measured values is then calculated.

E.2 CALCULATION OF ERROR

The calculation of error for a parameter where all the variables are assumed to be linear dependent with one another is

$$\epsilon^2 = \epsilon_1^2 + \epsilon_2^2 + \epsilon_3^2 + \epsilon_4^2 \dots \quad (\text{E.1})$$

Equation (E.1) is used to calculate the error for measured quantities where the dependence of each source of error is proportional to the other sources of error.

When determining the error for parameters calculated from equations, a more fundamental method is applied:

$$w_y^2 = \left(\frac{\partial y}{\partial x_1} w_{x_1} \right)^2 + \left(\frac{\partial y}{\partial x_2} w_{x_2} \right)^2 + \left(\frac{\partial y}{\partial x_3} w_{x_3} \right)^2 + \dots \quad (\text{E.2})$$

where w is the variation in a particular variable, y is the parameter being calculated, and the x 's are the variables in the equation. For proof sake, consider a function y whose variables are linearly dependent on one another, $y=x_1x_2x_3$. Taking the appropriate partial

derivatives, and then dividing both sides of Eqn. (E.2) by y , the following formulation is produced

$$\left(\frac{w_y}{y}\right)^2 = \left(\frac{w_{x_1}}{x_1}\right)^2 + \left(\frac{w_{x_2}}{x_2}\right)^2 + \left(\frac{w_{x_3}}{x_3}\right)^2 \quad (\text{E.3})$$

or,

$$\epsilon_y^2 = \epsilon_{x_1}^2 + \epsilon_{x_2}^2 + \epsilon_{x_3}^2 \quad (\text{E.4})$$

Equation (E.4) is, as expected, equivalent to (E.1).

E.3 ERROR IN PARAMETERS

E.3.1 Measured Species Concentrations

The measurement error of CO, CO₂, O₂ and UHC concentrations was attributed to four sources:

- analyzer repeatability, ϵ_{AR} ,
- calibration gas, ϵ_{CG} ,
- calibration uncertainty, ϵ_{CU} , and
- experimental repeatability, ϵ_{ER} .

The CO, CO₂ and O₂ concentrations were all measured dry while the UHC were measured wet.

The repeatability of the analyzers was noted by the manufactures as being $\pm 1\%$ ($\epsilon_{AR}=0.01$). The maximum error in the calibration gas concentration, determined by the supplier using a gas chromatograph, was $\pm 1.5\%$ ($\epsilon_{CG}=0.015$). The last two sources of error depended upon whether the gases were being sampled in the hallway (or

Table E.1. The uncertainty induced in the measurement of the species concentrations.

Species	$\epsilon_{CU,ex}$	$\epsilon_{ER,ex}$	ϵ_{ex}	$\epsilon_{CU,h/c}$	$\epsilon_{ER,h/c}$	$\epsilon_{h/c}$
CO	0.01	0.04	0.045	0.015	0.1	0.103
CO ₂	0.005	0.04	0.044	0.015	0.07	0.074
O ₂	0.005	0.005	0.02	0.005	0.05	0.053
UHC	0.01	0.025	0.036	0.01	0.15	0.102

compartment) or in the exhaust duct, and the species which was being measured. Tabulated values for these errors are given in Table E.1. Utilizing these values for the error, the error when measuring species in the exhaust duct, ϵ_{ex} , and in the hallway/compartment, $\epsilon_{h/c}$, was determined by applying Eqn. (E.3).

E.3.2 Wet Species Concentrations

Assuming the CO₂ and H₂O are present in a stoichiometric proportions, the wet concentrations of CO, CO₂ and O₂ can be calculated from

$$X_{j,w} = \frac{X_{j,d}}{(1 + 1.167 X_{CO_2,d})} \quad (E.5)$$

Gottuk estimated the assumption of the CO₂ and H₂O being in stoichiometric proportions as being valid to within $\pm 6\%$. Utilizing the tabulated values for the error in the dry concentration measurement, the error in the calculation of the wet concentrations is determined, see Table E.2.

E.3.3 Gas Temperature

Gas temperatures were measured in both the compartment and the hallway. The error in the temperature measurements was due to the aspiration process (utilized to shield the thermocouples from radiation) and the repeatability of the experiment.

Table E.2. The uncertainty in the calculation of the wet concentrations of CO, CO₂ and O₂.

Species	ϵ_{ex}	$\epsilon_{h/c}$
CO	0.075	0.119
CO ₂	0.074	0.095
O ₂	0.063	0.080

Inside the compartment, the error in the aspiration was approximated to be 1.0%. The repeatability of the experimental values was determined to be approximately 3% through comparison of two experiments run under the same conditions. The result was an error of $\pm 3.2\%$.

In the hallway, the temperatures in the hallway are more transient compared to the compartment. The error due to aspiration was determined to again be 3%. Through the comparison of the same experiments utilized in the compartment error analysis, the experimental repeatability of the temperatures was within 13%. The error in the hallway temperatures was calculated to be $\pm 13.2\%$.

E.3.4 Fuel Weight

The error induced on the weight of the fuel was attributed to the thermal drift in the load cell, the resolution of the load cell and the A/D conversion. The thermal drift was considered to be the most significant of the three sources, and was estimated by comparing the weight of the fuel pan before and after the experiment. The error was found to be approximately 1%. With the load cell being accurate to within 1 gram, the error in the resolution was considered to be negligible as was the A/D conversion. The error in the fuel weight was, therefore, $\pm 1\%$.

E.3.5 Air Mass Flow Rate into Compartment

The measurement of air mass flow rate into the compartment was determined to have three sources of error: the temperature measurement (used to determine the density) (1%), the location of the velocity probe relative to the location average velocity (4%), and the use of the average velocity instead of an integrated velocity profile (1%). Based on these sources of error, the error in the measurement was calculated to be $\pm 4.2\%$.

E.3.6 Global Equivalence Ratio

The global equivalence ratio is defined as

$$\phi = \frac{\dot{m}_v / \dot{m}_{air}}{\left(\dot{m}_{fuel} / \dot{m}_{air} \right)_{st}} \quad (\text{E.6})$$

Since the stoichiometric fuel to air ratio is a constant, the error in the fuel volatilization rate and the air entrainment rate into the compartment need only be considered. The error in the fuel volatilization rate was determined from

$$w_{\dot{m}_v} \leq \frac{1}{6} h^2 \ddot{m}_v \quad (\text{E.7})$$

which corresponds to the maximum variation in the numerical derivative of the fuel weight performed over a ± 10 , h, second band around the point. The maximum value of \ddot{m}_v of 9.5×10^{-6} was found to occur just prior to post-flashover. Using a value of $h=10$, the maximum variation in the fuel volatilization rate is expected to be 1.58×10^{-4} . Using the fuel volatilization rate at that instant where the maximum second derivative of the fuel volatilization rate was found, the error was determined to be $\pm 6\%$.

Using the error in the air entrainment rate into the compartment, $\pm 4.2\%$, in conjunction with the error in the fuel volatilization rate, the error in the global equivalence ratio was calculated to be $\pm 7.3\%$.

Table E.3 The uncertainty in the post-hallway yields for the different species measured in the study.

Species	ϵ_{yld}
CO	0.139
CO ₂	0.139
O ₂	0.134
UHC	0.107

E.3.7 Species Yields

The sources of error in the species yield

$$Y_{j,ex} = \frac{X_{j,w} MW_j \dot{n}_{ex}}{\dot{m}_v} \quad (E.8)$$

calculation were the error of all variables in Eqn. (E.8) and the time shift in the data to align the gas measurement data with the instantaneous measurement of the fuel weight. Assuming the shift results in at most 1% error, the molecular weight is within 0.5% of that of air and that \dot{n}_{ex} is within 10% of the actual molar flow rate within the duct; the error in the yields for each species is given in Table E.3.

E.3.8 Fire Size

The error in the ideal fire size is dependent upon the fuel volatilization rate, since the error in the heat of combustion multiplying the fuel volatilization rate is comparatively negligible. The error in the fire size is, therefore, calculated to be $\pm 6\%$.

E.3.9 Nondimensional Hallway Upper-Layer Depth

The sources of error in the determination of the nondimensional hallway upper-layer depth, $\gamma = \delta/z$, are from the measurement of the upper-layer within the hallway, δ , and the measurement of the distance between the bottom of the opening and the ceiling, z . The error in the measurement in the upper-layer depth was found to be 12.5%, while the value

of z only varied less than 0.5%. The analysis determined the error the nondimensional upper-layer depth to be $\pm 12.5\%$

E.3.10 Entrainment Function

With the entrainment function defined as the ratio between the entraining velocity and the velocity of the gases entering the hallway. The inlet velocity was known to within 10%. The velocity of the entraining air depended on the mass flow of air entrained, the density of the entraining air, and the wetted area of the jet. The largest errors were calculated for the mass flow of air entrained (15%) and the wetted area of the jet (19%), resulting in a 24% error in the entrained velocity. The entrainment function error is, therefore, $\pm 26\%$.

E.3.11 Richardson Number

The sources of error in the Ri is attributed to the density of the gases entering the hallway and the entraining gases (10%), the velocity of the gases entering the hallway (10%) and the hydraulic diameter of the opening (15%). The error in the Ri number is expected to be no greater than $\pm 25\%$.

E.3.12 Ignition Index

The majority of the error in the ignition index is from the estimation of H_2 from the CO , and the assumption that all the UHC are ethylene. The other sources of error are the measurement of CO and temperature. The error for the H_2 was estimated by Gottuk (1992a) as being 10%, while the UHC error was taken from Table E.1 to be 10.2%. The error in the CO measurement was 11.9%, but the temperature is accurate to within 3%. The application of these errors to Eqn. (E.1) produces a 18.8% error in the ignition index.

E.4 SUMMARY

Table E.4 lists the errors associated with the measured and calculated parameters.

Table E.4 The errors of all the parameters measured and calculated in the study.

PARAMETER	ERROR, (\pm)
$[\text{CO}]_{\text{dry}}$ (Ex. Duct/ Hall-Comp.)	4.5% / 10.3%
$[\text{CO}_2]_{\text{dry}}$ (Ex. Duct/ Hall-Comp.)	4.4% / 7.4%
$[\text{O}_2]_{\text{dry}}$ (Ex. Duct/ Hall-Comp.)	2% / 5.3%
$[\text{UHC}]_{\text{wet}}$ (Ex. Duct/ Hall-Comp.)	3.6% / 10.2%
$[\text{CO}]_{\text{wet}}$ (Ex. Duct/ Hall-Comp.)	7.5% / 11.9%
$[\text{CO}_2]_{\text{wet}}$ (Ex. Duct/ Hall-Comp.)	7.4% / 9.5%
$[\text{O}_2]_{\text{wet}}$ (Ex. Duct/ Hall-Comp.)	6.3% / 8.0%
Compartment Temperatures	3.2%
Hallway Temperatures	13.2%
\dot{m}_v	6.0%
\dot{m}_{air}	4.2%
ϕ	7.3%
CO Yield (Post-Hallway)	13.9%
CO ₂ Yield (Post-Hallway)	13.9%
O ₂ Yield (Post Hallway)	13.4%
UHC Yield (Post Hallway)	10.7%
Ideal Fire Size, Q	6%
γ	12.5%
E	26%
Ri	25%
Ignition Index, I.I.	18.8%

NIST-114
(REV. 9-92)
ADMAN 4.09

U.S. DEPARTMENT OF COMMERCE
NATIONAL INSTITUTE OF STANDARDS AND TECHNOLOGY

(ERB USE ONLY)

ERB CONTROL NUMBER	DIVISION
PUBLICATION REPORT NUMBER NIST-GCR-97-713	CATEGORY CODE
PUBLICATION DATE April, 1997	NUMBER PRINTED PAGES

MANUSCRIPT REVIEW AND APPROVAL

INSTRUCTIONS: ATTACH ORIGINAL OF THIS FORM TO ONE (1) COPY OF MANUSCRIPT AND SEND TO:
THE SECRETARY, APPROPRIATE EDITORIAL REVIEW BOARD.

TITLE AND SUBTITLE (CITE IN FULL)

The Transport of High Concentrations of Carbon Monoxide to Locations Remote from the Burning Compartment

CONTRACT OR GRANT NUMBER
60NANB4D1651

TYPE OF REPORT AND/OR PERIOD COVERED
September 1, 1995 - August 31, 1996

AUTHOR(S) (LAST NAME, FIRST INITIAL, SECOND INITIAL)
Lattimer, B.Y.; Vandsburger, U.
Roby, R.J.

PERFORMING ORGANIZATION (CHECK (X) ONE BOX)

<input checked="" type="checkbox"/>	NIST/GAITHERSBURG
<input type="checkbox"/>	NIST/BOULDER
<input type="checkbox"/>	JILA/BOULDER

LABORATORY AND DIVISION NAMES (FIRST NIST AUTHOR ONLY)

SPONSORING ORGANIZATION NAME AND COMPLETE ADDRESS (STREET, CITY, STATE, ZIP)
Department of Commerce
National Institute of Standards and Technology
Gaithersburg, MD 20899

RECOMMENDED FOR NIST PUBLICATION

<input type="checkbox"/>	JOURNAL OF RESEARCH (NIST JRES)	<input type="checkbox"/>	MONOGRAPH (NIST MN)	<input type="checkbox"/>	LETTER CIRCULAR
<input type="checkbox"/>	J. PHYS. & CHEM. REF. DATA (JPCRD)	<input type="checkbox"/>	NATL. STD. REF. DATA SERIES (NIST NSRDS)	<input type="checkbox"/>	BUILDING SCIENCE SERIES
<input type="checkbox"/>	HANDBOOK (NIST HB)	<input type="checkbox"/>	FEDERAL INF. PROCESS. STDS. (NIST FIPS)	<input type="checkbox"/>	PRODUCT STANDARDS
<input type="checkbox"/>	SPECIAL PUBLICATION (NIST SP)	<input type="checkbox"/>	LIST OF PUBLICATIONS (NIST LP)	<input checked="" type="checkbox"/>	OTHER NIST-GCR-
<input type="checkbox"/>	TECHNICAL NOTE (NIST TN)	<input type="checkbox"/>	NIST INTERAGENCY/INTERNAL REPORT (NISTIR)		

RECOMMENDED FOR NON-NIST PUBLICATION (CITE FULLY)

U.S. FOREIGN

PUBLISHING MEDIUM

<input type="checkbox"/>	PAPER	<input type="checkbox"/>	CD-ROM
<input type="checkbox"/>	DISKETTE (SPECIFY)		
<input type="checkbox"/>	OTHER (SPECIFY)		

SUPPLEMENTARY NOTES

ABSTRACT (A 1500-CHARACTER OR LESS FACTUAL SUMMARY OF MOST SIGNIFICANT INFORMATION. IF DOCUMENT INCLUDES A SIGNIFICANT BIBLIOGRAPHY OR LITERATURE SURVEY, CITE IT HERE. SPELL OUT ACRONYMS ON FIRST REFERENCE.) (CONTINUE ON SEPARATE PAGE, IF NECESSARY.)

An experimental study was conducted to measure the effects of oxygen entrainment on the transport of CO in building fires, and to develop a procedure for estimating CO levels at positions remote from the fire room. Experiments were performed with an insulated 1/4-scale room connected to the side of a 1/4-scale hallway forming an L-shape. Measurements of CO, unburned hydrocarbons, CO₂, and O₂ concentrations and temperatures were performed within the compartment, the hallway, and post-hallway in the exhaust duct. The CO yield increased by as much as 23% when the fire gases entering the hallway were completely surrounded by oxygen-deficient gases, while partial burn out of CO occurred when these gases had better access to oxygen. The distribution of CO within the upper layer of the hallway was highly nonuniform when the gases first entered from the fire room. A simple procedure has been developed for predicting CO levels at locations remote from the fire room which accounts for the effects of external burning, the non-uniform transport of toxic gases in the hallway, the hallway upper-layer depth, and the stoichiometry.

KEY WORDS (MAXIMUM 9 KEY WORDS; 28 CHARACTERS AND SPACES EACH; ALPHABETICAL ORDER; CAPITALIZE ONLY PROPER NAMES)

carbon monoxide, ceiling jets, corridors, exhaust gases, fire behavior, room fires, stoichiometry, toxic products

AVAILABILITY

<input type="checkbox"/>	UNLIMITED	<input type="checkbox"/>	FOR OFFICIAL DISTRIBUTION. DO NOT RELEASE TO NTIS.
<input type="checkbox"/>	ORDER FROM SUPERINTENDENT OF DOCUMENTS, U.S. GPO, WASHINGTON, D.C. 20402		
<input type="checkbox"/>	ORDER FROM NTIS, SPRINGFIELD, VA 22161		

NOTE TO AUTHOR(S) IF YOU DO NOT WISH THIS MANUSCRIPT ANNOUNCED BEFORE PUBLICATION, PLEASE CHECK HERE.

ELECTRONIC FORM